AD_____

Award Number: W81XWH-04-1-0509

TITLE: The Role of Drosophila Merlin in the Control of Mitosis Exit and Development

PRINCIPAL INVESTIGATOR: Long-Sheng Chang, Ph.D.

CONTRACTING ORGANIZATION: Children's Research Institute
Columbus, Ohio 43205-2696

REPORT DATE: July 2008

TYPE OF REPORT: Final

PREPARED FOR: U.S. Army Medical Research and Materiel Command
Fort Detrick, Maryland 21702-5012

REPORT DOCUMENTATION PAGE

Form Approved
OMB No. 0704-0188

1. REPORT DATE	2. REPORT TYPE	3. DATES COVERED
01-07-2008	Final	1 Jul 2004 – 30 Jun 2008

4. TITLE AND SUBTITLE

The Role of Drosophila Merlin in the Control of Mitosis Exit and Development

5a. CONTRACT NUMBER

5b. GRANT NUMBER
W81XWH-04-1-0509

5c. PROGRAM ELEMENT NUMBER

6. AUTHOR(S)

Long-Sheng Chang, Ph.D.

Email: lchang@chi.osu.edu

5d. PROJECT NUMBER

5e. TASK NUMBER

5f. WORK UNIT NUMBER

7. PERFORMING ORGANIZATION NAME(S) AND ADDRESS(ES)

Children's Research Institute
Columbus, Ohio 43205-2696

8. PERFORMING ORGANIZATION REPORT NUMBER

9. SPONSORING / MONITORING AGENCY NAME(S) AND ADDRESS(ES)
U.S. Army Medical Research and Materiel Command
Fort Detrick, Maryland 21702-5012

10. SPONSOR/MONITOR'S ACRONYM(S)

11. SPONSOR/MONITOR'S REPORT NUMBER(S)

12. DISTRIBUTION / AVAILABILITY STATEMENT
Approved for Public Release; Distribution Unlimited

13. SUPPLEMENTARY NOTES

14. ABSTRACT To better understand the mechanism by which Merlin functions as a tumor suppressor, we have confirmed that Drosophila Merlin plays important roles in the control of mitosis exit and in the determination of dorsal/ventral compartment border during wing imaginal disc development. We show that the Merlin protein is dynamically redistributed during meiosis and demonstrate, for the first time, Merlin immunoreactivity in mitochondria. Also, we have found that Merlin colocalizes with Wingless morphogen in the cells at the dorsal/ventral compartment border of the wing imaginal disc. Merlin inactivation may alter the determination/maintenance of Wingless stripe expression. Cells lacking Merlin possess greater ability to overcome vein restriction. In addition, we provide evidence for potential genetic interactions between Merlin and the proteins involved in vesicular trafficking, including Porcupine, Shibire, and Lap. By analyzing the evolution, diversity, and overall distribution of Merlin among different taxa, we demonstrate a monophyletic origin of the Merlin proteins with their root in the early metazoa. The overall similarity among the primary and secondary structures of all merlin proteins and the conservation of several functionally important residues suggest a universal role for merlin in a wide range of metazoa. Furthermore, we show that the AKT pathway is frequently activated in NF2- tumor cells. We have tested two novel compounds, OSU03012 and (S)-HDAC-42, which inhibit AKT phosphorylation, and found that these drugs effectively inhibit the growth of vestibular schwannoma cells. These findings set the stage for a phase I clinical trial on VS in the future.

15. SUBJECT TERMS Neurofibromatosis 2 (NF2), NF2 Gene, Merlin, ezrin-radixin-moesin (ERM), Drosophila melanogaster, mitosis exit, development, imaginal disc, receptor-mediated endocytosis, vesicular trafficking, Lap, spermatogenesis, and schwannomas

16. SECURITY CLASSIFICATION OF:			17. LIMITATION OF ABSTRACT	18. NUMBER OF PAGES	19a. NAME OF RESPONSIBLE PERSON
a. REPORT	b. ABSTRACT	c. THIS PAGE			USAMRMC
U	U	U	UU	154	19b. TELEPHONE NUMBER *(include area code)*

TABLE OF CONTENTS

INTRODUCTION:

Neurofibromatosis type 2 (NF2) is a hereditary disorder characterized by the development of bilateral vestibular schwannomas and associated with mutations in the *Neurofibromatosis 2* (*NF2*) tumor suppressor gene. The *NF2* gene encodes a protein named Merlin for moesin-ezrin-radixin like protein (Trofatter et al., 1993). Merlin shares a great deal of homology with the ezrin, radixin, and moesin (ERM) proteins, which belong to the protein 4.1 superfamily of cytoskeleton-associated proteins that link cell surface glycoproteins to the actin cytoskeleton. Presently, the mechanism by which Merlin functions as a tumor suppressor is poorly understood.

Drosophila melanogaster provides a genetic and developmental system, which is amenable to experimental manipulation, and has been very valuable to the study of tumor genetics. The *Drosophila* homolog of Merlin shares sequence similarity to the human Merlin protein (McCartney and Fehon, 1996; Fehon et al., 1997). In addition, the human *NF2* gene can rescue the lethal Merlin mutant allele in *Drosophila*, implying functional conservation (LaJeunesse et al., 1998). Molecular genetic analysis reveals that Merlin is essential for the regulation of proliferation and differentiation in the imaginal disc. However, understanding the tumor suppressor function of Merlin requires additional knowledge about specific cell-cycle points where Merlin regulates proliferation and coordinates it with morphogenesis.

We have found that cells in the wing imaginal disc of fly larva with a Merlin mutation (Mer^4) displayed abnormalities in the control of mitosis exit. Cytological images of mutant cells frequently showed asynchronous anaphase and telophase. We have also isolated adult Mer^4 pharates. Interestingly, these *Mer* mutant adults showed abnormal leg morphology. Some of them displayed duplication of the wing disc, and in some cases, abnormalities were seen in the dorsal/ventral compartment border of the *Mer* mutant wing disc. These results suggest that Merlin is important not only for the control of mitosis exit but also for the determination/maintenance of morphogen gradients in the wing imaginal disc.

The goal of our proposed research is to examine the novel role of Merlin in the control of mitosis and development. Specifically, we plan to confirm the role of Merlin in the control of mitosis and determine whether there are any additional points in the cell cycle where Merlin executes its functional activity. We will examine the role of Merlin in wing imaginal disc development and the effect of Merlin mutation on specific regulatory protein expression within the wing imaginal disc. In addition, we will attempt to investigate whether the abnormalities in mitosis observed in Merlin mutant flies could also be seen in mouse and human schwannoma cells lacking *NF2* function. From this study, we hope to better understand how Merlin regulates proliferation and how it coordinates proliferation, mitosis, and morphogenesis. Future investigation of the signaling pathways that link Merlin to intracellular signals regulating cell division may enable designs for novel therapeutic regiments to cure NF2 schwannomas and other associated tumors.

BODY:

Aim 1: To conduct cytological analysis on additional Merlin mutant alleles and allelic combinations for the control of mitosis exit and morphogenesis

Task 1: We previously studied the effect of a *Merlin* mutation, Mer^4 ($Gln^{170\rightarrow stop}$), on mitosis of neural ganglia and wing imaginal disks isolated from third-instar larvae of *Drosophila*. We examined neural ganglia and imaginal disk cells because they are similar to diploid somatic cells in mammals. We found that, compared to the same cell types from wild-type larvae, the Mer^4 cells showed abnormalities in the relative duration of mitosis phases and chromosome segregation in anaphase and telophase. To confirm these observations, we obtained additional merlin mutant alleles, including mer^1 ($Gln^{324\rightarrow stop}$), mer^2 ($Gln^{318\rightarrow stop}$), mer^3 ($Met^{177\rightarrow Ile}$), and $mer^4;mer^+$ (Fehon et al., 1997) Larvae with the hemizygous mer^1, mer^2, mer^3, or $mer^4;mer^+$ genetic background were prepared. For comparison, larvae from three wild-type strains were used. The wing imaginal discs and neural ganglia were isolated from these wild-type and mutant larvae, and used in cytological analysis as previously described for the mer^4 mutant. This task was accomplished in Year One.

Task 2: We performed cytological analysis on tissues isolated from three wild-type strains, various *Merlin* mutants [Mer^1, Mer^2, Mer^3, and Mer^4], as well as the $Mer^4;Mer^+$ strain, which contains a wild-type *Merlin* transgene in the Mer^4 genetic background. As shown in Figure 1, the normal flow of mitosis in both the brain and the wing imaginal disc from the wild-type larva is characterized by synchronous changes in the morphology of all chromosomes simultaneously (Figure 1A-1F). Dissociation of sister chromatids also occurs simultaneously in all chromosomes in metaphase or during the transition from metaphase to anaphase. In contrast, we observed that *Merlin mutants* frequently *displayed* two types of mitosis exit asynchrony. The first type of mitosis exit asynchrony was the asynchronous anaphase-telophase figures with one sister chromosome set in anaphase and the other in telophase (Figures 1G and 1H). The second type of mitosis exit asynchrony is the asynchronous telophase-interphase figures with one sister chromosome set in telophase and the other in interphase (Figures 1I and 1J).

*Figure 1. Images of normal mitosis in neural brain cells from third-instar wild-type larvae (A-F) as compared with those of asynchronous mitosis exit in neural brain cells from the Mer^4 mutant larvae. During normal mitosis, chromosome condensation at heterochromatin regions begins at early prophase P1 (A). Condensed homologous chromosomes are paired at late prophase P2 (B). Sister chromatids are connected at precentromeric heterochromatin regions in metaphase (C). Chromosomes are separated along their lengths at late metaphase (D). Two sister chromosome sets are separating from each other and oriented toward the opposite poles in anaphase (E). Fully-separated sister chromosome sets begin to undergo chromosome decondensation in telophase (F). Unlike normal mitosis, the Mer^4 mutant cells frequently display asynchronous anaphase-telophase figures. While tw*o sister chromosome sets are separating from each other and

orienting toward the opposite poles, one set of chromosomes is already undergoing chromosome decondensation (G,H). *The Mer^4 mutant cells also frequently show asynchronous telophase-interphase figures (I,J).*

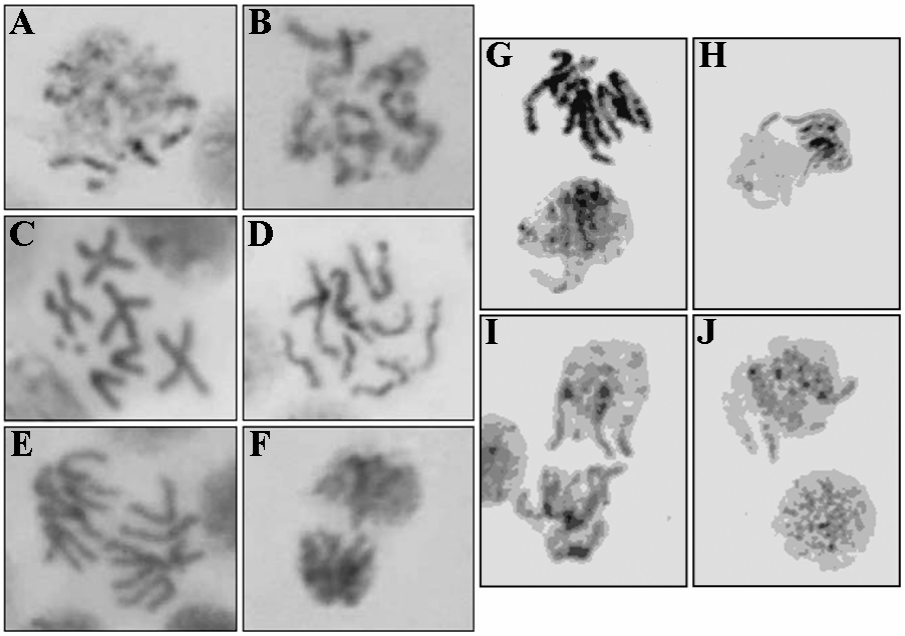

Table 1 summarizes the frequency of mitotic exit asynchrony in various mutant alleles compared with the three wild-type strains, Lausenne, Hikkone A-W, and Oregon R. In contrast to those from the wild-type strains, neural brain cells from all four *Merlin* mutants showed both types of mitosis exit asynchrony at higher frequencies. The frequency of asynchronous figures was lower in the weak *Mer^3* allele (a missense mutation) than in the other three truncated *Merlin* alleles, *Mer^1*, *Mer^2*, and *Mer^4*. Importantly, when a wild-type *Merlin* transgene was introduced back to the *Mer^4* genetic background, the asynchronous mitosis exit phenotype was substantially diminished. Collectively, these results suggest that Merlin is important for the control of mitosis exit.

Table 1. Mitotic exit asynchrony in various Merlin alleles, compared with the wild-type Lausenne, Hikkone A-W, and Oregon R strains.

Strain	No. of cells in anaphase analyzed[a]	No. of cells with asynchronous anaphase-telophase figures[b]	% of cells in anaphase with asynchronous anaphase-telophase figures	No. of cells in telophase analyzed[c]	No. of cells with asynchronous telophase-interphase figures[d]	% of cells in telophase with asynchronous telophase-interphase figures
Lausenne	298	0	0	11	0	0
Hikkone A-W	93	0	0	14	0	0
Oregon R	101	0	0	26	0	0
Mer^4	118	14	11.9	40	16	40
Mer^4;Mer$^+$	257	7	2.7	18	1	5.6
Mer^3	161	16	9.9	29	5	17.2
Mer^2	80	14	17.5	10	3	30
Mer^1	38	5	13.2	7	2	28.6

[a]Cells with at least one sister chromosome set in anaphase
[b]One sister chromosome set in anaphase while the other in telophase.
[c]Cells with at least one sister chromosome set in telophase but none in anaphase
[d]One sister chromosome set in telophase while the other in interphase.

Task 3: To test the effect of various *Merlin* allelic combinations on mitosis, we generated pUASP constructs carrying myc-tagged Mer^{+}, Mer^{3}, $Mer^{\Delta BB}$, Mer^{1-379}, or $Mer^{345-635}$ DNA ($mycMer^{+}$, $mycMer^{3}$, $mycMer^{\Delta BB}$, $mycMer^{1-379}$, or $mycMer^{345-635}$, respectively) and used them to transform *Drosophila* embryos. We found that both *pUASP-mycMer*$^{+}$ and *pUASP-mycMer*^{3} could rescue the lethality of Mer^{4} mutation when ectopically activated by the *Act5C-Gal4* driver (Table 2; also see Dorogova et al., 2008 [Appendices]). We also showed that only over-expression of *Mer*+ restored the fertility of flies carrying the Mer^{4} mutation. These results are consistent with the observation that male flies hemizygous for Mer^{3} are viable but sterile (LaJeunesse et al., 1998).

Table 2. The ability of various transgenes to restore the viability and fertility of the Mer^{4} allele.

Genetic cross	Males carrying Mer^{4}	Viability	Fertility
♀♀ *y w Mer^{4}/FM7i, GFP; +/+; +/+* X ♂♂ *w sn/Y; +/+ ; P{w^{+}=cosMer^{+}}/+*	*y w Mer^{4}/Y; +/+; P{w^{+}=cosMer^{+}}/+*	+	+
	y w Mer^{4}/Y; +/+; +/+	-	-
♀♀ *y w Mer^{4}/M-5, B w^{a}; +/+; +/+* X ♂♂ *y w/Y; Act5C-Gal4/If; P{w^{+}=UASP-Mer^{+}}/TM6, Tb*	*y w Mer^{4}/Y; Act5C-Gal4/+; P{w^{+}=UASP-Mer^{+}}/+*	+	+
	y w Mer^{4}/Y; Act5C-Gal4/+; +/TM6, Tb	-	-
	y w Mer^{4}/Y; If/+; TM6, Tb/+	-	-
	y w Mer^{4}/Y; If/+; P{w^{+}=UASP-Mer^{+}}/+	-	-
♀♀ *y w Mer^{4}/M-5, B w^{a}; +/+; +/+* X ♂♂ *y w/Y; Act5C-Gal4/If; P{w^{+}=UASP-Mer^{3}}/TM6, Tb*	*y w Mer^{4}/Y; Act5C-Gal4/+; P{w^{+}=UASP-Mer^{3}}/+*	+	-
	y w Mer^{4}/Y; Act5C-Gal4/+ ; +/TM6, Tb	-	-
	y w Mer^{4}/Y; If/+; TM6, Tb/+	-	-
	y w Mer^{4}/Y; If/+; P{w^{+}=UASP-Mer^{3}}/+	-	-

We also ectopically expressed the Mer^{3} transgene in the wing pouch using the *1096-Gal4* driver and examined the effect of Mer^{3} over-expression on mitosis in the wing imaginal disc. Since the flies we used also carried a *UAS-GFP (green fluorescent protein)* transgene, we were able to mark the wing pouch with GFP expression. To detect mitotic cells, the imaginal discs were stained with an anti-phospho-histone H3 antibody (Mattila et al. 2005) and the number of mitotic cells in the wing pouch, the region in which the *1096-Gal4* driver and GFP were expressed, was counted. We found that ectopic expression of Mer^{3} resulted in an increased number of mitotic cells in the wing pouch (Figure 2A), compared with that in the wild-type wing imaginal disc (Figure 2B).

These results indicate that *Merlin* mutation leads to increased mitosis and are consistent with the finding that the Mer^{3} mutant fly has larger wings (Fehon et al., 1997; LaJeunesse et al., 1998).

Figure 2. Anti-phospho-histone H3 labeling of mitosis in the wing pouch. Wing imaginal discs with a genetic background of Mer^{3}/1096-Gal4;UAS-GFP/+ (A) or 1096-Gal4/+;UAS-GFP/+, which served as a wild-type control (B), were immuno-stained with an anti-phospho-histone H3 antibody (red). The dorsal region of the wing pouch was marked by GFP expression (green) due to the

1096-Gal4 activity. Note that there were more mitotic cells in the wing pouch when Mer^3 was over-expressed.

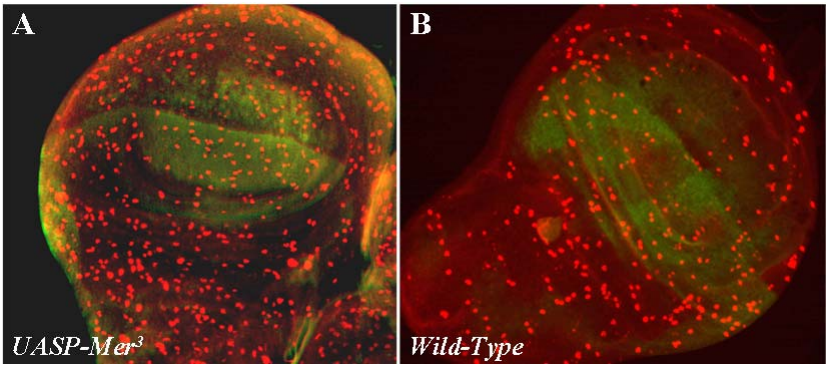

Aim 2: To examine and compare the duration of the cell cycle and mitosis phases using various Merlin mutants and to study subcellular localization of Merlin at various phases of mitosis

Task 4: Labeled mitotic curve provides information about the cell-cycle duration (time between two mitotic waves), and the duration of S-phase (duration of mitotic wave) and G_2 phase (time of appearance of the first labeled mitoses). To measure the duration of the cell cycle and mitosis phases, we conducted a mitotic labeling experiment using imaginal discs isolated from the wild-type Hikkone A/W strain, the strain with the homozygous overgrowth mutation *ft*^{4} (benign tumor), the strain with the homozygous tumor-suppressor mutation *l(2)gl*^{DV275} (malignant tumor), and the strain with the homozygous *Mer*^{4} mutation (benign tumor). Figure 3 shows that the time between the two cell cycle peaks in wild-type cells is about 9~10h, consistent with our previous observation (Trunova et al., 1998, 2001; Dubatolova and Omelyanchuk, 2004).

Figure 3. Labeled mitosis curves for the imaginal disc cells from the wild-type Hikkone A/W, l(2)gl^{DV275}, ft^4, and mer^4 strains. Two different ages (6 and 10 days) of ft^4 larvae were used.

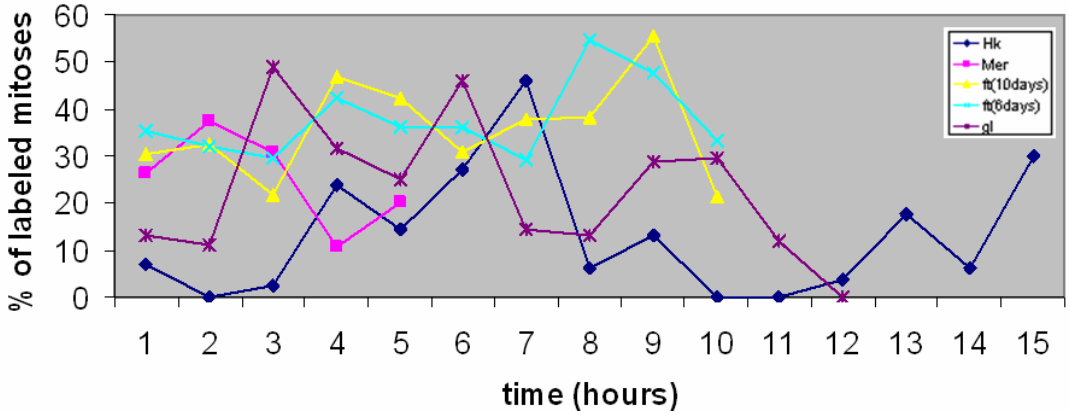

Unlike wild-type cells, which display one major peak during each cell cycle, the labeled mitosis curve for *l(2)gl* cells shows 3 peaks (Figure 3). The left peak constitutes the cell population with a shorter G_2 phase than that in the wild type. The middle peak represents the cell population with the same G_2 duration as that in the wild type. The right peak corresponds to the cell population with a longer G_2 phase. Similarly, we detected two different

populations of *ft*^{4} cells: one with a shorter G_2 phase and the other with a longer G_2 phase. For *Mer*^{4} cells, a subpopulation of cells with a shorter G_2 period was also seen; however, we could not cultivate M*er*^{4} imaginal discs for more than 5 h *in vitro*. Nevertheless, the results indicate that M*er*^{4} cells display a shorter G_2 period in the cell cycle, compared with wild-type cells.

Task 5: With the use of Schneider's *Drosophila* cell culture medium (Sigma-Aldrich), we were able to cultivate wing imaginal discs for a longer period of time. To determine the effect of *Merlin* mutation on the duration of cell-cycle phases, we performed a double labeling experiment incorporating BrdU labeling and anti-phospho-histone H3 staining of wing imaginal discs isolated from 3rd-instar wild-type or *Mer*^{4} larvae. Briefly, cultured wing imaginal discs were pulse-labeled with BrdU for six minutes and then chased for various periods of time. BrdU-labeled imaginal discs were doubly immunostained with anti-BrdU and anti-phospho-histone H3 antibodies. Stained imaginal discs were visualized under a confocal microscope, and representative images of such doubly-labeled imaginal discs are illustrated in Figure 4. The BrdU-labeled cells are seen in green and those in mitosis are in red, while cells that are doubly-labeled for both BrdU and phospho-histone H3 are shown in yellow (Figures 4A and 4B). The cell spots that are red or yellow were projected onto a map of a wing imaginal disc (Figures 4C and 4D) and counted.

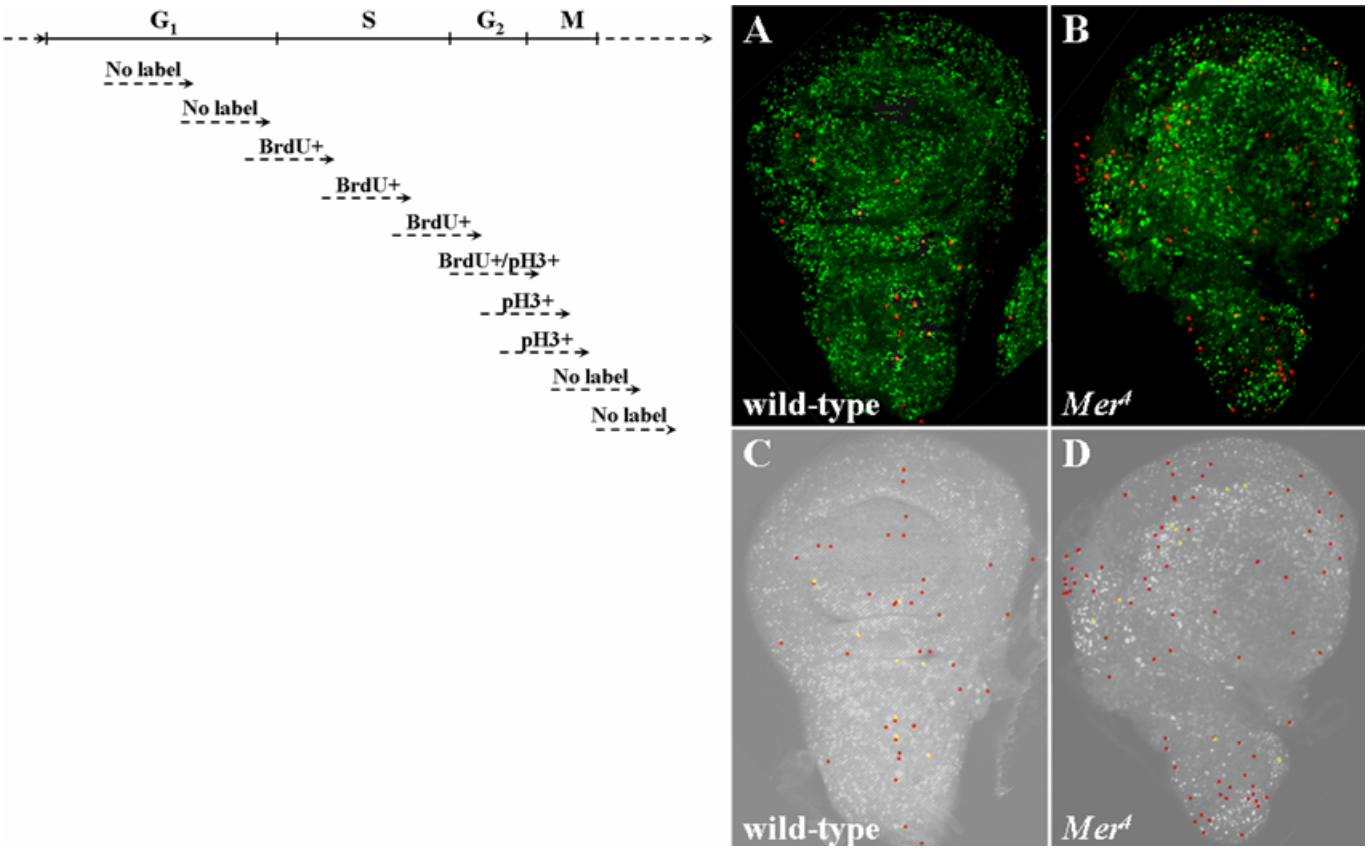

Figure 4. Double immuno-labeling of cultured wing imaginal discs from the wild-type control (FM7,GFP/Y) (A) or the Mer^4 *mutant (y w Mer*^{4}*/Y) (B) with anti-BrdU and anti-phospho-histone H3 antibodies. The wing imaginal discs were briefly pulsed labeled with BrdU, chased for 2 hr (dash arrow in the diagram), and then stained with anti-BrdU and anti-phospho-histone H3 antibodies. Four optical sections for each wing disc were obtained and*

merged for the illustration. The disc images of the wild-type (C) and the Mer^4 mutant (D) with mapped mitoses are shown. Red spots correspond to mitotic cells that are labeled only by the anti-phospho-histone H3 antibody. Yellow spots represent mitotic cells that are doubly-labeled by both anti-BrdU and anti-phospho-histone H3 antibodies.

Figure 5 summarizes the results from this double labeling experiment. The peak of the labeled mitosis curve for *Mer*^{4} mutant cells takes place about one to two hours earlier than that for the wild-type control. Consistent with that found in Task 4 (i.e., a decreased G2 period in the *Mer*^{4} cell cycle), this result indicates a shorter G2 phase for *Mer*^{4} mutant cells. Other parameters of the cell-cycle including the overall cell-cycle time (time between two mitotic waves) and the duration of S-phase (half-width of mitotic wave) appear to be not significantly affected by *Mer*^{4} mutation (also see below).

Taken together, our results show that *Mer*^{4} mutation alters the cell-cycle duration so that *Merlin* mutant cells display a shorter G_2 period and a compensatory longer G_1 phase.

Figure 5. Labeled mitosis curve for the Mer^4 (pink line) and wild-type (blue line) imaginal disc cells. Ordinate – the ratio of doubly-labeled cells to the total number of anti-phospho-H3-labeled cells. Abscissa – the chase time period.

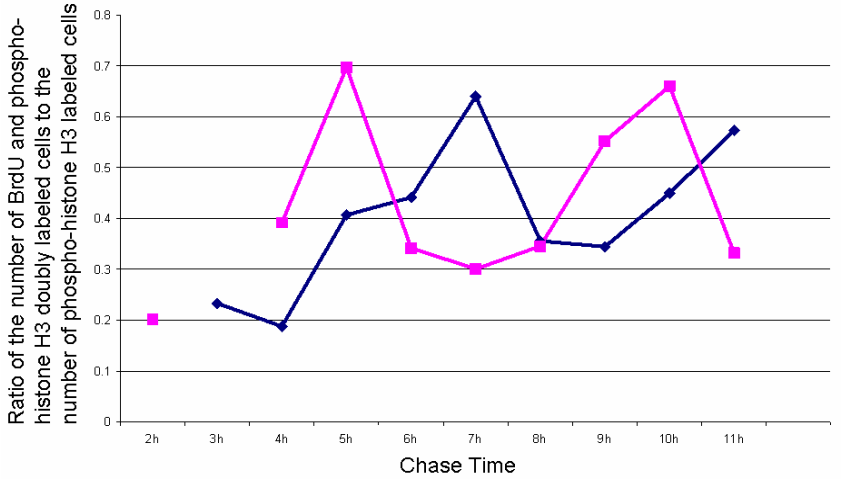

Task 6: To estimate the cell-cycle duration of cells in the wing imaginal disc, mosaic clone spots of multiple wing hairs (mwh) were induced by irradiating the +/mwh larvae of the wild-type and *Mer*^{3} homozygotes at different developmental stages with 1000R of γ-rays. Irradiated larvae were grown to the adult stage. Adult male wings were removed, and mosaic clone spots were photographed and projected onto a map of an adult wing. The clone dimension was determined by hair counting (Garcia-Bellido and Merriam, 1971; Gonzalez-Gaitan et al. 1994). By calculating clone frequency as a function of the time between egg laying and irradiation of larvae, we estimated the cell-cycle duration to be 9.4h for wild-type cells and 9.2h for *Mer*^{3} mutant cells Thus, the overall cell-cycle duration appears to be not significantly affected by *Merlin* mutation.

To further study the effect of *Merlin* mutation on cell proliferation in different regions of the wing imaginal disc, mosaic *mwh* clones were induced in the *+/mwh* larvae with or without *Mer*^{3}

mutation at 96 hr after egg laying (AEL) by 1000R of γ-rays irradiation. Irradiated larvae were grown to the adult stage, and the *mwh/mwh* clone spots in the male wings were photographed. Clone spots from 70 *Mer*^{3} and 76 wild-type wings were projected onto a map of an adult wing. The distribution of mosaic mwh clones in the wild-type and *Mer*^{3} wings is shown in Figure 6. Consistent with previous findings (Gonzalez-Gaitan et al., 1994), the wild-type mosaic clones induced at such a late developmental stage (96 hr AEL) respected the vein restriction and resided within the boundary of veins. However, the *Mer*^{3} mutant clones did not follow such a rule, and some of them crossed the vein boundary (arrows in Figure 6 point to these clones). In addition to crossing the vein, the mosaic clones that abut the vein were also found more frequently in the *Mer*^{3} wing than those in the wild-type control (Table 3). These results further support the role of Merlin in cell motility, cell adhesion, and cell proliferation. Cells lacking Merlin may possess a greater ability to overcome vein restriction.

Figure 6. Mer^3 *mutation delimits normal clonal restriction of mosaic clones to cross veins. Arrows point to the mer*^{3} *mutant clones that cross the vein boundary. Colors distinguish clone overlaps with the brown color for two overlapping clones, violet for three overlapping clones, and blue for four overlapping clones. The red color denotes uni-cell clones and the green color indicates two-cell clones.*

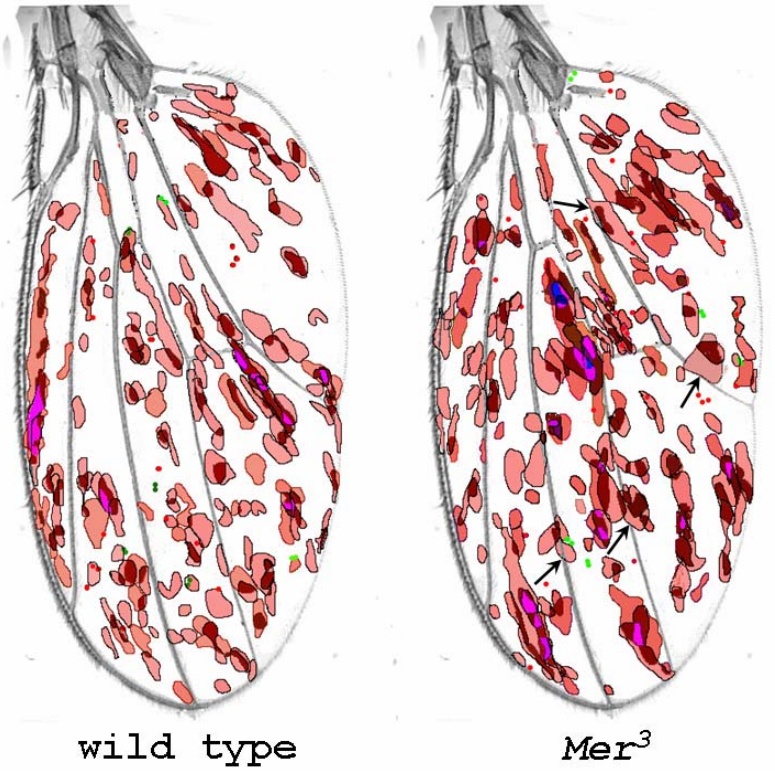

Table 3. Vein boundary restriction of mosaic clones with the wild-typeord Mer^3 *genetic background. Mosaic clones induced in each wing were carefully examined on an enlarged image. Data were collected from the analysis of 70 Mer*^{3} *and 76 wild-type wings.*

Genetic background of mosaic clones	No. of clones abutting the wing vein	No. of clones crossing the vein	Total No. of clones analyzed
Mer^3	16	6	240
Wild type	6	0	193

In addition, we induced mosaic clones in the wild-type and *Mer*^{3} wings late in development (48h after puparium formation). Consistent with a previous report showing little or no cell proliferation in the wing disc at this late developmental time-point (Garcia-Bellido and Merriam, 1971), we found only three uni-cell clones among 62 wild-type wings examined (Figure 7). In contrast, we identified 26 mosaic clones in 47 *Mer*^{3} wings; among them, three were two-cell clones and five others contained multiple cells. These results indicate that significant cell proliferation took place 48 hr after puparium formation in the *Mer*^{3} wings.

Taken together, our results further argue the possibility of a temporal difference in developmental timing between the wild-type and *Mer*^{3} mutant larvae.

Figure 7. Mosaic clone induction in wild-type and Mer^3 *wings 48h after puparium formation. Each cell is marked by a colored dot. Two-cell clones are indicated in green. The cells in multi-cell clones are connected by lines. The picture represents the summary of mosaic clones found on 62 wild-type and 47 Mer*^{3} *wings.*

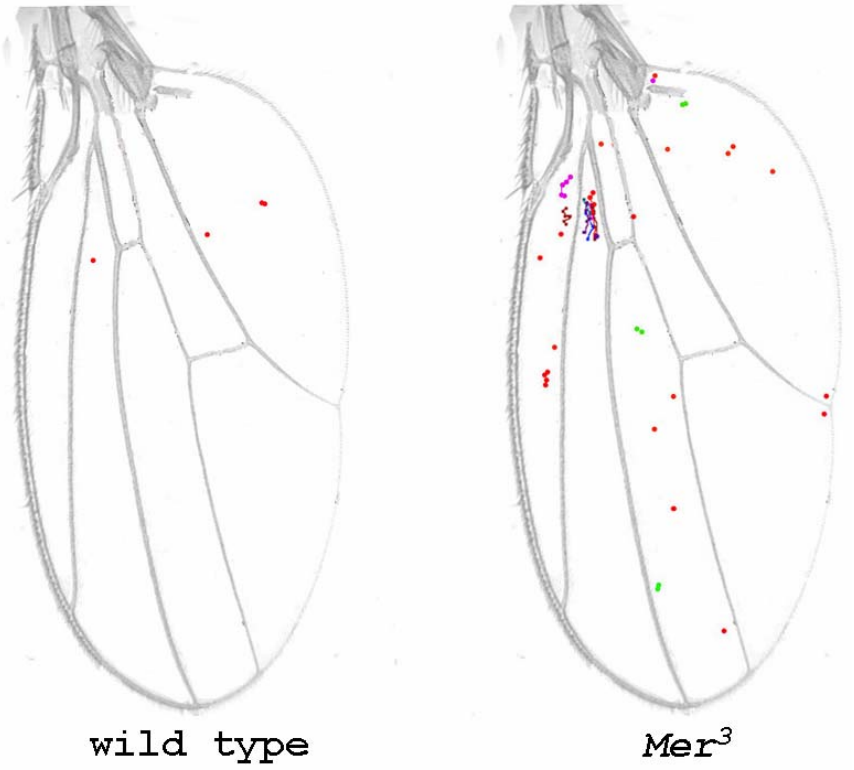

Task 7: By immunostaining using an anti-dMerlin antibody (kindly provided by Rick Fehon of Duke University; McCartney and Fehon, 1996), we demonstrated that the Merlin protein displayed cortical localization and some cytoplasmic staining throughout the wing imaginal disc (Figure 8A). Previously, Johnston and Edgar (1998) showed that the Wingless (Wg)-expressing cells at the dorsal/ventral (D/V) compartment border of the wing imaginal disc were arrested at the G_1 phase of the cell cycle. Furthermore, the G_1-arrested, Wg-expressing cells at the D/V border in the anterior compartment were surrounded by two stripes of G_2-arrested cells. Consistently, we detected strong Wg staining in cells at the D/V compartment border of the wing imaginal disc, and the majority of Wg protein staining was

found in the plasma membrane of cells (Figure 8B). By superimposing the Merlin and Wg staining images, we found that Merlin and Wg appeared to colocalize in the cells at the D/V compartment border (Figure 8C). In conjunction with those previous findings (Johnston and Edgar, 1998), these results suggest that the majority of Merlin protein is localized in the plasma membrane of cells that are at both the G_1 and G_2 phases. Also, the finding of Merlin-Wg colocalization implies a role for Merlin in Wg trafficking.

Figure 8. Colocalization of the Merlin protein with the Wg morphogen at the D/V compartment border. Wing imaginal discs from third-instar wild-type larvae were fixed and stained for Merlin (green) and Wg (red) using the anti-Merlin polyclonal antibody (McCartney and Fehon, 1996) and the anti-Wg monoclonal antibody 4D4 (Brook and Cohen, 1994), respectively. (A) The Merlin protein localized to the plasma membrane and some within the cytoplasm. (B) The Wg protein was detected in the cells at the D/V compartment border. Within this stripe of Wg-expressing cells, the Wg protein appeared to associate with the plasma membrane. In addition, Wg protein expression spread from the stripe of expressing cells to the adjacent cells in a gradient fashion by vesicle trafficking (punctuate structures). (C) The Merlin protein colocalizes with the Wg protein in cells at the D/V compartment border.

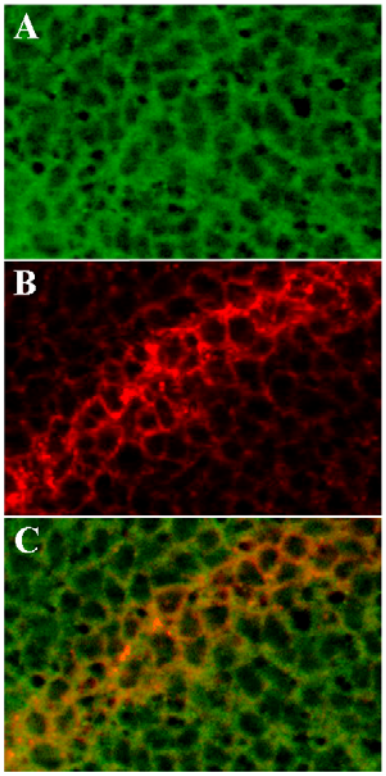

Spermatogenesis is a model that facilitates studies of the effect of gene mutations on mitosis, meiosis, and the remodeling of many cell structures. Since flies carrying a *Mer*^{3} allele are sterile, we examined the role of Merlin during spermatogenesis. We showed that *Merlin* mutations affected meiotic cytokinesis of spermatocytes, cyst polarization and nuclear shaping during spermatid elongation, and spermatid individualization Immunostaining analysis reveals that the Merlin protein is dynamically redistributed during meiosis (Figure 9; also see Dorogova et al., 2008 [Appendices]). Merlin is redistributed to the area covering the presumptive contractile ring

in telophase and near the newly-formed cellular membrane during cytokinesis. In addition, we demonstrated, for the first time, the mitochondrial localization of Merlin. The results suggest that Merlin may play a role in mitochondrial formation and function during spermatogenesis.

Figure 9. Intracellular distribution of the Merlin protein at various stages of spermatogenesis. Merlin was detected in the cellular cortex of spermatocytes (A). In prometaphase (B) and metaphase (C) of meiosis, the cortical localization of Merlin became more evident. In telophase (D), Merlin redistributed and accumulated in the area associated with the microtubules of the central spindle. During cytokinesis (E), Merlin staining remained associated with the microtubules but was less intense in the region of the contractile ring. In the onion-stage spermatids (F), Merlin was highly concentrated in the mitochondrial Nebenkern. This localization pattern was maintained through the comet stage of spermatid elongation (G). The insert in panel G shows intense Merlin staining in the two subunits of the Nebenkern in spermatids. In the cyst containing mature sperm, bright Merlin staining was also seen as a punctate dot in the acrosomal region (H). Merlin staining was also detected in the Mer^3 cyst at the comet stage; however, their sperm nuclei were scattered throughout the cyst, and the arrangement of spermatids was irregular (I).

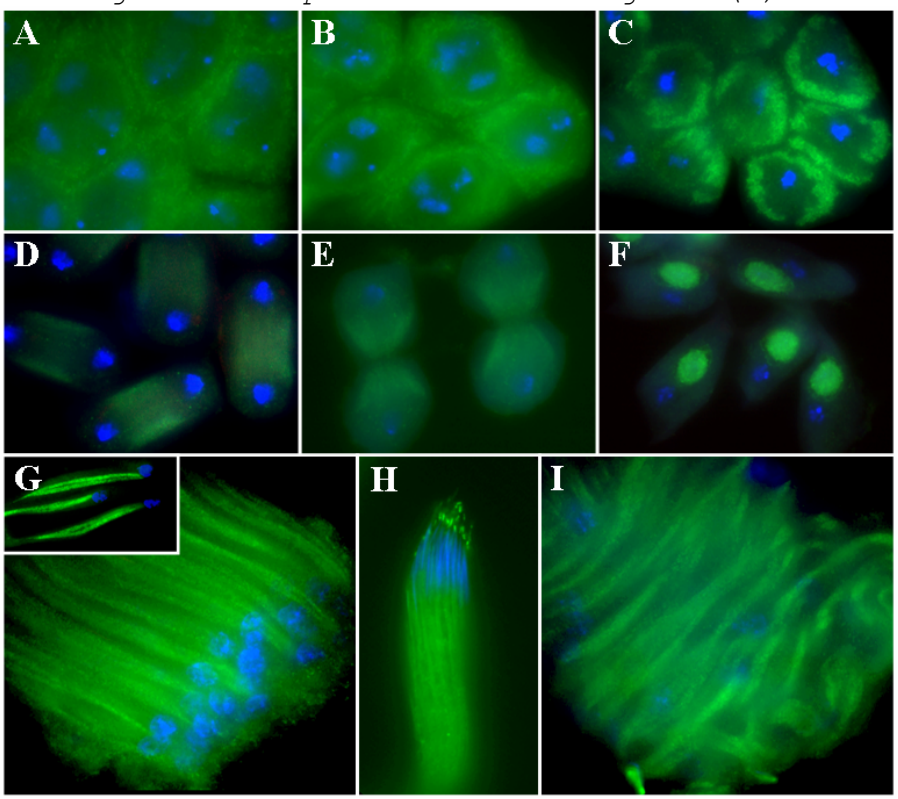

Aim 3: To further examine the role of Merlin in the determination/maintenance of the D/V compartment border in the *Drosophila* wing imaginal disc and to investigate how Merlin mutation affects the expression of proteins important for the determination of the compartment border

Task 8: To confirm the effect of various Merlin mutations on wing morphology, we first examined pupal wings because the Mer^4 allele does not yield adult flies. We found that the crossveins in the Mer^4 wing

were completely absent (Figure 10B). Similarly, adult viable *Mer*^{3} individuals showed a complete loss of anterior crossveins and a partial loss of posterior crossveins (Figure 10A). With the use of the Gal4 driver 1096, which is active in the wing pouch region, ectopic expression of the UAS-*Mer*$^{+}$ transgene did not affect the overall morphology of wings (Figure 10C). In contrast, over expression of UAS-*Mer*$^{\Delta BB}$, a Blue-Box deletion mutant of *Merlin*, led to the reduction of both crossveins (Figure 10D). These results confirm that Merlin plays an important role in the determination of wing morphology.

Figure 10. The morphology of wing in the fly carrying different merlin allele: (A) Mer^{3}*, (B) Mer*^{4}*, (C) 1096;UAS-Mer*$^{+}$*, and (D) 1096;UAS-Mer*$^{\Delta BB}$*.*

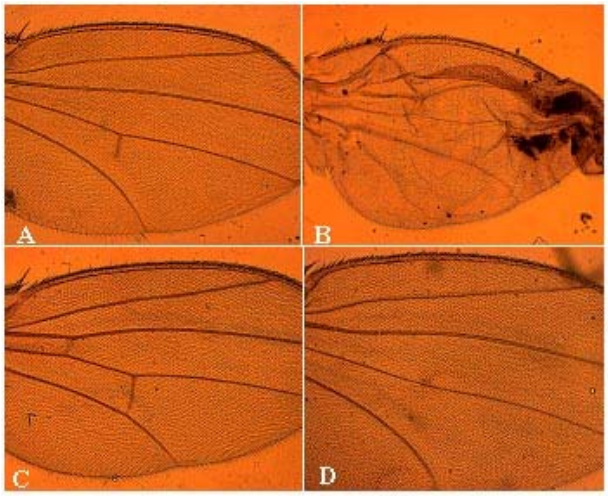

Task 9: It is well-documented that the Wg morphogen protein is synthesized by the cells at the D/V compartment boundary and then distributed in a spatial concentration gradient (Seto and Bellen, 2004). To examine the role of Merlin in the determination of the D/V compartment border in the wing imaginal disc, we analyzed the distribution pattern of the Wg protein in the wild-type and *Mer*^{4} wing imaginal discs. In contrast to the tight-stripe expression pattern of Wg seen in the wild-type wing imaginal disc (Figures 11A and 11B), the Wg stripe in the *Mer*^{4} mutant disc appeared frequently more diffuse. In about 40% of the cases, some diffuse regions of the Wg stripe were particularly notable (indicated with arrows in Figures 11C and 11D). These results indicate that Merlin inactivation affects the distribution of Wg expression in the D/V compartment border.

Figure 11. Wg protein distribution in the wild-type and Mer^{4} *wing imaginal discs. Wing imaginal discs were dissected and stained with an anti-Wg monoclonal antibody. The Wg expression stripe (red) was readily detected at the D/V compartment border in the wild-type wing pouch (A). At a higher magnification, the Wg protein showed a cortical localization in the cell (B). However, the Wg stripe at the D/V border of the Mer*^{4} *disc appeared more diffuse (C), particularly notable in some regions of the stripe (indicated by arrows). An enlarged area of a diffused region (arrowhead in C) showed that while the cortical localization of the Wg protein was still seen, Wg granules were diffusely distributed (D).*

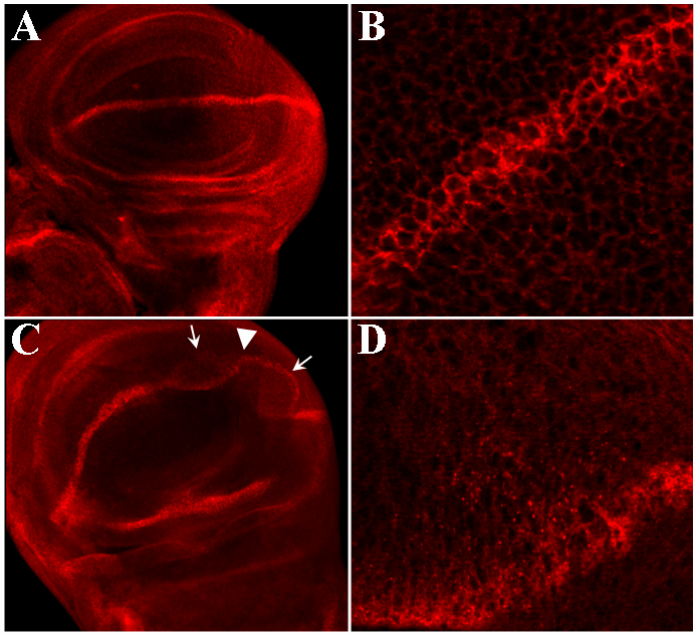

Recent data suggest a role for Merlin in receptor-mediated endocytosis (McCartney and Fehon, 1996; McCartney et al., 2000). Since Merlin co-localizes with the Wg protein in the plasma membrane of cells at the D/V compartment border of the wing imaginal disc (Figure 8), Merlin may participate in regulating vesicular trafficking of the Wg morphogen (Entchev and Gonzalez-Gaitan, 2002). To test this hypothesis, we performed experiments to examine potential genetic interactions between Merlin and the proteins involved in the vesicular trafficking process. By searching FlyBase, we identified fly strains carrying UAS constructs for *sgl*, *frc*, *Rab5*, *Rab7*^{DN}, *Csp*, or *shi*^{K44A}, as well as strains with an EP-insertion for *Damp*, *garnet*, *α-Adaptin*, *Scamp*, *Cirl*, *Gdi*, *Rop*, *lap*, or *AP-47*. We used the wing-pouch specific *Gal4* driver 1096 to ectopically express these constructs and examined any changes in the wing morphology. We found that ectopic expression of *porc* (*porcupine*), *shi*^{K44A}, a dominant negative *shibire* allele (s*hi*^{DN}), and *lap* (*like-AP180*) resulted in abnormal wing morphology.

The *porcupine* gene (*porc*), which is involved in segment polarity, encodes a putative multi-pass transmembrane protein belonging to the membrane-bound *O*-acyltransferase superfamily (Hofmann, 2000). Genetic and immunocytological studies indicate that *porc* is required for the secretion of active Wg ligand. The Porcupine (Porc) protein stimulates the posttranslational N-glycosylation of Wg in the endoplasmic reticulum. Porc over-expression stimulates the N-glycosylation of both endogenously and exogenously expressed Wg (Tanaka et al., 2002). To examine potential genetic interactions between *Mer* and *porc*, we over-expressed *Mer*$^{\Delta BB}$, a dominant-negative *Merlin* mutant with a deletion of the conserved Blue-Box in the N-terminal FERM domain of Merlin (LaJeunesse et al., 1998; Golovnina et al., 2006 [Appendices]), in the wing pouch using the 1096 driver. Over-expression of *Mer*$^{\Delta BB}$ alone led to a loss of the posterior cross vein and a slightly enlarged wing but did not affect the overall wing structure (Figure 12A). In contrast, over-expression of *porc* in the wing pouch completely disrupted the wing structure, yielding

abnormally small wings with no veins (Figure 12B). Interestingly, when both *porc* and $Mer^{\Delta BB}$ were over-expressed together in the wing pouch, flies with normal wing morphology were recovered; however, the defects in the posterior crossvein were still present, presumably due to the effect of $Mer^{\Delta BB}$ over-expression (Figure 12C). Similarly, when *porc* was over-expressed together with the wild-type *Mer* gene (Mer^{+}), flies with completely normal wing morphology, including crossveins, were obtained (Figure 12D).

Figure 12. A potential genetic interaction between Mer and porc. (A) Over-expression of $Mer^{\Delta BB}$ *in the wing pouch using the 1096 driver did not affect the overall morphology of the wing. (B) Over-expression of porc in the wing pouch completely disrupted the wing morphology. (C) Over-expression of porc together with* $Mer^{\Delta BB}$ *resulted in some flies with normal wing morphology. (D) Over-expression of porc together with* Mer^{+} *completely rescued the overall wing morphology.*

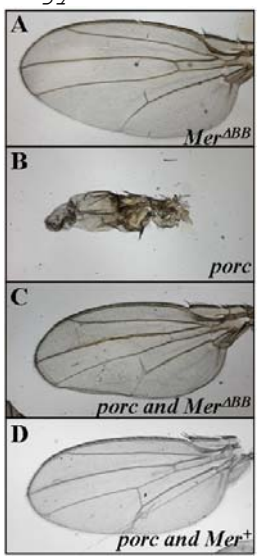

Next, we examined the effect of over-expression of $Mer^{\Delta BB}$ alone, *porc* alone, $Mer^{\Delta BB}$ plus *porc*, or *porc* plus Mer^{+} in the wing pouch on Wg protein distribution. Immunostaining with the anti-Merlin antibody revealed that the 1096 driver, as predicted, was active in the wing pouch, resulting in over-expression of the $Mer^{\Delta BB}$ and the wild-type Merlin protein (Figure 13A-D). When $Mer^{\Delta BB}$ was over-expressed in the wing pouch, no obvious effect on the Wg stripe expression pattern at the D/V compartment border was found (Figure 13E). In contrast, over-expression of *porc* resulted in a complete loss of the Wg stripe at the D/V compartment border (Figure 13F). Interestingly, simultaneous over-expression of $Mer^{\Delta BB}$ or *Mer+* ith *porc* led to re-appearance of the Wg stripe at the D/V compartment border; however, a broad Wg stripe was observed particularly in the case of simultaneous over-expression of *porc* and $Mer^{\Delta BB}$ (Figures 13G and 13H). Together, these results suggest a potential genetic interaction between *porc* and *Mer*. Such a genetic interaction appears to have a profound effect on regulating the Wg distribution pattern at the D/V compartment border.

Figure 13. The effect of over-expression of $Mer^{\Delta BB}$ *alone (A and E), porc*

alone (B and F), porc plus Mer$^{\Delta BB}$ (C and G), or porc plus Mer^{+} (D and H) on Wg expression at the D/V compartment border. (A-D) Immunostaning for Merlin. (E-H) Immunostaining for Wg. White arrowheads point to the Wg stripe at the D/V compartment border.

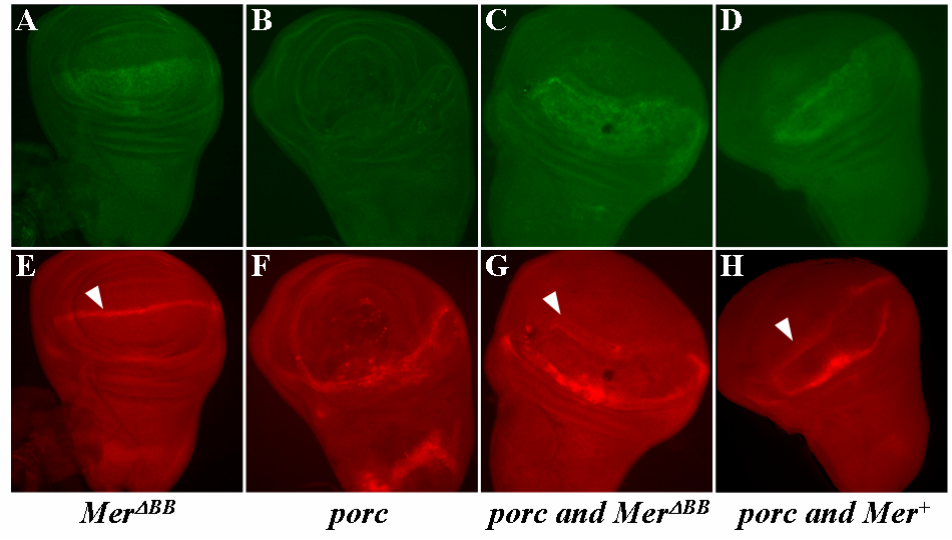

The *shibire* gene (*shi*) encodes the Dynamin protein, a GTPase essential for cytokinesis and endocytosis (van der Bliek and Meyerowitz, 1991; Kitamoto, 2002). The Shibire (Shi) protein is involved in vesicle trafficking of various neurotransmitters and the Wg protein during early embryogenesis (Strigini and Cohen, 2000). We also performed a similar analysis on the potential genetic interaction between *Mer* and *shi^{K44A}*, a dominant negative *shi* allele. Over-expression of *shi^{K44A}* in the wing pouch using the 1096 driver resulted in flies with abnormally small wings, which did not have any veins or staut bristles, but had some disorganized sensory bristles (Figure 14). Staut bristles originate from the Wg-expressing cells at the D/V compartment border. The disappearance of staut bristles implies that these cells did not undergo normal differentiation processes during wing development. Interestingly, when *Mer$^{\Delta BB}$* was over-expressed together with *shi^{K44A}* in the wing disc using the 1096 driver, a partial restoration of triple rows, including the medial triple row of staut bristles was observed; however, the wings remained small in size and had no vein (Figure 14). Similarly, simultaneous over-expression of *Mer^{+}* and *shi^{K44A}* in the wing pouch partially restored the formation of triple rows, including the medial triple row of staut bristles, as well as the ventral and dorsal triple rows of sensory bristles. However, the spacing and organization of ventral and dorsal triple rows still appeared abnormal, and there were no veins in the wing. These results suggest a potential genetic interaction between *Merlin* and *shibire*.

Figure 14. A potential genetic interaction between Mer and shi. Over-expression of Mer$^{\Delta BB}$ in the wing pouch did not affect the overall morphology of the wing. Over-expression of shi^{K44A} in the wing pouch completely disrupted the wing morphology. Over-expression of shi^{K44A} together with Mer$^{\Delta BB}$ partially restored the formation of staut bristles in the wing margin. Simultaneous over-expression of shi^{K44A} and Mer^{+} also partially restored the formation of the medial triple row of staut bristles, as well as the ventral and dorsal triple rows of sensory bristles.

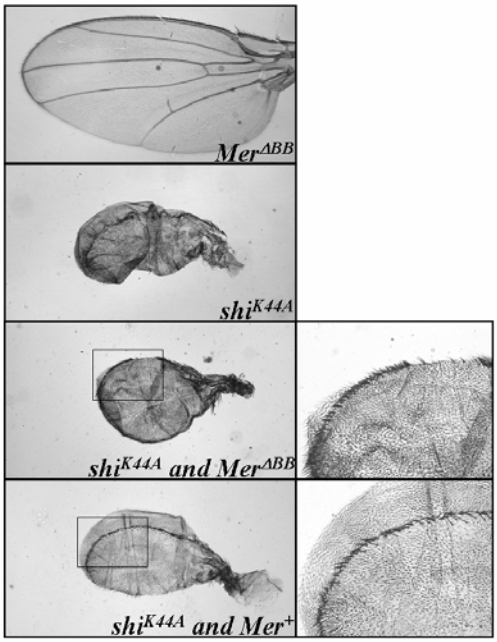

The *lap* (*like-AP180*) gene encodes a pre-synaptically-enriched clathrin adaptor protein. The Lap protein plays an important role in clathrin-mediated endocytosis of synaptic vesicles (SVs) and regulates the size of SVs (Zhang et al. 1998). We also found that over-expression of *lap* in the wing pouch using the 1096 driver resulted in wings with ectopic vein formation, frequently seen at the distal part of vein V (Figure 15; Kopyl et al., 2008 [Appendices]). When *lap* was over-expressed together with $Mer^{\Delta BB}$, excessive ectopic vein material, which was even more than that observed with *lap* over expression alone, appeared in many parts of the wing blade. In contrast, simultaneous over-expression of Mer^{+} and *lap* in the wing pouch resulted in wings with a normal or almost normal vein pattern. These results indicate that dominant-negative Merlin, $Mer^{\Delta BB}$, enhances the effect of Lap over-expression on vein fate determination, while wild-type Merlin suppresses such an effect.

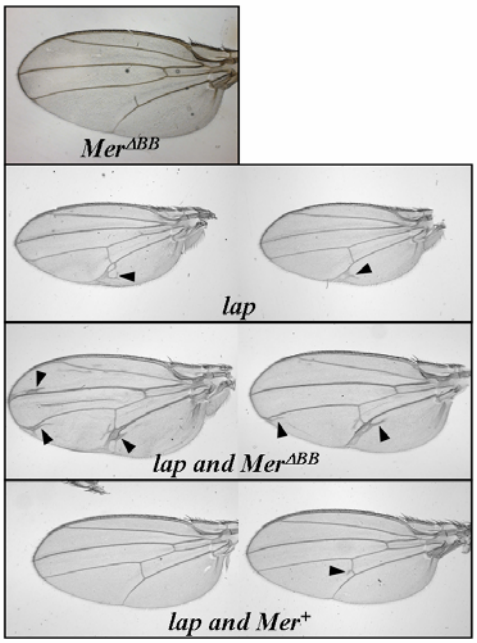

Figure 15. A potential genetic interaction between Mer and lap. Over-expression of $Mer^{\Delta BB}$ *in the wing pouch did not affect the overall morphology*

of the wing. Over-expression of lap in the wing pouch completely disrupted the wing morphology. Over-expression of lap together with $Mer^{\Delta BB}$ resulted in some flies with normal wing morphology. Over-expression of lap together with Mer^{+} completely rescued the overall wing morphology. Arrowheads denote the sites of ectopic vein material.

To determine which region of Merlin was required for the genetic interaction with *lap*, we simultaneously over-expressed Lap together with various truncated Merlin proteins in the wing pouch using the 1096 driver. When Mer^{1-169} was simultaneously over-expressed together with Lap in the wing disc, ectopic vein formation was still detected in the wing, similar to that observed with Lap over-expression alone (Figure 16). When other N-terminal fragments of Merlin, Mer^{1-330} and Mer^{1-375}, were over-expressed together with Lap, ectopic vein material continued to be seen. Also, when the first 600 amino acids of Merlin, Mer^{1-600}, were co-expressed with Lap in the wing disc, some ectopic veins were still present in the wing; however, the amount of ectopic vein material was reduced. Importantly, when the C-terminal fragment of Merlin, $Mer^{351-635}$, was co-expressed with Lap, the normal wing was restored. Similarly, normal vein restoration was observed when Mer^{+} was simultaneously over-expressed together with Lap. These results indicate that the C-terminal region of the Merlin protein is important for a genetic interaction with *lap*.

Figure 16. The C-terminal region of Merlin required for a genetic interaction with lap. Arrowheads point to ectopic vein materials.

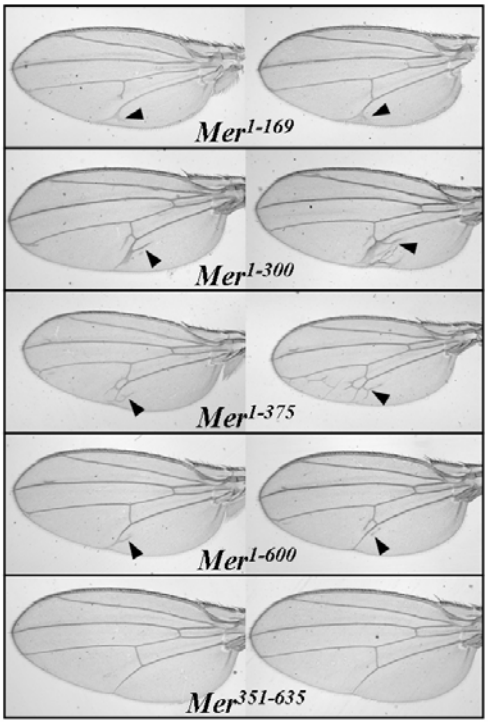

Recent studies suggest that Merlin may function to antagonize the epidermal growth factor receptor (EGFR) pathway which controls vein fate determination in the wing (LeJeunesse et al., 2001; Maitra et al., 2006). Merlin and Expanded, another member of the protein 4.1 family, function cooperatively to modulate receptor endocytosis and signaling, including EGFR. Taken together, our data suggest that Merlin may counteract Lap by direct or indirect interaction. We

hypothesize that by interacting with Lap, Merlin may participate in regulating the EGFR pathway required for vein fate determination in the wing (Figure 17).

Figure 17. Model for Merlin's function through interaction with Lap to regulate the EGFR pathway required for vein fate determination.

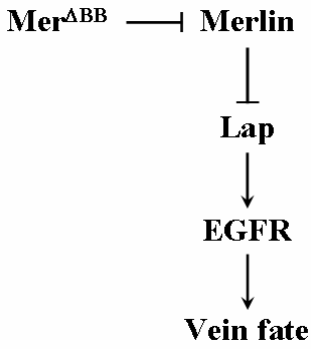

Task 10: To study the intracellular distribution of the Merlin protein, we performed immunostaining on wing imaginal discs that carried homozygous mutations in the *Mer*, *expanded (ex)*, or *fat (ft)* genes using the anti-Merlin antibody (McCartney and Fehon 1996; McCartney et al., 2000; Boedigheimer and Laughon, 1993; Reuter and Szidonya, 1983). Expanded is another member of the protein 4.1 family and is known to interact with Merlin (McCartney et al., 2000). Recent data indicate that both Fat and Merlin are involved in the Hippo signaling pathway (Hamaratoglu et al., 2006). As shown in Figure 18, the Merlin protein has a cortical localization pattern in cells in the wild-type wing imaginal disc. A similar Merlin distribution pattern was also noted in the wing imaginal disc with homozygous *ex*, *ft*, or Mer^3 mutations. These results indicate that Merlin protein distribution in the wing imaginal disc is not affected by other tumor suppressor mutations.

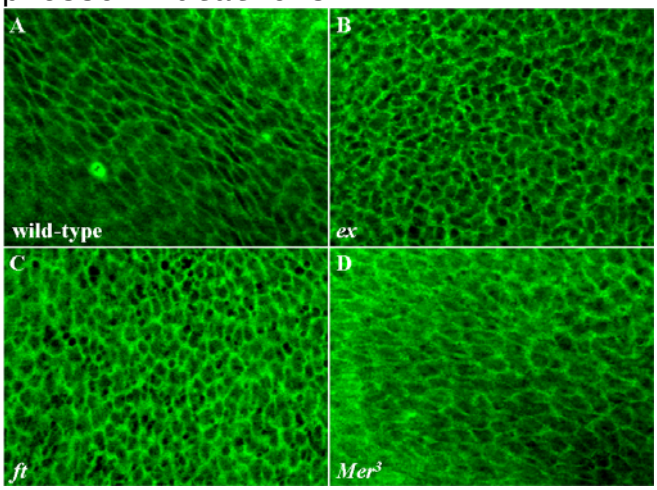

Figure 18. Immunostaining of the Merlin protein in the wing imaginal discs from the wild-type (A), expanded^{K12913} (B), fat^4 (C), and Mer^3 (D) mutants.

The *Drosophila* Merlin protein is phosphorylated by Slik kinase (Hughes and Fehon, 2006); however, the exact amino-acid residue at which the phosphorylated event occurs is not known. Studies in mammalian cells reveal that Merlin is phosphorylated by the p21-

activated kinase at the Serine-518 residue (Shaw et al., 1998; Xiao et al., 2002; Surace et al., 2004; Rong et al., 2004). Previously, we showed that the Merlin proteins are evolutionary conserved across species (Golovnina et al., 2005 [Appendices]). The equivalent position of Serine-518 in the *Drosophila* Merlin protein is a Threonine-501 residue, which could also be a phosphorylation site. To examine whether the Threonine-501 residue is a phosphorylation site, we generated antibodies recognizing the phosphorylated or non-phosphorylated peptide with the amino acid sequence covering the Threonine-501 residue. Interestingly, both the anti-phospho- and non-phospho-Merlin antibodies recognized a specific band with a molecular weight equivalent to the Merlin protein in *Drosophila* S2 cells (Figure 19A). In cells devoid of growth factor, the Merlin protein appeared to migrate slightly faster on the gel, while in fetal bovine serum (FBS)-stimulated cells, the Merlin protein migrated slower, presumably due to phosphorylation (Figure 19B). In addition, we found that in cells grown at high density, the non-phospho-Merlin protein appeared mostly in the cytoplasm, while the phospho-Merlin protein could be seen in the membrane region (Figure 19C-D).

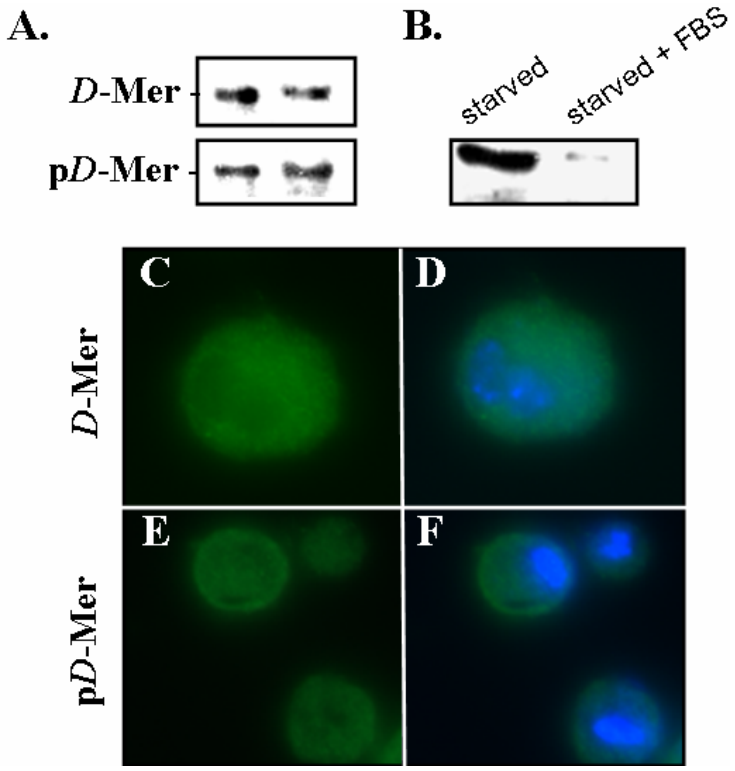

Figure 19. Immuno-detection of phospho- and non-phospho-Merlin proteins in Drosophila S2 cells. (A) Western blot analysis using either the anti-nonphospho- (D-Mer) or the phospho-Merlin (pD-Mer) antibody. (B) Merlin protein expression changes when stimulated with growth factors. (C-F) Immunostaining using the anti-nonphospho-Merlin (C,D) or phospho-Merlin (E,F) antibody (green) in S2 cells grown at high density. DAPI stained nuclei blue.

To further examine the functional significance of the Threonine-501 residue, we generated a Mer^{T501A} mutant with the Threonine-501 residue changed to an Alanine. The Mer^{T501A} mutant was inserted into pUASP vector to generate the pUASP-Mer^{T501A} construct. We

microinjected the pUASP-*Mer*^{T501A} construct into *Drosophila* embryos and transgenic flies carrying the pUASP-*Mer*^{T501A} construct were isolated. We crossed *w Mer*^{4}*/M-5* females with males containing *da-Gal4; UASP-Mer*^{T501A}*/ TSTL, Tb Hu* and checked for the presence of the *w Mer*^{4}*/Y; da-Gal4/+; UASP-Mer*^{T501A} adult individuals in the progeny; however, we did not observe flies of this genotype. Also, we attempted to collect male pupae with this genotype and the results indicate that *Mer*^{T501A} expression could not rescue the *Mer*^{4} defects.

In addition, we over-expressed *Mer*^{T501A} in otherwise normal individuals by using the *nanos-Gal4* driver. Interestingly, over-expression of *Mer*^{T501A} in the testis resulted in an abnormal mitochondrial phenotype (Figure 20), in contrast to that seen in *Mer*$^{+}$ over-expression (Table 2; Dorogova et al., 2008 [Appendices]).

Taken together, these results show that the Threonine-501 residue is important for Merlin function.

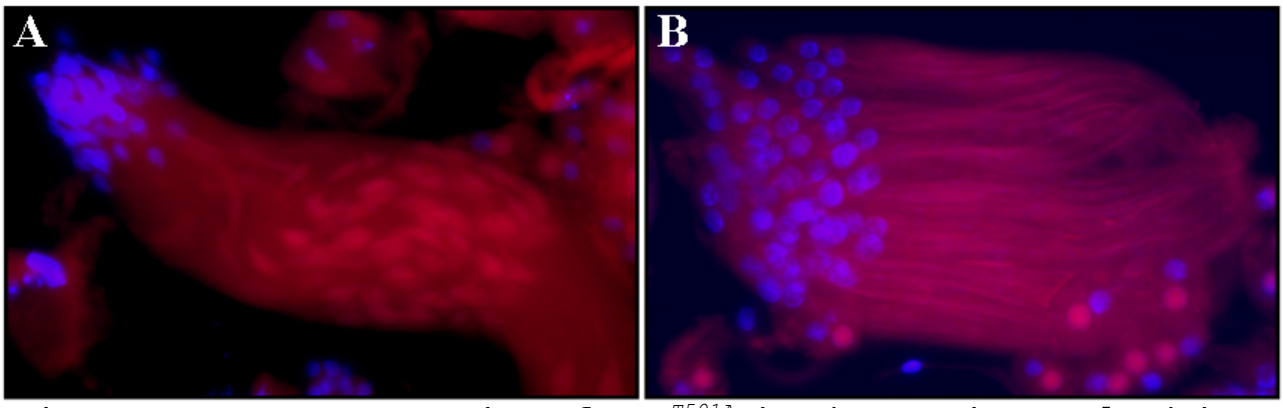

Figure 20. Over-expression of *Mer*^{T501A} in the testis resulted in an abnormal mitochondrial phenotype. The structure of the mitochondrial body in the spermatid was revealed by MitoTraker Red (Invitrogen). (A) Abnormal mitochondrial bodies seen in the spermatid with ectopic expression of Mer^{T501A} by the nanos-Gal4 driver. (B) Mitochondrial bodies in the wild-type spermatid. Note that there is no elongated mitochondrial body in the spermatid with Mer^{T501A} over-expression. MitoTraker Red dye stained mitochondria red, while DAPI stained nuclei blue.

Aim 4: To investigate whether *NF2*$^{-/-}$ mouse schwannoma cells also show cytological abnormalities in mitosis similar to those seen in the *Drosophila* imaginal discs.

Task 11: We have made a collaborative agreement with Dr. Marco Giovannini of INSERM, France for his *Nf2*$^{flox2/flox2}$ and *P0Cre* mice (Giovannini et al., 2000). These mice were imported into our vivarium and bred to produce various types of compound mice for conditional *Nf2*-inactivation in Schwann cells (see below).

Task 12: To generate a conditional *Nf2* knockout in Schwann cells, the *Nf2*$^{flox2/flox2}$ mice were mated with the *P0Cre* mice to generate compound *P0Cre*;*Nf2*$^{flox2/flox2}$ mice. Since expression of the Cre recombinase in Schwann cells (specified by the myelin protein *P0* promoter) results in deletion of exon 2 of the *Nf2* gene, Giovannini et al. (2000)

previously showed that a fraction of the *P0Cre*;*Nf2*$^{flox2/flox2}$ mice developed schwannoma after 10 months of age or older. We have also observed that the *P0Cre*;*Nf2*$^{flox2/flox2}$ mice developed schwannomas after about one year old. Histopathological examination revealed that the tumor was a grayish, creamy globoid mass. Histologically, it consisted of spindle-shaped cells with mitotic figures (Figure 21).

Figure 21. Histology of a schwannoma produced in the P0Cre;Nf2$^{flox2/flox2}$ mouse. Note that the tumor consisted of actively growing, spindle-shaped cells.

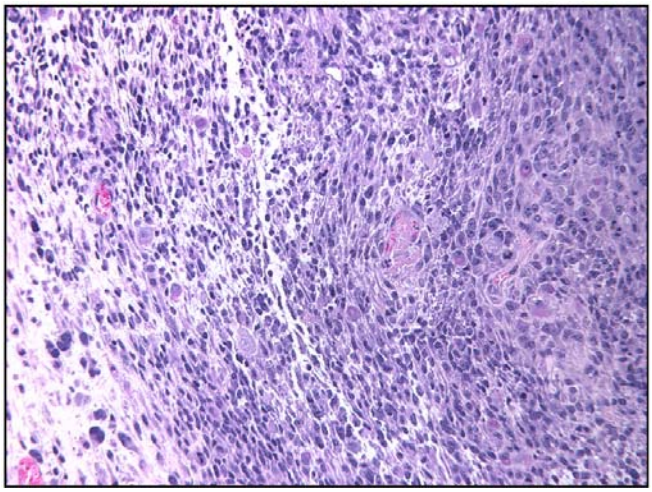

Task 13: In addition to *Nf2*$^{-/-}$ mouse schwannoma cells that we prepared, we isolated Schwann cells from phenotypically-normal *Nf2*$^{flox2/flox2}$ mice. By infecting these *Nf2*$^{flox2/flox2}$ Schwann cells with an adenovirus carrying a Cre recombinase expressing unit (AdCMV-Cre), we generated *Nf2*$^{-/-}$ Schwann cells. Using these mouse Schwann cells and schwannoma cells together with human vestibular schwannoma tumor cells carrying *NF2* mutations, we found that the PI3-kinase AKT pathway was frequently activated in *NF2*$^{-}$ vestibular schwannomas (Jacob et al., 2008 [Appendices]). Because the PI3-kinase/AKT pathway serves as a convergence point for many growth stimuli, and through its downstream substrates, controls cellular processes and responses such as cell survival, cell proliferation, insulin response, stress response, and differentiation (LoPiccolo et al., 2008), its activation expectedly contributes to tumorigenesis. Thus, the PI3-kinase/AKT pathway is an attractive therapeutic target for vestibular schwannomas, and small-molecule inhibitors of AKT signaling may have therapeutic potential in suppressing schwannoma growth.

Recently, we evaluated the growth inhibitory and anti-tumor activities of OSU-03012, a celecoxib-derived small-molecule inhibitor of phosphoinositide-dependent kinase 1 (PDK1), on cultured human and mouse Schwann cells and schwannoma cells, as well as schwannoma xenografts in severe combined immunodeficiency (SCID) mice (Chang et al., 2006). Our results demonstrated that OSU-03012 effectively inhibited cell proliferation, and induced apoptosis in human schwannoma cells as well as mouse *Nf2*$^{-/-}$ Schwann cells and *Nf2*$^{-/-}$ schwannoma cells with IC_{50} values in the low micro-molar range. We also showed that OSU-03012 possessed potent anti-tumor activity and induced massive necrosis in malignant schwannoma xenografts in SCID

mice (Lee et al., 2008. Abstract presented to the CTF International Consortium for Molecular Biology of NF1 and NF2, Bonita Springs, FL).

Task 14: To investigate whether *Nf2*$^{-/-}$ schwannoma cells showed any cytological abnormalities in mitosis, we conducted cytological analysis on Schwann cells and schwannoma cells. Although we did not find any asynchrony in anaphase and telophase (Figure 22A-6D), we observed some *Nf2*$^{-/-}$ schwannoma cells with multiple nuclei, reminiscent of that frequently seen in transformed and cancer cells (Figures 22E and 22F).

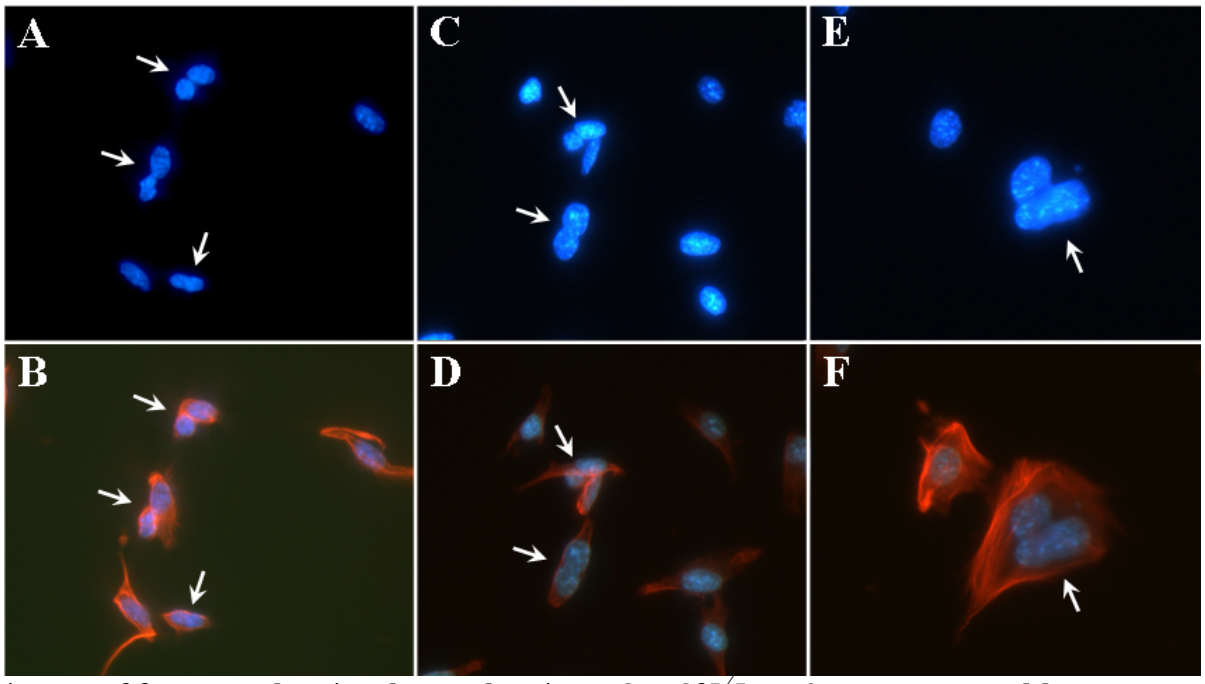

Figure 22. Cytological analysis of Nf2$^{-/-}$ *schwannoma cells. Actively-growing cells were stained with anti-*α*- and* β*-tubulin antibodies and Texas red-conjugated phalloidin in order to visualize the cytoskeleton. Shown in panels A, C, and D were DAPI-stained nuclei, while those in panels B, D, and F are merged images with the cytoskeletal staining. Arrows point to mitotic cells at various cell-cycle phases.*

Task 15: As a result of this grant support, we were able to present our research findings to the annual international neurofibromatosis conferences. Ten research abstracts were presented, and a total of nine publications were generated during this grant period. Detailed description of these research abstracts and publications can be found in Reportable Outcome and Appendices sections.

KEY RESEARCH ACCOMPLISHMENTS:

(1) We have confirmed mitosis exit abnormalities in various *Drosophila Merlin* mutants. Two types of mitosis exit asynchrony, the asynchronous anaphase-telophase figures and the asynchronous telophase-interphase figures, were frequently observed in the mutants. The asynchronous mitosis exit phenotype in the *Mer*^{4} genetic background could be rescued by the introduction of a wild-type *Merlin*

transgene. These results suggest that Merlin is important for the control of mitosis exit.

(2) *Merlin* mutations lead to increased mitosis. *Merlin* mutant cells display a longer G_2 period than the wild-type cells, suggesting that *Merlin* mutation alters the duration of this cell-cycle phase.

(3) Merlin is important for the determination of wing morphology. Merlin and Wingless (Wg) morphogen colocalize in the cells at the D/V compartment border of the wing imaginal disc. Merlin inactivation alters the Wg stripe expression pattern. Cells lacking Merlin possess greater ability to overcome vein restriction.

(4) We provide evidence for potential genetic interactions between Merlin and the proteins involved in vesicular trafficking, including porcupine, which controls the acetylation of the Wg morphogen during the development of the wing imaginal disc, shibire, a Dynamin participating in cytokinesis and endocytosis and involved in Wg protein trafficking during early embryogenesis, and lap, a clathrin-adapter protein involved in vesicular trafficking. These results suggest that Merlin may regulate receptor-mediated endocytosis through these interactions (Kopyl et al., 2008).

(5) The *Drosophila* Merlin protein plays important roles during spermatogenesis. *Merlin* mutants display abnormalities in meiotic cytokinesis of spermatocytes, cyst polarization and nuclear shaping during spermatid elongation, and spermatid individualization. The *Drosophila* Merlin protein is dynamically redistributed during meiosis. Merlin immunoreactivity has been detected in the mitochondria, suggesting a role for Merlin in mitochondrial formation and function (Dorogova et al., 2008).

(6) The distribution of the *Drosophila* Merlin protein in the wing imaginal disc is not affected by other tumor suppressor mutations. The Merlin protein is regulated by phosphorylation. In cells grown at high density, the non-phospho-Merlin protein appears mostly in the cytoplasm, while the phospho-Merlin protein can be found in the membrane region.

(7) By combining bioinformatic and phylogenetic approaches, we demonstrate a monophyletic origin of the Merlin proteins with the root in early metazoa. The overall similarity among the primary and secondary structures of Merlin proteins across species and the conservation of several functionally important residues suggest a universal role for Merlin in a wide range of metazoa (Golovnina et al., 2005).

(8) The *NF2* promoter is strongly expressed in the developing mouse brain and in sites containing migrating cells. A transition change of *NF2* promoter expression occurs during neural tube closure and neural crest cell migration. Considerable *NF2* promoter activity could be detected in various NF2-affected tissues (Akhmametyeva et al., 2006). By conditional knockout approaches and by using the

tamoxifen-inducible Cre/LoxP recombination system, we show that Merlin plays an important role during neural tube closure, neural crest cell adhesion and migration, and brain development.

(9) The AKT pathway is frequently activated in the *NF2*$^{-/-}$ tumor cells (Jacob et al., 2008). We have tested two novel compounds, OSU03012 and (S)-HDAC-42, which inhibit AKT phosphorylation, and found that these drugs effectively inhibit the growth of vestibular schwannoma cells and xenografts (Chang et al., 2006). These findings set the stage for a phase I clinical trial on VS in the future.

REPORTABLE OUTCOMES:

During this grant period, we presented ten research abstracts to Annual International Neurofibromatosis Conferences. Nine publications were produced as a result of this grant support. We acknowledged the support from the Department of Defense Neurofibromatosis Research Programs in all these publications. Summaries of the abstracts and publications are provided below.

Abstracts Presented to National Meetings

(1) Omelyanchuk, L.V., Dorogova, N.V., Kopyl, S., Akhmameteva, E.M., Perceva, J., Fehon, R.G., and Chang, L.S. 2005. The Role of Merlin in *Drosophila* Spermatogenesis. Abstract presented to the 2005 CTF International Consortium for the Molecular Biology of NF1, NF2, and Schwannomatosis.

We reported that merlin plays important roles in spermatogenesis. By examining the viable, but completely sterile, merlin mutant mer^{3} *for any defects in this process, we found that the mer*^{3} *mutant showed abnormalities in male meiosis due to cytokinesis failure. During the cyst polarization (comet) stage, mer*^{3} *sperm nuclei displayed abnormal shape and failed to group near the cyst wall. Immuno-localization experiments suggested that Merlin might be involved in the control of acrosome-nucleus association and/or participate in the process of nucleus migration and condensation during cyst polarization.*

(2) Golovnina, K., Blinov, A., Akhmametyeva, E.M., Omelyanchuk, L.V., and Chang, L.-S. 2005. Evolution and Origin of Merlin, the Product of the *Neurofibromatosis Type 2* Tumor-Suppressor Gene. Abstract presented to the 2005 CTF International Consortium for the Molecular Biology of NF1, NF2, and Schwannomatosis.

By combining bioinformatics and phylogenetic approaches, we demonstrate a monophyletic origin of the Merlin proteins with the root in early metazoa. Amino acid sequence alignment reveals the absence of an actin-binding site in the C-terminal region of all Merlin proteins from various species but the presence of a conserved internal binding site in the N-terminal domain of the Merlin and ERM proteins. Examination of sequence variability at functionally significant sites, including the serine-518 residue, the phosphorylation of which modulates Merlin's intra-molecular association and function as a tumor suppressor, identifies several

potentially important sites that are conserved among all Merlin proteins but divergent in the ERM proteins. Conservation of several functionally important sites among all Merlin proteins suggests a universal role of Merlin in a wide range of metazoa.

(3) Omelyanchuk, L.V., Dorogova, N.V., Kopyl, S., Akhmameteva, E.M., Fehon, R.G., and Chang, L.-S. 2006. The Role of *Drosophila* Merlin in Spermatogenesis and Wg Morphogen Trafficking in the Imaginal Disc. Abstract presented to the 2006 CTF International Consortium for the Molecular Biology of NF1, NF2, and Schwannomatosis.

Flies with a Mer^3 allele (Met^{177}→Ile) are viable but sterile, and display abnormalities in cyst polarization during spermatogenesis. The Merlin protein normally localizes to the acrosome of mature sperm; however, this localization pattern is altered in the Mer^3 mutant. A more severe defect in cyst polarization could also be seen in the adult male pharates carrying the Mer^4 allele (Gln^{170}→stop). Similarly, both the clathrin mutant Chc4 and the meiotic mutant ff16 displayed defective nuclei polarization and nuclear shaping. Because Merlin has been shown to associate with the endocytic compartments and because mutations in the genes, such as clathrin and ff16, that are known to be important for vesicle formation and cytokinesis, also affect nuclei polarization, we examined whether Merlin is involved in the vesicular traffic in somatic tissues. We first examined a potential interaction between Merlin and shibere, a dynamin participating in various microtubule-mediated processes, such as cytokinesis and endocytosis. Ectopic expression of a dominant-negative mutant of shibere (shi^{DN}), Shi^{K44A}, by the 1096 wing pouch driver led to a disrupted wing morphology, including the loss of MTR staut bristles. The shi^{DN} wing margin phenotype was rescued by simultaneous introduction of a UAS-Mer construct carrying the Mer^+ or Mer^{1-600} transgene. Partial restoration of the phenotype was also seen when truncated Merlin expression constructs Mer^{1-330} and Mer^{1-375} were used, while no restoration was detected with Mer^{1-169} and $Mer^{\Delta BB}$. These results suggest that Merlin plays a role in vesicular trafficking and that the FERM domain including the Blue Box is required for the interaction with Shibere. The MTR staut bristles are derived from the cells normally expressing the wingless (Wg) morphogen, whose movement through the tissue is related to the vesicular traffic. We found that the expression pattern of patched (ptc), which marks the A/P compartment border in the wing imaginal disc, did not change in the Mer^4 mutant, suggesting that Decapentaplegic (Dpp) morphogen trafficking is likely not affected by Merlin mutation. In contrast, the stripe expression pattern of Wg at the D/V compartment border was altered in the Mer^4 mutant. Intriguingly, wg-lacZ insertion in the Mer^4 background revealed no change in the wg regulatory zone when compared to the wild-type control. While the expression of neuralized, which participates in the determination of dTR and vTR bristles, was controlled by Wg, its expression pattern deviated significantly in the Mer^4 mutant. In addition, the Wg-regulated cycE expression pattern at the D/V border was also affected by the Mer^4 mutation. These results suggest that Merlin plays an important role in Wg trafficking. It has been shown that Porcupine (Porc) facilitates Wg glycosylation in the endoplasmic reticulum, and the

wing margin is subjected to Wg regulation. We found that both Mer^3 and Mer^4 mutations did not significantly affect the wing margin morphology and only caused additional sensory bristles within the row of staut bristles. While over-expression of Mer^+ or $Mer^{\Delta BB}$ did not change the wing margin pattern, over-expression of Porc led to complete disappearance of Staut bristles and irregularities of sensory and mechano-sensory bristles. In contrast, simultaneous over-expression of Mer and porc restored the staut bristles and normalized the arrangement of the mechano- and chemo-sensory bristles. In addition, while over-expression of $Mer^{\Delta BB}$ did not affect Wg transcription and protein expression in the wing imaginal disc, porc over-expression results in complete absence of the Wg protein at the D/V border. Importantly, over-expression of both porc and Mer^+ or $Mer^{\Delta BB}$ restored the Wg stripe at the D/V border. These results suggest that over-expression of Merlin may facilitates Wg secretion. Together, our data support the notion that Merlin participates in vesicular trafficking.

(4) Dorogova, N., Akhmametyeva, E.M., Kopyl, S., Dubatolova, T., Fehon, R.G., Omelyanchuk, L.V., and Chang, L.-S. 2007. Tumor-Suppressor Merlin Regulates Epidermal Growth Factor Receptor Signaling in the *Drosophila* Wing through the Clathrin Adapter Protein LAP. Abstract presented to the 2007 CTF NF Conference – Models, Mechanisms, and Therapeutic Targets, Park City, UT.

We reported the genetic interaction between Merlin and lap. We showed that over-expression of the clathrin adaptor protein Lap in the wing pouch resulted in the formation of extra vein material. Co-expression of Merlin with Lap restored the normal venation phenotype in the wing. By using various Merlin truncation mutants, we identified the C-terminal portion of Merlin to be important for the Merlin-lap genetic interaction. Furthermore, we showed that the LAP protein colocalized with the Merlin protein at the internal face of the plasma membrane. In conjunction with previous findings, these results suggest that both Merlin and Lap may control wing venation through the EGFR signaling pathway. By mosaic clone analysis, we found that, unlike wild-type cells, Merlin mutant clones could cross vein restriction borders, similar to that observed for the mosaic clones of the overgrowth mutant fat. These results corroborate the recent report indicating that Fat cadherin and Merlin function in the Hippo tumor suppressor signaling pathway, which regulates cell proliferation and likely, cell migration.

(5) Dorogova, N.V., Akhmameteva, E.M., Kopyl, S., Gubanova, N., Fehon, R.G., Omelyanchuk, L.V., and Chang, L.-S. 2007. The Role of Merlin in Drosophila Spermatogenesis. Abstract presented to the 2007 CTF NF Conference – Models, Mechanisms, and Therapeutic Targets, Park City, UT.

Drosophila Mer^3 mutants are viable but sterile. We showed that adult males hemizygous for the Mer^3 allele had seminal vesicles, but they were almost devoid of sperm. Although most Mer^3 spermatocytes underwent normal meiotic divisions, some showed abnormal onion-stage spermatids or defects in spindle organization. During the sperm

individualization stage, both the sperm nuclei and actin cone bundles were abnormally distributed in the Mer^3 cyst. Not all nuclei within a Mer^3 cyst had sperm heads with a normal needle shape; instead, the sperm heads were round, suggesting defects in sperm head packaging. At the cyst polarization or comet stage, the Mer^3 cyst failed to group the sperm nuclei near a defined region of the cyst wall. Immunostaining of testis tissues revealed that during meiotic prophase and metaphase the Merlin protein was detected in the cellular cortex of spermatocytes, similar to that seen in somatic tissues. In telophase, Merlin was redistributed to the periphery of spindles in the vicinity of the presumptive contractile ring. During cytokinesis, Merlin was found mostly near the newly-formed cellular membranes. In the onion-stage spermatids, the Merlin protein accumulated in the nebenkern. This mitochondrial localization was maintained until mature sperm formation. In mature sperms, Merlin expression was also seen as a dot in the acrosome. Consistently, electron microscopy analysis demonstrated the loss of the axoneme-mitochondrial derivative association in the Mer^3 and Mer^4 spermatids. Collectively, these results suggest that Merlin is important for the control of cyst polarization and axoneme-nebenkern association during spermatogenesis.

(6) Akhmametyeva, E.M., Kuan, C.-Y., Giovannini, M., Welling, D.B., and Chang, L.-S. 2007. Merlin, the Product of the *Neurofibromatosis 2* (*NF2*) Gene, is Important for Neural Tube Closure, Neural Crest Cell Adhesion and Migration, and Brain Development. Abstract presented to the 2007 CTF NF Conference – Models, Mechanisms, and Therapeutic Targets, Park City, UT.

We previously showed that NF2 promoter expression is dynamically regulated during neural tube closure and neural crest cell migration. To examine whether Merlin plays an important role during these processes, we generated a conditional Nf2 knockout using the Wnt1 promoter to drive Cre recombinase expression in the mesencephalon and dorsal neural tube. We found that mutant embryos lacking Nf2 function in the dorsal neural tube were smaller in size than wild-type embryos or those heterozygous for Nf2, and displayed defects in neural tube closure. The neural tube closure defects in the mutant embryos could be seen as early as embryonic day 8.5, which corresponded to the time of Wnt1 expression. Importantly, while cultures of neural tube explants from the wild-type embryo displayed typical neural crest cell migration and differentiation, neural tube explants from the mutant embryo adhered poorly to the fibronectin-coated substratum, and mutant neural crest cells were unable to migrate. These results indicate that Merlin plays an important role during neural tube closure and neural crest cell adhesion and migration. To further examine the role of Merlin at various stages of embryonic development, we employed the tamoxifen-inducible Cre/LoxP recombination system. For this system, we generated transgenic mice carrying the nestin enhancer/hsp68 minimal promoter-driven Cre recombinase fused with the mutated ligand binding domain of the estrogen receptor (nestin-CreER) or the NF2 promoter-driven CreER (NF2-CreER). Interestingly, we found that Nf2 inactivation in neural progenitor cells using nestin-CreER resulted in embryos with

defects in brain development. Together, our results demonstrate that Merlin plays key roles at various stages of nervous system development during embryogenesis.

(7) Packer, M., Akhmametyeva, E.M., Chang, L.-S., and Welling, D.B. 2007. An Unusually Large, Recurrent Vestibular Schwannoma. Abstract presented to the 2007 CTF NF Conference – Models, Mechanisms, and Therapeutic Targets, Park City, UT.

Recurrence of vestibular schwannomas after complete excision is seen in less than one percent of our patients (6 of >600 excisions). When tumors recur, they generally grow slowly at one to two millimeters per year. We have identified a patient who underwent a complete translabyrinthine excision of a moderate-sized (2.4 cm diameter) primary VS of the left cerebello-pontine angle, but experienced unusually rapid regrowth. Surveillance MR imaging four years after the initial excision showed a recurrent mass measuring 2.8 cm. Neuropathology confirmed a benign schwannoma. Growth of the recurrent tumor in cell culture demonstrated remarkable growth of schwannoma cells with S100-positive reactivity. Excision of both the primary and recurrent tumors showed tenacious adherence of both masses to their surrounding environment, specifically to the facial nerve. Prolonged surgical times were required for successful anatomical salvage of the seventh cranial nerve; however, recovery of facial function was partial and prolonged. Facial function three months after excision of the recurrent schwannoma is still House-Brackmann grade VI/VI. Immunohistochemical analysis of both the primary and recurrent tumor tissue sections reveals elevated immunoreactivities to the phospho-PTEN and p53 proteins. The molecular difference in the expression of these key tumor suppressor proteins might explain the clinical aggression of this otherwise pathologically benign tumor.

(8) Lee, T., Jacob, A., Packer, M., Chen, C.-S. Welling, D.B., and Chang, L.-S. 2007. OSU03012 and (S)-HDAC-42, Two Novel Inhibitors of the PI3K/AKT Pathway, Are Potential Therapeutic Agents for Vestibular Schwannomas. Abstract presented to the 2007 CTF NF Conference – Models, Mechanisms, and Therapeutic Targets, Park City, UT.

The ultimate goal of our research is to develop new drugs for the cure of neurofibromatosis type 2 (NF2)-associated tumors. To approach this goal, we identified novel signaling pathways that were deregulated in vestibular schwannomas (VS) with NF2 mutations. We found that the phosphatidylinositol-3 kinase (PI3K)/AKT pathway was frequently activated in VS compared to normal vestibular nerve from the same patient. Given the fact that Merlin may exert its growth suppressive activity by inhibiting PI3K via binding to the PI3K enhancer long isoform (PIKE-L), the loss of functional Merlin in VS cells could result in activation of the PI3K/AKT pathway. Thus, drugs targeting the PI3K/AKT pathway have potential as therapeutic agents for VS. We tested two such compounds, OSU03012 and (S)-HDAC-42, which were recently developed. The OSU03012 compound is a novel derivative of the COX2 inhibitor Celecoxib (Celebrex™). It is a potent inhibitor of phosphoinositide-dependent kinase 1 (PDK1), an upstream kinase that phosphorylates and activates AKT, but lacks the

COX2 inhibitory activity of the parent drug, which limits its side effect profile. These unique features may make it a well-tolerated drug for long-term treatment of benign tumors, such as VS. To assess the efficacy of OSU03012, we prepared primary VS cells and human malignant schwannoma HMS-97 cells, and grew them in the medium containing varying concentrations of OSU03012. The levels of cell proliferation and AKT phosphorylation were measured using the MTS assay and Western blot analysis, respectively. We found that treatment with OSU03012 resulted in inhibition of cell proliferation in both VS and HMS-97 with the IC_{50} values in the low micromolar range. Concomitantly, treatment with OSU03012 led to decreased AKT phosphorylation at both the Ser-308 and Thr-473 sites in a dose-dependent manner. By TUNEL staining, we showed that OSU03012 induced apoptosis in both VS and HMS 97 cells. These results indicate that the OSU03012 compound efficiently inhibits cell proliferation and promotes apoptosis in schwannoma cells via decreased AKT phosphorylation. The (S)-HDAC-42 compound belongs to a novel class of anti-tumor drugs that act by inhibiting histone deacetylase (HDAC). Recent studies showed that this phenylbutyrate-derived HDAC inhibitor could down-regulate the AKT pathway by disrupting interactions between protein phosphatase-1 (PP1) and HDAC6, an isoform of HDAC, and consequently, allowing free PP1 to interact with and dephosphorylate AKT. We found that (S)-HDAC-42 could also inhibit the proliferation of both VS and HMS-97 cells with IC_{50} values in the low micromolar range. These results indicate that both the OSU03012 and (S)-HDAC-42 compounds are potential therapeutic agents for VS. Further investigation of these novel compounds in a VS xenograft model is ongoing. In addition, experiments are in progress to examine the possible synergistic action of these two drugs, since they both inhibit the PI3K/AKT pathway, but through different targets. All of these experiments may set the stage for a phase I clinical trial on VS in the future.

(9) Akhmametyeva, E.M., J. Hunag, C.-Y. Kuan, M. Giovannini, D.B. Welling, and L.-S. Chang. 2008. Merlin Is Important for Neural Tube Closure, Neural Progenitor Cell Adhesion and Cerebral Cortex Development. Abstract presented to The CTF International Consortium for Molecular Biology of NF1 and NF2, Bonita Springs, FL.

To examine whether Merlin plays an important role during neural tube closure and neural crest cell migration, we generated a conditional Nf2 knockout using the Wnt1 promoter to drive Cre recombinase expression in the mesencephalon and dorsal neural tube. We showed that the mutant embryos lacking Nf2 function in the dorsal neural tube were smaller in size than those of the wild-type or heterozygous Nf2 embryos, and displayed defects in neural tube closure. Importantly, while cultures of neural tube explants from the wild-type embryo displayed typical neural crest cell migration and differentiation, neural tube explants from the mutant embryo adhered poorly to the fibronectin-coated substratum and mutant neural crest cells were unable to migrate. These results indicate that Merlin plays an important role during neural tube closure and neural crest cell adhesion and migration. By using the tamoxifen-inducible Cre/LoxP recombination system, we further examined Merlin function at

various time points during nervous system development. Transgenic nestin-CreER mice carrying the nestin enhancer/hsp68 minimal promoter-driven Cre recombinase fused with the mutated ligand binding domain of estrogen receptor were mated with $Nf2^{flox2/flox2}$ mice to generate compound nestin-CreER;$Nf2^{flox2/flox2}$ mice. Upon tamoxifen induction, Nf2 inactivation in neural progenitor cells resulted in embryos with defects in neural tube closure, such as exencephaly and encephalocele. Immuno-histochemical analysis reveals that neuroprogenitor cells are poorly attached to each other. Although immature neurons were present, the cerebral cortex was not developed. Together, our results indicate that Merlin plays important roles during neural tube closure, neural crest cell migration, and brain development.

(10) Lee, T.X., M. Packer, E.M. Akhmametyeva, J. Huang, A. Jacob, S.K. Kulp, C.-S. Chen, D.B. Welling, and L.-S. Chang. 2008. OSU03012, A Novel Inhibitor of The PI3k/Akt Pathway, Is A Potential Therapeutic Agent For Vestibular Schwannomas and Malignant Schwannomas. The CTF International Consortium for Molecular Biology of NF1 and NF2, Bonita Springs, FL.

Previously, we showed that the phosphatidylinositol-3 kinase (PI3K)/AKT pathway is frequently up-regulated in vestibular schwannomas (VS). Thus, drugs targeting the PI3K/AKT pathway have potential as therapeutic agents for VS. The goal of this study is to investigate growth inhibitory and anti-tumor activities of OSU03012, a novel derivative of Celecoxib and a potent inhibitor of phosphoinositide-dependent kinase 1 (PDK1), an upstream kinase of AKT, on VS and malignant schwannoma cells. We showed that both VS and malignant schwannoma HMS-97 cells were more sensitive to inhibition of cell proliferation by OSU03012 than normal human Schwann cells. The IC_{50} of OSU03012 at 48 hours was 3.1 μM for VS cells and 2.6 μM for HMS-97 cells. We also demonstrated that OSU03012 induced apoptosis in both VS and HMS-97 cells and caused marked reduction of AKT phosphorylation at both the Ser-308 and Thr-473 sites in a dose-dependent manner. Similarly, we showed that $Nf2^{-/-}$ mouse schwannoma and Schwann cells were more sensitive to growth inhibition by OSU03012 than wild-type mouse Schwann cells and schwannoma cells established from transgenic mice carrying the NF2 promoter-driven SV40 T antigen gene. In vivo xenograft analysis in SCID mice demonstrated that OSU-03012 was well-tolerated and inhibited the growth of HMS-97 schwannoma xenografts by 55% after four weeks of oral treatment as demonstrated by high-field small animal MRI. Together, our results suggest that OSU03012 has thepotential to become a chemotherapeutic agent for treating VS and malignant schwannomas.

Publications and Manuscripts Submitted or In Press

(1) Golovnina, K., Blinov, A., Akhmametyeva, E.M., Omelyanchuk, L.V., and Chang, L.-S. 2005. Evolution and Origin of Merlin, the Product of the Neurofibromatosis Type 2 Tumor-Suppressor Gene. BMC Evolutionary Biology 5:69-86. http://www.ncbi.nlm.nih.gov/pubmed/16324214?ordinalpos=3&itool=EntrezSystem2.PEntrez.Pubmed.Pubmed_ResultsPanel.Pubmed_RVDocSum

In this paper, we examined the evolution, diversity, and overall

distribution of Merlin among different taxa. By combining bioinformatic and phylogenetic approaches, we demonstrate that merlin homologs are present across a wide range of metazoan lineages. While the phylogenetic tree shows a monophyletic origin of the ERM family, the origin of the Merlin proteins is robustly separated from that of the ERM proteins. The derivation of Merlin is thought to be in early metazoa. We have also observed the expansion of the ERM-like proteins within the vertebrate clade, which occurred after its separation from Urochordata (Ciona intestinalis). Amino acid sequence alignment reveals the absence of an actin-binding site in the C-terminal region of all Merlin proteins from various species but the presence of a conserved internal binding site in the N-terminal domain of the Merlin and ERM proteins. In addition, a more conserved pattern of amino acid residues is found in the region containing the so-called "Blue Box," although some amino acid substitutions in this region exist in the merlin sequences of worms, fish, and Ciona. Examination of sequence variability at functionally significant sites, including the serine-518 residue, the phosphorylation of which modulates Merlin's intra-molecular association and function as a tumor suppressor, identifies several potentially important sites that are conserved among all Merlin proteins but divergent in the ERM proteins. Secondary structure prediction reveals the presence of a conserved α-helical domain in the central to C-terminal region of the Merlin proteins of various species. The conserved residues and structures identified correspond to the important sites highlighted by the available crystal structures of the Merlin and ERM proteins. Furthermore, analysis of the Merlin gene structures from various organisms revealed the increase of gene length during evolution due to the expansion of introns; however, a reduction of intron number and length appeared to occur in the merlin gene of the insect group. Our results demonstrated a monophyletic origin of the Merlin proteins with their root in the early metazoa. The overall similarity among the primary and secondary structures of all Merlin proteins and the conservation of several functionally important residues suggest a universal role for Merlin in a wide range of metazoa.

(2) Dorogova, N.V., Akhmametyeva, E.M., Kopyl, S.A., Gubanova, N.V., Yudina, O.S., Omelyanchuk, L.V., and Chang, L.-S. 2008. The role of Merlin in spermatogenesis. BMC Cell Biology 9:1-15. http://www.ncbi.nlm.nih.gov/pubmed/18186933?ordinalpos=1&itool=EntrezSystem2.PEntrez.Pubmed.Pubmed_ResultsPanel.Pubmed_RVDocSum

In this paper, we examined the effect of *Merlin* mutations on mitosis, meiosis, and morphogenesis in *Drosophila*. Previous studies showed that flies carrying a *Mer3* allele, a missense mutation (Met177→Ile) in the *Merlin* gene, are viable but sterile. Testis examination revealed that hemizygous *Mer3* mutant males have small seminal vesicles that contain only a few, but immotile, sperm. By cytological and electron microscopy analyses of the *Mer3*, *Mer4* (Gln170→stop), and control testes at various stages of spermatogenesis, we showed that *Merlin* mutations affect meiotic cytokinesis of spermatocytes, cyst polarization and nuclear shaping during spermatid elongation, and spermatid individualization. We also demonstrated that the lethality and sterility phenotypes of the *Mer4*

mutant are rescued by the introduction of a wild-type Merlin gene. Immunostaining demonstrates that the Merlin protein is redistributed to the area covering the presumptive contractile ring in telophase and near the newly-formed cellular membrane during meiotic cytokinesis. At the onion stage, Merlin is concentrated in the Nebenkern of spermatids, and this mitochondrial localization is maintained throughout sperm formation. Also, Merlin exhibits punctate staining in the acrosomal region of mature sperm. In summary, we showed that *Merlin* mutations affect spermatogenesis at multiple stages. The Merlin protein is dynamically redistributed during meiosis of spermatocytes and is concentrated in the Nebenkern of spermatids. Our results demonstrated for the first time the mitochondrial localization of Merlin and suggest that Merlin may play a role in mitochondrial formation and function during spermatogenesis.

(3) Jacob, A., T.X. Lee, B.A. Neff, S. Miller, D.B. Welling, and L.-S. Chang. 2008. Activation of the AKT Pathway in Human Vestibular Schwannomas. Otol. Neurotol. 29:58-68. http://www.ncbi.nlm.nih.gov/pubmed/18199958?ordinalpos=1&itool=EntrezSystem2.PEntrez.Pubmed.Pubmed_ResultsPanel.Pubmed_RVDocSum

Despite advances in diagnosis and treatment, vestibular schwannomas (VS) continue to cause patient morbidity. A more thorough understanding of the signaling pathways deregulated in VS will aid in the development of novel medical therapeutics. We performed cDNA microarray analysis and found that total AKT gene expression was up-regulated in VS, compared to normal vestibular nerves. By immunohistochemical analysis of 14 VS tissue sections, we detected positive staining for activated AKT that are phosphorylated at both serine-473 and threonine-308 in all VS tumors. Western blots comparing VS specimens to normal vestibular nerves revealed that the AKT pathway is activated in VS but not in normal nerve. Total AKT, p-AKT, PI3-kinase, p-PTEN, p-PDK1, p-FOXO, p-GSK3β, and p-mTOR are also upregulated in VS. Together, these results indicate that the PI3-kinase/AKT pathway is activated in VS. Using our recently reported, quantifiable VS xenograft model, novel inhibitors of the PI3-kinase/AKT pathway may be tested for VS growth inhibition in vivo.

(4) Kopyl, S.A., Akhmametyeva, E.M., Dorogova, N.V., Omelyanchuk, L.V., and Chang, L.-S. 2008. *Drosophila* Merlin Genetically Interacts with the Clathrin Adaptor Protein LAP. Submitted to BMC Genetics.

Recent studies show that Merlin and Expanded, another member of the protein 4.1 family, cooperatively regulate the recycling of membrane receptors, such as the epidermal growth factor receptor (EGFR). To better understand the role of Merlin in receptor-mediated endocytosis, we performed a search for potential genetic interactions between *Merlin* and the genes important for vesicular trafficking. We showed that ectopic expression of the clathrin adaptor protein Lap, an adapter protein involved in clathrin-mediated receptor endocytosis, in the wing pouch results in the formation of extra vein material. Co-expression of wild-type Merlin and lap in the wing pouch restores normal venation, while over-expression of a dominant-negative Merlin mutant $Mer^{\Delta BB}$ together with lap enhances ectopic vein

formation. Using various Merlin truncation mutants, we have identified the C-terminal portion of Merlin to be important for the Merlin-lap genetic interaction. Furthermore, we showed that the Merlin and Lap proteins colocalize at the cellular cortex in the wing imaginal disc cells. Together with previous findings, our results suggest that Merlin may regulate receptor-mediated endocytosis through interaction with Lap.

The research described in the following four publications were supported in part by the present grant:

(5) Neff, B.A., D.B. Welling, E.M. Akhmametyeva, and L.-S. Chang. 2006. The Molecular Biology of Vestibular Schwannomas: Dissecting the Pathogenic Process at the Molecular Level. Otol. Neurotol. 27:197-208.
http://www.ncbi.nlm.nih.gov/sites/entrez?Db=pubmed&Cmd=ShowDetailView&TermToSearch=16436990&ordinalpos=4&itool=EntrezSystem2.PEntrez.Pubmed.Pubmed_ResultsPanel.Pubmed_RVDocSum

The goal of this article is to concisely review what is currently known about the tumorigenesis of vestibular schwannomas. Recent advances in molecular biology have led to a better understanding of the cause of vestibular schwannomas. Mutations in the Neurofibromatosis type 2 tumor suppressor gene (NF2) have been identified in these tumors. In addition, the interactions of Merlin, the protein product of the NF2 gene, and other cellular proteins are beginning to give us a better idea of NF2 function and the pathogenesis of vestibular schwannomas. We have reviewed the clinical characteristics of vestibular schwannomas and neurofibromatosis type 2 syndromes and their relation to the alteration of the NF2 gene. We have highlighted studies demonstrating our current understanding of tumor developmental pathways. In addition, we outline methods of clinical and genetic screening for neurofibromatosis type 2 disease. We also discuss avenues for the development of potential future research and therapies. In conclusion, great strides have been made to identify why vestibular schwannomas develop at the molecular level. Continued research is needed to find targeted therapies with which to treat these tumors.

(6) Neff, B.A., E. Oberstein, M. Lorenz,, A. Chadhury, D.B. Welling, and L.-S. Chang. 2006. Cyclin D_1 and D_3 Expression in Vestibular Schwannomas. Laryngoscope 116:423-426.
http://www.ncbi.nlm.nih.gov/sites/entrez?Db=pubmed&Cmd=ShowDetailView&TermToSearch=16540902&ordinalpos=3&itool=EntrezSystem2.PEntrez.Pubmed.Pubmed_ResultsPanel.Pubmed_RVDocSum

The purpose of this study is to evaluate the expression of the G1 regulators cyclin D1 and D3 and the corresponding clinical characteristics of vestibular schwannomas. By immunohistochemical analysis, we show that while the breast carcinoma control expresses abundant cyclin D1 protein, none of the 15 vestibular schwannomas shows detectable cyclin D1 staining. In contrast, seven of 15 vestibular schwannomas stain positive for the cyclin D3 protein. Cyclin D3 staining is taken up in the nucleus of schwannoma tumor cells in a greater proportion than Schwann cells of the adjacent vestibular nerve. Although the sample size is small, no significant

difference in the average age of presentation, tumor size, and male to female ratios for the cyclin D3+ or cyclin D3- groups is found. In conclusion, the cyclin D1 protein does not appear to play a prominent role in promoting cell-cycle progression in vestibular schwannomas. In contrast, cyclin D3 expression was seen in nearly half of the tumors examined, suggesting that it may have a growth-promoting role in some schwannomas.

(7) Akhmametyeva, E.M., M.M. Mihaylova, H. Luo, S. Kharzai, D.B. Welling, and L.-S. Chang. 2006. Regulation of *NF2* Gene Promoter Expression during Embryonic Development. Dev. Dyn. 235:2771-2785. http://www.ncbi.nlm.nih.gov/sites/entrez?Db=pubmed&Cmd=ShowDetailView&TermToSearch=16894610&ordinalpos=2&itool=EntrezSystem2.PEntrez.Pubmed.Pubmed_ResultsPanel.Pubmed_RVDocSum

We describe, in this paper, the examination of NF2 expression during embryonic development. We generated transgenic mice carrying a 2.4-kb NF2 promoter driving β-galactosidase (β-gal) with a nuclear localization signal. Whole-mount embryo staining revealed that the NF2 promoter directs β-gal expression as early as embryonic day E5.5. Strong expression is detected at E6.5 in the embryonic ectoderm containing many mitotic cells. β-gal staining was also found in parts of the embryonic endoderm and mesoderm. The β-gal staining pattern in the embryonic tissues is corroborated by in situ hybridization analysis of endogenous Nf2 RNA expression. Importantly, we observe strong NF2 promoter activity in the developing brain and in sites containing migrating cells, including the neural tube closure, branchial arches, dorsal aorta, and paraaortic splanchnopleura. Furthermore, we note a transient change of NF2 promoter activity during neural crest cell migration. While little β-gal activity is detected in premigratory neural crest cells at the dorsal ridge region of the neural fold, significant activity is seen in the neural crest cells already migrating away from the dorsal neural tube. In addition, we detect considerable NF2 promoter activity in various NF2-affected tissues, such as acoustic ganglion, trigeminal ganglion, spinal ganglia, optic chiasma, the ependymal cell-containing tela choroidea, and the pigmented epithelium of the retina. The NF2 promoter expression pattern during embryogenesis suggests specific regulation of the NF2 gene during neural crest cell migration and further supports the role of Merlin in cell adhesion, motility, and proliferation during development.

(8) Chang, L.-S., A. Jacob, M. Lorenz, J. Rock, E.M. Akhmametyeva, G. Mihai, P. Schmalbrock, A.R. Chaudhury, R. Lopez, J. Yamate, M.R. John, H. Wickert, B.A. Neff, E. Dodson, and D.B. Welling. 2006. Magnetic Resonance Imaging Noninvasively Quantifies Schwannoma Xenografts in SCID Mice. Laryngoscope 116:2018-2026. http://www.ncbi.nlm.nih.gov/sites/entrez?Db=pubmed&Cmd=ShowDetailView&TermToSearch=17075413&ordinalpos=1&itool=EntrezSystem2.PEntrez.Pubmed.Pubmed_ResultsPanel.Pubmed_RVDocSum

The purpose of this study is to establish a quantifiable human VS xenograft model in mice. SCID mice implanted with malignant schwannoma cells develop visible tumors within 2 weeks. By using a 4.7-tesla magnetic resonance imaging and immunohistopathologic

examination, we have identified solid tumors in all KE-F11 and HMS-97 xenografts, whereas RT4 xenografts consistently develop cystic schwannomas. VS xenografts demonstrate variability in their growth rates similar to human VS. The majority of VS xenografts do not grow but persist throughout the study, whereas two of 15 xenografts grow significantly. By histopathologic examination and immunohistochemistry, we have confirmed that VS xenografts retain their original microscopic and immunohistochemical characteristics after prolonged implantation. In conclusion, this study describes the first animal model for cystic schwannomas. Also, we demonstrate the use of high-field magnetic resonance imaging to quantify VS xenograft growth over time. The VS xenografts represent a model complimentary to Nf2 transgenic and knockout mice for translational VS research.

(9) Welling, D.B., M.D. Packer, and L.-S. Chang. 2007. Molecular Studies of Vestibular Schwannomas: A Review. Curr. Opin. Otolaryngol. Head Neck Surg. 15:341-346. http://www.ncbi.nlm.nih.gov/pubmed/17823551?ordinalpos=9&itool=EntrezSystem2.PEntrez.Pubmed.Pubmed_ResultsPanel.Pubmed_RVDocSum

This paper summarizes advances in understanding the molecular biology of vestibular schwannomas over the past year. The role of the Neurofibromatosis type 2 (NF2) protein, denoted as Merlin or schwannomin, in embryonic development, cellular adherence, and cell proliferation has become better elucidated in the past year. Likewise, the role of merlin in Schwann cell-axon interaction has been studied. Additionally, two comprehensive analyses of the spectrum of human neurofibromatosis type 2 mutations have been compiled which make up a valuable resource in understanding critical regions of the neurofibromatosis type 2 gene. Neurofibromatosis type 2 screening guidelines for young patients with solitary vestibular schwannomas have been published. The role of electromagnetic radiation via cellular and portable telephones as a predisposing factor to vestibular schwannoma formation has also been the topic of several studies. Based on increased knowledge of the pathways in which Merlin functions and the available transgenic and xenograft mouse models, preliminary data regarding directed pharmacotherapy are also summarized. With increased knowledge of the pathologic mechanisms and interacting proteins associated with merlin, the research community is poised to begin trials of targeted interventions in vitro and in the current mouse models.

CONCLUSIONS:

We have confirmed that *Drosophila* Merlin plays important roles in the control of mitosis exit and in the determination of dorsal/ventral compartment border during wing imaginal disc development. Merlin mutations lead to two types of mitosis exit asynchrony, the asynchronous anaphase-telophase figures and the asynchronous telophase-interphase figures. *Merlin* mutant cells display a longer G_2 period than the wild-type cells, indicating that *Merlin* mutation alters the duration of this cell-cycle phase. The Merlin protein colocalizes with the Wingless morphogen in the cells

at the dorsal/ventral compartment border of the wing imaginal disc. Merlin inactivation may lead to an alteration in the determination/maintenance of Wg stripe expression. Cells lacking Merlin possess greater ability to overcome vein restriction. Also, we have found that the Merlin protein is dynamically redistributed during meiosis. Merlin immunoreactivity has been detected in the mitochondria, suggesting a role for Merlin in mitochondrial formation and function. In addition, we have found that Merlin genetically interacts with proteins involved in vesicular trafficking, including porcupine, Shibire, and Lap. These results suggest that Merlin may regulate receptor-mediated endocytosis through interaction with Lap. The Merlin protein is regulated by phosphorylation. In cells grown at high density, the non-phospho-Merlin protein appears mostly in the cytoplasm, while the phospho-Merlin protein is seen in the membrane region. By analyzing the evolution, diversity, and overall distribution of Merlin among different taxa, we demonstrate a monophyletic origin of the Merlin proteins with their root in the early metazoa. The overall similarity among the primary and secondary structures of all Merlin proteins and the conservation of several functionally important residues suggest a universal role for merlin in a wide range of metazoa. Furthermore, we show that the AKT pathway is frequently activated in the *NF2*$^{-/-}$ tumor cells. We have tested two novel compounds, OSU03012 and (S)-HDAC-42, which inhibit AKT phosphorylation, and found that these drugs effectively inhibit the growth of vestibular schwannoma cells and xenografts. These findings set the stage for a phase I clinical trial on VS in the future.

REFERENCES:

Akhmametyeva, E.M., M.M. Mihaylova, H. Luo, S. Kharzai, D.B. Welling, and L.-S. Chang. 2006. Regulation of the *NF2* Gene Promoter Expression During Embryonic Development. Dev. Dyn. 235:2771-2785.

Boedigheimer, M.J., Laughon, A.S. 1993. expanded: a gene involved in the control of cell proliferation in Drosophila imaginal discs. Development 118:1291—1301.

Brook, W.J., S.M. Cohen. 1996. Antagonistic interaction between Wingless and Decapentaplegic responsible for dorsal-ventral pattern in the Drosophila leg. Science 273, 1373-1377.

Chang, L.-S., A. Jacob, M. Lorenz, J. Rock, E.M. Akhmametyeva, G. Mihai, P. Schmalbrock, A.R. Chaudhury, R. Lopez, J. Yamate, M.R. John, H. Wickert, B.A. Neff, E. Dodson, and D.B. Welling. 2006. Magnetic Resonance Imaging Noninvasively Quantifies Schwannoma Xenografts in SCID Mice. Laryngoscope 116:2018-2026.

Dorogova, N.V., Akhmametyeva, E.M., Kopyl, S.A., Gubanova, N.V., Yudina, O.S., Omelyanchuk, L.V., and Chang, L.-S. 2008. The role of Merlin in spermatogenesis. BMC Cell Biology 9:1-15.

Dubatolova, T.D. and Omelyanchuk, L.V. 2004. Analysis of cell proliferation in Drosophila wing imaginal discs using mosaic clones. Heredity 92:299—305.

Entchev, E.V. and Gonzalez-Gaitan, M.A. 2002. Morphogen gradient formation and vesicular trafficking. Traffic 3:98-109.

Fehon, R.G., Oren, T., LaJeunesse, D.R., Melby, T.E., McCartney. B.M.

1997. Isolation of mutations in the Drosophila homologues of the human Neurofibromatosis 2 and yeast CDC42 genes using a simple and efficient reverse-genetic method. Genetics 146:245-252.
Garcia-Bellido, A. and Merriam, J.R. 1971a. Parameters of the wing imaginal disc development of *Drosophila melanogaster*. Dev. Biol. 24:61-87.
Garcia-Bellido, A. and Merriam, J.R. 1971b. Genetic analysis of cell heredity in imaginal discs of *Drosophila melanogaster*. Proc. Natl. Acad. Sci. USA 68:2222-2226.
Giovannini, M., Robanus-Maandag, E., van der Valk, M., Niwa-Kawakita, M., et al. 2000. Conditional biallelic *Nf2* mutation in the mouse promotes manifestations of human neurofibromatosis type 2. Genes Dev. 14:1617-1630.
Golovnina, K., A. Blinov, E.M. Akhmametyeva, L.V. Omelyanchuk, and L.-S. Chang. 2005. Evolution and Origin of Merlin, the Product of the *Neurofibromatosis Type 2* (*NF2*) Tumor-Suppressor Gene. BMC Evol. Biol. 5:69-86.
Gonzalez-Gaitan, M., Capdevila, M.P., and Garcia-Bellido, A. 1994. Cell proliferation pattern in the wing imaginal disc of *Drosophila*. Mech. Dev. 40:183-200.
Hamaratoglu F, Willecke M, Kango-Singh M, Nolo R, Hyun E, Tao C, Jafar-Nejad H, Halder G. 2006. The tumour-suppressor genes NF2/Merlin and Expanded act through Hippo signalling to regulate cell proliferation and apoptosis. Nat. Cell Biol. 8:27-36.
Hofmann, K. 2000. A superfamily of membrane-bound O-acyltransferases with implications for Wnt signaling. *Trends Biochem. Sci.* 25:111–112.
Hughes, S.C., Fehon, R.G. 2006. Phosphorylation and activity of the tumor suppressor Merlin and the ERM protein Moesin are coordinately regulated by the Slik kinase. J. Cell Biol. 175:305-313.
Jacob, A., T.X. Lee, B.A. Neff, S. Miller, D.B. Welling, and L.-S. Chang. 2008. Activation of the AKT Pathway in Human Vestibular Schwannomas. Otol. Neurotol. 29:58-68.
Johnston L.A. and Edgar B.A. 1998 Wingless and Notch regulate cell-cycle arrest in the developing Drosophila wing. Nature 394:82-84.
Kitamoto, T. 2002. Targeted expression of temperature-sensitive dynamin to study neural mechanisms of complex behavior in Drosophila. J. Neurogenet. 16:205-228.
Kopyl, S.A., Akhmametyeva, E.M., Dorogova, N.V., Omelyanchuk, L.V., and Chang, L.-S. 2008. *Drosophila* Merlin Genetically Interacts with the Clathrin Adaptor Protein LAP. Submitted to BMC Genetics.
LaJeunesse, D.R., McCartney, B.M., Fehon, R.G. 1998. Structural analysis of Drosophila merlin reveals functional domains important for growth control and subcellular localization. J. Cell Biol. 141:1589-1599.
LoPiccolo, J., Blumenthal, G.M., Bernstein, W.B., Dennis, P.A. 2008. Targeting the PI3K/Akt/mTOR pathway: effective combinations and clinical considerations. Drug Resist. Updat. 11:32-50.
Maitra, S., Kulikauskas, R.M., Gavilan, H., and Fehon, R.G. 2006. The tumor suppressors Merlin and expanded function cooperatively to modulate receptor endocytosis and signaling. Curr. Biol. 16:702-709.
Mattila J, Omelyanchuk L, Kyttala S, Turunen H, Nokkala S. 2005. Role of Jun N-terminal Kinase (JNK) signaling in the wound healing and

regeneration of a Drosophila melanogaster wing imaginal disc. Int. J. Dev. Biol. 49:391-399.
McCartney, B.M., Fehon, R.G. 1996. Distinct cellular and subcellular patterns of expression imply distinct functions for the Drosophila homologues of moesin and the neurofibromatosis 2 tumor suppressor, merlin. J. Cell Biol. 133:843-852.
McCartney BM, Kulikauskas RM, LaJeunesse DR, Fehon RG. 2000. The neurofibromatosis-2 homologue, Merlin, and the tumor suppressor expanded function together in Drosophila to regulate cell proliferation and differentiation. Development 127:1315-1324.
Neff, B.A., D.B. Welling, E.M. Akhmametyeva, and L.-S. Chang. 2006. The Molecular Biology of Vestibular Schwannomas: Dissecting the Pathogenic Process at the Molecular Level. Otol. Neurotol. 27:197-208.
Neff, B.A., E. Oberstein, M. Lorenz,, A. Chadhury, D.B. Welling, and L.-S. Chang. 2006. Cyclin D_1 and D_3 Expression in Vestibular Schwannomas. Laryngoscope 116:423-426.
Ramaswami, M., Rao, S., van der Bliek, A., Kelly, R.B., and Krishnan, K.S. 1993. Genetic studies on dynamin function in Drosophila. J. Neurogenet. 9:73-87.
Reuter, G., Szidonya, J. 1983. Cytogenetic analysis of variegation suppressors and a dominant temperature-sensitive lethal in region 23-26 of chromosome arm 2L in Drosophila melanogaster. Chromosoma 88:277--285.
Rong, R., Surace, E.I., Haipek, C.A., Gutmann, D.H., Ye, K. 2004. Serine 518 phosphorylation modulates merlin intramolecular association and binding to critical effectors important for NF2 growth suppression. Oncogene 23:8447-8454.
Seto, E.S. and Bellen, H.J. 2004. The ins and outs of Wingless signaling. Trends Cell Biol. 14:45-53.
Strigini, M. and Cohen, S.M. 2000. Wingless gradient formation in the Drosophila wing. Curr. Biol. 10:293-300.
Surace, E.I., Haipek, C.A., Gutmann, D.H. 2004. Effect of merlin phosphorylation on neurofibromatosis 2 (NF2) gene function. Oncogene 23:580-587.
Shaw, R.J., McClatchey, A.I., Jacks, T. 1998. Regulation of the neurofibromatosis type 2 tumor suppressor protein, merlin, by adhesion and growth arrest stimuli. J. Biol. Chem. 273:7757-7764.
Tanaka, K., Kitagawa, Y., Kadowaki, T. 2002. Drosophila segment polarity gene product porcupine stimulates the posttranslational N-glycosylation of wingless in the endoplasmic reticulum. J. Biol. Chem. 277:12816-12823.
Trofatter JA, MacCollin MM, Rutter JL, Murrell JR, et al. 1993. A novel Moesin-, Ezrin-, Radixin-like gene is a candidate for the neurofibromatosis 2 tumor-suppressor. Cell 72:791-800.
Trunova, S.A., Dubatolova, T.D., Omel'ianchuk, L.V. 2001. Phase-specific elements of the regulatory zone of the *Drosophila melanogaster* string gene. Genetika 37:1616—1620.
Trunova, S.A., Dubatolova, T.D., Omel'ianchuk, L.V. 1998. Determination of the expression phase of chb(V40) gene in the cell cycle of Drosophila melanogaster. Ontogenez 29:342—346.
Xiao, G.H., Beeser, A., Chernoff, J. Testa, J.R. 2002. p21-activated kinase links Rac/Cdc42 signaling to merlin. J. Biol. Chem. 277:883-

886.
van der Bliek, A.M. and Meyerowitz, E.M. 1991. Dynamin-like protein encoded by the Drosophila shibire gene associated with vesicular traffic. Nature 351:411-414.
Zhang, B., Koh, Y.H., Beckstead, R.B., Budnik, V., Ganetzky, B., and Bellen, H.J. 1998. Synaptic vesicle size and number are regulated by a clathrin adaptor protein required for endocytosis. Neuron 21:1465-1475.

LIST OF PERSONNEL RECEIVING PAY FROM THE RESEARCH EFFORT

Long-Sheng Chang, Ph.D., Principal Investigator and Professor, Columbus Children's Research Institute, Columbus, Ohio
Elena M. Akhmameteyva, M.D., Ph.D., Research Associate Scientist, Columbus Children's Research Institute, Columbus, Ohio
Sarah S. Burns, Research Aide, Columbus Children's Research Institute, Columbus, Ohio
Jie Huang, Ph.D., Postdoctoral Research Fellow, Columbus Children's Research Institute, Columbus, Ohio

Leonid V. Omelyanchuk, Ph.D., Co-Investigator and Chief of Laboratory of Cell Cycle Genetics, Institute of Cytology and Genetics, Russian Academy of Sciences, Novosibirsk, Russia
Sergei Kopyl, Ph.D., Postdoctoral Researcher, Institute of Cytology and Genetics, Russian Academy of Sciences, Novosibirsk, Russia
Natalia Dorogova, Ph.D., Postdoctoral Researcher, Institute of Cytology and Genetics, Russian Academy of Sciences, Novosibirsk, Russia
Natalia V. Gubanova, Ph.D., Postdoctoral Researcher, Institute of Cytology and Genetics, Russian Academy of Sciences, Novosibirsk, Russia
Tatiana Yu. Baymak, Ph.D., Postdoctoral Researcher, Institute of Cytology and Genetics, Russian Academy of Sciences, Novosibirsk, Russia
Anna M. Gusachenko, Ph.D., Postdoctoral Researcher, Institute of Cytology and Genetics, Russian Academy of Sciences, Novosibirsk, Russia
Olga Yudina, M.S., Ph.D. Student, Institute of Cytology and Genetics, Russian Academy of Sciences, Novosibirsk, Russia
Julia Pertseva, M.S., Ph.D. Student, Institute of Cytology and Genetics, Russian Academy of Sciences, Novosibirsk, Russia
Olga O. Nerusheva, M.S., Ph.D. Student, Institute of Cytology and Genetics, Russian Academy of Sciences, Novosibirsk, Russia
Elena Gordeeva, M.S., Ph.D. Student, Institute of Cytology and Genetics, Russian Academy of Sciences, Novosibirsk, Russia
Tatyana D. Dubatolova, M.S., Staff Researcher, Institute of Cytology and Genetics, Russian Academy of Sciences, Novosibirsk, Russia
Irina E. Shilova, M.S., Staff Researcher, Institute of Cytology and Genetics, Russian Academy of Sciences, Novosibirsk, Russia
Alexander Blinov, Ph.D., Chief of Laboratory of Bioinformatics, Institute of Cytology and Genetics, Russian Academy of Sciences, Novosibirsk, Russia
Ksenya Golovnina, Ph.D., Postdoctoral Researcher, Institute of Cytology and Genetics, Russian Academy of Sciences, Novosibirsk, Russia
Anna Kabanova, M.S., Ph.D. Student, Institute of Cytology and Genetics, Russian Academy of Sciences, Novosibirsk, Russia
Nina G. Darkina, Drosophila Kitchen Staff, Institute of Cytology and Genetics, Russian Academy of Sciences, Novosibirsk, Russia
Tatiana V. Ivanova, Drosophila Kitchen Staff, Institute of Cytology and Genetics, Russian Academy of Sciences, Novosibirsk, Russia

Tatiana K. Lepehina, Drosophila Kitchen Staff, Institute of Cytology and Genetics, Russian Academy of Sciences, Novosibirsk, Russia
Tatiana D. Ulazovska, Drosophila Kitchen Staff, Institute of Cytology and Genetics, Russian Academy of Sciences, Novosibirsk, Russia

ABSTRACT

To better understand the mechanism by which Merlin functions as a tumor suppressor, we have confirmed that *Drosophila* Merlin plays important roles in the control of mitosis exit and in the determination of dorsal/ventral compartment border during wing imaginal disc development. We show that the Merlin protein is dynamically redistributed during meiosis and demonstrate, for the first time, Merlin immunoreactivity in mitochondria. Also, we have found that Merlin colocalizes with Wingless morphogen in the cells at the dorsal/ventral compartment border of the wing imaginal disc. Merlin inactivation may alter the determination/maintenance of Wingless stripe expression. Cells lacking Merlin possess greater ability to overcome vein restriction. In addition, we provide evidence for potential genetic interactions between Merlin and the proteins involved in vesicular trafficking, including Porcupine, Shibire, and Lap. By analyzing the evolution, diversity, and overall distribution of Merlin among different taxa, we demonstrate a monophyletic origin of the Merlin proteins with their root in the early metazoa. The overall similarity among the primary and secondary structures of all merlin proteins and the conservation of several functionally important residues suggest a universal role for merlin in a wide range of metazoa. Furthermore, we show that the AKT pathway is frequently activated in *NF2*$^{-}$ tumor cells. We have tested two novel compounds, OSU03012 and (S)-HDAC-42, which inhibit AKT phosphorylation, and found that these drugs effectively inhibit the growth of vestibular schwannoma cells. These findings set the stage for a phase I clinical trial on VS in the future.

APPENDICES:

Publications listed below can also be found in the indicated web link.

(1) Golovnina, K., Blinov, A., Akhmametyeva, E.M., Omelyanchuk, L.V., and Chang, L.-S. 2005. Evolution and Origin of Merlin, the Product of the Neurofibromatosis Type 2 Tumor-Suppressor Gene. BMC Evolutionary Biology 5:69-86. http://www.ncbi.nlm.nih.gov/pubmed/16324214?ordinalpos=3&itool=EntrezSystem2.PEntrez.Pubmed.Pubmed_ResultsPanel.Pubmed_RVDocSum

(2) Neff, B.A., D.B. Welling, E.M. Akhmametyeva, and L.-S. Chang. 2006. The Molecular Biology of Vestibular Schwannomas: Dissecting the Pathogenic Process at the Molecular Level. Otol. Neurotol. 27:197-208. http://www.ncbi.nlm.nih.gov/sites/entrez?Db=pubmed&Cmd=ShowDetailView&TermToSearch=16436990&ordinalpos=4&itool=EntrezSystem2.PEntrez.Pubmed.Pubmed_ResultsPanel.Pubmed_RVDocSum

(3) Neff, B.A., E. Oberstein, M. Lorenz,, A. Chadhury, D.B. Welling, and L.-S. Chang. 2006. Cyclin D_1 and D_3 Expression in Vestibular Schwannomas. Laryngoscope 116:423-426. http://www.ncbi.nlm.nih.gov/sites/entrez?Db=pubmed&Cmd=ShowDetailView&TermToSearch=16540902&ordinalpos=3&itool=EntrezSystem2.PEntrez.Pubmed.Pubmed_ResultsPanel.Pubmed_RVDocSum

(4) Akhmametyeva, E.M., M.M. Mihaylova, H. Luo, S. Kharzai, D.B. Welling, and L.-S. Chang. 2006. Regulation of the *NF2* Gene Promoter Expression During Embryonic Development. Dev. Dyn. 235:2771-2785. http://www.ncbi.nlm.nih.gov/sites/entrez?Db=pubmed&Cmd=ShowDetailView&TermToSearch=16894610&ordinalpos=2&itool=EntrezSystem2.PEntrez.Pubmed.Pubmed_ResultsPanel.Pubmed_RVDocSum

(5) Chang, L.-S., A. Jacob, M. Lorenz, J. Rock, E.M. Akhmametyeva, G. Mihai, P. Schmalbrock, A.R. Chaudhury, R. Lopez, J. Yamate, M.R. John, H. Wickert, B.A. Neff, E. Dodson, and D.B. Welling. 2006. Magnetic Resonance Imaging Noninvasively Quantifies Schwannoma Xenografts in SCID Mice. Laryngoscope 116:2018-2026. http://www.ncbi.nlm.nih.gov/sites/entrez?Db=pubmed&Cmd=ShowDetailView&TermToSearch=17075413&ordinalpos=1&itool=EntrezSystem2.PEntrez.Pubmed.Pubmed_ResultsPanel.Pubmed_RVDocSum

(6) Welling, D.B., M.D. Packer, and L.-S. Chang. 2007. Molecular Studies of Vestibular Schwannomas: A Review. Curr. Opin. Otolaryngol. Head Neck Surg. 15:341-346. http://www.ncbi.nlm.nih.gov/pubmed/17823551?ordinalpos=9&itool=EntrezSystem2.PEntrez.Pubmed.Pubmed_ResultsPanel.Pubmed_RVDocSum

(7) Dorogova, N.V., Akhmametyeva, E.M., Kopyl, S.A., Gubanova, N.V., Yudina, O.S., Omelyanchuk, L.V., and Chang, L.-S. 2008. The role of Merlin in spermatogenesis. Submitted to BMC Cell Biology 9:1-15.

http://www.ncbi.nlm.nih.gov/pubmed/18186933?ordinalpos=1&itool=EntrezSystem2.PEntrez.Pubmed.Pubmed_ResultsPanel.Pubmed_RVDocSum

(8) Jacob, A., T.X. Lee, B.A. Neff, S. Miller, D.B. Welling, and L.-S. Chang. 2008. Activation of the AKT Pathway in Human Vestibular Schwannomas. Otol. Neurotol. 29:58-68. http://www.ncbi.nlm.nih.gov/pubmed/18199958?ordinalpos=1&itool=EntrezSystem2.PEntrez.Pubmed.Pubmed_ResultsPanel.Pubmed_RVDocSum

Manuscripts Submitted or In Press:

(9) Kopyl, S.A., Akhmametyeva, E.M., Dorogova, N.V., Omelyanchuk, L.V., and Chang, L.-S. 2008. *Drosophila* Merlin Genetically Interacts with the Clathrin Adaptor Protein LAP. Submitted to BMC Genetics.

BMC Evolutionary Biology

BioMed Central

Research article

Evolution and origin of merlin, the product of the *Neurofibromatosis type 2* (*NF2*) tumor-suppressor gene

Kseniya Golovnina[1], Alexander Blinov[1], Elena M Akhmametyeva[2], Leonid V Omelyanchuk[1] and Long-Sheng Chang*[2]

Address: [1]Institute of Cytology and Genetics, Russian Academy of Sciences, 10 Lavrent'ev Ave., 630090, Novosibirsk, Russia and [2]Center for Childhood Cancer, Children's Research Institute, Children's Hospital and Department of Pediatrics, The Ohio State University, 700 Children's Drive, Columbus, OH 43205-2696, USA

Email: Kseniya Golovnina - ksu@bionet.nsc.ru; Alexander Blinov - blinov@bionet.nsc.ru; Elena M Akhmametyeva - akhmamee@pediatrics.ohio-state.edu; Leonid V Omelyanchuk - ome@bionet.nsc.ru; Long-Sheng Chang* - lchang@chi.osu.edu

* Corresponding author

Published: 02 December 2005

BMC Evolutionary Biology 2005, **5**:69 doi:10.1186/1471-2148-5-69

Received: 18 March 2005
Accepted: 02 December 2005

This article is available from: http://www.biomedcentral.com/1471-2148/5/69

Abstract

Background: Merlin, the product of the *Neurofibromatosis type 2* (*NF2*) tumor suppressor gene, belongs to the ezrin-radixin-moesin (ERM) subgroup of the protein 4.1 superfamily, which links cell surface glycoproteins to the actin cytoskeleton. While merlin's functional activity has been examined in mammalian and *Drosophila* models, little is understood about its evolution, diversity, and overall distribution among different taxa.

Results: By combining bioinformatic and phylogenetic approaches, we demonstrate that merlin homologs are present across a wide range of metazoan lineages. While the phylogenetic tree shows a monophyletic origin of the ERM family, the origin of the merlin proteins is robustly separated from that of the ERM proteins. The derivation of merlin is thought to be in early metazoa. We have also observed the expansion of the ERM-like proteins within the vertebrate clade, which occurred after its separation from Urochordata (*Ciona intestinalis*). Amino acid sequence alignment reveals the absence of an actin-binding site in the C-terminal region of all merlin proteins from various species but the presence of a conserved internal binding site in the N-terminal domain of the merlin and ERM proteins. In addition, a more conserved pattern of amino acid residues is found in the region containing the so-called "Blue Box," although some amino acid substitutions in this region exist in the merlin sequences of worms, fish, and *Ciona*. Examination of sequence variability at functionally significant sites, including the serine-518 residue, the phosphorylation of which modulates merlin's intra-molecular association and function as a tumor suppressor, identifies several potentially important sites that are conserved among all merlin proteins but divergent in the ERM proteins. Secondary structure prediction reveals the presence of a conserved α-helical domain in the central to C-terminal region of the merlin proteins of various species. The conserved residues and structures identified correspond to the important sites highlighted by the available crystal structures of the merlin and ERM proteins. Furthermore, analysis of the merlin gene structures from various organisms reveals the increase of gene length during evolution due to the expansion of introns; however, a reduction of intron number and length appears to occur in the merlin gene of the insect group.

Conclusion: Our results demonstrate a monophyletic origin of the merlin proteins with their root in the early metazoa. The overall similarity among the primary and secondary structures of all merlin proteins and the conservation of several functionally important residues suggest a universal role for merlin in a wide range of metazoa.

Background

The advancement in genome sequencing projects, the accumulation of knowledge in bioinformatics, and the molecular genetic analysis of genes and their functions in a variety of model organisms provides us with an unprecedented opportunity to identify novel genes based on sequences related to characterized genes [1]. This process is conducted using pairwise sequence comparison with the understanding that genes form families wherein related sequences likely share similar functions. Although initial identification of new genes may not yield a clear indication of their respective functions, studies on their evolution may allow validation of their sequence identity and provide information on their putative functional characteristics. For genes evolved from duplication and/or adapted to different evolutionary niches during speciation, detailed sequence comparison can provide additional information regarding their biological and biochemical characteristics [2].

Neurofibromatosis type 2 (NF2) is a highly penetrant, autosomal dominant disorder, whose hallmark is the development of bilateral vestibular schwannomas [3,4]. The tumor suppressor gene associated with NF2 has been identified and termed the *neurofibromatosis type 2* gene (*NF2*) [5,6]. The *NF2* gene encodes a protein named merlin, for moesin-ezrin-radixin like protein, or schwannomin, a word derived from schwannoma, the most prevalent tumor seen in NF2. For simplicity, we refer to the *NF2* gene product as merlin hereafter.

Merlin shares sequence similarity with the ezrin, radixin, and moesin (ERM) proteins, which belong to the protein 4.1 superfamily of cytoskeleton-associated proteins that link cell surface glycoproteins to the actin cytoskeleton [7,8]. Like ERM proteins, merlin consists of three predicted structural domains [5,6,9]. The N-terminal domain, termed the FERM (F for 4.1) domain, is highly conserved among all members of the ERM family and is important for interactions with cell surface glycoproteins, including CD44 and intercellular adhesion molecules [10-13]. Crystal structure analysis shows that the tertiary structure of the FERM domain of merlin closely resembles those of the FERM domain of moesin and radixin [14-18]. The FERM domain of merlin exists as a clover-shaped molecule consisting of three structural subdomains A, B, and C, which are homologous to lobes F1, F2, and F3 in moesin and radixin. Subdomain A, composed of residues 20–100, possesses a ubiquitin-like fold. Subdomain B, consisting of residues 101–215, folds itself into a topology like that of the acetyl-CoA-binding protein. Subdomain C, containing residues 216–313, adopts the pleckstrin homology/phosphotyrosine-binding fold found in a broad range of signaling molecules [14-16]. The second half of merlin contains a predicted α-helix domain, which is also present in the ERM proteins [19]. Although the unique C-terminus of merlin lacks the conventional actin-binding domain found in the ERM proteins [20,21], merlin can directly bind actin using the residues at the N-terminal domain and indirectly through its association with βII-spectrin or fodrin [22-24].

The merlin and ERM proteins are thought to be key regulators of interactions between the actin cytoskeleton and the plasma membrane in polarized cells. They act as important members of signal transduction pathways that control cell growth and participate in the sorting of membrane proteins during exocytic traffic [25,26]. However, unlike the ERM proteins, merlin has a distinct function as a tumor suppressor [27]. Growth suppression by merlin is dependent on its ability to form intramolecular associations [28,29]. In this regard, merlin exists in an "open" (inactive form) or "closed" (active growth-suppressive form) conformation that is regulated by phosphorylation [30-35].

While previous studies have focused primarily on the functional analysis of merlin, limited information is available about its overall distribution across eukaryotes and its evolution. A phylogenetic study indicates that the FERM domains of ERM homologs from sea urchins, *Caenorhabditis elegans*, *Drosophila melanogaster*, and vertebrates share 74–82% amino acid identity and have about 60% identity with those of merlin [25,36-42]. These levels of identity are exceptionally high, suggesting that the protein structures of the merlin and ERM proteins from these species may be well-conserved. The most divergent ERM proteins are found in tapeworms and schistosomes [36-39]. The FERM domains of these parasite proteins share only 44–58% similarity to their vertebrate homologs. The high degree of structural conservation among these proteins points to possible similarities or functional redundancies. Intriguingly, no FERM domain-encoding genes have been identified in the genome of the yeast *Saccharomyces cerevisiae*, implying that FERM domains evolved in response to multicellularity, rather than as a cytoskeletal component [25].

The goal of the present study was to expand our understanding of the taxonomic diversity of merlin and the phylogenetic relationships using experimentally annotated and predicted sequences. By the integration of the BLAST-based analysis using the available partial and whole genome sequences with phylogeny reconstruction, we have generated an evolutionary tree for the entire ERM-family members from various taxa and identified some interesting details about their phylogenetic origin. In addition, we compared sequence variability at functionally significant sites, including the major phosphorylation site of merlin, predicted the secondary structure of the

Table 1: The list of the predicted and experimentally annotated merlin and ERM proteins included in this study.

Species	Proteins	UniProtKB/Swiss-Prot Identifiers	GenBank Accession No.	Entries from Genome Sequencing Projects	Related Resources
Homo sapiens	merlin (NF2)	P35240	AAA36212		http://www.ncbi.nlm.nih.gov/entrez/query.fcgi?db=gmd=Retrieve&dopt=Overview&list_uids=9558
	ezrin	P15311	CAA35893		
	radixin	P35241	AAA36541		
	moesin	P26038	AAA36322		
Pan troglodytes	similar to NF2		XP_515061		http://www.hgsc.bcm.tmc.edu/projects/chimpanzee/
Papio anubis	merlin	P59750	AAO23133		http://www.ncbi.nlm.nih.gov/entrez/query.fcgi?db=gmd=Retrieve&dopt=Overview&list_uids=12965
Bos taurus	ezrin	P31976	AAA30510		http://www.hgsc.bcm.tmc.edu/projects/bovine/
Sus scrofa	radixin	P26044	AAB02865		http://www.tigr.org/tigr-scripts/tgi/T_index.cgi?spec
	moesin	P26042	AAB02864		
Canis familiaris	similar to NF2		XP_534729		http://www.tigr.org/tigr-scripts/tgi/T_index.cgi?spec
Oryctolagus cuniculus	ezrin	Q8HZQ5	AAN06818		http://www.ncbi.nlm.nih.gov/entrez/query.fcgi?db=gmd=Retrieve&dopt=Overview&list_uids=12818
Mus musculus	ezrin	P26040	CAA43086		http://www.tigr.org/tigr-scripts/tgi/T_index.cgi?spec
	radixin	P26043	CAA43087		
	merlin	P46662	CAA52737		
Rattus norvegicus	ezrin	P31977	AAR91694		http://www.tigr.org/tigr-scripts/tgi/T_index.cgi?spec
	NF2		XP_341249		
Gallus gallus	ezrin	Q9YGW6	BAA75497		http://www.tigr.org/tigr-scripts/tgi/T_index.cgi?spec
	radixin	Q9PU45	CAB59977		
	merlin		NP_989828		
Xenopus laevis	unknown protein		AAH77822		http://www.xenbase.org/
Danio rerio	nf2a	Q6Q413	AAS66973		http://www.ensembl.org/Danio_rerio/
	moesin	Q503E6	AAH95359		
Fugu rubripes	radixin			FRUP00000132603	http://genome.jgi-psf.org/
	moesin			FRUP00000156313	
	merlin			FRUP00000136298	
Tetraodon nigroviridis	unnamed protein 1		CAG08868		http://www.ensembl.org/Tetraodon_nigroviridis/
	unnamed		CAG08250		

Table 1: The list of the predicted and experimentally annotated merlin and ERM proteins included in this study. *(Continued)*

	protein 2				
Ciona intestinalis	erm-like			ci0100149701	http://genome.jgi-psf.org/
	merlin-like			ci0100130636	
Ciona savignyi	merlin-like			paired_scaffold_109	http://www.broad.mit.edu/ftp/
Biomphalaria glabrata	erm-like		AAK61353		http://biology.unm.edu/biomphalaria-genome/
Lytechinus variegates	moesin	P52962	AAC46514		http://www.hgsc.bcm.tmc.edu/projects/seaurchin/
Apis mellifera	similar to schwannomin		XP_392673		http://racerx00.tamu.edu/PHP/bee_search.php
Drosophila melanogaster	merlin	Q24564	AAB08449		http://fbserver.gen.cam.ac.uk:7081/
	moesin	P46150	AAB48934		
Drosophila yakuba	merlin-like			predicted in this work	http://genome.wustl.edu/blast/client.pl
Anopheles gambiae	merlin-like fragment		EAA07087		http://www.tigr.org/tigr-scripts/tgi/T_index.cgi?spec
Caenorhabditis elegans	erm1a	P91015	AAB37643		http://www.wormbase.org/
	erm1b	P91016	AAB37642		
	nfm 1a	Q20307	AAA19073		
	nfm 1b	Q95QG5	AAK68385		
Caenorhabditis briggsae	erm-like			BP:CBP03133	http://www.wormbase.org/
	nfm1			BP:CBP05025	
Caenorhabditis remanie	merlin-like			predicted in this work	http://genome.wustl.edu/blast/client.pl
	erm-like				
Brugia malayi	merlin-like			316.m00022	http://www.tigr.org/tdb/e2k1/bma1/
Schistosoma japonicum	JF2		AAB49033		http://www.nhm.ac.uk/hosted_sites/schisto/
Taenia saginata	myosin-like	Q94815	CAA65728		http://www.ncbi.nlm.nih.gov/entrez/query.fcgi?CMD=protein
Echinococcus multilocularis	EM10		A45620		http://www.sanger.ac.uk/Projects/Echinococcus/
Echinococcus granulosus	EG10	Q24796	CAA82625		
Phanerochaete chrysosporium	---				http://genome.jgi-psf.org/whiterot1/whiterot1.home
Aspergillus flavus	---				http://www.tigr.org/tigr-scripts/tgi/T_index.cgi?spec
Arabidopsis thaliana	---				http://www.tigr.org/tigr-scripts/tgi/T_index.cgi?spec
Oryza sativa	---				http://www.tigr.org/tigr-scripts/tgi/T_index.cgi?spec
Trypanosoma brucei	---				http://www.tigr.org/tigr-scripts/tgi/T_index.cgi?spec
Cryptosporidium parvum	---				http://www.tigr.org/tigr-scripts/tgi/T_index.cgi?species=c_parvum

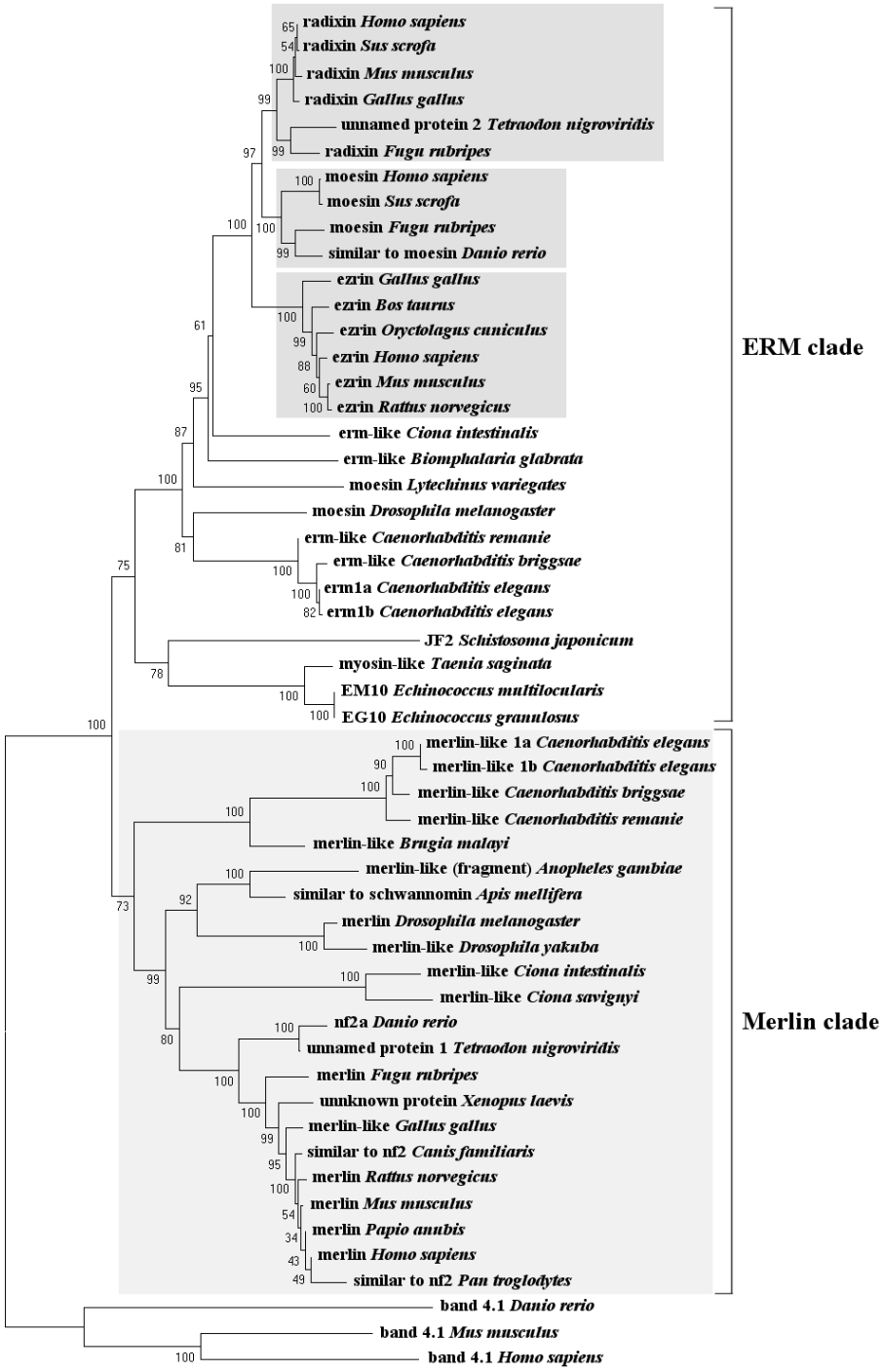

Figure 1

The neighbor-joining tree of the ERM family. The diagram illustrates the basic resolution of the ERM-family members into two major clades, merlin and ERM. Bootstrap support values are shown above each node. Shaded boxes denote different subgroups of the ERM clade in vertebrates, which appeared after the expansion of the ERM-like ancestor. The *Tetraodon nigroviridis* "unnamed protein 1 and 2" sequences (GenBank Accession No. CAG08868 and CAG08250, respectively) and the *Xenopus laevis* "unknown protein" sequence (GenBank Accession No. AAH77822) were grouped based on their similarity to the merlin or ERM sequences.

merlin proteins of various species, and examined the exon-intron structural evolution of the *NF2* gene.

Results and Discussion

BLAST identification of merlin sequences

To identify putative merlin and ERM sequences in a wide range of eukaryotes, we performed BLAST analysis of 15 available genome databases. By searching through all annotated proteins and genome sequences, we identified 50 sequences from 30 species. Table 1 summarizes the full list of the predicted and annotated merlin and ERM proteins identified, and their GenBank and available UniProtKB/Swiss-Prot accession numbers and related resources. No merlin-like sequences were found in the genomes of fungi, plants, and protozoa. While the sequencing projects of the hard ticks are still ongoing at The Institute for Genomic Research (TIGR), amino acid sequences deduced from partial cDNAs of salivary glands, which share a similarity with the FERM domain of merlin, have been noted from *Rhipicephalus appendiculatus* [43], *Amblyomma variegatum* [44], and *Boophilus microplus* [45].

Assembly of predicted merlin sequences from whole genome shotgun

To date, the genomes of *Caenorhabditis remanei and Drosophila yakuba* are represented by a set of contigs [46]. When contigs are ordered, oriented, and positioned with respect to each other by mate-pair reads, they are described as a scaffold. Scaffolds are the main product of the Whole Genome Shotgun strategy and can be assigned to chromosomes using chromosome-specific markers. Although the extensive scaffolds for the genomes of *Caenorhabditis remanei* and *Drosophila yakuba* are not currently available, we were able to assemble predictive protein sequences, which most resemble the merlin sequence of the closely-related organism, *Caenorhabditis elegans* or *Drosophila melanogaster*, respectively, using TBLASTN search across the available sets of contigs. In the *Drosophila yakuba* contig 49.37, we identified a predicted merlin sequence, which is nearly identical to that of the *Drosophila melanogaster* protein with the exception of three positions at the C-terminus, two substitutions at Glu^{468}→Asp and Asn^{579}→Ser and an insertion of Lys at position 575. Also, we found three *Caenorhabditis remanei* contigs, 564.6, 2151.1, and 2151.2, which contained merlin-like sequences with similarity, ranging from 81% to 100%, to its *Caenorhabditis elegans* counterpart. It should be noted that the deduced amino acid sequences were assembled manually, and in some cases, only partial or approximate amino acid sequences could be obtained. Nevertheless, they were useful for the identification of the definite gene in the respective genome and were valuable for the following phylogenetic reconstruction in order to validate the functional relationship and evolution of the definite gene.

Construction of a phylogenetic tree for the ERM family of proteins

To understand the origin and evolution of merlin, we conducted a phylogenetic analysis of the 50 proteins of the ERM family, which were identified from 30 different taxa (Table 1) using the neighbor-joining method [47,48] combined with the molecular evolutionary genetics analysis program MEGA2 [49]. Three protein 4.1 sequences from humans, mice, and zebrafish, respectively, were used as an outgroup. By comparing the bootstrap support values, which denote the number of times a grouping occurs out of 1,000 random samples from the alignment, we constructed a phylogenetic tree for the ERM family of proteins (Figure 1). Based on this phylogenetic analysis, the entire ERM family can be subdivided into the ERM clade and the merlin clade. While both clades show a strongly supported monophyletic origin, the merlin clade can be robustly defined and separated from the ERM clade (the bootstrap support value = 100). We identified a total of 22 sequences for the merlin clade and 28 sequences for the ERM clade. The topology of the phylogenetic tree within the merlin clade appears to agree with the general concept of evolutionary history of speciation.

The merlin clade can be further divided into three groups according to the order of derivation: worms, insects, and Chordata, with the earliest separated genus, *Ciona*, in the last taxonomic unit (Figure 1). The predicted merlin-like sequence from *Caenorhabditis remanei* branched from that of *Caenorhabditis elegans*, and similarly, *Drosophila yakuba* diverged from its *Drosophila melanogaster* counterpart. Both the "unnamed protein 1" of *Tetraodon nigroviridis* and the "unknown protein" of *Xenopus laevis* from the GenBank database are clustered in the Chordata merlin-like group with high bootstrap probabilities (Figure 1), which confirms their identity as merlin homologs. The protein fragment from *Anopheles gambiae*, which bears a sequence similarity to merlin, is grouped together with the *Apis mellifera* merlin-like protein by a bootstrap support value of 100.

Although the ERM-like proteins have been identified in *Taenia saginata*, *Schistosoma japonicum*, *Echinococcus granulosus*, and *Echinococcus multilocularis* [36-39], we did not find any merlin-like sequences in the genomes of these species. The lack of merlin-like sequences in these parasite genomes may be due to incomplete genome sequences in the database; however, this explanation is unlikely because the merlin-like sequence was also not observed in the genome of *Schistosoma mansoni*, which has been rigorously studied [50]. Another possibility is that the absence of merlin-like sequences in these organisms may reflect their adaptation to a parasitic lifestyle and the reduction of various organ systems. Alternatively, the merlin protein may emerge later during evolution. Similarly, no merlin-

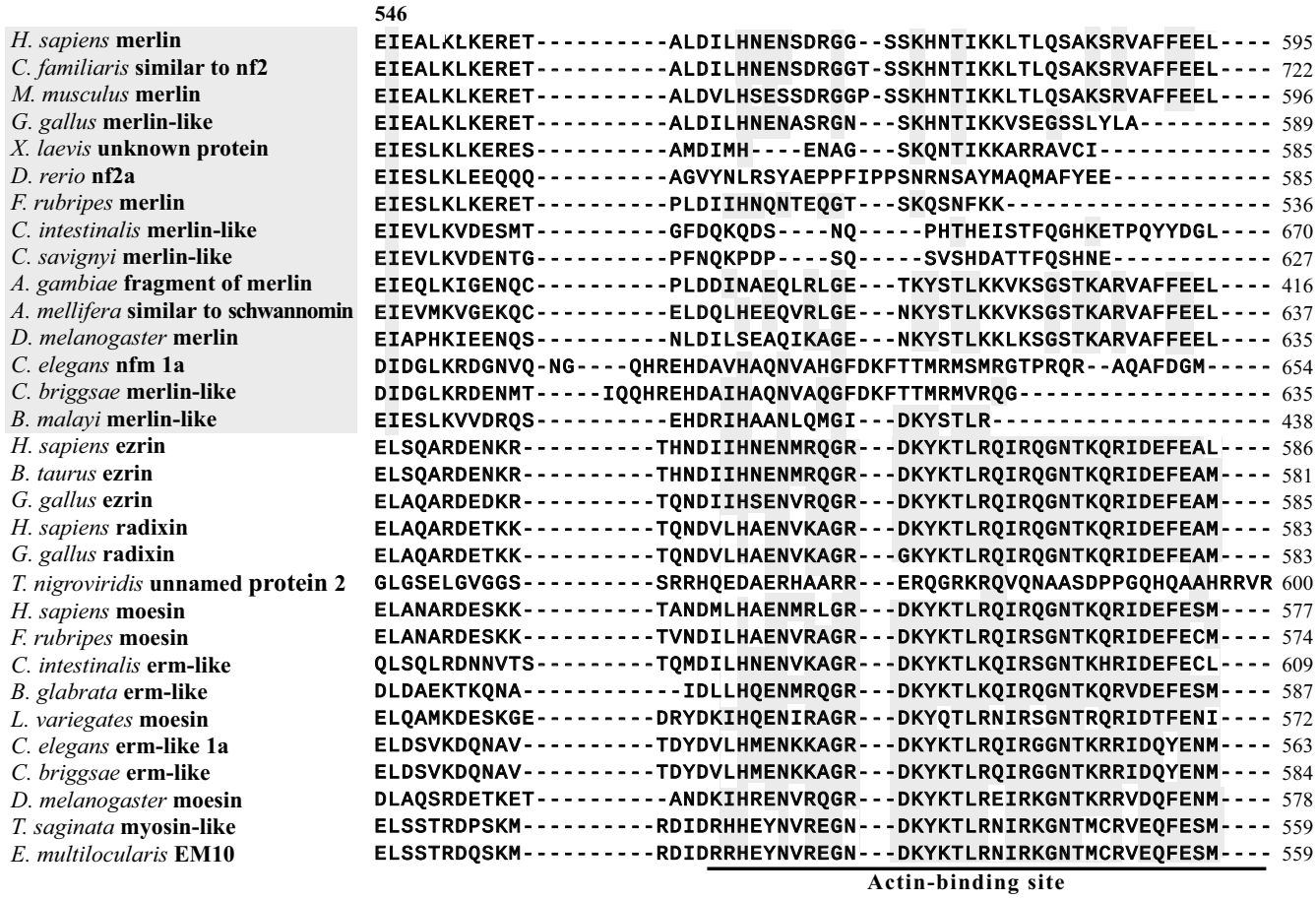

Figure 2

Sequence alignments of functionally important sites in the merlin and ERM proteins of various species. Comparison of the C-terminal region including the actin-binding site and two other predicted significant residues. Databank resources for the ERM-family proteins listed in Table 1 were used in the analysis, and only typical representatives from each group are displayed.

like sequence was found in the complete genomes of protozoa, fungi, and plants. Based on these results, we suppose that the derivation of merlin occurred in the early metazoa after its separation from flatworms.

As illustrated in the ERM clade in Figure 1, the ERM-like proteins found in parasites can be grouped together but form a separate branch from the rest of ERM proteins. Based on the phylogenetic analysis, the clustering of the "unnamed protein 2" of *Tetraodon nigroviridis* with the *Fugu rubripes* radixin protein defines it as a radixin-like protein. It should be noted that the two predicted ERM proteins, erm1a and erm1b of *Caenorhabditis elegans* [51], may represent different transcript variants of the same gene (also see below).

Furthermore, we have observed the evident expansion of the ERM-like ancestor in vertebrates (Figure 1). Since the ERM homolog of *Ciona* emerged prior to the vertebrate clade, it appears that the first duplication of the vertebrate ERM sequence occurred after its divergence from *Ciona*. Subsequent expansion within this sub-family has led to the present existence of three related groups of proteins, ezrin, radixin and moesin; among which, the ezrin group is the most ancient. Such an expanded complement may only be common to the ERM proteins of vertebrates because other metazoa have only one predicted ERM-like homolog [52-56]. Curiously, the increasing number of ERM members that occurred within the vertebrate clade paralleled the evolutionary complexity of the organism. It will be important to understand how these proteins

	Blue Box	204
H. sapiens **merlin**	INLYQ-MTPEMWEERITAWYAEHRGRARDEAEMEYLK	209
C. familiaris **similar to nf2**	INLYQ-MTPEMWEERITAWYAEHRGRARDEAEMEYLK	318
M. musculus **merlin**	INLYQ-MTPEMWEERITAWYAEHRGRARDEAEMEYLK	209
G. gallus **merlin-like**	INLYQ-MTPEMWEERITAWYAEHRGRARDEAEMEYLK	209
X. laevis **unknown protein**	INLYQ-MTPEMWEERITAWYAEHRGRTRDEAEMEYLK	209
D. rerio **nf2a**	LMQYQ-MTPDMWEEKITAWYAEHRNITRDEAEMEYLK	201
F. rubripes **merlin**	INLYQ-MTAEMWEERITACYAEHRGRTRDEAEMEYLK	170
C. intestinalis **merlin-like**	RDQFQSVTGEMWETQITSWYAQHHGLTRDEAELEYLK	207
C. savignyi **merlin-like**	IDQYQSVTGQMWEAQITPWYAGHHGLTRDEAELEYLK	179
A. gambiae **fragment of merlin**	--QYQ-MTPQMWEERIKTWYADHRGMSRDEAEMEYLK	34
A. mellifera **similar to schwannomin**	IDQYQ-MTPEMWEDRIKIWYADHRGMSRDEAEMEYLK	201
D. melanogaster **merlin**	TDQYQ-MTPEMWEERIKTWYMDHEPMTRDEVEMEYLK	203
C. elegans **nfm-1a**	IDQYD-MSADMWRDRIKRWWSRNAGQSREEAELEYLR	203
C. briggsae **merlin-like**	IDQYD-MSADMWRDRIKRWWSRNAGQSREEAELEYLR	203
B. malayi **merlin-like**	IKQYD-MTPOMWEERIKRWWINNSGQSREDAEMEYLR	196
H. sapiens **ezrin**	MDQHK-LTRDQWEDRIQVWHAEHRGMLKDNAMLEYLK	193
B. taurus **ezrin**	MDQHK-LTRDQWEDRIQVWHAEHRGMLKDSAMLEYLK	193
G. gallus **ezrin**	MDQHK-LSRDQWEERIQVWHAEHSGMLKENAMLEYLK	193
H. sapiens **radixin**	LEQHK-LTKEQWEERIQNWHEEHRGMLREDSMMEYLK	193
G. gallus **radixin**	LEQHK-LTKEQWEERIQNWHEEHRGMLREDSMMEYLK	193
T. nigroviridis **unnamed protein 2**	LEQHK-LTKEQWEERIQTWHEEHRSMLREDAMMEYLK	189
H. sapiens **moesin**	LEQHK-LNKDQWEERIQVWHEEHRGMLREDAVLEYLK	193
F. rubripes **moesin**	LDQHK-LNKDQWEERIQVWHEEHKGMMREESMMEYLK	189
C. intestinalis **erm-like**	YEQHK-MTKEQWEERIQTWHCEHGSMTREDAMIEYLK	217
B. glabrata **erm-like**	YDQHK-LTKEQWEERIKSWYAEHKAMLREDAMIEYLK	194
L. variegates **moesin**	IEQHK-MTKEQWYERVSNWHQEHLSLSKEDAITEYMK	192
C. elegans **erm-like 1a**	LGQFK-LNSEEWERRIMTWWADHRATTREQAMLEYLK	194
C. briggsae **erm-like**	LGQFK-LNSEEWERRIMTWWADHRATTREQAMLEYLK	189
D. melanogaster **moesin**	IDQHK-MSKDEWEQSIMTWWQEHRSMLREDAMMEYLK	194
T. saginata **myosin-like**	KDQYD-QTDEQWFDRIVTYYKDHHDMSREDAMVQYLQ	195
E. multilocularis **EM10**	KEQYD-QTDEQWYERIIAYYKDHHDMSREDAMVQYLQ	195

Figure 3
Alignment of the N-terminal domain, containing the Blue Box and the amino acid residue 204, conserved among the merlin proteins but divergent in the ERM proteins.

evolved and how their functions coordinated because of the important and diverse functions of ERM proteins [8,25,26].

Evolution of the functionally important residues in merlin

Although initial identification of proteins via sequence similarities does not yield a clear indication of their respective functions, analysis of specific conserved regions and residues may provide important information regarding their putative functional characteristics. We conducted pairwise sequence comparison among all obtained merlin and ERM sequences, and identified several regions of interest. The results of the entire sequence alignment are provided in the Additional File 1 and are summarized in

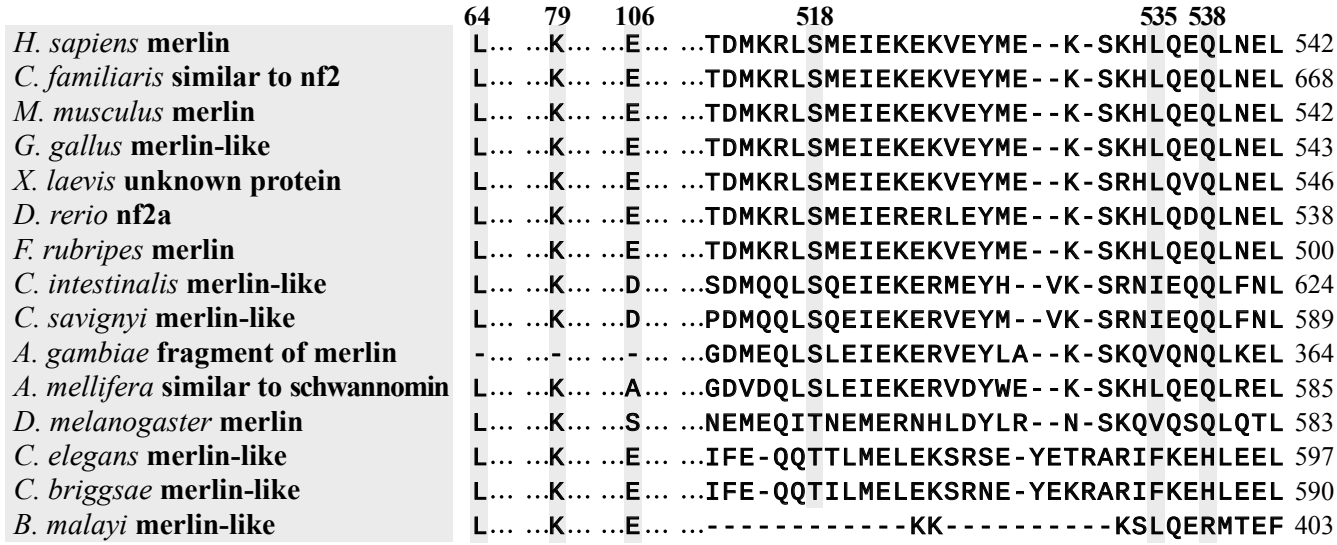

Figure 4
Sequence alignments reveal conservation of several functionally important residues, including the major phosphorylation site of the merlin group.

Figures 2, 3, and 4. Previously, the conservation of the N-terminal FERM domain among human ERM proteins and their functional importance were described [10-13]. In our alignment, we showed that this conservation extended to the merlin and ERM proteins of various species for which sequences were available to date. These data suggest a universal role for the presence of the FERM domain during evolution and further imply an existence of certain evolutionary constraints on the changes of their amino acid residues.

Although merlin lacks the C-terminal actin-binding site found in ERM proteins [7,20,21,57], it can directly interact with the actin cytoskeleton [22,58] or indirectly bind via the actin-binding protein βII spectrin/fodrin [23,24]. Sequence alignment showed extensive amino acid variability in the C-terminal region of the merlin proteins of various species, while a noncontiguous stretch of 25 amino acid residues, including the well-defined actin-binding site, was reliably aligned among all predicted ERM proteins with the exception of the "unnamed protein 2" of *Tetraodon nigroviridis* (Figure 2). According to the phylogenetic tree, the "unnamed protein 2" of *Tetraodon nigroviridis* is classified in the radixin group (Figure 1), and its sequence visibly differs from other radixin proteins only at the C-terminus. The reason for this sequence variability is presently unknown. It may be due to an inaccuracy in sequence assembly from the scaffold. Alternatively, the "unnamed 2 protein" may possess a unique characteristic and will be of considerable interest for functional comparison with other radixin proteins.

Sequence variability at the C-terminal domain of the merlin proteins of various species appears to be high, while some conservation can be found within separate taxonomic groups such as vertebrates, insects, and worms (Figure 2 and Additional File 1). A part of the C-terminal region is absent in *Fugu rubripes*, *Danio rerio*, *C. briggsae*, and *Brugia malayi*. This may be due to partial assembly of the protein sequences, as all of them were predicted by bioinformatics using the available genomes and cDNA sequences. Alternatively, the lack of conservation in the C-terminal region of merlin in these species may imply that this region does not share the same function. In the remaining organisms, the C-terminal amino acid residues have a specific charge distribution, in spite of decreased hydrophilicity, when compared with the C-terminal part of moesin [15]; however, they likely form structures similar to the B, C, and D helices found in moesin.

Unlike ERM proteins, two regions (residues 1–27 and 280–323) in the N-terminal half of merlin have been mapped that are sufficient for binding to F-actin [59,60]. The first 17 amino acids in the N-terminus of human merlin are present in the merlin proteins of various species but not in any ERM proteins (see Additional File 1). The merlin proteins of higher vertebrates contain these residues, eight of which are absent in the merlin proteins of other organisms. Crystal structure analysis suggests that the structure of these extreme N-terminal residues of merlin is disordered in solution but likely becomes ordered as merlin binds to some effector targets [17]. Our sequence alignment indicates that the conservation in the extreme

N-terminus of merlin extends to the first 27 residues. The distribution of specific positively-charged residues also appears to be conserved in this N-terminal portion of the merlin proteins of lower vertebrates and insects. These results suggest that the first 27 amino acids of merlin serve as a common protein-binding motif. It is noteworthy that a similar sequence can be found in the ERM-like protein of *Ciona*; however, the N-terminal region of the *Ciona* protein contains ten positively-charged, basic amino acids, which may affect the binding to actin and/or other proteins (Additional File 1).

The internal actin-binding site, containing residues 280–323 in the N-terminal half of merlin, was found to be highly conserved among all merlin and ERM proteins analyzed, particularly the last 30 amino acid residues (Additional File 1). This region contains an extended helix at the beginning of the α-helical domain and its importance is supported by the identification of several disease-causing mutations (S315F, L316F, L316W, Q324L), which were predicted to destabilize the α-helical segment and disrupt its hydrogen bonding with subdomain A [16-18]. In addition, these residues have been shown to associate with F-actin in moesin [61,62] and to contribute to the ICAM-2-binding site in radixin [14].

Previously, LaJeunesse et al. [63] identified seven functionally important amino acid residues (^{170}YQMTPEM^{177}) in the N-terminal domain of *Drosophila* merlin, called the "Blue Box." These seven amino acids are identical between the human and *Drosophila* merlin proteins but differ from the ERM proteins. Sequence comparison revealed a more conserved pattern of the Blue Box; all seven amino acid residues of the Blue Box were found to be identical in the merlin sequences from vertebrates, fruit flies, and honeybees (Figure 3); however, several amino acid substitutions were found in the Blue Box of worms, fish, and *Ciona*. The most interesting substitutions were found in the merlin-like protein of *Caenorhabditis* from ^{174}ThrProGlu^{176} to ^{174}SerAlaAsp^{176}. It is noteworthy that the methionine residue at position 177 in the Blue Box is conserved among all merlin proteins but not in the ERM proteins. These results further corroborate the functional importance of the seven amino acids in the Blue Box [63].

According to the crystal structure of the FERM domain in human merlin, the Blue Box residues are located in helix α3B of subdomain B [18] and form a defined area that is located on the surface of the protein [17]. Intriguingly, the three-dimensional conformation of merlin's Blue Box region is similar to that of the equivalent region in radixin [18], suggesting that regions in addition to the Blue Box are required for merlin to function as a tumor suppressor. Note that regions closely adjacent to the Blue Box-equivalent residues in human ERM proteins have been shown to participate in the N-terminal to C-terminal intramolecular interaction and ligand-binding, enabling increased mobility and structural changes in the activated FERM domain [14-16,64]. In light of the functional importance of the Blue Box in *Drosophila* merlin, its sequence conservation during evolution, and its location on the surface of merlin, the Blue Box probably participates in specific protein-protein interactions and contributes to other activities of merlin.

As in ERM proteins, phosphorylation affects the subcellular localization and intra- and inter-molecular associations of merlin [13,30-32]. In addition, it modulates the ability of merlin to suppress cell growth [34,35]. Two phosphorylation sites have been mapped to the Ser^{518} and Thr^{576} residues in the merlin protein. Phosphorylation on Ser^{518} has been shown to modulate the ability of merlin to form intramolecular associations and to bind to critical effectors important for growth suppression [34,35]. In contrast, phosphorylation on the Thr^{576} residue has no effect on merlin's functional activity, while phosphorylation on this residue is important for the function of ERM proteins [57,65-67]. Sequence alignment shows that the Ser^{518} residue is conserved across all merlin proteins of various species with the exception of the fruit fly and the worm, which contain a related threonine residue at the corresponding position (Figure 4). Since both the serine and threonine residues can be phosphorylated, we suggest that the corresponding threonine residue in merlin proteins of the fly and the worm may act as a phosphorylation site.

Gutmann et al. showed that mutations within the predicted α-helical region of the human merlin protein had little effect on its function, whereas those in its N- or C-terminus rendered the protein inactive as a negative growth regulator [28,29]. Specifically, five naturally occurring missense mutations, L64P, K79E, E106G, L535P and Q538P, were found to inactivate merlin function. Interestingly, we found that the Leu^{64} and Lys^{79} residues were conserved among the merlin and ERM proteins of various species (Figure 4). According to the crystal structure of the FERM domain of merlin, the L64P substitution would create a cavity in the hydrophobic core of subdomain A and affect its β-sheet structure [17,18]. The significance of this structural information was further supported by the finding that the L64P mutation impaired the ability of merlin to form an intramolecular complex between its two N-terminal interaction sites [28]. Moreover, the L64P mutant lost its ability to bind the cytoplasmic tail of CD44; this interaction correlates with the ability of merlin to function as a growth suppressor [29].

The Lys[79] residue is situated at the end of helix α4A, and mutation at this residue (K79E) may cause the formation of a salt bridge with its neighboring Lys[76] residue, which is normally hydrogen bonded to Tyr[66] in helix α3A [17]. Two equivalent lysine residues, Lys[60] and Lys[63], were found in module F1 of moesin and were predicted to be involved in specific protein interactions, consequently changing the structure of an activated molecule [15,16]. Together with a group of positively-charged amino acids at the beginning of the helix module F3 (R275, K278, R279), these lysine residues interact with the negatively-charged residues (342-REKEE-346) in the C-terminal region [16]. Importantly, most of the homologous positively-charged residues located between lobes F1 and F3 in the radixin protein have been shown to bind to inositol 1,4,5-trisphosphate (IP3) [15]. In addition to Lys[79], the Lys[76] residue was also found to be highly conserved among various merlin and ERM proteins with the exception of the worm protein, which has a Gln[76] instead of Lys[76] (Figure 4 and Additional File 1). Also, the ERM-like proteins of parasites *Taenia saginata*, *Echinococcus granulosus*, and *Echinococcus multilocularis* contain an Arg[76] residue, which is also a basic amino acid residue and may be capable of participating in interactions similar to those of the corresponding lysine residue. On the contrary, in the JF2 protein of *Shistosoma mansoni*, the position equivalent to Lys[60] of moesin is occupied by a glutamic acid residue, and no conservation of residues 275, 278, and 279 in the JF2 protein was found, suggesting a unique structural feature for this S*histosoma* protein.

Several other naturally-occurring missense mutations on human merlin, including E106G, L535P and Q538P, have also been found to affect its functional activity [29,68]. Our sequence alignment revealed that the Glu[106], Leu[535], and Gln[538] residues were conserved among the merlin proteins of the Chordata group (Figure 4), highlighting the general importance of these residues for merlin function. Similar to the L64P mutation described above, the E106G mutation resulted in impaired intramolecular associations of merlin [29]. However, the Leu[64] residue is highly conserved among all merlin and ERM proteins of various species, while Glu[106] is conserved only in the merlin proteins of Chordata and worms. In the crystal structure of the FERM domain of merlin, the Glu[106] residue is located at the linker A-B (α1'B) and participates in the inter-subdomain interaction by forming a hydrogen bond with the Lys[289] residue [17,18]. This interaction may enable subdomain B to rotate closer to subdomain C. Intriguingly, Lys[289] is conserved only among the merlin proteins of mammals, chickens, frogs, honeybees, and mosquitoes (Additional File 1). In the merlin proteins of other species, a negatively-charged aspartic or glutamic acid occupies this position, except in fish. Instead of lysine, an arginine residue was found in the homologous position of all ERM proteins (e.g., Arg[273] for moesin), except for the ERM-like proteins in parasites (Additional File 1). This Arg[273] residue, located at the beginning of the helix of subdomain F3, lies in a specific cleft between subdomains F1 and F3 with the positively-charged R275, K278, and R279 residues. According to the structure of radixin, the IP_3-binding site is located at this basic cleft [14]. This region in the moesin protein has also been shown to interact with its C-terminal domain [16].

It should be mentioned that residues that are conserved in the merlin proteins, but not in the ERM proteins, of various species may be important for elucidating the functional difference between the merlin and ERM proteins. We found that the glutamic acid residue at position 204 of human merlin was conserved among all merlin proteins (Figure 3). In contrast, variable and uncharged amino acids were found at the corresponding position of the ERM proteins. Crystal structure of the FERM domain of human merlin shows that the Glu[204] residue lies in the beginning of helix α4B and is included in a specific stretch of amino acids in subdomain B [17]. By sequence alignment of human merlin and ERM proteins, about 70 amino acids, including this specific stretch of residues, which are unique to merlin but different in ERM proteins, were identified (see Additional File 1). The majority of these amino acids can be subdivided into three clusters; each of them is specific to its corresponding subdomain and is located on the surface of the protein. These results suggest that these 70 amino acids likely take part in protein-protein interactions. Note that the conserved stretch of amino acids in subdomain B also includes the functionally important "Blue Box" discussed above.

Similarly, the isoleucine residue at position 546 was found to be conserved among the merlin proteins of various species, while a leucine residue was present in the corresponding position in all ERM proteins (Figure 2). The residue homologous to Leu[529] in the C-terminal domain of moesin is located at the end of helix A with other hydrophobic residues, tightly contacting the hydrophobic faces of helices B and D of subdomain F2 [15]. Although the information about such an interaction in merlin is presently unavailable, additional crystal structure analysis should allow us to better understand the importance of this amino acid residue. In addition, it will be interesting to test whether mutations in the conserved amino acid residues identified in this study could affect protein function.

Predicted secondary structure of merlin and comparative analysis of the predicted α-helical region

Turunen et al. previously reported that the central region of ERM proteins contained approximately 200 residues that were predicted to be mostly α-helical [19]. To exam-

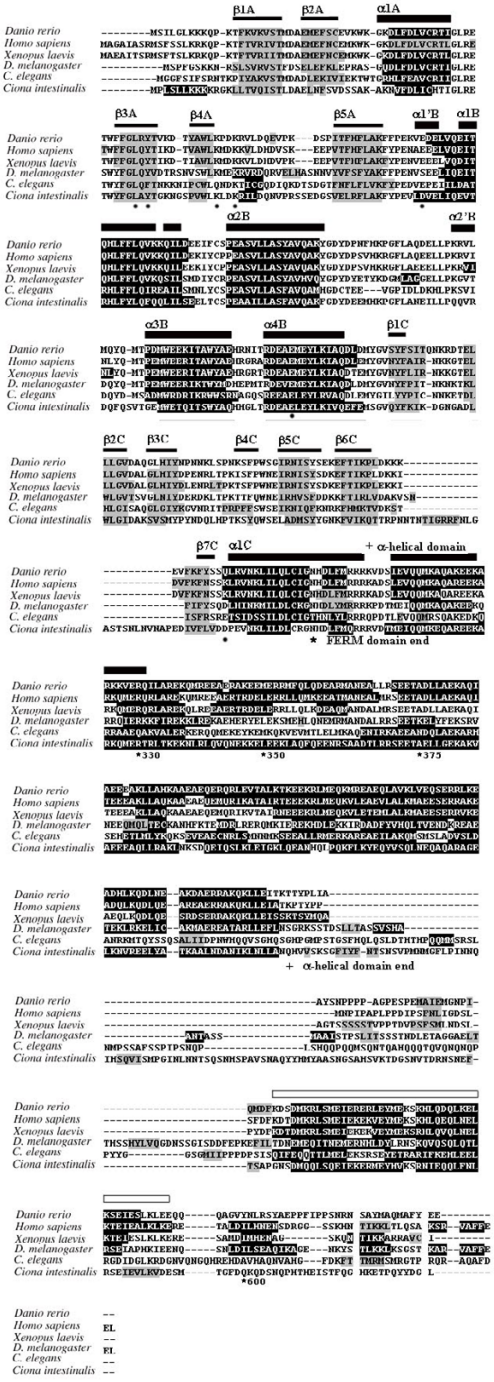

Figure 5

The predicted secondary structures for the merlin proteins of various species. The region with a predicted β-sheet structure is shaded in grey, while the region with an α-helix structure is shaded in black. These predicted secondary structures correspond to the crystal structural data [18], which are shown above the alignment with the α-helix region indicated with a thick black bar and the β-sheet region with a thin black bar. The predicted α-helical domain in the central-to-C-terminal region of merlin is marked with an open bar. Asterisks denote known domains of the merlin protein with numbers pointing to the end of truncated *Drosophila* merlin protein discussed in the text. "+" denotes the beginning and the end of the predicted α-helical domain. The positions of specific residues in the FERM domain discussed in the text are denoted by black dots below the aligned sequences.

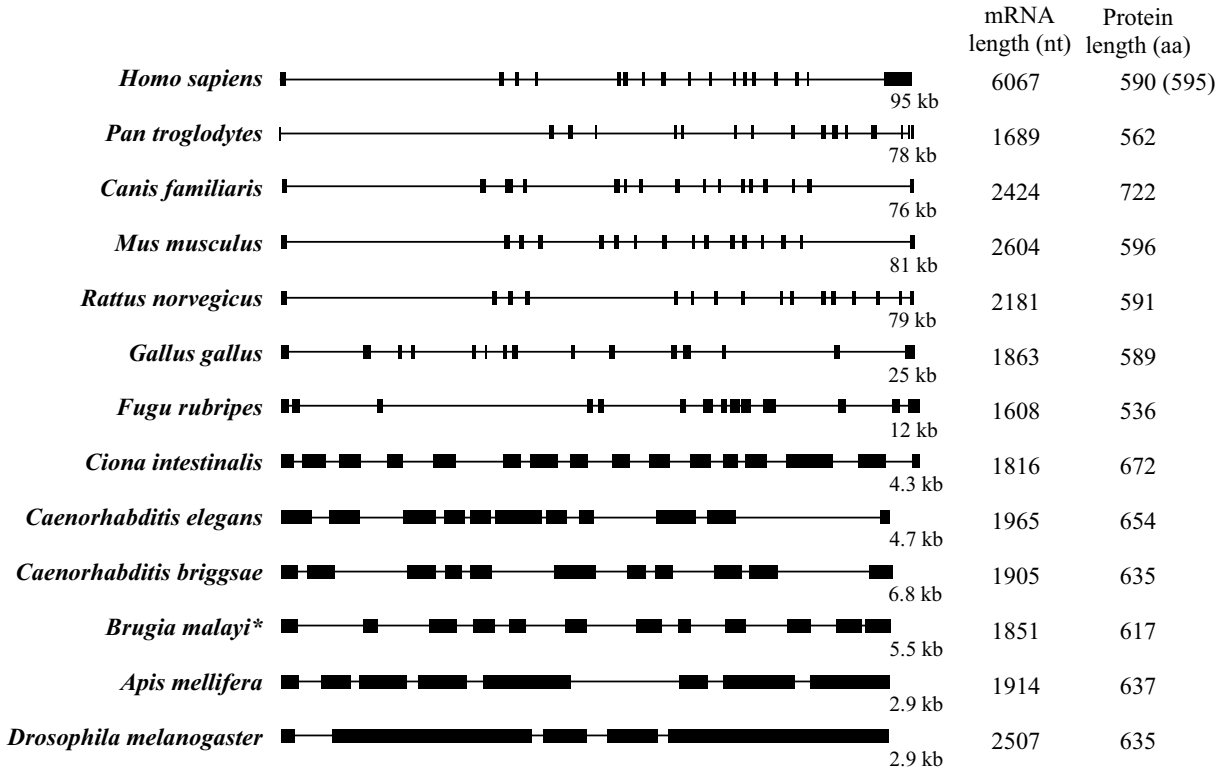

Figure 6

Schematic diagram of the exon and intron structures for the merlin genes of various species. The horizontal line depicts the merlin gene with its size indicated in base pairs (bp) on the right. The upright boxes represent exons. The lengths of the merlin mRNA sequences available in the database are shown in nucleotides (nt) and the lengths of the predicted merlin proteins are also indicated in amino acids (aa). The indicated human *NF2* mRNA refers to the longest, full-length transcript identified, which contains a long 3' untranslated region [72]. Two major *NF2* isoforms I and II are produced via alternative splicing and the lengths of their protein products are shown with that of isoform I indicated in the parentheses. It should be noted that Northern blot analysis detected the rat and mouse *NF2* mRNAs of about 4.5 kb, indicating that the sizes of the rodent *NF2* mRNAs shown here are not full-length. The asterisk (*) denotes the exon-intron structure of *Brugia malayi* predicted from this study.

ine whether there was a similar structure present in all merlin proteins, we analyzed 21 merlin sequences from various organisms and predicted their secondary structures using the JPRED program [69]. The results of such an analysis for six representative species are presented in Figure 5. The predicted locations of α-helices and β-sheets in the N-terminal domain support the experimental findings from the structural analysis of the FERM domain of human merlin protein [18]. In addition, a predicted α-helical structure in the central-to-C-terminal region was found to be conserved among the merlin proteins of various species analyzed. Previously, it was shown that a truncated merlin protein of *Drosophila*, containing residues 1–600, lost the ability to localize to the cytoplasm and was concentrated at the plasma membrane [63]. However, two smaller truncated proteins, consisting of residues 1–350 or 1–375, were only loosely associated with the plasma membrane. These results suggest that the predicted α-helical region of merlin is important for its intracellular localization. Since almost the entire α-helical domain was absent in these truncated proteins, we suggest that it may contain a determinant for membrane association. This notion is further supported by the observation that additional truncated proteins, containing residues 1–300 or missing almost the entire α-helical domain, were diffusely localized to the cytoplasm.

In human merlin, the predicted α-helical structure is situated between residues K312 and K478 (Figure 5 and Additional File 1). The N-terminal border of this structure was clearly recognized for 21 merlin sequences analyzed, whereas the C-terminal boundary could be traced only up to Urochordata (*Ciona*) and Nematoda (*Caenorhabditis*). This α-helical domain, predicted from all 21 merlin

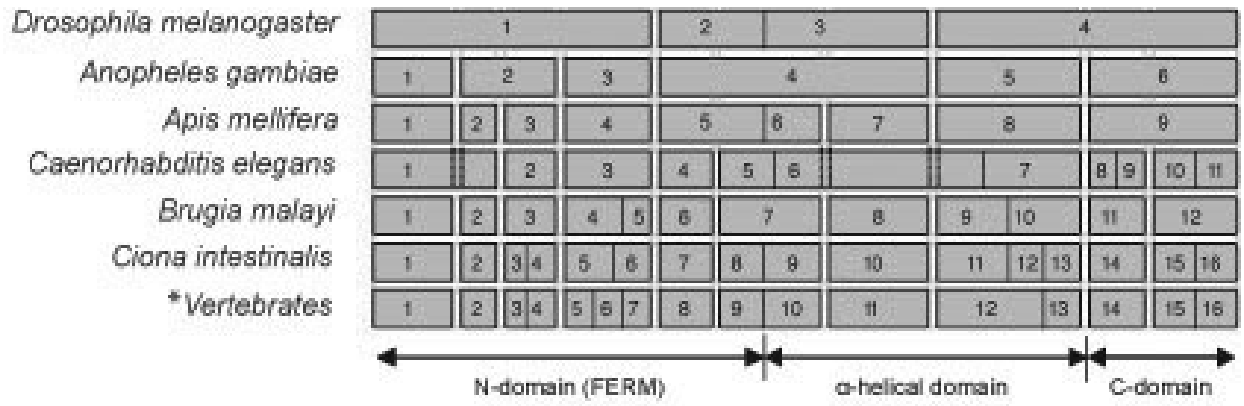

Figure 7

The alignment of exons with specific domains of merlin reveals the presence of homologous introns. Boxes represent the coding exons with numbers indicated accordingly. The locations of the three commonly discussed domains are marked with horizontal arrows under exons. The boundaries among these domains were defined according to the human merlin protein. The asterisk indicates that the exon structure shown is common to the merlin genes of all vertebrate species studied, including *Homo sapiens*, *Pan troglodytes*, *Canis familaris*, *Mus musculus*, *Rattus norvegicus*, *Danio rerio*, *Fugu rubripes*, *and Xenopus laevis*. The overall merlin gene structure of *Gallus gallus* is similar, except that exons 15 and 16 are fused together in this species.

sequences, contains a high density of charged amino acids (from about 25% in *Ciona* to greater than 40% in vertebrates). Sequence alignment reveals 19 conserved amino acid residues in this predicted α-helical domain (Additional File 1). The amino acid identity for the predicted α-helical domain within each phylogenetic group is as follows: 1) Genus *Drosophila* (*D. melanogaster* and *D. yakuba*) – 99% (one amino acid substitution), 2) Genus *Caenorhabditis* (*C. elegans*, *C. briggsae*, and *C. remanie*) – 85.7%, 3) Genus *Ciona* (*C. intestinalis* and *C. savignyi*) – 71.7%, 4) vertebrates – 63.5%, and 5) mammals – 90%. Taken together, these results indicate that the merlin proteins of various species contain a conserved α-helical domain in the central to C-terminal region.

Exon-intron structural evolution of the merlin gene

Recent progress in automated computational analysis of partially and completely sequenced genomes using a gene prediction method and the analysis of expressed sequence tag (EST) has provided considerable opportunities not only to describe novel genes but also their exon-intron structures. Such an approach also allows the examination of the presence of different splicing variants/isoforms. To understand the evolution of the exon-intron structure of the merlin gene, we assembled all available *NF2* gene-related sequences from various taxa. Using the sequences of proteins, mRNAs, and combined contigs [70], we established the structure of the merlin-like gene for *Brugia malayi*, which consists of 12 exons and 11 introns (Figure 6). Analogously, the homolog of the *NF2* gene in *Caenorhabditis elegans* was found to contain 11 exons and 10 introns. It should be mentioned that the two *NF2*-like sequences, nfm-1a and nfm-1b of *Caenorhabditis elegans*, differ from each other only by the sequence of the last exon (Additional File 1), suggesting that they represent cDNA isoforms.

As shown in Figure 6, the general arrangement of the merlin gene structure is conserved among mammalian species, especially at the region that encodes the N-terminal domain, albeit the length of the genes may differ slightly. The human *NF2* gene consists of 17 exons and spans about 95 kb of DNA [5,6,71,72]. *NF2* transcripts undergo alternative splicing, generating multiple isoforms [72-79]. Isoform I, missing exon 16, and isoform II, containing all 17 exons, are the two predominant species. As the result of alternative splicing, isoform 1 encodes a 595 amino acid protein. Isoform II differs from isoform I only at the C-terminus. Insertion of exon 16 into the mRNA provides a new stop codon, resulting in a 590 amino acid protein that is identical to isoform I over the first 579 residues. Because of the presence of a long 3' untranslated region, the longest *NF2* isoform I RNA, containing the sequence from all 17 exons, is about 6.1 kb [72]. The merlin genes of other mammalian species, R*attus norvegicus*, *Canis familiaris*, *Mus musculus* and *Pan troglodytes*, contain 16 exons (Figures 6 and 7). In addition, alternatively spliced merlin isoforms have been found in rodent species [80-82]. On the contrary, the structure of the merlin genes of *Gallus gallus* and *Fugu rubripes* are arranged differently from those of mammalian species, with 15 and 14 exons spanning much shorter DNAs of only about 25 kb and 12.3 kb, respectively (Figure 6). Although the *NF2* gene of *Fugu rubripes* has not yet been completely assembled, we

predict that it lacks the sequences of the first and the last exons of the mammalian *NF2* gene based on our sequence alignment (see Additional File 1).

In spite of the presence of 16 exons and the size of transcript similar to those found in some vertebrates, the gene for the merlin-like protein of *Ciona intestinalis* is relatively small with only about 4.3 kb (Figure 6). This tendency towards reduction of intron length and number continues to be seen in the merlin gene of worms and insects (Figures 6 and 7). The gene for the merlin-like protein of *Caenorhabditis elegans*, consisting of 11 exons, spans about 4.7-kb DNA, and that of *Brugia malayi*, containing 12 exons, is about 5.5 kb in length. The *NF2* homolog of *Drosophila melanogaster* and the gene for the merlin-like protein of *Apis mellifera* are only about 2.9 kb, the smallest in the merlin clade, and consist of 5 and 8 exons, respectively (Figure 6). Interestingly, some conservation of the positions of homologous introns can be found in the *NF2* gene from various species (Figure 7); however, the sizes of their introns are variable. Such an evolutionary conservation of homologous introns implies that the presence of regulatory sequences in the introns to regulate the transcriptional event.

Unlike the sizes and structures of the merlin or merlin-like genes in various organisms, the lengths of the merlin proteins and transcripts have not changed very much during evolution (Figure 6). Moreover, several functionally important domains of merlin also remain conserved. Since the merlin protein of the insect emerged after deviation from that of the worm, which was anciently derived from the common ancestor (Figure 1), it appears that the decrease in gene size and exon number occurred specifically within the insect group. This branch of merlin evolution is likely to develop independently and in the opposite direction from those more recently developed merlin proteins of Chordata. Parallel evolution towards the increase in merlin gene size and exon number between the worm and Chordata appears to be less likely. Thus, it is possible that the common ancestor for the merlin genes of the worm, the insect, and Chordata may contain a few more exons. During evolution, reduction of introns and/or fusion of exons occur within the insect group.

It is evident that the genome of the insect is more complicated than that of the worm. The simplification of the merlin gene structure in the insect is unique and may have a functional significance. This observation may explain the lack of splicing variants of the *NF2* homolog in *Drosophila*, in contrast to those merlin isoforms found in mammals [72-82] and in *Caenorhabditis elegans* as we predicted in this study.

Conclusion

We have conducted the phylogenetic analysis of merlin diversity across metazoan genomes using the experimentally annotated and predicted sequences in conjunction with bioinformatic tools. We show that the merlin proteins have a monophyletic origin with a root in the early metazoa. We have also established the expansion of the ERM-like ancestors within the vertebrate clade that occurred after its separation from Urochordata. Several potentially important sites that are conserved among all merlin proteins but are divergent in the ERM members have been identified. As supported by the crystal structure data, these conserved residues are likely to be important for merlin function. Analysis of the evolution of the merlin gene structure reveals the existence of common splicing variants in human and *Caenorhabditis elegans*. While a trend toward the increase of gene length during evolution was observed, a reduction of intron number and length appears to occur in the merlin gene of the insect group. Taken together, our results have important implications for the evolution of the merlin proteins and their possible functional variability in different taxa.

Methods

BLAST search

Initial sequences of genes and proteins of interest from various organisms were identified from the National Center for Biotechnology Information (NCBI) database [83] using the BLAST algorithm [84]. We then searched the desirable sequences across genomic databases of completely or partially sequenced genomes available at The Sanger Institute [85] and The Institute for Genomic Research (TIGR; [86]). Also, we investigated other available sequence databases that contain information for specific organisms. The sources of sequences of the predicted or experimentally annotated merlin and ERM proteins are summarized in Table 1.

To obtain the entire amino acid sequence of an annotated protein, we used UniProt from Universal Protein Resource [87]. The erythrocyte membrane proteins 4.1 sequences of *Homo sapiens* (GenBank: CAI21970), *Mus musculus* (GenBank: NP_001006665), and *Danio rerio* (GenBank: AAQ97985) were also included in the analysis as an outgroup. Because of the presence of many non-conserved and large introns in the genes of interest, we conducted BLAST search using TBLASTN alignment algorithm in the cases where no protein sequences were available.

Alignments and phylogeny

The CLUSTAL_X program [88] was used to align the characterized or predicted protein sequences from different species. Phylogenetic analysis was carried out using the MEGA2.1 program [49].

Secondary structure prediction

The secondary structure prediction program JPRED [69] was used to predict the secondary structure of each merlin protein from various species. This program uses physical-chemical properties of the amino acid sequence and neural network for recognition of α-helices and β-sheets.

List of Abbreviations

NF2 – Neurofibromatosis type 2

NF2 – the *Neurofibromatosis type 2* gene

ERM – ezrin, radixin, and moesin

FERM – 4.1, ezrin, radixin, and moesin

IP3 – inositol 1,4,5-trisphosphate

TIGR – The Institute for Genomic Research

EST, expressed sequence tag

NCBI – National Center for Biotechnology Information

Authors' contributions

KG and AB carried out the phylogenetic analysis of merlin diversity across metazoan genomes and drafted the manuscript. EMA and LVO helped with the design of the study and preparation of data for the figures. LSC was the principal investigator of the project and participated in the design, coordination, and writing of the manuscript. All authors read and approved the final manuscript

Additional material

Additional File 1

Complete amino acid sequence alignment of the merlin and ERM proteins. *Letters shaded in grey illustrate the conservation pattern of aligned sequences. The names of the merlin proteins from various species are shown in yellow. The conserved residues of the 'Blue Box' are also shaded in yellow. The positions of residues discussed in the text are colored in red. Blue letters denote the conserved residues within the predicted α-helical domain. Numbers indicated at the end of each sequence refer to the positions of the last residue within each protein analyzed.*

Click here for file

[http://www.biomedcentral.com/content/supplementary/1471-2148-5-69-S1.pdf]

Acknowledgements

We sincerely thank Sarah S. Burns, Maria Mihaylova, and D. Bradley Welling for critical reading of the manuscript, and Hui-Chun Hsiao and Kiselev Arkadyi for the help with the diagrams. This study was supported by grants from the US Department of Defense Neurofibromatosis Research Program and Russian Fund of Fundamental Investigations.

References

1. Dacks JB, Doolittle WF: **Novel syntaxin gene sequences from *Giardia*, *Trypanosoma* and algae: implications for the ancient evolution of the eukaryotic endomembrane system.** *J Cell Sci* 2002, **115:**1635-1642.
2. Hsu S: **Bioinformatics in reproductive biology – functional annotation based on comparative sequence analysis.** *J Rep Immunol* 2004, **63:**75-83.
3. NIH Consensus Statement on Acoustic Neuroma: *Neurofibromatosis Res. Newsletter* 1992, **8:**1-7.
4. Bull. World Health Org: **Prevention and control of neurofibromatosis: Memorandum from a joint WHO/NNFF meeting.** 1992, **70:**173-182.
5. Rouleau GA, Merel P, Luchtman M, Sanson M, Zucman J, Marineau C, Hoang-Xuan K, Demczuk S, Desmaze C, Plougastel B, Pulst SM, Le noir G, Bijlsma E, Fashold R, Dumanski J, de Jong P, Parry D, Eldridge R, Aurias A, Delattre O, Thomas G: **Alteration in a new gene encoding a putative membrane-organizing protein causes neuro-fibromatosis type 2.** *Nature* 1993, **363:**515-521.
6. Trofatter JA, MacCollin MM, Rutter JL, Murrell JR, Duyai MP, Parry DM, Eldridge RE, Kley N, Menon AG, Pulaski K, Haase VH, Ambrose CM, Munroe D, Bove C, Haines JL, Martuza RL, MacDonald ME, Seizinger BR, Short MP, Buckner AJ, Gusella JF: **A novel moezin-, ezrin-, radixin-like gene is a candidate for the neurofibromatosis 2 tumor suppressor.** *Cell* 1993, **72:**791-800.
7. Algrain M, Arpin M, Louvard D: **Wizardry at the cell cortex.** *Current Biol* 1993, **3:**451-454.
8. Tsukita S, Oishi K, Sato N, Sagara J, Kawai A, Tsukita S: **ERM family members as molecular linkers between the cell surface glycoprotein CD44 and actin-based cytoskeleton.** *J Cell Biol* 1994, **126:**391-401.
9. Takeuchi K, Kawashima A, Nagafuchi A, Tsukita S: **Structural diversity of band 4.1 superfamily members.** *J Cell Sci* 1994, **107:**1921-1928.
10. Chishti AH, Kim AC, Marfatia SM, Lutchman M, Hanspal M, Jindal H, Liu SC, Low PS, Rouleau GA, Mohandas N, Chasis JA, Conboy JG, Gaskard P, Takakuwa Y, Huang SC, Benz EJ Jr, Bretcher A, Fenon RG, Gusella JF, Ramesh V, Solomon F, Marchesi VT, Tsukita S, Hoover KB: **The FERM domain: a unique module involved in the linkage of the cytoplasmic proteins to the membrane.** *Trends Biochem Sci* 1998, **23:**281-282.
11. Hamada K, Shimizu T, Matsui T, Tsukita S, Hakoshima T: **Structural basis of the membrane-targeting and unmasking mechanisms of the radixin FERM domain.** *EMBO J* 2000, **19:**4449-4462.
12. Herrlich P, Morrison H, Sleeman J, Orian-Rousseau V, Konig H, Weg-Remers S, Ponta H: **CD44 acts both as a growth- and invasiveness-promoting molecule and as a tumor-suppressing cofactor.** *Ann NY Acad Sci* 2000, **910:**106-118.
13. Morrison H, Sherman LS, Legg J, Banine F, Isacke C, Haipek CA, Gutmann DH, Ponta H, Herrlich P: **The NF2 tumor suppressor gene product, merlin, mediates contact inhibition of growth through interactions with CD44.** *Genes Dev* 2001, **15:**968-980.
14. Hamada K, Shimizu T, Yonemura S, Tsukita Sh, Tsukita S, Hakoshima T: **Structural basis of adhesion – molecule recognition by ERM proteins revealed by the crystal structure of the radixin – ICAM-2 complex.** *EMBO J* 2003, **22:**502-514.
15. Pearson MA, Reczek D, Bretscher A, Karplus PA: **Structure of the ERM protein moesin reveals the FERM domain fold masked by an extended actin binding tail domain.** *Cell* 2000, **101:**259-270.
16. Edwards SD, Keep NH: **The 2.7 Å crystal structure of the activated FERM domain of moesin: an analysis of structural changes on activation.** *Biochemistry* 2001, **40:**7061-7068.
17. Kang BS, Cooper DR, Devedjiev Y, Derewenda U, Derewenda ZS: **The structure of the FERM domain of merlin, the neurofibromatosis type 2 gene product.** *Acta Crystollogr Sec D* 2002, **58:**381-391.
18. Shimizu T, Seto A, Maita N, Hamada K, Tsukita Sh, Tsukita S, Hakoshima T: **Structural basis for neurofibromatosis type2.** *J Biol Chem* 2002, **277:**10332-10336.
19. Turunen O, Sainio M, Jaaskelainen J, Carpen O, Vaheri A: **Structure-function relationships in the ezrin family and the effect of tumor-associated point mutations in neurofibromatosis 2 protein.** *Biochim Biophys Acta* 1998, **1387:**1-16.

20. Turunen O, Wahlström T, Vaheri A: **Ezrin has a COOH-terminal acting-binding site that is conserved in the ezrin protein family.** *J Cell Biol* 1994, **126:**1445-1453.
21. Gary R, Bretscher A: **Ezrin self-association involves binding of an N-terminal domain to a normally masked C-terminal domain that includes the F-actin binding site.** *Mol Biol Cell* 1995, **6:**1061-1075.
22. Sainio M, Zhao F, Heiska L, Turunen O, den Bakker M, Zwarthoff E, Lutchman M, Rouleau GA, Jaaskelainen J, Vaheri A, Carpen O: **Neurofibromatosis 2 tumor suppressor protein colocalizes with ezrin and CD44 and associates with actin-containing cytoskeleton.** *J Cell Sci* 1997, **110:**2249-2260.
23. Scoles DR, Huynh DP, Morcos PA, Coulsell ER, Robinson NG, Tamanoi F, Pulst SM: **Neurofibromatosis 2 tumor suppressor schwannomin interacts with βII-spectrin.** *Nature Genet* 1998, **18:**354-359.
24. Neill GW, Crompton MR: **Binding of the merlin-I product of the neurofibromatosis type 2 tumour suppressor gene to a novel site in beta-fodrin is regulated by association between merlin domains.** *Biochem J* 2001, **358:**727-735.
25. Bretscher A, Edwards K, Fehon RG: **ERM proteins and merlin: integrators at the cell cortex.** *Nature Rev Mol Cell Biol* 2002, **3:**586-599.
26. Ramesh V: **Merlin and ERM proteins in Schwann cells, neurons and growth cones.** *Nature Rev Neurosci* 2004, **5:**462-470.
27. McClatchey AI: **Merlin and ERM proteins: unappreciated roles in cancer development?** *Nature Rev Cancer* 2003, **3:**877-883.
28. Gutmann DH, Haipek CA, Hoang Lu K: **Neurofibromatosis 2 tumor suppressor protein, merlin, forms two functionally important intramolecular associations.** *J Neurosci Res* 1999, **58:**706-716.
29. Gutmann DH, Hirbe AC, Haipek CA: **Functional analysis of neurofibromatosis 2 (NF2) missense mutations.** *Hum Mol Genet* 2001, **10:**1519-1529.
30. Shaw RJ, Paez JG, Curto M, Yaktine A, Pruitt WM, Saotome I, O'Bryan JP, Gupta V, Ratner N, Der CJ, Jacks T, McClatchey AI: **The Nf2 tumor suppressor, merlin, functions in Rac-dependent signaling.** *Dev Cell* 2001, **1:**63-72.
31. Kissil JL, Johnson KC, Eckman MS, Jacks T: **Merlin phosphorylation by p21-activated kinase 2 and effects of phosphorylation on merlin localization.** *J Biol Chem* 2002, **277:**10394-10399.
32. Xiao GH, Beeser A, Chernoff J, Testa JR: **p21-activated kinase links Rac/Cdc42 signaling to merlin.** *J Biol Chem* 2002, **277:**883-886.
33. Alfthan K, Heiska L, Gronholm M, Renkema GH, Carpen O: **Cyclic AMP-dependent protein kinase phosphorylates merlin at serine 518 independently of p21-activated kinase and promotes merlin-ezrin heterodimerization.** *J Biol Chem* 2004, **279:**18559-18566.
34. Surace EI, Haipek CA, Gutmann DH: **Effect of merlin phosphorylation on neurofibromatosis 2 (NF2) gene function.** *Oncogene* 2004, **23:**580-587.
35. Rong R, Surace EI, Haipek CA, Gutmann DH, Ye K: **Serine 518 phosphorylation modulates merlin intramolecular association and binding to critical effectors important for NF2 growth suppression.** *Oncogene* 2004, **23:**8447-8454.
36. Frosch PM, Frosch M, Pfister T, Schaad V, Bitter-Suermann D: **Cloning and characterisation of an immunodominant major surface antigen of *Echinococcus multilocularis*.** *Mol Biochem Parasitol* 1991, **48:**121-130.
37. Frosch PM, Muhlschlegel F, Sygulla L, Hartmann M, Frosch M: **Identification of a cDNA clone from the larval stage of *Echinococcus granulosus* with homologies to the *E. multilocularis* antigen EM10-expressing cDNA clone.** *Parasitol Res* 1994, **80:**703-705.
38. Kurtis JD, Ramirez BL, Wiest PM, Dong KL, El-Meanawy A, Petzke MM, Johnson JH, Edmison J, Maier RA Jr, Olds GR: **Identification and molecular cloning of a 67-kilodalton protein in *Schistosoma japonicum* homologous to a family of actin-binding proteins.** *Infect Immun* 1997, **65:**344-347.
39. Hubert K, Cordero E, Frosch M, Solomon F: **Activities of the EM10 protein from *Echinococcus multilocularis* in cultured mammalian cells demonstrate functional relationships to ERM family members.** *Cell Motil Cytoskeleton* 1999, **42:**178-188.
40. McCartney BM, Fehon RG: **Distinct cellular and subcellular patterns of expression imply distinct functions for the *Drosophila* homologues of moesin and the neurofibromatosis 2 tumor suppressor, merlin.** *J Cell Biol* 1996, **133:**843-852.
41. Hansson CM, Ali H, Bruder CE, Fransson I, Kluge S, Andersson B, Roe BA, Menzel U, Dumanski JP: **Strong conservation of the human NF2 locus based on sequence comparison in five species.** *Mamm Genome* 2003, **14:**526-536.
42. Chen Y-X, Gutmann DH, Haipek CA, Martinsen BJ, Bronner-Fraser M, Krull CE: **Characterization of chicken Nf2/merlin indicates regulatory roles in cell proliferation and migration.** *Dev Dyn* 2004, **229:**541-54.
43. [http://www.tigr.org/tigr-scripts/tgi/est_report.pl?GB=CD797075&species=r_appendiculatus].
44. [http://www.tigr.org/tigr-scripts/tgi/est_report.pl?GB=BM291669&species=a_variegatum].
45. [http://www.tigr.org/tigr-scripts/tgi/est_report.pl?GB=CK190110&species=B.microplus].
46. [http://genome.wustl.edu/blast/client.pl].
47. Saitou N, Nei M: **The neighbor-joining method: A new method for reconstructing phylogenetic trees.** *Mol Biol Evol* 1987, **4:**406-425.
48. Kumar S, Gadagkar SR: **Efficiency of the neighbor-joining method in reconstructing deep and shallow evolutionary relationships in large phylogenies.** *J Mol Evol* 2000, **51:**544-53.
49. Kumar S, Tamura K, Jakobsen IB, Nei M: **MEGA2: molecular evolutionary genetics analysis software.** *Bioinformatics* 2001, **17:**1244-1245.
50. [http://www.tigr.org/tdb/e2k1/sma1/].
51. [http://www.wormbase.org/db/gene/gene?name=F42A10.2a;class=Transcript].
52. The C. elegans Sequencing Consortium: **Genome sequence of the nematode C. elegans: a platform for investigating biology.** *Science* 1998, **282:**2012-2018.
53. Adams MD, Celniker SE, Holt RA, Evans CA, *et al.*: **The genome sequence of Drosophila melanogaster.** *Science* 2000, **287:**2185-2195.
54. Dehal P, Satou Y, Campbell RK, Chapman J, *et al.*: **The draft genome of Ciona intestinalis: insights into chordate and vertebrate origins.** *Science* 2002, **298:**2157-2167.
55. Stein LD, Bao Z, Blasiar D, Blumenthal T, *et al.*: **The genome sequence of Caenorhabditis briggsae: a platform for comparative genomics.** *PLoS Biol* 2003, **1:**E45.
56. Foster JM, Kumar S, Ganatra MB, Kamal IH, Ware J, Ingram J, Pope-Chappell J, Guiliano D, Whitton C, Daub J, Blaxter ML, Slatko BE: **Construction of bacterial artificial chromosome libraries from the parasitic nematode *Brugia malayi* and physical mapping of the genome of its Wolbachia endosymbiont.** *Int J Parasitol* 2004, **34:**733-746.
57. Matsui T, Maeda M, Doi Y, Yonemura S, Amano M, Kaibuchi K, Tsukita S: **Rho-kinase phosphorylates COOH-terminal threonines of ezrin/radixin/moezin (ERM) proteins and regulates their head-to-tail association.** *J Cell Biol* 1998, **140:**647-657.
58. Deguen B, Merel P, Goutebroze L, Giovannini M, Reggio H, Arpin M, Thomas G: **Impaired interaction of naturally occurring mutant NF2 protein with actin-based cytoskeleton and membrane.** *Hum Mol Genet* 1998, **7:**217-226.
59. Xu H, Gutmann DH: **Merlin differentially associates with the microtubule and acting cytoskeleton.** *J Neurosci Res* 1998, **51:**403-415.
60. Brault E, Gautreau A, Lamarine M, Callebaut I, Gilles T: **Normal membrane localization and actin association of the NF2 tumor suppressor protein are dependent on folding of its N-terminal domain.** *J Cell Sci* 2001, **114:**1901-1912.
61. Roy C, Martin M, Mangeat P: **A dual involvement of the amino terminal domain of ezrin in F- and G-actin binding.** *J Biol Chem* 1997, **272:**20088-20095.
62. Martin M, Roy C, Montcourrier P, Sahuquet A, Mangeat P: **Three determinants in ezrin are responsible for cell extension activity.** *Mol Cell Biol* 1997, **8:**1543-1557.
63. LaJeunesse DR, McCartney BM, Fehon RG: **Structural analysis of *Drosophila* merlin reveals functional domains important for growth control and subcellular localization.** *J Cell Biol* 1998, **141:**1589-1599.
64. Smith WJ, Nassar N, Bretscher A, Cerione RA, Karplus PA: **Structure of the active N-terminal domain of ezrin.** *J Biol Chem* 2003, **278:**4949-4956.

65. Nakamura F, Amieva MR, Furthmayr H: **Phosphorylation of threonine 558 in the carboxyl-terminal actin-binding domain of moesin by thrombin activation of human platelets.** *J Biol Chem* 1995, **270:**31377-31385.
66. Oshiro N, Fukata Y, Kaibuchi K: **Phosphorylation of moesin by rho-associated kinase (Rho-kinase) plays a crucial role in the formation of microvilli-like structures.** *J Biol Chem* 1998, **273:**34663-34666.
67. Dard N, Louvet-Vallee S, Santa-Maria A, Maro B: **Phosphorylation of ezrin on threonine T567 plays a crucial role during compaction in the mouse early embryo.** *Dev Biol* 2004, **271:**87-97.
68. Stokowski RP, Cox DR: **Functional analysis of the neurofibromatosis type 2 protein by means of disease – causing point mutations.** *Am J Hum Genet* 2000, **66:**873-891.
69. [http://www.compbio.dundee.ac.uk/~www-jpred/].
70. [http://www.tigr.org/tdb/e2k1/bma1/].
71. Zucman-Rossi J, Legoix P, Der Sarkissian H, Cheret G, Sor F, Bernardi A, Cazes L, Giraud S, Ollagnon E, Lenoir G, Thomas G: **NF2 gene in neurofibromatosis type 2 patients.** *Hum Mol Genet* 1998, **7:**2095-2101.
72. Chang L-S, Akhmametyeva EM, Wu Y, Zhu L, Welling DB: **Multiple transcription initiation sites, alternative splicing, and differential polyadenylation contribute to the complexity of human neurofibromatosis 2 transcripts.** *Genomics* 2002, **79:**63-76.
73. Arakawa H, Hayashi N, Nagase H, Ogawa M, Nakamura Y: **Alternative splicing of the NF2 gene and its mutation analysis of breast and colorectal cancers.** *Hum Mol Genet* 1994, **3:**565-568.
74. Bianchi AB, Hara T, Ramesh V, Gao J, *et al.*: **Mutations in transcript isoforms of the neurofibromatosis 2 gene in multiple human tumour types.** *Nature Genet* 1994, **6:**185-192.
75. Hara T, Bianchi AB, Seizinger BR, Kley N: **Molecular cloning and characterization of alternatively spliced transcripts of the mouse neurofibromatosis 2 gene.** *Cancer Res* 1994, **54:**330-335.
76. Hitotsumatsu T, Kitamoto T, Iwaki T, Fukui M, Tateishi J: **An exon 8-spliced out transcript of neurofibromatosis 2 gene is constitutively expressed in various human tissues.** *J Biochem (Tokyo)* 1994, **116:**1205-1207.
77. Pykett MJ, Murphy M, Harnish PR, George DL: **The neurofibromatosis 2 (*NF2*) tumor suppressor gene encodes multiple alternatively spliced transcripts.** *Hum Mol Genet* 1994, **3:**559-564.
78. Nishi T, *et al.*: **Neurofibromatosis 2 gene has novel alternative splicing which control intracellular protein binding.** *Int J Oncol* 1997, **10:**1025-1029.
79. Schmucker B, Tang Y, Kressel M: **Novel alternatively spliced isoforms of the neurofibromatosis type 2 tumor suppressor are targeted to the nucleus and cytoplasmic granules.** *Hum Mol Genet* 1999, **8:**1561-1570.
80. Haase VH, Trofatter JA, MacCollin M, Tarttelin E, Gusella JF, Ramesh V: **The murine NF2 homologue encodes a highly conserved merlin protein with alternative forms.** *Hum Mol Genet* 1994, **3:**407-411.
81. Huynh DP, Nechiporuk T, Pulst SM: **Alternative transcripts in the mouse neurofibromatosis type 2 (NF2) gene are conserved and code for schwannomins with distinct C-terminal domains.** *Hum Mol Genet* 1994, **3:**1075-1079.
82. Gutmann DH, Wright DE, Geist RT, Snider WD: **Expression of the neurofibromatosis 2 (NF2) gene isoforms during rat embryonic development.** *Hum Mol Genet* 1995, **4:**471-478.
83. [http://www.ncbi.nlm.nih.gov/BLAST].
84. Altschul SF, Madden TL, Schaffer AA, Zhang J, Zhang Z, Miller W, Lipman DJ: **Gapped BLAST and PSI-BLAST: a new generation of protein database search programs.** *Nucleic Acids Res* 1997, **25:**3389-3402.
85. [http://www.sanger.ac.uk/DataSearch].
86. [http://tigrblast.tigr.org/tgi/].
87. [http://www.ebi.uniprot.org/index.shtml].
88. Thompson JD, Gibson TJ, Plewniak F, Jeanmougin F, Higgins DG: **The CLUSTAL_X windows interface: flexible strategies for multiple sequence alignment aided by quality analysis tools.** *Nucleic Acids Res* 1997, **15:**4876-4882.

Otology & Neurotology
27:197–208 © 2006, Otology & Neurotology, Inc.

The Molecular Biology of Vestibular Schwannomas: Dissecting the Pathogenic Process at the Molecular Level

*Brian A. Neff, *D. Bradley Welling, †Elena Akhmametyeva, and *†‡§¶Long-Sheng Chang

*Departments of *Otolaryngology, †Pathology, ‡Pediatrics, §Molecular Cellular Biochemistry, and ¶Veterinary Biosciences, The Ohio State University College of Medicine and Children's Hospital, Columbus, Ohio*

Objective: The goal of this article was to review concisely what is currently known about the tumorigenesis of vestibular schwannomas.
Background: Recent advances in molecular biology have led to a better understanding of the cause of vestibular schwannomas. Mutations in the neurofibromatosis type 2 tumor suppressor gene (*NF2*) have been identified in these tumors. In addition, the interactions of merlin, the protein product of the *NF2* gene, and other cellular proteins are beginning to give us a better idea of *NF2* function and the pathogenesis of vestibular schwannomas.
Methods: Review of the relevant basic science studies at our institution as well as the basic science and clinical literature.
Results: The clinical characteristics of vestibular schwannomas and neurofibromatosis type 2 syndromes are reviewed and related to alterations in the *NF2* gene. Studies demonstrating our current understanding of tumor developmental pathways are highlighted. In addition, methods of clinical and genetic screening for neurofibromatosis type 2 disease are outlined. Avenues for the development of potential future research and therapies are discussed.
Conclusion: Great strides have been made to identify why vestibular schwannomas develop at the molecular level. Continued research is needed to find targeted therapies with which to treat these tumors. **Key Words:** Acoustic neuroma—*NF2* gene—Merlin—Neurofibromatosis type 2—Vestibular schwannoma.

Otol Neurotol **27:**197–208, 2006.

Vestibular schwannomas are histologically benign tumors of the neural sheath that originate on the superior or inferior vestibular branches of Cranial Nerve VIII. The term "vestibular schwannoma" is preferred over the more commonly used term "acoustic neuroma" because these tumors are not neuromas, nor do they arise from the acoustic (cochlear) nerve. They occur either as sporadic unilateral tumors or bilateral tumors; the development of bilateral vestibular schwannomas is the hallmark of neurofibromatosis type 2 (NF2). Various types of vestibular schwannomas can be loosely grouped into unilateral sporadic vestibular schwannomas, bilateral or NF2-associated schwannomas, and cystic schwannomas.

This study was supported by the National Institutes of Health and the Department of Defense Neurofibromatosis Research Program.

Address correspondence and reprint requests to Bradley Welling, M.D., Ph.D., 456 West 10th Avenue, Columbus, OH 43210, U.S.A.; E-mail: welling.1@osu.edu

Unilateral schwannomas are the most common presentation, and they constitute 95% of all vestibular schwannomas. Sporadic vestibular schwannomas occur in approximately 10 per 1 million persons per year (1). However, the true incidence may be higher, as highlighted by Anderson et al., who demonstrated an incidence of 7 unsuspected schwannomas per 10,000 brain magnetic resonance imaging (MRI) studies (0.07%) (2). Sporadic tumors usually occur in the fourth and fifth decades, with a mean presentation of 50 years of age. Although histologically benign, schwannomas can, if large enough, cause hydrocephalus, brainstem compression, herniation, and death. Most commonly, however, they are associated with hearing loss, tinnitus, imbalance, and other symptoms related to compression of adjacent cranial nerves.

NF2 is clinically an autosomal dominant disease that is highly penetrant (3). NF2-associated tumors account for approximately 5% of all vestibular schwannomas. Patients who inherit an abnormal copy of the *NF2* tumor suppressor gene have a 95% chance of

developing bilateral vestibular schwannomas. However, approximately one-half of the cases have no family history of NF2, and thus they represent new germline mutations that were not inherited. Other disease features of NF2 include intracranial meningiomas, ependymomas, spinal schwannomas, and presenile lens opacities (4,5). Of the four different sets of diagnostic criteria for NF2, the Manchester criteria are the most sensitive, and they are summarized in Table 1 (6). NF2 is now recognized as a disease that is distinctly different from neurofibromatosis type 1 (NF1) or von Recklinghausen's disease. NF1, which is associated with multiple peripheral neuromas, is caused by a mutation in the *NF1* tumor suppressor gene on chromosome 17.

NF2 is currently subdivided into three groups on the basis of clinical presentation and severity of disease (7). The Wishart type has a more severe clinical presentation. In addition to bilateral vestibular schwannomas, patients often suffer from associated spinal tumors, with a typical onset in the late teens or early 20s (8). The Gardner type has a later onset and a less severe presentation. Although patients present with bilateral schwannomas, the incidence of associated intracranial tumors is less common (9). A more recently recognized third category of NF2 has been termed mosaic NF2, where a mutation occurs in embryogenesis rather than in the germline DNA; therefore, only a portion of the patients' cells carry the mutation (10,11). This is different from those patients with traditional NF2 who inherit the mutation from their parent. Kluwe et al. recently estimated that mosaicism may account for 24.8% (58 of 233) of NF2 cases of any subtype among patients whose parents did not display the disease (11). Patients with somatic mosaicism can display bilateral vestibular schwannomas if the postzygotic mutation occurred early in embryogenesis. However, they may also display an atypical presentation, or segmental NF2, in which the patient has a unilateral vestibular schwannoma and an ipsilateral, additional intracranial tumor, such as a meningioma, if the postzygotic mutation occurred late in development (10). Unlike the traditional forms of NF2, the risk of passing NF2 caused by mosaicism to future offspring is very low (12); however, in the unlikely event that NF2 is inherited from a mosaic parent, the offspring will carry the mutation in all their cells, and the clinical presentation would be severe and consistent with the conventional form of NF2.

Schwannomatosis, a recently defined form of neurofibromatosis, is characterized by multiple schwannomas without any NF2-associated vestibular schwannomas. Patients with schwannomatosis frequently present with intractable pain rather than cranial nerve deficits. They do not develop other intracranial tumors or malignancies. MacCollin et al. noted that approximately one-third of patients with schwannomatosis had tumors in an anatomically limited distribution, such as a single limb, several contiguous segments of the spine, or one side of the body (13). Sporadic cases of schwannomatosis are as common as NF2, but few cases of familial schwannomatosis have been identified. This is in contradistinction to NF1 and NF2, which are autosomal dominant, highly penetrant syndromes that are frequently found clustered in families. The underlying molecular disruption in schwannomatosis is a pattern of somatic *NF2* gene inactivation incompatible with NF1 or NF2, but this has not been completely defined.

Cystic vestibular schwannomas are a particularly aggressive group of unilateral, sporadic schwannomas that invade the surrounding cranial nerves, splaying them throughout the tumors. Cystic vestibular schwannomas are associated with either intratumoral or extratumoral cysts that develop in the loosely organized Antoni B tissues. In addition, a higher degree of nuclear atypia is seen in cystic tumors (14). Careful distinction must be drawn between the truly cystic schwannomas and the very common heterogeneous schwannomas, which are not as aggressive in their clinical behavior. MRI clearly distinguishes between the solid and cystic vestibular schwannomas. Cystic regions of the tumors are hyperintense on T2-weighted images, and the cysts do not enhance with gadolinium administration. The noncystic component of the cystic tumors enhances with gadolinium in a manner similar to the unilateral and NF2-associated schwannomas (Fig. 1). Cystic tumors may grow rapidly, and they are very difficult to manage because of the high rate of hearing loss and facial nerve paralysis that occurs after surgical removal (15). When compared with solid tumors of a similar size, the rate of complete facial nerve paralysis (House-Brackmann Grade VI) with surgical removal of cystic tumors was 41%, as compared with 27% for that of solid unilateral schwannomas (16). Cystic tumors are also more likely to have continued growth and facial nerve paralysis even with stereotactic radiation treatments than either the unilateral

TABLE 1. *Manchester criteria for the diagnosis of NF2*[a,b]

A. Bilateral vestibular schwannomas
B. First-degree relative with NF2 and unilateral vestibular schwannoma or any two of the following: meningioma, schwannoma, glioma, neurofibroma, juvenile posterior subcapsular lens opacity
C. Unilateral vestibular schwannoma and any two of the following: meningioma, schwannoma, glioma, neurofibroma, posterior subcapsular lenticular opacities
D. Multiple meningiomas (two or more) and unilateral vestibular schwannoma or any two of the following: schwannoma, glioma, neurofibroma, cataract

[a]Data from Baser et al. (6).

[b]Note: "any two of" refers to two individual tumors or cataract. For example, a unilateral schwannoma and two gliomas would meet the criteria.

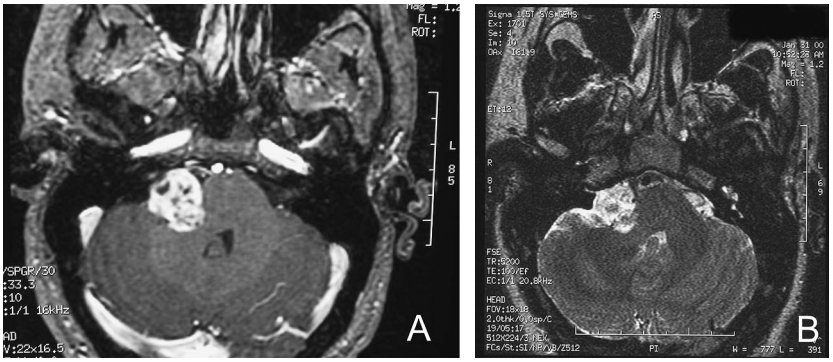

FIG. 1. MRI scans of vestibular schwannomas. (*A*) Axial T1-weighted MRI scan with gadolinium contrast. There is an enhancing right-sided cerebellopontine angle tumor with areas of central low intensity that correspond with cysts within this pathologically confirmed vestibular schwannoma. (*B*) Axial T2-weighted MRI scan. The tumor is more hyperintense than the typical T2 signal characteristics of a vestibular schwannoma. In addition, there are focal areas of increased signal intensity that correspond with the intratumoral cysts.

spontaneous or NF2-associated schwannomas (17,18). To date, some differences in the gene expression profiles of cystic tumors have been identified, compared with those of sporadic and NF2-associated tumors (19,20); however, there has not been a clear tumorigenic pathway demonstrated to definitively explain the aggressive growth seen with cystic schwannomas, and this is an area of current investigation.

Although the effectiveness of treatment with current surgical and radiation treatments for vestibular schwannomas are generally good, treatment-related morbidity continues to be problematic. The field of molecular biology is proposed as the discipline to advance the level of diagnosis and to improve the treatment of vestibular schwannomas. When applied to various neurotologic abnormalities, "molecular neurotology" may soon develop as a medical discipline in a manner similar to the advent of surgical neurotology in the 1960s. A brief review of the recent discoveries and advances in the molecular biology of vestibular schwannomas follows.

THE *NF2* GENE

The *NF2* gene was localized to chromosome 22 through a genetic linkage analysis (21). Subsequently, 23 patients from a large NF2 kindred were studied, and the *NF2* locus was further mapped close to the center of the long arm of chromosome 22 (22q12) (22). After genetic and physical mapping, positional cloning studies led to the discovery of the *NF2* gene. In 1993, Trofatter et al. and Rouleau et al. independently identified the *NF2* gene, which is frequently mutated in NF2-related vestibular schwannomas (23, 24). Since that time, mutations in the *NF2* gene have been found not only in NF2 tumors but also in sporadic unilateral schwannomas and cystic schwannomas (Table 2) (25–39). In addition, mutations within the *NF2* gene have been frequently identified in meningiomas and occasionally identified in other tumor types such as mesotheliomas (26,39–42).

NF2 MUTATIONS AND THEIR CLINICAL CORRELATION

Several groups have attempted to correlate clinical expression of tumors with specific *NF2* mutations in vestibular schwannomas and other NF2-associated tumors. A number of somatic mutations and their specific clinical behavior in vestibular schwannomas have been characterized in sporadic unilateral tumors and NF2 tumors (25–31,38–40,43–47). We previously studied a series of patients who had vestibular schwannomas and found that the frequency, type, and distribution of *NF2* mutations were shown to be different between the sporadic and familial NF2 tumors (25). Mutations were identified in 66% of the sporadic cases but in only 33% of the NF2 cases; therefore, the rate of detection of a mutation in unilateral schwannomas was significantly higher than that in familial schwannomas. Point mutations accounted for the majority of mutations identified in NF2 patients, whereas small deletions accounted for the majority of mutations found in the sporadic unilateral tumors (28,30,43).

Studies were also conducted to determine whether the genotype could be a predictor of disease severity. The clinical phenotypes of NF2, Wishart and Gardner, were further examined, as was a potential third phenotype, mosaic or segmental NF2. Deletion mutations that cause truncation of the NF2 protein have been reported to cause a more severe phenotype in NF2 pedigrees (28,30,43), whereas missense mutations or small in-frame insertions in the *NF2*-coding region have been reported to associate with a mild phenotype (25,26,31,39,46). However, this has not held true in other studies, which showed that some missense mutations associated with a severe phenotype. In addition, missense mutations within the α-helical domain of the NF2 protein appear to associate with a less severe phenotype than those within the conserved FERM domain (48). This lack of genotype-phenotype correlation was also seen for large deletions, which could give rise to mild phenotypes and the previously reported severe disease expression (49).

TABLE 2. *Summary of NF2 mutation detection*

Reference	No. of NF2 patients	No. of non-NF2 patients	% Detected	Methods*
Jacoby[28] 1994	8	30	53	SSCP
MacCollin[27] 1994	33		64	SSCP
Merel[26] 1995	91		35	DGGE
Welling[25] 1996	32	29	54	HA, DS
Ruttledge[31] 1996	111		54	SSCP
Mautner[32] 1996	9	3	75	SSCP
Parry[30] 1996	32		66	SSCP
Kluwe[29] 1996	59		34	SSCP
Evans[34] 1998	125		43	DS
Zucman-Rossi[33] 1998	19		84	DGGE, DS
Antinheimo[35] 2000	8	12	70	CGH
Hung[36] 2000	20		80	NIRCA

*HA, heteroduplex analysis; DS, direct sequencing; DGGE, denaturing gradient gel electrophoresis; SSCP, single-stranded conformation polymorphism analysis; CGH, comparative genomic hybridization; NIRCA, nonisotopic RNAase cleavage assay.

Given the heterogeneity of clinical response to various types of mutations, no clear genotype-to-phenotype correlation has been established, and this is further evidenced by the fact that phenotypic variability within the NF2 families with the same mutation has been seen (32). By extensive screening of the *NF2* gene, Zucman-Rossi et al. reported an 84% mutation detection rate in vestibular schwannomas; thus, additional mechanisms for inactivation of the *NF2* gene in some patients may exist (33). The possibility of a modifier gene has been suggested (50). Also, mutation or methylation in the regulatory region of the *NF2* gene has been suggested as a possible mechanism of gene inactivation (51,52). The complexity of *NF2* transcripts generated by posttranscriptional alternative splicing and differential polyadenylation may also be considered as possible means of inactivating the *NF2* gene (52).

ALTERNATIVELY SPLICED *NF2* MRNA ISOFORMS IN VESTIBULAR SCHWANNOMAS

DNA consists of regions called exons and introns. The exons are the segments of DNA that are transcribed and brought together as a mature mRNA product. The introns represent the sections of DNA that are transcribed but are spliced out during RNA processing. Alternative splicing is the mechanism by which different exon combinations are brought together to produce multiple mRNA transcripts from the same gene. These alternatively spliced transcripts can include all of the gene's exons or can be missing one or multiple exons. The different RNA transcripts produced from this process are termed mRNA isoforms.

The coding region of the *NF2* gene consists of 17 exons, and the *NF2* gene undergoes alternative splicing of these coding exons. An example of *NF2* mRNA isoforms is shown in Figure 2. Multiple alternatively spliced *NF2* transcripts have been identified in various human cells. The most common isoforms in these cells were isoforms II (containing all 17 exons) and I (without exon 16) (26,52–54).

We have also examined the expression of alternatively spliced *NF2* mRNA isoforms in vestibular schwannomas (one NF2 schwannoma, seven sporadic schwannomas, and two cystic schwannomas). Cloning and sequencing analysis showed that the expression pattern and relative frequency of the alternatively spliced *NF2* transcripts appeared to be different from those detected in other human cell types described above. Particularly, in addition to isoforms I and II, these schwannomas expressed a high percentage of the *NF2* mRNA isoform lacking exons 15 and 16 (Fig. 2). These alternatively spliced *NF2* transcripts could encode different protein products (Please provide name and initials of source of unpublished dataunpublished data).

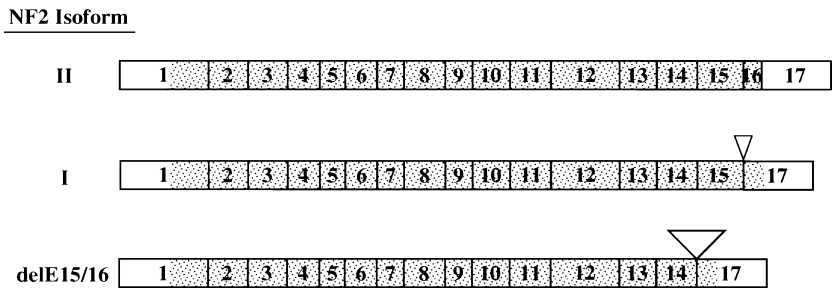

FIG. 2. The *NF2* gene is transcribed into mRNA; however, alternative splicing can produce different mRNA transcripts or isoforms. Different exon combinations can be brought together to produce multiple mRNAs from the same gene. Our studies showed that isoform I, II, and delE15/16 were the most common isoforms found in vestibular schwannomas examined.

Presently, the role of alternative splicing of *NF2* mRNA is not well understood. It is possible that the functional contribution of the *NF2* tumor suppressor may require a balanced expression of various isoform proteins in Schwann cells and/or other cell lineages (52,55). Alternative splicing may be another mechanism for Schwann cells to inactivate merlin function and/or to generate isoforms that have additional properties conducive to tumor formation. We are presently conducting experiments to test these possibilities.

THE *NF2* GENE PROMOTER

The upstream and downstream untranslated regions of the *NF2* gene have been characterized so that these regions could be screened for mutations in both sporadic and familial tumors in which no mutation was found in the *NF2*-coding region. Our laboratory has mapped the major transcription initiation site of the *NF2* gene and found that multiple regions in the *NF2* promoter are required for full *NF2* promoter activity (52,56). Both positive and negative *cis*-acting regulatory elements required for transcription of the *NF2* gene have been found in the 5′ flanking region of the promoter. A G/C-rich sequence located in the proximal promoter region, which can be bound by the Sp1 transcription factor, serves as a positive regulatory element. Both the 5′ and 3′ flanking regions of the human *NF2* locus are G/C rich and could serve as targets for gene methylation and inactivation (52).

THE NF2 PROTEIN: STRUCTURE AND FUNCTION

The *NF2*-coding region encompasses 90 kb of DNA on chromosome 22 (23,24,33). It encodes a 595–amino acid protein product which has been named merlin (for *m*oesin-*e*zrin-*r*adixin *l*ike prote*in*) or *schwannomin* (derived from schwannoma) (23,24). For simplicity, the *NF2* protein will be referred to as merlin in this article.

Merlin shares a high degree of homology to the erythrocyte protein 4.1–related superfamily of proteins, which act to link the actin cytoskeleton to the plasma membrane. In particular, three proteins, ezrin, radixin, and moesin, referred to as the ERM family, share a great deal of structural similarity with merlin (24). The proteins belonging to this family all have a similar N-terminal globular domain, also known as the FERM domain, followed by an α-helical stretch, and finally a charged C-terminus (57). The key functional domains of merlin may lie within the highly conserved FERM domains and the unique C-terminus of the protein. The ERM proteins have been shown to be involved in cellular remodeling involving the actin cytoskeleton (58). These proteins bind actin filaments in the cytoskeleton via a conserved C-terminal domain and possibly via a second actin-binding site in the N-terminal half of the protein (59,60).

Like the ERM proteins, merlin is expressed in a variety of cell types, where it localizes to the areas of membrane remodeling, particularly membrane ruffles, although its precise distribution may differ from the ERM proteins expressed in the same cell (61). Interestingly, schwannoma cells from NF2 tumors show dramatic alterations in the actin cytoskeleton and display abnormalities in cell spreading (62). These results suggest that merlin may play an important role in regulating both the actin cytoskeleton-mediated processes and cell proliferation (63). However, it should be noted that merlin has a growth suppression role, whereas other ERM-family members seem to facilitate cell growth.

MERLIN ACTS AS A TUMOR SUPPRESSOR

Overexpression of the *NF2* gene in mouse fibroblasts or rat schwannoma cells can limit cell growth (46,64) and suppress cell transformation by the ras oncogene (65). The growth control of certain Schwann cells and meningeal cells is lost in the absence of *NF2* function, suggesting that *NF2* mutations and merlin deficiency disrupt some aspect of intracellular signaling that leads to cellular transformation. Together with animals, these findings demonstrate merlin's ability to act as a tumor suppressor.

Mouse Models

Scientists have developed *Nf2* knockout mice that were designed to be missing one or both copies of the *Nf2* gene in the germline. Intriguingly, heterozygous *Nf2* knockout mice go on to develop osteosarcomas and, less often, fibrosarcomas or hepatocellular carcinomas (66). Genetic analysis of these tumors shows that nearly all of them are missing both *Nf2* alleles because of a mutation causing a loss of the second *Nf2* allele. The fact that tumor growth occurs in the absence of both *Nf2* alleles indicates that the *Nf2* gene possesses a classical tumor suppressor function. However, none of the heterozygous *Nf2* mice develop tumors or clinical manifestations associated with human NF2.

Homozygous *Nf2* mutant mice, which are designed to be missing both *Nf2* alleles, also do not demonstrate clinical characteristics of human NF2, and the mutant embryos die at approximately seven days of gestation, indicating that a homozygous *Nf2* mutation is embryonic lethal (67). Together with our preliminary data showing that the *Nf2* gene is expressed early in embryogenesis (Akhmametyeva EM, et al. Data unpublished.), these results indicate that the *Nf2* gene product plays an important role during early embryonic development.

By engineering mice whose Schwann cells have exon 2 excised and removed from both *Nf2* alleles,

conditional homozygous *Nf2* knockout mice have been produced that display some characteristics of NF2 including schwannomas, Schwann cell hyperplasia, cataracts, and osseous metaplasia (68). Although these results argue that loss of merlin is sufficient for schwannoma formation in vivo, none of the tumors observed in these conditional knockout mice were found on the vestibular nerve. This is in contrast to those vestibular schwannomas commonly found in patients with NF2. Although these mouse models are a valuable tool with which to study potential therapeutic interventions for NF2, further work is needed to develop a mouse model that phenotypically displays schwannomas originating from the VIIIth cranial nerve.

MERLIN CELL SIGNALING AND REGULATION

In addition to the actin cytoskeleton, merlin has been shown to associate with cell membrane domains, which are highly enriched in signaling molecules that regulate cellular responses to proliferative and antiproliferative stimuli (69). To date, several proteins that are likely to interact with merlin have been identified. These include the ERM proteins, hyalurin receptor CD44, F-actin, paxillin, microtubules, βII-spectrin, β1-integrin, β-fodrin, the regulatory cofactor of Na^+-H^+ exchanger, SCHIP-1, hepatocyte growth factor-regulated tyrosine kinase substrate, p21-activated kinase 1 and 2 (Pak1 and Pak2), Rac1, RalGDS, N–WASP, Erbin, and RIB subunit of protein kinase A (70–83, 112–114).

Presently, how these protein–protein interactions relate to the tumor suppressor activity of merlin is largely not understood. The association of merlin with CD44 and β1-integrin raises the possibility that merlin might function as a molecular switch in the signaling pathways. CD44 is a transmembrane hyaluronic acid receptor implicated in cell–cell adhesion, cell–matrix adhesion, cell motility, and metastasis (82,83). Recent evidence suggests that merlin mediates contact inhibition of cell growth through signals from the extracellular matrix. At high cell density, merlin becomes hypophosphorylated and inhibits cell growth in response to hyaluronate, a mucopolysaccharide that surrounds cells. Merlin's growth-inhibitory activity depends on specific interaction with the cytoplasmic tail of CD44. At low cell density, merlin is phosphorylated; growth permissive; and exists in a complex with ezrin, moesin, and CD44. These data indicate that merlin and CD44 form a molecular switch that specifies cell growth arrest or proliferation (84). Also, merlin colocalizes and interacts with adherens components in confluent cells. Mouse fibroblasts lacking *Nf2* function do not undergo contact–dependent growth and can not form stable cadherin–containing cell:cell junctions. These results indicate that merlin functions as a tumor and metastasis suppressor by controlling cadherin–mediated cell:cell contact (111). Rac1, a member of the RhoGTPase family, has recently been demonstrated to promote phosphorylation of merlin, thereby inactivating its growth suppressor mechanism. In addition, among the Rac/Cdc42 effectors, p21-activated kinase 2 (Pak2) has been shown to phosphorylate merlin at serine 518 and inactivates its function (69,85,86). Kissil et al. also recently reported an interaction between merlin and Pak1. Merlin inhibits the activation dynamic of Pak1. Loss of merlin expression leads to the inappropriate activation of Pak1, whereas overexpression of merlin results in the inhibition of Pak1 activity (72) (Fig. 3).

MERLIN'S GROWTH REGULATORY FUNCTION IS RELATED TO ITS CONFORMATION AND PROTEIN–PROTEIN INTERACTIONS

The activities of the ERM proteins are controlled by self-association of the proteins' N-terminal and C-terminal regions (87). The ERM proteins can exist in the ''closed'' conformation, where the N- and C-terminal regions undergo an intramolecular interaction, thus folding the protein to mask the conserved actin-binding site (Fig. 3). The molecule can be converted to the open conformation in which the intramolecular interaction is disrupted by signals such as phosphorylation or treatment with phosphoinositides (46,72,86,88).

Merlin's ability to function as a growth regulator is also related to its ability to form such intramolecular associations. Two such interactions have been identified. The first interaction is between residues that fold the N-terminal end of the protein onto itself, whereas the second interaction folds the entire protein so that there is contact between N- and C-terminal

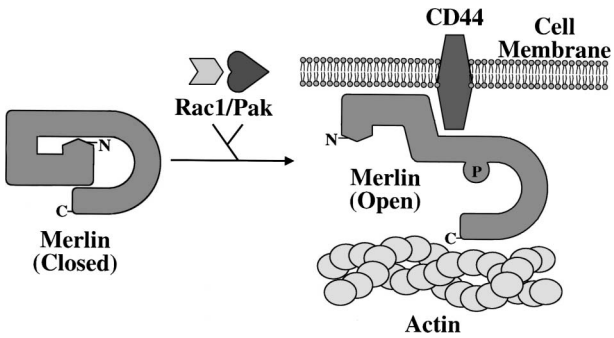

FIG. 3. Schematic diagram of merlin action. This diagram shows how Rac1 and Pak help convert the merlin protein from a closed conformation to an open conformation by phosphorylation of the protein. Consequently, merlin, in its open conformation, can interact with CD44 and facilitate linking the actin cytoskeleton to the cell membrane.

ends of the protein (46,89,90) (Fig. 3). In a fashion similar to the ERM proteins, merlin may cycle between the open and 'closed' conformations that differentially determine whether it binds with the ERM proteins or other molecules to transduce merlin's growth inhibition signal (91). In addition, the association between merlin and hepatocyte growth factor-regulated tyrosine kinase substrate, a substrate implicated in the signaling pathway initiated by hepatocyte growth factor binding to the c-met receptor (92), appears to be regulated by merlin folding, suggesting that the ability of merlin to cycle between the open and closed conformations may integrate CD44 and hepatocyte growth factor signaling pathways relevant to growth regulation (90).

IMMUNOHISTOCHEMICAL MARKERS OF GROWTH IN VESTIBULAR SCHWANNOMAS: CLINICAL CORRELATION

Attempts to correlate clinical parameters with immunohistologic evaluation of protein expression in vestibular schwannomas have been performed. An increase in Ki-67, which is an index of nuclear proliferation, was shown to correlate with the growth of solid schwannomas on MRI (93). Higher rates of tumor recurrence have also been suggested in tumors with an increased rate of nuclear proliferation and mitotic indexes, although the supporting data for this claim are not conclusive (94). Positron emission tomography scanning has been conducted to assess the metabolic activity of vestibular schwannomas preoperatively and to correlate the metabolic activity with the proliferation index, Ki-67. No correlation was found between the large and recurrent tumors and the uptake of 18-fluorodeoxyglucose as a radionucleotide tracer to measure glucose metabolism by positron emission tomography scanning. In additiion, there was no correlation between 18-fluorodeoxyglucose uptake and Ki-67 expression measured by immunostaining (95). A possible reason for this is that vestibular schwannomas are slow-growing tumors with only a small proportion of the tumor cells being in S-phase (active division) (96). Cystic schwannomas are associated with a 36-fold decrease in nuclear proliferation as measured with Ki-67 staining when compared with solid tumors. This suggests that the rapid clinical growth seen in cystic schwannomas is related to the accumulation of fluid during cyst formation and not by an actual increase in the growth rate of tumor cells (97). However, before this can be stated as fact, the cellular mechanism leading to the development of cystic schwannomas needs to be better understood. Lastly, *NF2*-associated schwannomas have been shown to have an increased proliferation index by Ki-67 and proliferating cell nuclear antigen immunostaining when compared with unilateral solid schwannomas (98).

Another possible marker for tumor growth is the transforming growth factor-β1. Immunostaining for transforming growth factor-β1 was positive in 96% of blood vessels within schwannomas and in 84% of schwannoma tissue samples; however, again, no clinical correlation with tumor types or tumor growth was found (99). Immunohistochemical association of β1-integrin with merlin has been demonstrated but has not been related directly to tumor phenotypes (77).

Considered together, these studies demonstrate a degree of correlation between clinical growth as assessed by MRI scans and historical data, and nuclear growth indexes in solid unilateral and *NF2*-associated schwannomas. However, cystic tumor growth appears to occur via a different mechanism. Although the defective *NF2* gene is the underlying common denominator in tumor formation of unilateral sporadic, *NF2*-associated, and cystic schwannomas, other differences at the molecular level likely account for the variable clinical presentations of these tumors.

CLINICAL SCREENING FOR NF2

Routine clinical and radiographic examinations are required for at-risk patients including patients with a first-degree relative with NF2. In addition, patients younger than 30 years with a unilateral vestibular schwannoma, or any patient with multiple intracranial or spinal tumors or other stigmata associated with NF2, should have a surveillance plan initiated. Any offspring of patients with NF2 should have annual ocular examinations starting soon after birth and annual neurologic examinations starting at 7 years of age. Biannual audiography and annual MRI evaluations should be conducted beginning at age 7. Others have recommended starting a similar screening process at 10 years of age, with an MRI every other year and annually if a vestibular schwannoma is found (100). We do not perform screening spinal imaging in undiagnosed, at-risk patients because nonsurgical management is usually recommended in cases of asymptomatic spinal tumors (101). The only time we would recommend spinal imaging in an at-risk patient is if they presented with complaints suggesting a symptomatic spinal tumor. Once a diagnosis of NF2 is made secondary to intracranial schwannomas and/or other tumors, we suggest obtaining a baseline spinal MRI scan, but the spinal scans should only be repeated if symptoms or physical examination findings suggest a new or progressive spinal tumor. The important point in this discussion is to begin some form of screening at an early age to pick up tumors while hearing preservation surgery is still possible.

GENETIC SCREENING FOR NF2

There are three scenarios worth considering in reference to genetic screening for NF2. Each instance

deals with an asymptomatic, undiagnosed child that is at-risk for developing NF2 disease. The first scenario pertains to an NF2 parent who has already had their specific mutation detected in the DNA of peripheral blood cells and/or a previously excised vestibular schwannoma. Another possibility is that the parent has a mosaic form of NF2 in which a mutation is often not detectable in the peripheral blood cells because only a portion of their cells carries the mutation. In these mosaic individuals, the mutation can often only be found when testing an excised vestibular schwannoma. In either case, if a mutation had been previously characterized in a parent, the sensitivity of genetic testing in this circumstance is nearly 100%, because the DNA being screened can be directly compared with the known mutation in the parent. Therefore, if the screening test was negative, then the child would not be at any higher risk for developing NF2 than the normal population and could avoid annual MRI screenings.

The second scenario is when multiple family members have been diagnosed with NF2 and none of them have had mutational analysis performed. In this case, we feel that it would be prudent to perform mutational screening on the affected family members to find a specific mutation that can be used to screen their children. Again, this would have a sensitivity of nearly 100%, and frequent testing could thus be avoided. If a specific mutation cannot be identified in any of the family members, linkage analysis of multiple NF2 family members may be used to screen children for NF2 (102).

The last scenario involves whether to screen children whose NF2 parent has not previously had a mutation identified or a previous attempt to find a mutation was unsuccessful. Several physicians feel that genetic screening is a useful tool in directing surveillance in this scenario; however, currently, this is a controversial position. We do not perform routine genetic screening in this specific instance, and the following discussion highlights the reasons why. It is important to note that this scenario is quite common because testing has only been available in the last decade; therefore, it is not uncommon to have 30- and 40-year-old NF2 patients who have not undergone mutational analysis. Furthermore, it is not unusual to have only one family member affected with NF2 because new mutations account for up to 50% of NF2 cases (7). In this instance, when screening a child whose NF2 mutation is unknown in their parent, probing the *NF2* gene for a specific known mutation is not possible, but rather a general probe for an unknown mutation is performed. In other words, instead of looking at a child's DNA to see whether it matches a known parental mutation that is located in a specific stretch of DNA within the *NF2* coding region, one is searching the entire *NF2* coding region for an unknown mutation, and consequently, in this instance, the sensitivity of genetic screening drops from nearly 100% to between 34 and 84%. Obviously, this leaves a significant number of patients whose NF2 mutation is not detected by this screening process and makes it difficult to predict those patients who will develop NF2 (25–36). Taking this fact into consideration, those children who had a negative screening test would still need annual MRI scans and biannual audiometric testing. In addition, if a mutation was detected during DNA sequencing, we would still recommend annual MRI scans and biannual audiometric testing to detect the development of vestibular schwannomas at the earliest possible stage. Early detection in NF2 does make a significant difference in the ability to successfully treat vestibular schwannomas. Therefore, because a positive or a negative NF2 mutation screen does not alter the recommended clinical follow-up of these at-risk children, when a mutation has not already been identified in a parent, we do not recommend routine genetic screening. Our current position may need to be reconsidered as the sensitivity of screening increases and the cost of mutation detection decreases.

IDENTIFYING DEREGULATED GENES IN VESTIBULAR SCHWANNOMAS

With 69,227 mRNA sequences representing unique human genes and more than 3 million expressed sequence tags in the UniGene database, the success of the Human Genome Project is evident. However, the expression, function, and regulation of the majority of genes are not yet known (103). The study of large-scale gene expression profiles using cDNA microarrays allows examination of the so-called transcriptome of a tissue, and gives a means of exploring a broad view of the basic biology of tumors (104). Data from the human genome project makes the expression profiles more readily searchable, and organization of the genes into functional groupings allows examination of distinct pathways. For example, cell cycle control, DNA damage repair, or signal transduction and transcription factors can be organized and reviewed for various tumors (105). Biochips that contain thousands of oligonucleotides representing genes from the human genome have been created and are used to perform cDNA microarrays.

To evaluate the gene expression profile in a tumor, RNA is isolated from the tumor and converted into cDNA or cRNA. This cDNA or cRNA is then labeled with a fluorescent dye and hybridized to the oligonucleotides on the biochip. The same process can be used to evaluate RNA expressed in a normal tissue and then to compare gene expression differences between the affected and normal tissues. Consequently, deregulated genes in the affected tissues can be identified. Microarray gene expression analysis has been successfully used in recent years to evaluate a number of solid tumors including breast carcinoma, colon

carcinoma, prostate carcinoma, ovarian carcinoma, and vestibular schwannomas (19,20,106–109).

Gene expression analysis has revealed differences among tumors that are not distinguishable histologically. Molecular classification, rather than histologic classification, may also better predict the response of certain tumor types to specific therapies (110). This genomic scale approach has helped to identify subclasses of colon carcinoma, breast carcinoma, melanoma, leukemias, and lymphomas (108,109). In several instances, cDNA microarray analysis has identified genes that appear to be useful for predicting clinical behavior.

Vestibular schwannoma characteristics cannot be explained by the current understanding of the mutation types alone. Investigating intertumor variability of gene expression profiles shows promise in helping to unravel the clinical differences among subtypes of vestibular schwannomas. To better understand the pathways leading to schwannoma formation, we have used cDNA microarray analysis to evaluate gene expression profiles of vestibular schwannomas (19,20). Three sporadic vestibular schwannomas, two NF2-associated schwannomas, and three cystic schwannomas were compared with a normal vestibular nerve from a patient with a sporadic schwannoma. The goal was to seek patterns of gene expression consistently elevated or decreased across all tumors. Of 25,920 genes or expressed sequence tags screened, 42 genes were significantly upregulated (by a factor of three or more) consistently across at least six of the eight tumors examined. In addition, multiple genes were found to be significantly downregulated in the majority of vestibular schwannomas examined. Of these genes, eight genes involved with cell signaling and division were downregulated, including an apoptosis-related, putative tumor suppressor gene, *LUCA-15*, which was downregulated in seven of eight schwannomas studied. Two mediators of angiogenesis, endoglin and osteonectin, were highly elevated in most of the tumors examined. Osteonectin is a secreted glycoprotein that interacts with extracellular matrix proteins to decrease adhesion of cells from the matrix, thereby inducing a biological state conducive to cell migration, and endoglin is a transforming growth factor-α receptor that is known to be an endothelial marker for angiogenesis in solid tumors. Osteonectin was elevated in all of the tumors studied, and endoglin was found to be significantly upregulated in all of the solid tumors but not in any of the cystic tumors examined. The difference in endoglin gene expression may be a future avenue of investigation into why some schwannomas develop the aggressive cystic phenotype (19). An example of a deregulated signaling pathway suggested by the microarray data is the retinoblastoma protein-cyclin-dependent kinase (CDK) pathway. Among genes involved in G_1 to S progression, CDK2 was found to be downregulated in seven of eight tumors, and every tumor examined had multiple genes deregulated in this pathway (20). To further validate the microarray results, quantitative real-time polymerase chain reaction and immunohistochemistry have been used to confirm RNA and protein expression levels, respectively, but the significance of these findings in the role of tumorigenesis is still under investigation (19,20).

CONCLUSION

The discovery of molecular mechanisms underlying vestibular schwannoma formation is rapidly moving forward. Understanding merlin's interactions with other proteins, signaling pathways, and regulation of the *NF2* gene will possibly lead to the development of novel drug therapies for vestibular schwannomas. In the future, it may also be possible to develop a targeted molecular therapy that will stop tumor progression or altogether eradicate preexisting tumors. It is hoped that these new avenues of treatment will offer improved alternatives to the current options of untreated observation of tumor growth, stereotactic radiation, or surgical removal. These are the challenges facing the "molecular neurotologist" of the future.

REFERENCES

1. Howitz MF, Johansen C, Tos M, et al. Incidence of vestibular schwannoma in Denmark, 1977–1995. *Am J Otol* 2000;21: 690–4.
2. Anderson TD, Loevner LA, Bigelow DC, et al. Prevalence of unsuspected acoustic neuroma found by magnetic resonance imaging. *Otolaryngol Head Neck Surg* 2000;122:643–6.
3. Bull. World Health Org. Prevention and control of neurofibromatosis: Memorandum from a joint WHO/NNFF meeting. *Bull World Health Org* 1992;70:173–82.
4. Kanter WR, Eldridge R, Fabricant R, et al. Central neurofibromatosis with bilateral acoustic neuroma: genetic, clinical and biochemical distinctions from peripheral neurofibromatosis. *Neurology* 1980;30:851–9.
5. Martuza RL, Eldridge R. Neurofibromatosis 2 (bilateral acoustic neurofibromatosis). *N Engl J Med* 1988;318:684–8.
6. Baser ME, Friedman JM, Wallace AJ, et al. Evaluation of clinical diagnostic criteria for neurofibromatosis 2. *Neurology* 2002;59:1759–65.
7. Evans DGR, Huson SM, Donnai D, et al. A genetic study of type 2 neurofibromatosis in the United Kingdom: I. Prevalence, mutation rate, fitness, and confirmation of maternal transmission effect on severity. *J Med Genet* 1992;29:841–6.
8. Wishart JH. Case of tumors in the skull, dura mater, and brain. *Edinburgh Med Surg J* 1822;18:393–7.
9. Gardner WJ, Frazier CH. Bilateral acoustic neurofibromatosis: a clinical study and field survey of a family of five generations with bilateral deafness in thirty-eight members. *Arch Neurol Psychiatry* 1930;23:266–302.
10. Ruggieri M, Huson SM. The clinical and diagnostic implications of mosaicism in neurofibromatosis. *Neurology* 2001;56:1433–43.
11. Kluwe L, Mautner V, Heinrich B. Molecular study of frequency of mosaicism in neurofibromatosis 2 patients with bilateral vestibular schwannomas. *J Med Genet* 2003;40:109–14.
12. Moyhuddin A, Baser MG, Watson C. Somatic mosaicism in neurofibromatosis 2: prevalence and risk of disease transmission to offspring. *J Med Genet* 2003;40:459–63.

13. MacCollin M, Willett C, Heinrich B, et al. Familial schwannomatosis: exclusion of the NF2 locus as the germline event. *Neurology* 2003;60:1968–74.
14. Charabi S, Tos M, Thomsen J, et al. Cystic vestibular schwannoma: clinical and experimental studies. *Acta Otolaryngol* 2000;543(Suppl):11–3.
15. Charabi S, Tos M, Borgesen SE, et al. Cystic acoustic neuromas: results of translabyrinthine surgery. *Arch Otolaryngol Head Neck Surg* 1994;120:1333–8.
16. Fundova P, Charabi S, Tos M, et al. Cystic vestibular schwannoma: surgical outcome. *J Laryngol Otol* 2000;114: 935–9.
17. Pendl G, Ganz JC, Kitz K, et al. Acoustic neurinomas with macrocysts treated with gamma knife radiosurgery. *Stereotact Funct Neurosurg* 1995;66(Suppl):103–11.
18. Shirato H, Sakamoto T, Takeichi N, et al. Fractionated stereotactic radiotherapy for vestibular schwannoma (VS): comparison between cystic-type and solid-type VS. *Int J Radiat Oncol Biol Phys* 2000;48:1395–401.
19. Welling DB, Lasak JM, Akhmametyeva EM, et al. cDNA microarray analysis of vestibular schwannomas. *Otol Neurotol* 2002;23:736–48.
20. Lasak JM, Welling DB, Salloum M, et al. Deregulation of the pRb-CDK pathway in vestibular schwannomas. *Laryngoscope* 2001;112:1555–61.
21. Rouleau GA, Wertelecki W, Haines JL, et al. Genetic linkage of bilateral acoustic neurofibromatosis to a DNA marker on chromosome 22. *Nature* 1987;329:246–8.
22. Wertelecki W, Rouleau GA, Superneau DW, et al. Neurofibromatosis 2: clinical and DNA linkage studies of a larger kindred. *N Engl J Med* 1988;319:278–83.
23. Rouleau GA, Merel P, Lutchman M, et al. Alteration in a new gene encoding a putative membrane-organizing protein causes neurofibromatosis type 2. *Nature* 1993;363:515–21.
24. Trofatter JA, MacCollin MM, Rutter JL, et al. A novel Moesin-, Exrin-, Radixin-like gene is a candidate for the neurofibromatosis 2 tumor-suppressor. *Cell* 1993;72:791–800.
25. Welling DB, Guida M, Goll F, et al. Mutational spectrums in the neurofibromatosis type 2 gene in sporadic and familial schwannomas. *Hum Genet* 1996;98:189–93.
26. Merel P, Khe HX, Sanson M, et al. Screening for germ-line mutations in the NF2 gene. *Genes Chromosome Cancer* 1995; 12:117–2.
27. MacCollin M, Ramesh V, Jacoby LB, et al. Mutational analysis of patients with neurofibromatosis 2. *Am J Hum Genet* 1994;55:314–20.
28. Jacoby LB, MacCollin M, Louis DN, et al. Exon scanning for mutation of the NF2 gene in schwannomas. *Hum Mol Genet* 1994;3:413–9.
29. Kluwe L, Bayer S, Baser ME, et al. Identification of NF2 germ-line mutations and comparison with neurofibromatosis 2 phenotypes. *Hum Genet* 1996;98:534–8.
30. Parry DM, MacCollin MM, Kaiser-Kupfer MI, et al. Germline mutations in the neurofibromatosis 2 gene: correlation with disease severity and retinal abnormalities. *Am J Hum Genet* 1996;59:529–3.
31. Ruttledge MH, Andermann AA, Phelan CM, et al. Type of mutation in the neurofibromatosis type 2 gene (NF2) frequently determines severity of disease. *Am J Hum Genet* 1996;59:331–42.
32. Mautner VF, Baser ME, Kluwe L. Phenotypic variability in two families with novel splice-site and frameshift NF2 mutations. *Hum Genet* 1996;98:203–6.
33. Zucman-Rossi J, Legoix P, Der Sarkissian H, et al. NF2 gene in neurofibromatosis type 2 patients. *Hum Mol Genet* 1998; 7:2095–101.
34. Evans DG, Trueman L, Wallace A, et al. Genotype/phenotype correlations in type 2 neurofibromatosis (NF2): evidence for more severe disease associated with truncating mutations. *J Med Genet* 1998;35:450–5.
35. Antinheimo J, Sallinen SL, Sallinen P, et al. Genetic aberrations in sporadic and neurofibromatosis 2 (NF2)-associated schwannomas studied by comparative genomic hybridization (CGH). *Acta Neurochir (Wien)* 2000;142:1099–104.
36. Hung G, Faudoa R, Baser ME, et al. Neurofibromatosis 2 phenotypes and germ-line NF2 mutations determined by an RNA mismatch method and loss of heterozygosity analysis in NF2 schwannomas. *Cancer Genet Cytogenet* 2000;118:167–8.
37. Welling DB. Clinical manifestations of mutations in the neurofibromatosis type 2 gene in vestibular schwannomas (acoustic neuromas). *Laryngoscope* 1998;108:178–89.
38. Jacoby LB, MacCollin M, Barone R, et al. Frequency and distribution of NF2 mutations in schwannomas. *Genes Chromosomes Cancer* 1996;17:45–55.
39. Merel P, Hoang-Xuan K, Sanson M, et al. Predominant occurrence of somatic mutations of the NF2 gene in meningiomas and schwannomas. *Genes Chromosomes Cancer* 1995;13:1211–6.
40. Bianchi AB, Hara T, Ramesh V, et al. Mutations in transcript isoforms of the neurofibromatosis 2 gene in multiple human tumour types. *Nat Genet* 1994;6:185–92.
41. Ruttledge MH, Sarrazin J, Rangaratnam S, et al. Evidence for the complete inactivation of the NF2 gene in the majority of sporadic meningiomas. *Nat Genet* 1994;6:180–4.
42. Deguen B, Goutebroze L, Giovannini M, et al. Heterogeneity of mesothelioma cell lines as defined by altered genomic structure and expression of the NF2 gene. *Int J Cancer* 1998; 77:554–60.
43. Irving RM, Moffat DA, Hardy DG, et al. Somatic NF2 gene mutations in familial and non-familial vestibular schwannoma. *Hum Mol Genet* 1994;3:347–50.
44. Sainz J, Figueroa K, Baser ME, et al. High frequency of nonsense mutations in the NF2 gene caused by C to T transitions in five CGA codons. *Hum Genet* 1995;4:137–9.
45. Sainz J, Huynh DP, Figueroa K, et al. Mutations of the neurofibromatosis type 2 gene and lack of the gene product in vestibular schwannomas. *Hum Mol Genet* 1994;3:885–91.
46. Gutmann DH, Geist RT, Xu H, et al. Defects in neurofibromatosis 2 protein function can arise at multiple levels. *Hum Mol Genet* 1998;7:335–4.
47. Stokowski RP, Cox DR. Functional analysis of the neurofibromatosis type 2 protein by means of disease-causing point mutations. *Am J Hum Genet* 2000;66:873–91.
48. Gutmann DH, Hirbe AC, Haipek CA. Functional analysis of neurofibromatosis 2 (NF2) missense mutations. *Hum Mol Genet* 2001;10:1519–2.
49. Bruder DEG, Kirvela C, Tapia-Paez I, et al. High resolution deletion analysis of constitutional DNA from neurofibromatosis type 2 (NF2) patients using microarray-CGH. *Hum Mol Genet* 2001;10:271–82.
50. Bruder CE, Ichimura K, Blennow E, et al. Severe phenotype of neurofibromatosis type 2 in a patient with a 7.4-MB constitutional deletion on chromosome 22: possible localization of a neurofibromatosis type 2 modifier gene? *Genes Chromosomes Cancer* 1999;25:184–90.
51. Kino T, Takeshima H, Nakao M, et al. Identification of the cis-acting region in the NF2 gene promoter as a potential target for mutation and methylation-dependent silencing in schwannoma. *Genes Cells* 2001;6:441–54.
52. Chang LS, Akhmametyeva EM, Wu Y, et al. Multiple transcription initiation sites, alternative splicing, and differential polyadenylation contribute to the complexity of human neurofibromatosis 2 transcripts. *Genomics* 2002;79:63–76.
53. Hitotsumatsu T, Kitamoto T, Iwaki T, et al. An exon 8-spliced out transcript of neurofibromatosis 2 gene is constitutively expressed in various human tissues. *J Biochem* 1994;116: 1205–7.
54. Pykett MJ, Murphy M, Harnish PR, et al. The neurofibromatosis type 2 tumor suppressor gene encodes multiple alternatively spliced transcripts. *Hum Mol Genet* 1994;3: 559–64.
55. Giovannini M, Robanus-Maandag E, Niwa-Kawakita M, et al. Schwann cell hyperplasia and tumors in transgenic mice

expressing a naturally occurring mutant NF2 protein. *Genes Dev* 1999;13:978–86.
56. Welling DB, Akhmametyeva EM, Daniels RL, et al. Analysis of the human neurofibromatosis type 2 gene promoter and its expression. *Otolaryngol Head Neck Surg* 2000;123:413–8.
57. Chishti AH, Kim AC, Marfatia SM, et al. The FERM domain: a unique module involved in the linkage of cytoplasmic proteins to the membrane. *Trends Biochem Sci* 1998;23:281–2.
58. Bretscher A, Chambers D, Nguyen R, et al. ERM-Merlin and EBP50 protein families in plasma membrane organization and function. *Annu Rev Cell Dev Biol* 2000;16:113–43.
59. Turunen O, Wahlstrom T, Vaheri A. Ezrin has a COOH-terminal actin-binding site that is conserved in the ezrin protein family. *J Cell Biol* 1994;126:1445–53.
60. Roy C, Martin M, Mangeat P. A dual involvement of the amino-terminal domain of ezrin in F- and G-actin binding. *J Biol Chem* 1997;272:20088–95.
61. Gonzalez-Agosti C, Xu L, Pinney D, et al. The merlin tumor suppressor localizes preferentially in membrane ruffles. *Oncogene* 1996;13:1239–47.
62. Pelton PD, Sherman LS, Rizvi TA, et al. Ruffling membrane, stress fiber, cell spreading, and proliferation abnormalities in human schwannoma cells. *Oncogene* 1998;17:2195–209.
63. Deguen B, Merel P, Goutebroze L, et al. Impaired interaction of naturally occurring mutant NF2 protein with actin-based cytoskeleton and membrane. *Hum Mol Genet* 1998;7: 217–26.
64. Lutchman M, Rouleau GA. The neurofibromatosis type 2 gene product, schwannomin, suppresses growth of NIH 3T3 cells. *Cancer Res* 1995;55:2270–4.
65. Tikoo A, Varga M, Ramesh V, et al. An anti-Ras function of neurofibromatosis type 2 gene product (NF2/Merlin). *J Biol Chem* 1994;269:23387–90.
66. McClatchey AI, Saotome I, Mercer K, et al. Mice heterozygous for a mutation at the NF2 tumor suppressor locus develop a range of highly metastatic tumors. *Genes Dev* 1998; 12:1121–33.
67. McClatchey AI, Saotome I, Ramesh V, et al. The NF2 tumor suppressor gene product is essential for extraembryonic development immediately prior to gastrulation. *Genes Dev* 1997;11:1253–65.
68. Giovannini M, Robanus-Maandag E, van der Valk M, et al. Conditional biallelic *Nf2* mutation in the mouse promotes manifestations of human neurofibromatosis type 2. *Genes Dev* 2000;14:1617–30.
69. Shaw RJ, Paez JG, Curto M, et al. The NF2 tumor suppressor, merlin, functions in Rac-dependent signaling. *Dev Cell* 2001;1:63–72.
70. Fernandez-Valle C, Tang Y, Ricard J, et al. Paxillin binds schwannomin and regulates its density-dependent localization and effect on cell morphology. *Nat Genet* 2000;31:354–62.
71. Gronholm M, Vossebein L, Carlson CR, et al. Merlin links to the cAMP neuronal signaling pathway by anchoring the R1 beta subunit of protein kinase A. *J Biol Chem* 2003;278: 41167–72.
72. Kissil JL, Wilker EW, Johnson KC, et al. Merlin, the product of the NF2 tumor suppressor gene, is an inhibitor of the p21-activated kinase, PAK1. *Mol Cell* 2003;12:841–9.
73. Takeshima H, Izawa I, Lee PS, et al. Detection of cellular proteins that interact with the NF2 tumor suppressor gene product. *Oncogene* 1994;9:2135–44.
74. Sainio M, Zhao F, Heiska L, et al. Neurofibromatosis 2 tumor suppressor protein co-localizes with ezrin and CD44 and associates with actin-containing cytoskeleton. *J Cell Sci* 1997;110:2249–60.
75. Huang L, Ichimaru E, Pestonjamasp K, et al. Merlin differs from moesin in binding to F-actin and in its intra- and intermolecular interactions. *Biochim Biophys Res Commun* 1998;248:548–53.
76. Murthy A, Gonzalez-Agosti C, Cordero E, et al. NHE-RF, a regulatory cofactor for Na(+)-H+ exchange, is a common interactor for merlin and ERM (MERM) proteins. *J Biol Chem* 1998;273:1273–6.
77. Obremski VJ, Hall AM, Fernandez-Valle C. Merlin, the neurofibromatosis type 2 gene product, and β1 integrin associate in isolated and differentiating Schwann cells. *J Neurobiol* 1998;37:487–501.
78. Scoles DR, Huynh DP, Morcos PA, et al. Neurofibromatosis 2 tumor suppressor schwannomin interacts with βII-spectrin. *Nat Genet* 1998;18:354–9.
79. Scoles DR, Huynh DP, Chen MS, et al. The neurofibromatosis 2 tumor suppressor protein interacts with hepatocyte growth factor-regulated tyrosine kinase substrate. *Hum Mol Genet* 2000;9:1567–74.
80. Xu HM, Gutmann DH. Merlin differentially associates with the microtubule and actin cytoskeleton. *J Neurosci Res* 1998; 51:403–15.
81. Goutebroze L, Brault E, Muchardt C, et al. Cloning and characterization of SCHIP-1, a novel protein interacting specifically with spliced isoforms and naturally occurring mutant NF2 proteins. *Mol Cell Biol* 2000;20:1699–712.
82. Herrlich P, Morrison H, Sleeman J, et al. CD44 acts both as a growth and invasiveness-promoting molecule and as a tumor-suppressing cofactor. *Ann N Y Acad Sci* 2000;910: 106–18.
83. Sherman L, Sleeman J, Herrlich P, et al. Hyaluronate receptors: key players in growth, differentiation, migration, and tumor progression. *Curr Opin Cell Biol* 1994;6:726–33.
84. Morrison H, Sherman LS, Legg J, et al. The NF2 tumor suppressor gene product, merlin, mediates contact inhibition of growth through interactions with CD44. *Genes Dev* 2001; 15:968–80.
85. Xiao GH, Beeser A, Chernoff J, et al. P21-activated kinase links Rac/Cdc42 signaling to merlin. *J Biol Chem* 2002;277: 883–6.
86. Kissil JL, Johnson KC, Eckman MS, et al. Merlin phosphorylation by p21-activated kinase 2 and effects of phosphorylation on merlin localization. *J Biol Chem* 2002;277: 10394–9.
87. Bretscher A, Reczek D, Berryman M. Ezrin: a protein requiring conformational activation to link microfilaments to the plasma membrane in the assembly of cell surface structures. *J Cell Sci* 1997;110:3011–8.
88. Hirao M, Sato N, Kondo T, et al. Regulation mechanism of ERM (ezrin/radixin/moesin) protein/plasma membrane association: possible involvement of phosphatidylinositol turnover and Rho-dependent signaling pathway. *J Cell Biol* 1996;135: 37–51.
89. Gutmann DH, Sherman L, Seftor L, et al. Increased expression of the NF2 tumor suppressor gene product, merlin, impairs cell motility, adhesion and spreading. *Hum Mol Genet* 1999;8:267–75.
90. Gutmann DH, Haipek CA, Burke SP, et al. The *NF2* interactor, hepatocyte growth factor-regulated tyrosine kinase substrate (HRS), associates with merlin in the 'open' conformation and suppresses cell growth and motility. *Hum Mol Genet* 2001;10:825–34.
91. Pearson MA, Reczek D, Bretscher A, et al. Structure of the ERM protein moesin reveals the FERM domain fold masked by an extended actin binding tail domain. *Cell* 2000;101:259–70.
92. Komada M, Kitamura N. Growth factor-induced tyrosine phosphorylation of HRS, a novel 115- kilodalton protein with a structurally conserved putative zinc finger domain. *Mol Cell Biol* 1995;15:6213–21.
93. Niemczyk K, Vaneecloo FN, Lecomte MH, et al. Correlation between Ki-67 index and some clinical aspects of acoustic neuromas (vestibular schwannomas). *Otolaryngol Head Neck Surg* 2000;123:779–83.
94. Light JP, Roland JT Jr, Fishman A, et al. Atypical and low-grade malignant vestibular schwannomas: clinical implications of proliferative activity. *Otol Neurotol* 2001; 22:922–7.

95. Chen JM, Houle S, Ang LC, et al. A study of vestibular schwannomas using positron emission tomography and monoclonal antibody Ki-67. *Am J Otol* 1998;19:840–5.
96. Kesterson L, Shelton C, Dressler L, et al. Clinical behavior of acoustic tumors: a flow cytometric analysis. *Arch Otolaryngol Head Neck Surg* 1993;119:269–71.
97. Charabi S, Klinken L, Tos M, et al. Histopathology and growth pattern of cystic acoustic neuromas. *Laryngoscope* 1994;104:1348–52.
98. Antinheimo J, Haapasalo H, Seppala M, et al. Proliferative potential of sporadic and neurofibromatosis 2-associated schwannomas as studied by MIB-1 (Ki-67) and PCNA labeling. *J Neuropathol Exp Neurol* 1995;54:776–82.
99. Cardillo MR, Filipo R, Monini S, et al. Transforming growth factor-beta1 expression in human acoustic neuroma. *Am J Otol* 1999;20:65–8.
100. Evans DGR, Sainio M, Baser ME. Neurofibromatosis type 2. *J Med Genet* 2000;37:897–904.
101. Mautner VF, Lindenau M, Baser ME, et al. The neuroimaging and clinical spectrum of neurofibromatosis 2. *Neurosurgery* 1996;38:880–85.
102. Sainio M, Strachan T, Blomstedt G, et al. Presymptomatic DNA and MRI diagnosis of neurofibromatosis 2 with mild clinical course in an extended pedigree. *Neurology* 1995;45: 1314–22.
103. Lander ES, Lenton LM, Birren B, et al. Initial sequencing and analysis of the human genome. *Nature* 2001;409:860–921.
104. Lockhart DJ, Winzeler EA. Genomics, gene expression, and DNA arrays. *Nature* 2000;405:827–36.
105. DeRisi JL, Iyer VR, Brown PO. Exploring the metabolic and genetic control of gene expression on a genomic scale. *Science* 1997;278:680–6.
106. Zhang DH, Salto-Tellez M, Chiu LL, et al. Tissue microarray study for classification of breast tumors. *Life Sci* 2003;73: 3189–99.
107. Nishizuku S, Chen ST, Gwadry FG, et al. Diagnostic markers that distinguish colon and ovarian adenocarcinomas: identification, genomic, proteomic, and tissue array profiling. *Cancer Res* 2003;63:5243–50.
108. Alizadeh AA, Ross DT, Perou CM, et al. Towards a novel classification of human malignancies based on gene expression patterns. *J Pathol* 2001;195:41–52.
109. Jordan CT. Unique molecular and cellular features of acute myelogenous leukemia stem cells. *Leukemia* 2002;16: 559–62.
110. Klausner RD. Cancer, genomics, and the National Cancer Institute. *J Clin Invest* 1999;104:S15–7.
111. Lallemand D, Curto M, Saotome I, Giovannini M, McClatchey AI. NF2 deficiency promotes tumorigenesis and metastasis by destabilizing adherens junction. *Genes Dev* 2003;17:1090–1100.
112. Ryu CH, Kim SW, Lee KH, et al. The merlin tumor suppressor interacts with Ral guanine nucleotide dissociation stimulator and inhibits its activity. *Oncogene* 2005;24: 5355–64.
113. Manchanda N, Lyubimova A, Ho HY, et al. The NF2 tumor suppressor Merlin and ERM proteins interact with N–WASP and regulate its actin polymerization function. *J Biol Chem* 2005;280:12517–22.
114. Rangwala R, Banine F, Borg JP, Sherman LS. Erbin regulates mitogen–activated protein (MAP) kinase activation and MAP kinase–dependent interactions between Merlin and adherens junction protein complexes in Schwann cells. *J Biol Chem* 2005;280:11790–7.

The Laryngoscope
Lippincott Williams & Wilkins, Inc.

Cyclin D_1 and D_3 Expression in Vestibular Schwannomas

Brian A. Neff, MD[1,4*]; Elly Oberstien, MS[4]; Mark Lorenz, MS[4]; Abhik R. Chaudhury, MD[2,4]; D. Bradley Welling, MD, PhD[1,4*]; Long-Sheng Chang, PhD[1,2,3,4,5*]

Objectives: **The G_1 regulators of the cell cycle, cyclin D_1 and D_3, have been implicated in the regulation of Schwann cell proliferation and differentiation. The purpose of this study is to evaluate cyclin D_1 and D_3 protein expression and the corresponding clinical characteristics of vestibular schwannomas.** ***Study Design and Methods:*** **Tissue sections of 15 sporadic vestibular schwannomas were prepared. Immunohistochemical analysis of the vestibular schwannomas was performed with anticyclin D_1 and anticyclin D_3 antibodies. The immunoreactivity was evaluated in comparison with adjacent vestibular nerves. Tissue sections of breast carcinoma and prostate carcinoma were used as positive controls for cyclin D_1 and D_3 staining, respectively. Patient demographics, tumor characteristics, and cyclin D expression were reviewed, and statistical analysis was performed.** ***Results:*** **While the breast carcinoma control expressed abundant cyclin D_1 protein, none of the 15 vestibular schwannomas showed detectable cyclin D_1 staining. In contrast, seven of 15 vestibular schwannomas stained positive for the cyclin D_3 protein. Cyclin D_3 staining was taken up in the nucleus of schwannoma tumor cells in greater proportion than Schwann cells of adjacent vestibular nerve. Although sample size was small, no significant difference in the average age of presentation, tumor size, and male to female ratios for the cyclin D_3+ or cyclin D_3− groups was found.** ***Conclusion:*** **The Cyclin D_1 protein does not appear to play a prominent role in promoting cell cycle progression in vestibular schwannomas. In contrast, cyclin D_3 expression was seen in nearly half of the tumors examined, suggesting that it may have a growth-promoting role in some schwannomas. Further studies are needed to define its cellular mechanism.** ***Key words:*** **Vestibular schwannoma, cyclin D_1 and D_3, neurofibromatosis type 2, *NF2* gene, and cell cycle.**
***Laryngoscope*, 116:423–426, 2006**

INTRODUCTION

Vestibular schwannomas are benign tumors originating from the vestibular divisions of the eighth cranial nerve.[1] Although advances have been made in the clinical treatment of these tumors, the morbidity associated with the current treatment modalities continues to be a problem. For this reason, it is important to find new methods to eradicate or control these tumors. The most promising approaches require a fundamental understanding of the molecular mechanisms underlying vestibular schwannoma tumorigenesis.

Although mutations inactivating both alleles of the neurofibromatosis type 2 gene (*NF2*) are responsible for the development of vestibular schwannomas, the mutation type and/or location of the mutation alone is insufficient to predict the clinical behavior of the tumors. In particular, predictors of growth rate are not yet known, but would be important clinically if such could be determined. Several genes or pathways including the retinoblastoma protein (pRb)-cyclin dependent kinase (CDK) pathway have been found to be frequently deregulated in these tumors.[2,3] Among the genes involved in the pRb-CDK pathway, which regulates G_1-to-S progression during the cell cycle,[4] CDK2 was substantially under expressed in most vestibular schwannomas examined. In addition, all schwannomas displayed deregulated expression of at least one of the genes involved in the pRb-CDK pathway.[2]

Recent studies suggest important roles for the D-type cyclins in the control of Schwann cell proliferation. Mice lacking cyclin D_1 display defects in the growth of mature Schwann cells.[5] Schwann cell proliferative responses to cAMP and platelet-derived growth factor appear to be mediated by cyclin D_1.[6] Finally, microarray analysis has revealed a strong correlation between Schwann cell proliferation and cyclin D_3 expression, and synergistic induction of cyclin D_3 expression may be critical to the stimu-

[1]From the Department of Otolaryngology Head and Neck Surgery (B.A.N., D.B.W., L.C.), [2]Pathology (A.R.C., L.C.), and [3]Pediatrics (L.C.), The Ohio State University, Columbus, Ohio, U.S.A. From [4]The Ohio State University College of Medicine (B.A.N., E.O., M.L., A.R.C., D.B.W., L.C.). From [5]the Center for Childhood Cancer (L.C.), Children's Research Institute, Children's Hospital, Columbus, Ohio, U.S.A.

This study was supported by the Department of Defense Neurofibromatosis Research Program and the National Institute of Deafness and Other Communication Disorders.

Send Correspondence to D. Bradley Welling, 456 W. 10th Avenue, Columbus, OH 43210; E-mail: welling.1@osu.edu; and Long-Sheng Chang, 700 Children's Drive, Columbus, OH 43205 U.S.A; E-mail: lchang@chi.osu.edu; Phone: 614-355-2658; Fax: 614-722-5895

[*]Department of Otolaryngology Head and Neck Surgery (B.A.N.), The Mayo Clinic, Rochester, Minnesota, U.S.A.

DOI: 10.1097/01.mlg.0000195076.05466.6c

lation of Schwann cell proliferation by heregulin and forskolin.[7–9]

Alterations in the expression of the cyclin D family of proteins have been demonstrated in a variety of benign and malignant tumors.[10–16] The cyclin D_1 gene is rearranged, amplified, and/or over-expressed in several human neoplasms. Also, over-expression and/or amplification of cyclin D_3 occur in some malignancies. In addition, expression of cyclin D_1 and D_3 may be of prognostic value in several of these pathologies.[17–18] However, the role of cyclin D_1 and D_3 in vestibular schwannomas has not been previously examined. Since cyclin D_1 and D_3 have been implicated in the regulation of Schwann cell proliferation and differentiation, we evaluated the protein expression of cyclin D_1 and D_3 in vestibular schwannomas.

METHODS

Tissue Procurement

Vestibular schwannomas were resected with informed patient consent and utilized per the Human Subjects Protocol for tissue procurement approved by the Institutional Review Board. Paraffin-embedded tissue sections were evaluated by a neuropathologist and histologically confirmed as vestibular schwannomas. Fifteen sporadic vestibular schwannoma specimens were obtained and used in the study. None of the 15 patients included in the study had undergone previous surgery or irradiation to treat their tumor.

Immunohistochemistry

Immunostaining of vestibular schwannoma tissue sections was performed as previously described.[2,3] Sections of cyclin D_1-positive breast carcinomas and cyclin D_3-positive prostate carcinomas were used as positive controls. Deparaffinized tissue sections were incubated overnight at 4°C with either the anticyclin D_1 (HD11, sc-246) or anticyclin D_3 (D-7, sc-6283) monoclonal antibody (Santa Cruz Biotechnology, Santa Cruz, CA) at a 1:40,000 or 1:1000 dilution, respectively. The antibody concentration was determined by serial dilution and staining of positive control tissues. The optimal concentration was chosen in which positive control tissues demonstrated the most discrete immunoreactivity with the least amount of background staining. After extensive washing, slides were sequentially treated with biotinylated secondary antibody for 20 min, conjugated streptovidin for 20 min, and AEC+ High Sensitivity substrate chromogen (Dako Corp., Carpinteria, CA) for 5 min. A hematoxylin counterstain was then applied and light microscopy used to visualize the stained tissues. Tissues expressing the cyclin D_1 or D_3 protein stained brown while the hematoxylin counterstain appeared blue. Immunostained slides were evaluated by a neuropathologist and the immunoreactivity was graded as 0 (negative), 1+ (faint), 2+ (distinct), 3+ (strong, focal), 4+ (strong, diffuse) according to a modification of a previously reported intensity grading scale.[19] The staining intensity in the tumor tissue was compared to the adjacent vestibular nerve to evaluate whether or not the expression of the cyclin D_1 or D_3 protein was increased or decreased in the tumor.

A review of patient demographics was done for the 15 patients whose tumor was immunostained for cyclin D_3. The average age at presentation, patient sex, and average tumor size at presentation were tabulated for the group of patients with cyclin D_3+ and cyclin D_3− tumors. The size of the tumor was measured as the largest tumor diameter in either the axial, coronal, or sagittal MRI view. The age and tumor size data for the two groups were compared using the Student t test with statistical significance being set at $P < .05$.

RESULTS

Aberrant nuclear overexpression and accumulation of the cyclin D_1 protein are frequently detected in breast carcinomas, and thus, breast carcinoma tissues were used as a positive control.[20] The anticyclin D_1 antibody gave rise to abundant, mostly nuclear immunoreactivity in the breast carcinoma tissue section (Fig. 1a). We detected no staining signal in either the nucleus or the cytoplasm of all 15 vestibular schwannoma specimens (Fig. 1b, Table I). Additionally, we also detected no cyclin D_1-staining signal in the adjacent vestibular nerve tissue (data not shown).

For cyclin D_3 staining, prostate carcinoma tissues were utilized as a positive control.[14,21] As expected, strong immunoreactivity for cyclin D_3 was detected in the prostate carcinoma tissue (Fig. 2a). Intriguingly, the cyclin D_3 staining signal was found mostly in the cytoplasm. Seven schwannoma specimens stained positive for cyclin D_3. Five tumors showed a 2+ distinct nuclear staining pattern (Table I), and the other two schwannoma specimens were graded 3+ with several foci of strong nuclear staining (Fig. 2b, Table I). Interestingly, when the adjacent vestibular nerve was examined for cyclin D_3 expression, only a few Schwann cells exhibited faint 1+ nuclear staining; furthermore, their staining intensity was much weaker than that seen in the schwannoma cells (compare Fig. 2b to Fig. 2c).

A review of patient demographics was done for the cyclin D_3+ and D_3− tumors. There was no significant difference ($P = .44$) in the average age at presentation which was 51 years for the cyclin D_3+ group compared to 58 years for the cyclin D_3− group. The average tumor size was 1.3 cm for the cyclin D_3+ tumors and 0.9 cm for the cyclin D_3− tumors, and again, the tumor size was not statistically different between the two groups ($P = .42$). Lastly, male to female ratios were the same for both groups.

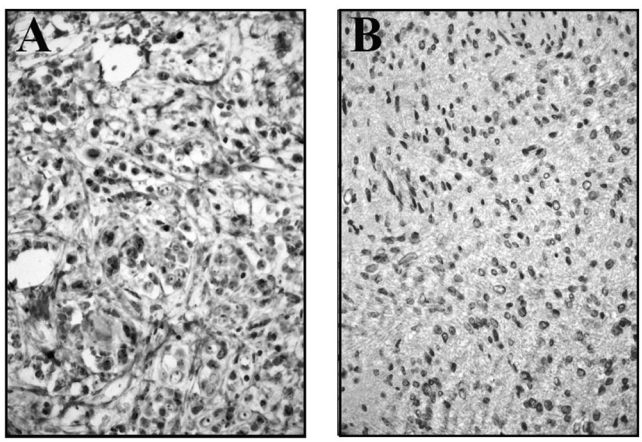

Fig. 1. Cyclin D_1 immunostaining. Tissue sections of a breast carcinoma (a) and a vestibular schwannoma (b) were stained with an anticyclin D_1 monoclonal antibody.

TABLE I.
Summary of Cyclin D_1 and D_3 Protein Expression in Vestibular Schwannomas.

Sample Number	Cyclin D_1	Cyclin D_3
17796 A1	Negative	2+ nuclear staining
17660 B1	Negative	Negative
1030012	Negative	2+ nuclear staining
1030069	Negative	Negative
0303C011	Negative	Negative
304577208	Negative	Negative
17607	Negative	3+ nuclear staining
17613	Negative	2+ nuclear staining
17644	Negative	Negative
17638	Negative	3+ nuclear staining
17579	Negative	Negative
17666	Negative	2+ nuclear staining
17661	Negative	2+ nuclear staining
17789	Negative	Negative
17696	Negative	Negative

DISCUSSION

The pRb-CDK pathway is frequently deregulated in human tumors including vestibular schwannomas.[2,3] Within this pathway, over expression of cyclin D_1 and/or D_3 has been detected in a variety of malignant tumors. In this study we showed that none of the 15 benign vestibular schwannomas examined displayed any cyclin D_1 staining signal, while 7 of 15 (47%) schwannomas over-expressed the cyclin D_3 protein, compared to the adjacent vestibular nerve.

The cyclin D proteins have been shown to contribute to oncogenic potential of tissues in a CDK-dependent and independent manner. In the CDK-dependent pathway, the D cyclins interact with CDK4 and CDK6, and through this interaction, phosphorylation of pRb occurs. In addition, the cyclin D-CDK 4/6 interaction sequesters the CIP/KIP (p21 and p27) and INK4 (p15, p16, p18, and p19) families of CDK inhibitors. This releases the cyclin E-CDK2 holoenzyme to further inactivate the pRb protein.

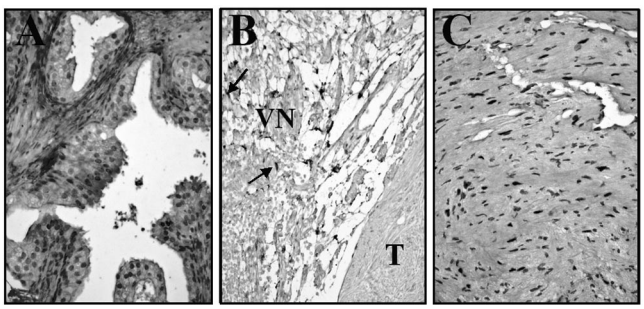

Fig. 2. Cyclin D_3 immunostaining. Tissue sections of a prostate carcinoma (a) and a vestibular schwannoma with (b) or without (c) adjacent vestibular nerve were stained with an anticyclin D_3 monoclonal antibody as described in Materials and Methods. Arrows indicate nuclear staining of some Schwann cells in the vestibular nerve (VN), adjacent to the vestibular schwannoma tumor (T).

Once pRb is hyperphosphorylated and inactivated, pRb dissociates from its pRb-E2F transcriptional repressor complex. The free E2F released from pRb inhibition binds and activates E2F target genes important for the cell to transit from G_1 to S phase.[22,23]

The cyclin D proteins can also affect the activity of several transcription factors including the cyclin D_1-interacting myb-like protein (DMP-1), the signal transducer and activator of transcription 3 (STAT 3), and the β-cell E-box transactivator 2 (BETA2/NeuroD) without the participation of CDK.[23] Furthermore, cyclin D_1 interacts with the transcription factor C/EBPβ and activating transcription factor 5 (ATF5) in a CDK-independent manner, and this may be a vital step in tumor formation.[22,23] Similar to cyclin D_1, cyclin D_3 may function in the CDK-independent pathway that involves C/EBPβ.[9]

In transgenic mice, cyclin D_3 over-expression in epithelial tissues results in epidermal hyperplasia.[24] Deregulated expression of cyclin D_3 and CDK6 could predispose cells to malignant transformation.[25] These results are consistent with the oncogenic role of cyclin D_3 activation in certain human malignancies. Our observation that cyclin D_3 is over-expressed in about half of vestibular schwannomas also suggests a role for cyclin D_3 in schwannoma formation. Given the fact that cyclin D_3 is important for Schwann cell proliferation,[7,8] vestibular schwannomas over-expressing cyclin D_3 may possess growth advantage. Due to the small sample size of tumors stained for cyclin D_3 expression, definitive clinical correlations between D_3+ expressing tumors and tumor size or age at presentation can not be made. However, a cursory review of patient data did not show any significant differences between D_3+ and D_3− patients. A larger clinical study will be needed to assess whether cyclin D_3 over-expression can act as a marker for increased vestibular schwannoma growth. This would require a study of patients who had an initial period of tumor observation and growth who subsequently underwent tumor resection and protein expression analysis of their schwannomas.

Similar to those found in human cancer cells,[19,26] we detected nuclear expression of the cyclin D_3 protein in Schwann cells and vestibular schwannomas. Intriguingly, intense cyclin D_3 immunoreactivity was detected in the cytoplasm of prostate carcinoma cells. Although the reason for this observation is presently not understood, it raises the question that cyclin D_3 may function in different cellular compartments. The subcellular localization of the cyclin D protein has been shown to play an important role in regulating Schwann cell proliferation.[27] Schwann cells in mature myelinating nerves expressed cyclin D_1 in the perinuclear region. After axon damage, cyclin D_1 expression is elevated in parallel with Schwann cell proliferation and translocates into Schwann cell nuclei. In contrast, cyclin D_1 expression is restricted to the perinuclear region of proliferating Schwann cells during normal development. These data indicate that there are different mechanisms regulating proliferation of Schwann cells during development or nerve injury.

CONCLUSION

The D-type cyclins are involved in cell-cycle progression from G_1 to S phase, and have been implicated in the oncogenesis of several human malignancies. Our study shows over expression of the cyclin D_3 protein in 7 of 15 vestibular schwannomas, and this suggests a role for cyclin D_3 in the growth of schwannoma cells.

BIBLIOGRAPHY

1. Welling DB. Clinical manifestations of mutations in the neurofibromatosis type 2 gene in vestibular schwannomas (acoustic neuromas). *Laryngoscope* 1998;108:178–189.
2. Lasak JM, Welling DB. Akhmametyeva EM, et al. Retinoblastoma-cyclin-dependent kinase pathway deregulation in vestibular schwannomas. *Laryngoscope* 2002;112: 1555–1561.
3. Welling DB, Lasak JM, Chang LS, et al. cDNA microarray analysis of vestibular schwannomas. *Otol Neurotol* 2002; 23:736–748.
4. Sherr CJ. Cell cycle control and cancer. *Harvey Lect* 2000-2001;96:73–92.
5. Kim HA, Pomeroy SL, Whoriskey W, et al. A developmentally regulated switch directs regenerative growth of Schwann cells through cyclin D1. *Neuron* 2000;26 (2):405–416.
6. Kim HA, Ratner N, Roberts TM, et al. Schwann cell proliferative responses to cAMP and *Nf1* are mediated by cyclin D1. *J Neurosci* 2001;21 (4):1110–1116.
7. Rahmatullah M, Schroering A, Rothblum K, et al. Synergistic regulation of Schwann cell proliferation by heregulin and forskolin. *Mol Cell Biol* 1998;18:6245–6252.
8. Schworer CM, Masker KK, Wood GC, et al. Microarray analysis of gene expression in proliferating Schwann cells: synergistic response of a specific subset of genes to the mitogenic action of heregulin plus forskolin. *J Neurosci Res* 2003;73:456–464.
9. Fuentealba L, Schworer C, Schroering A, et al. Heregulin and forskolin-induced cyclin D3 expression in Schwann cells: Role of a CCAAT promoter element and CCAAT enhancer binding protein. *Glia* 2004;45:238–248.
10. Seto M, Yamamoto K, Iida S, et al. Gene rearrangement and overexpression of PRAD1 in lymphoid malignancy with t(11;14)(q13;q32) translocation. *Oncogene* 1992;7: 1401–1406.
11. Leach FS, Elledge SJ, Sherr CJ, et al. Amplification of cyclin genes in colorectal carcinomas. *Cancer Res* 1993;53: 1986–1989.
12. Bartkova J, Lukas J, Strauss M, et al. Cyclin D1 oncoprotein aberrantly accumulates in malignancies of diverse histogenesis. *Oncogene* 1995;10:775–778.
13. Jares P, Fernandez PL, Campo E, et al. PRAD-1/cyclin D1 gene amplification correlates with messenger RNA overexpression and tumor progression in human laryngeal carcinomas. *Cancer Res* 1994;54:4813–4817.
14. Han EK, Lim JT, Arber N, et al. Cyclin D1 expression in human prostate carcinoma cell lines and primary tumors. *Prostate* 1998;35:95–101.
15. Oyama T, Kashiwabara K, Yoshimoto K, et al. Frequent overexpression of the cyclin D1 oncogene in invasive lobular carcinoma of the breast. *Cancer Res* 1998;58: 2876–2880.
16. Sonoki T, Harder L, Horsman DE, et al. Cyclin D3 is a target gene of t(6;14)(p21.1;q32.3) of mature B-cell malignancies. *Blood* 2001;98:2837–2844.
17. McIntosh GG, Anderson JJ, Milton I, et al. Determination of the prognostic value of cyclin D1 overexpression in breast cancer. *Oncogene* 1995;11:885–891.
18. Florenes VA, Faye RS, Maelandsmo GM, et al. Levels of cyclin D1 and D3 in malignant melanoma: deregulated cyclin D3 expression is associated with poor clinical outcome in superficial melanoma. *Clin Cancer Res* 2000;6: 3614–3620.
19. Doglioni C, Chiarelli C, Macri E, et al. Cyclin D3 expression in normal, reactive, and neoplastic tissues. *J Pathol* 1998; 185:159–166.
20. Bartkova J, Lukas J, Muller H, et al. Cyclin D1 protein expression and function in human breast cancer. *Int J Cancer* 1994;57:353–361.
21. Mukhopadhyay A, Banerjee S, Stafford LJ, et al. Curcumin-induced suppression of cell proliferation correlates with down-regulation of cyclin D1 expression and CDK4-mediated retinoblastoma protein phosphorylation. *Oncogene* 2002;21:8852–8861.
22. Lamb J, Ramaswamy S, Ford HL, et al. A mechanism of cyclin D1 action encoded in the patterns of gene expression in human cancer. *Cell* 2003;114:323–334.
23. Ewen ME, Lamb J. The activities of cyclin D1 that drive tumorigenesis. *Trends Mol Med* 2004;10:158–162.
24. Rodriguez-Puebla ML, LaCava M, Miliani DeMarval PL, et al. Cyclin D2 overexpression in transgenic mice induces thymic and epidermal hyperplasia whereas cyclin D3 expression results only in epidermal hyperplasia. *Am J Pathol* 2000;157:1039–1050.
25. Chen Q, Lin J, Jinno S, et al. Overexpression of Cdk6-cyclin D3 highly sensitizes cells to physical and chemical transformation. *Oncogene* 2003;22:992–1001.
26. Bartkova J, Zemanova M, Bartek J. Abundance and subcellular localization of cyclin D3 in human tumors. *Int J Cancer* 1996;65:323–327.
27. Atonasoski S, Shumas S, Dickson C, et al. Differential cyclin D1 requirements of proliferating Schwann cells during development and after injury. *Mol Cell Neurosci* 2001;18: 581–592.

DISEASE CONNECTIONS

Regulation of the *Neurofibromatosis 2* Gene Promoter Expression During Embryonic Development

Elena M. Akhmametyeva,[1,2] Maria M. Mihaylova,[1,2] Huijun Luo,[1,2] Sadeq Kharzai,[1] D. Bradley Welling,[3] and Long-Sheng Chang[1–4]*

Mutations in the *Neurofibromatosis 2* (*NF2*) gene are associated with predisposition to vestibular schwannomas, spinal schwannomas, meningiomas, and ependymomas. Presently, how *NF2* is expressed during embryonic development and in the tissues affected by neurofibromatosis type 2 (NF2) has not been well defined. To examine *NF2* expression in vivo, we generated transgenic mice carrying a 2.4-kb *NF2* promoter driving β-galactosidase (β-gal) with a nuclear localization signal. Whole-mount embryo staining revealed that the *NF2* promoter directed β-gal expression as early as embryonic day E5.5. Strong expression was detected at E6.5 in the embryonic ectoderm containing many mitotic cells. β-gal staining was also found in parts of embryonic endoderm and mesoderm. The β-gal staining pattern in the embryonic tissues was corroborated by in situ hybridization analysis of endogenous *Nf2* RNA expression. Importantly, we observed strong *NF2* promoter activity in the developing brain and in sites containing migrating cells including the neural tube closure, branchial arches, dorsal aorta, and paraaortic splanchnopleura. Furthermore, we noted a transient change of *NF2* promoter activity during neural crest cell migration. While little β-gal activity was detected in premigratory neural crest cells at the dorsal ridge region of the neural fold, significant activity was seen in the neural crest cells already migrating away from the dorsal neural tube. In addition, we detected considerable *NF2* promoter activity in various NF2-affected tissues such as acoustic ganglion, trigeminal ganglion, spinal ganglia, optic chiasma, the ependymal cell-containing tela choroidea, and the pigmented epithelium of the retina. The *NF2* promoter expression pattern during embryogenesis suggests a specific regulation of the *NF2* gene during neural crest cell migration and further supports the role of merlin in cell adhesion, motility, and proliferation during development. *Developmental Dynamics 235:2771–2785, 2006.* © 2006 Wiley-Liss, Inc.

Key words: *Neurofibromatosis 2* (*NF2*) gene promoter; neurofibromatosis type 2 (NF2); neural tube closure; neural crest cell migration; pigmented epithelium of the retina; transgenic mouse

Accepted 23 May 2006

INTRODUCTION

Neurofibromatosis type 2 (NF2) is an autosomal dominant disorder that predisposes affected individuals to bilateral vestibular schwannomas and the development of multiple meningiomas, intracranial tumors, ophthalmologic and skin abnormalities, and spinal schwannomas (NIH Consens. Statement, 1991). By positional cloning, the gene associated with NF2 has been identified and termed the *Neurofibromatosis 2* gene (*NF2*), which encodes a protein named "merlin" for moesin-

[1]Center for Childhood Cancer, Children's Research Institute, Children's Hospital, Columbus, Ohio
[2]Department of Pediatrics, The Ohio State University College of Medicine and Public Health, Columbus, Ohio
[3]Department of Otolaryngology, The Ohio State University College of Medicine and Public Health, Columbus, Ohio
[4]Department of Pathology, The Ohio State University College of Medicine and Public Health, Columbus, Ohio
Grant sponsor: US Department of Defense Neurofibromatosis Research Program; Grant number: DAMD17-02-1-0680; Grant sponsor: National Institute of Deafness and Other Communication Disorders; Grant number: DC5985; Grant sponsor: National Cancer Institute; Grant number: CA16058.
***Correspondence to: Dr. Long-Sheng Chang, Department of Pediatrics, Children's Hospital and The Ohio State University, WA-5104, 700 Children's Drive, Columbus, OH 43205-2696. E-mail: lchang@chi.osu.edu**

DOI 10.1002/dvdy.20883
Published online 7 August 2006 in Wiley InterScience (www.interscience.wiley.com).

ezrin-radixin like protein (Trofatter et al., 1993), or "schwannomin," a word derived from schwannoma, the most prevalent tumor seen in NF2 (Rouleau et al., 1993). Mutations in the *NF2* gene have been found in NF2-associated vestibular schwannomas, sporadic vestibular schwannomas, and cystic schwannomas, as well as meningiomas (reviewed in Neff et al., 2005).

The *NF2* protein shares a high degree of homology to ezrin, radixin, and moesin (ERM), a family of membrane-cytoskeleton-associated proteins that are important for cell adhesion, motility, regulation of cell shape, and signal transduction (McClatchey, 2004; McClatchey and Giovannini, 2005). Like the ERM proteins, merlin is expressed in a variety of cell types where it localizes to areas of membrane remodeling, particularly membrane ruffles, although its precise distribution may differ from the ERM proteins expressed in the same cell (Gonzalez-Agosti et al., 1996). In addition, schwannoma cells from NF2-associated tumors have dramatic alterations in the actin cytoskeleton and display abnormalities in cell spreading (Pelton et al., 1998). These results suggest that merlin may play an important role in regulating both actin cytoskeleton-mediated processes and cell proliferation. However, unlike the ERM proteins, merlin exerts a growth suppression effect. Over-expression of merlin in mouse fibroblasts or rat schwannoma cells can limit cell growth (Lutchman and Rouleau, 1995; Sherman et al., 1997; Gutmann et al., 1998) and suppress transformation by a *ras* oncogene (Tikoo et al., 1994). Recent studies demonstrate that cells lacking *NF2* function exhibit characteristics of cells expressing activated alleles of the small GTPase Rac, and the p21-activated kinase 2, a downstream target of Rac1/Cdc42, which directly phosphorylates merlin, affecting merlin's localization and function (Shaw et al., 2001; Xiao et al., 2002; Kissil et al., 2002; Surace et al., 2004; Rong et al., 2004).

Studies of *Nf2* gene knockout in mice show that merlin function is essential during early embryonic development. Homozygous *Nf2* mutant mouse embryos fail in development at approximately day 7 of gestation and die immediately prior to gastrulation (McClatchey et al., 1997). Conditional homozygous deletion of *Nf2* in Schwann cells or arachnoid cells leads to hyperplasia and tumor development, which are characteristics of NF2 (Giovannini et al., 2000; Kalamarides et al., 2002). Although these results argue that loss of merlin is sufficient for schwannoma and meningioma formation in vivo, none of the lesions detected in these mice were found in the vestibular nerve. This observation contrasts with the vestibular schwannomas commonly found in patients with NF2.

To better understand merlin function during development, previous studies examined merlin expression using Northern blot, in situ hybridization, RT-PCR, or immunostaining; however, these studies have not yielded consistent results. An earlier report indicated that the *NF2* gene was only expressed in tissues of ectodermal origin (World Health Org., 1992). Subsequently, Bianchi et al. (1994) reported that merlin RNA was not detected in the adult human heart and liver, whereas Haase et al. (1994) noticed abundant merlin RNA expression in the adult mouse heart. Similarly, no merlin RNA was detected in the adult mouse lung, whereas abundant expression could be found in the adult human lung. Northern blot analysis, however, detected *Nf2* transcripts in the adult mouse brain, kidney, cardiac muscle, skin, and lung (Claudio et al., 1994). By in situ hybridization and reverse transcription-polymerase chain reaction (RT-PCR) analyses, Gutmann et al. (1994) reported that rat merlin was widely expressed during mid to late embryogenesis. High levels of merlin expression were seen in cerebral cortex, brainstem, spinal cord, and heart during embryonic days E12–16. Merlin RNA expression becomes restricted to the brainstem, cerebellum, dorsal root ganglia, spinal cord, adrenal gland, and testis in adult animals, while no appreciable levels of merlin RNA could be detected in kidney, lung, and skeletal muscle. On the contrary, by in situ hybridization and immunostaining, Huynh et al. (1996) showed that merlin was detected in most differentiated tissues but not in undifferentiated tissues. In particular, merlin was not detectable in mitotic neuroepithelial cells, the perichondrium, the liver, the neocortex, and the ventricular zone of the developing cerebral cortex. Furthermore, in contrast to the phenotype of early embryonic lethality in mice lacking *Nf2* function, Gronholm et al. (2005) did not detect merlin protein expression until E11 in mouse embryos. In light of these inconsistent results, a detailed analysis of *NF2* expression during embryonic development is needed.

Previously, we have defined the 5′ flanking sequence of the human *NF2* gene and showed that the 2.4-kb *NF2* promoter could direct strong expression in several cell lines including neuronal cells (Welling et al., 2000; Chang et al., 2002). However, whether the *NF2* promoter is sufficient for expression in a variety of tissues including Schwann cells and neurons in vivo has not been tested. The objective of this study was to define the *NF2* expression pattern during embryonic development using two approaches. First, we generated a construct containing the 2.4-kb *NF2* promoter-driven β-galactosidase (β-gal) with a nuclear localization signal and used it to produce transgenic mice. Whole-mount X-gal staining of transgenic embryos at various days post coitus (p.c.) was conducted and tissue sections were analyzed. Second, we performed whole-mount in situ hybridization using various *Nf2* cDNA fragments as probes to confirm the expression pattern. Our results show that the *NF2* promoter could direct β-gal expression as early as E5.5. β-gal expression was first detected in the embryonic ectoderm and, to a lesser extent, in some parts of endoderm and mesoderm. Subsequently, strong β-gal staining was seen in the developing neural tube, migrating neural crest cells, the heart, the dorsal aorta, and the paraaortic mesenchyme. As the embryos matured, significant levels of β-gal expression were found in the cranial ganglia V and VIII, spinal ganglia, pigmented epithelium of the retina, and skin.

RESULTS

The NF2 Promoter Directed Transgene Expression as Early as E5.5

To examine the *NF2* promoter expression pattern in vivo, we generated the

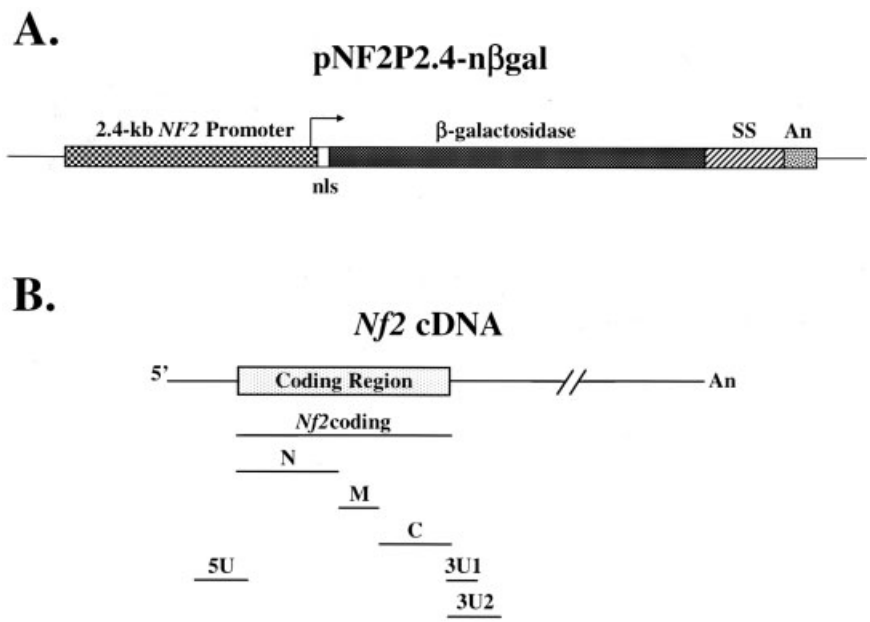

C.

Nf2 Primer	Sequence*	Position*
Coding-F	5'-ggtaccccgcgcc**atggccggagccatcgct**-3'	-13 ~ +18
Coding-R	5'-tcacctg**ctagagttcttcaaagaag**-3'	+1798 ~ +1773
5U-F	5'-acacgtgtgcgctcccaactactg-3'	-406 ~ -383
5U-R	5'-**cgatccgcaccgtgaatgtcttgg**-3'	+79 ~ +56
3U1-F	5'-**ggccttggacgtcctacacagcg**-3'	+1668 ~ +1690
3U1-R	5'-cggggccctcaactcaagagttcc-3'	+1913 ~ +1890
3U2-F	5'-**cagagcgccaagtcccgagtg**-3'	+1773 ~ +1798
3U2-R	5'-gcccatcccagaagcccagttg-3'	+2244 ~ +2223

Fig. 1. Schematic diagram of the pNF2P2.4-nβ-gal construct and various mouse cDNA fragments used in whole-mount RNA in situ hybridization. **A:** The pNF2P2.4-nβ-gal construct contains the 2.4-kb human *NF2* promoter fused with a nuclear localization signal (nls)-containing β-gal expression cassette. SS, SV40 splicing signal; An, SV40 polyadenylation sequence. **B:** Various mouse *Nf2* cDNA fragments were obtained by RT-PCR as described in the Experimental Procedures section and cloned into the pCRII-TOPO vector. The relative locations of the *Nf2* cDNA fragments are illustrated. **C:** Nucleotide sequences and locations of the mouse *Nf2*-specific primers. *Nucleotide position +1 is assigned to the A residue of the ATG translation start codon (GenBank accession No. L27090). +The ATG translation start codon is underlined. The primer sequence in the *Nf2* coding region is shown in bold letters while that in the 5′ or 3′ untranslated region is indicated in small letters.

pNF2P2.4-nβgal construct containing the β-gal reporter with a nuclear localization signal under the control of the 2.4-kb human *NF2* promoter (Fig. 1A), and used it to produce transgenic mice. Four lines of transgenic NF2P2.4-nβgal mice were generated. To detect the transgene-encoded β-gal, embryos were obtained from the mating of all four lines of transgenic mice at various days p.c. and whole-mount X-gal staining was performed. All four lines of the transgenic NF2P2.4-nβgal mice showed a similar β-gal staining pattern, eliminating the positional effect due to integration.

As shown in Figure 2A, β-gal staining could be seen in the transgenic embryo as early as E5.5. At this stage, β-gal expression was detected only in the embryonic tissue but not in the extraembryonic tissue. At E6.5, strong β-gal staining was found in the embryonic ectoderm. Cells in this embryonic tissue divided rapidly with visible mitotic figures, and were darkly stained (Fig. 2B). Significant β-gal expression was also seen in some parts of the proximal embryonic endoderm. Weak β-gal staining was detected in the mesoderm, while no staining was seen in the extraembryonic ectoderm (Fig. 2A). E7.5 is the stage when a portion of the dorsal embryonic ectoderm begins to specify into the neural ectoderm, a process important to the formation and shaping of the neural plate (Hogan et al., 1994; Rugh, 1994). High levels of β-gal expression continued to be observed in the embryonic ectoderm of the transgenic E7.5 embryo (Fig. 2A). Similar to that observed at E6.5, substantial β-gal staining was also detected in the embryonic endoderm. Intriguingly, the staining was not contiguous in this endoderm at E7.5; some regions were extensively labeled while others were not. In the mesoderm, only a few cells showed significant β-gal staining, while in the extraembryonic tissues, the ectoplacental cone and the chorionic ectoderm remained negative for β-gal expression.

The Transgene-Encoded β-gal Staining Pattern Coincided With the Endogenous Nf2 RNA Expression Pattern in the Embryonic Tissues

As mentioned earlier, previous studies examining merlin expression, particularly using in situ hybridization and immunostaining (Gutmann et al., 1994, 1996), did not yield consistent results. To examine whether the 2.4-kb *NF2* promoter could recapitulate the endogenous *Nf2* expression pattern, we performed whole-mount RNA in situ hybridization analysis. Various regions of the *Nf2* cDNA were cloned into the pCRII vector (Fig. 1B). Both sense and antisense riboprobes were synthesized from each plasmid by in vitro transcription and used in whole-mount embryo hybridization. We found that the antisense probe prepared from 3U1, containing the *Nf2* sequence immediately upstream of the translation termination codon to about 300 bp into the 3′ untranslated region (Fig. 1), consistently gave rise to a lower background when the

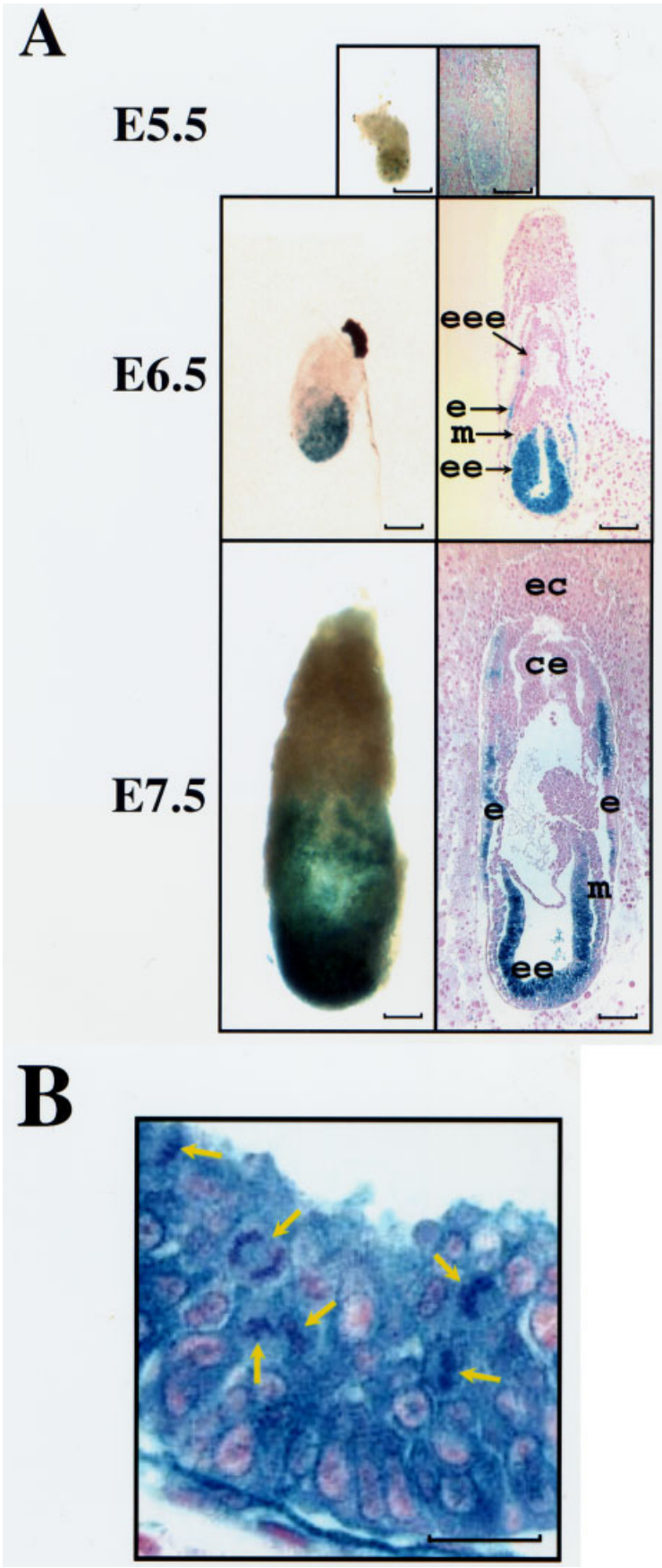

sense probe was compared with the antisense probe. The representative images of whole-mount RNA in situ hybridization of E7.5 embryos are shown in Figure 3. *Nf2* RNA expression was readily detected throughout the embedded embryo and its surrounding decidua, when the antisense probe, derived from 3U1, was used. In contrast, the sense probe yielded little hybridization (compare Fig. 3A with 3B). To visualize which embryonic tissues expressed *Nf2* RNA, dissected embryos were used in the in situ hybridization experiment. High levels of *Nf2* RNA expression were detected in the embryonic tissues, particularly in the developing neural ectoderm (Fig. 3C). For comparison, we performed whole-mount X-gal staining of transgenic E7.5 embryos. As shown in Figure 3D, the β-gal staining pattern in the embryonic tissue was similar to the endogenous *Nf2* RNA expression pattern, exhibiting the strongest staining in the neural ectoderm.

In addition, we performed whole-mount RNA in situ hybridization and β-gal staining of E8.5 and E9.5 embryos. Similar to that observed in the E7.5 embryo, *Nf2* RNA expression was detected throughout the E8.5 embryo with the strongest expression in the developing neural tube (compared Fig. 4A with 4B). Also, *Nf2* RNA expression was detected in the allantois and the yolk sac (Fig. 4A). Consistent with the RNA in situ hybridization result, strong β-gal staining was seen in the embryonic tissues of transgenic E8.5 embryo, particularly in the neural tube (Fig. 4C), while no β-gal staining was found in the wild-type E8.5 embryo (Fig. 4D). It should be noted that at this stage, β-gal expression was detected in the allantois and the yolk sac, but was not seen in the ectoplacental cone (Fig. 4C). As the

Fig. 2. Expression of β-gal in transgenic E5.5–7.5 embryos. **A:** Images of whole mount X-gal stained transgenic embryos at E5.5–7.5. eee, extraembryonic ectoderm; ee, embryonic ectoderm; m, mesoderm; e, endoderm; ec, ectoplacental cone; ce, chorionic ectoderm. Scale bar = 100 μm. **B:** Tissue section revealed strong β-gal staining in mitotic cells from embryonic ectoderm of the E6.5 embryo. Tissue section was photographed at 400× magnification. Arrows point to mitotic cells. Scale bar = 10 μm.

embryo matured to E9.5, *Nf2* RNA expression was consistently detected throughout the entire embryo with the strongest expression in the developing brain and spinal cord (compare Fig. 5A with 5B). The neural crest cell-populated branchial arches and the hematopoietic stem cell–containing paraaortic splanchnopleura also showed significant *Nf2* RNA expression (Fig. 5A). A similar β-gal staining pattern was detected in the transgenic E9.5 embryo (Fig. 5C). The tissues that gave rise to the strongest β-gal staining included the brain, spinal cord, and heart regions, the branchial arches, and the paraaortic splanchnopleura along with the dorsal aorta. Taken together, these results indicate that the β-gal staining pattern qualitatively matches most of the *Nf2* RNA distribution pattern, particularly in the embryonic tissues.

Changes in NF2 Promoter Activity During Neural Crest Cell Migration

Around E8.5, which is the early stage of organogenesis, the neural ectoderm-derived neural plate folds into the neural tube. Examination of β-gal-expressing cells in the E8.5 transgenic embryo section detected the highest level of expression in the neural tube, particularly in the rostral end, and the intensity of the β-gal staining gradually decreased toward the caudal extremity (Fig. 4E). Intriguingly, cells in the dorsal ridge of the neural folds in the cranial region and its adjacent non-neural ectoderm were only modestly stained (arrowheads pointed to this region in Fig. 4E). Previous studies have shown that the neural crest cells arise in the neural folds at the border between the neural and non-neural ectoderm (Hogan et al., 1994; LeDouarin and Kalcheim, 1999). Although initially contained within the central nervous system, the neural crest cells depart from the site of origin, migrate extensively throughout the embryo, and form many diverse derivatives including most of the peripheral nervous system, facial skeleton, and melanocytes of the skin. A detailed analysis of transversal sections of the anterior neural tube from transgenic embryos at around E8.5 revealed that while β-gal staining was detected in the neural folds, little staining was seen in the round-shaped neural crest cells that were in the process of delaminating from the dorsal ridge region of the neural fold (Fig. 4F). However, significant β-gal staining was detected in the neural crest cells already migrating away from the dorsal neural tube (Fig. 4G). Blue-stained cells were detected along the putative pathways of neural crest cell migration particularly in the dorsal trunk mesenchyme beneath the ectoderm and between the somite and neural tube (Fig. 4E and G; also see below). A number of markers on neural crest cells have been used to trace their migration. Among them, the Sox9 transcription factor is important for neural crest induction, survival, and delamination (Cheung and Briscoe, 2003; Mori-Akiyama et al., 2003). Interestingly, we observed abundant Sox9 protein expression in the migrating neural crest cells (Fig. 6A,B). Substantial β-gal expression was observed in the endocardium of the heart (Fig. 4E) and within the wall of the dorsal aorta (Fig. 4G). β-gal staining was also found in the yolk sac and allantois (Fig. 4E). At this embryonic stage, the yolk sac consists of an endodermal epithelium and underlying mesoderm within which blood islands and vessels develop. Significant β-gal expression was detected in the endodermal epithelium of the yolk sac and some labeled cells were seen within the blood island.

Upon examination of tissue sections of the transgenic E9.5 embryos, highly labeled cells continued to be detected in the neural tube. Within the neural tube, high levels of β-gal activity were found in the developing forebrain, midbrain, and hindbrain (Fig. 5C,D). As reported previously (LeDouarin and Kalcheim, 1999), the neural crest–derived cells from the posterior midbrain and hindbrain region migrate ventrolaterally and densely populate the first, second, and third branchial arches. Significant β-gal expression was seen in the cells of the craniofacial mesenchyme and the first branchial arch in the pharyngeal region (Fig. 5D). The entire mesenchymal component of the branchial arch, which was derived from the neural crest cells, was highly labeled, whereas the epithelium covering the branchial arch and the foregut endoderm were not labeled. Strong β-gal staining was also detected in the paraaortic splanchnopleura, and the heart region and the dorsal aorta were also positive for β-gal staining (Fig. 5D).

The Most Intense β-gal Staining Was Detected Along the Dorsal Midline of the Neural Tube

Whole-mount embryo staining showed that the *NF2* promoter-directed β-gal expression was predominantly observed in the anterior part of the transgenic embryo at E9.5 (Fig. 7A). The β-gal staining extended to the posterior extremity as the embryo matured from E10.5 to E14.5 (Fig. 7B–D). By E14.5, extensive β-gal expression was detected throughout the embryo (Fig. 7D).

Previous studies (Rugh, 1994; Wallingord, 2005) indicate that the neural tube begins to close at E8.5 from multiple sites in the middle portion of the embryo and extends toward the anterior and posterior ends in a zipper-like fashion. By E9.5, most parts of the neural tube have already closed, and only small openings, called neural pores, are left in both the anterior and posterior ends of the embryo. We found that the most intense β-gal staining was located along the dorsal midline, the line of the neural tube closure, in the E9.5 embryo (Fig. 8A). Deep staining was observed particularly in the area of the anterior neuropore, forming the fourth brain ventricle, also known as myelocoel. By E10.5, the anterior neuropore is completely closed (Rugh, 1994; Wallingord, 2005). Intense β-gal staining was still observed at the site of the thin roof of the fourth ventricle and along the dorsal midline of the neural tube (Fig. 8B). Consistent with those observed at the earlier stages of development, strong β-gal expression was detected in the branchial arches I–IV of the E10.5 embryo (Fig. 8C).

Strong β-gal Expression in the Embryonic Ectoderm-Derived Tissues

In tissue sections of the E10.5 embryo, very intense β-gal labeling was noted

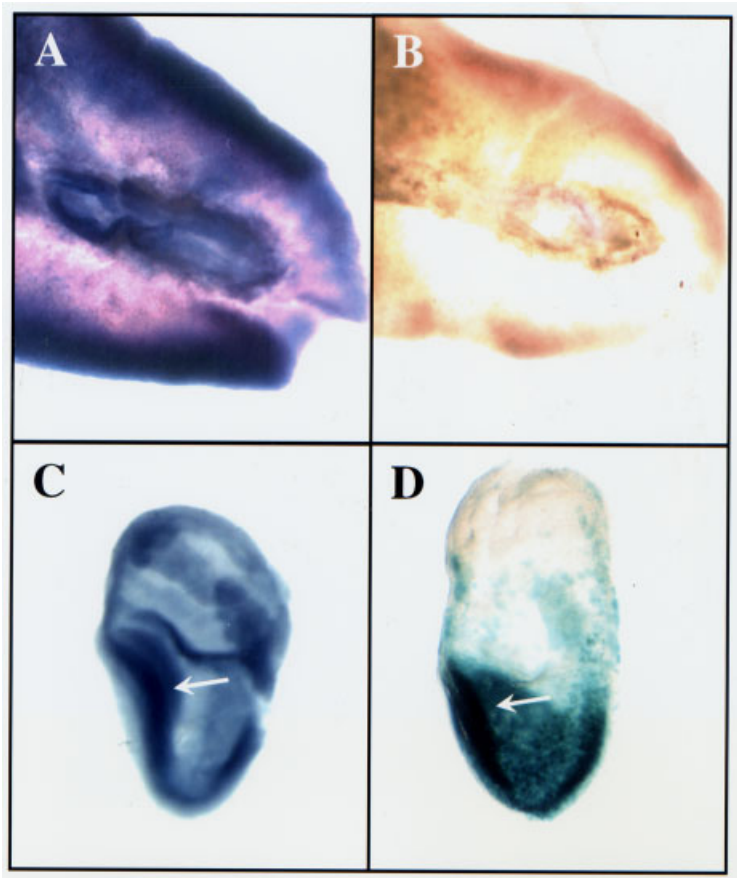

Fig. 3. Detection of endogenous *Nf2* RNA expression and β-gal staining in E7.5 embryos. Whole-mount RNA in situ hybridization of wild-type E7.5 embryos was performed using an antisense (**A,C**) or sense (**B**) *Nf2* 3U1 probe (Fig. 1) derived from the exon 17 region as described in the Experimental Procedures section. Compared to the results obtained from the sense probe control (B), strong *Nf2* RNA expression was detected in the embryo embedded in the decidua (A) or the dissected embryo (C), particularly in the developing neural ectoderm (arrow). Similarly, whole-mount X-gal staining showed strong β-gal expression in the developing neural ectoderm of the transgenic E7.5 embryo (**D**). The slight difference in the size and shape of the embryo shown in C and D was due to the procedures. The embryo processed for in situ hybridization was dehydrated with methanol, followed by proteinase K digestion and fixation. The embryo processed for β-gal was fixed in the fixation solution before X-gal staining. Nevertheless, the β-gal staining pattern in the embryonic tissue was similar to the endogenous *Nf2* RNA expression pattern.

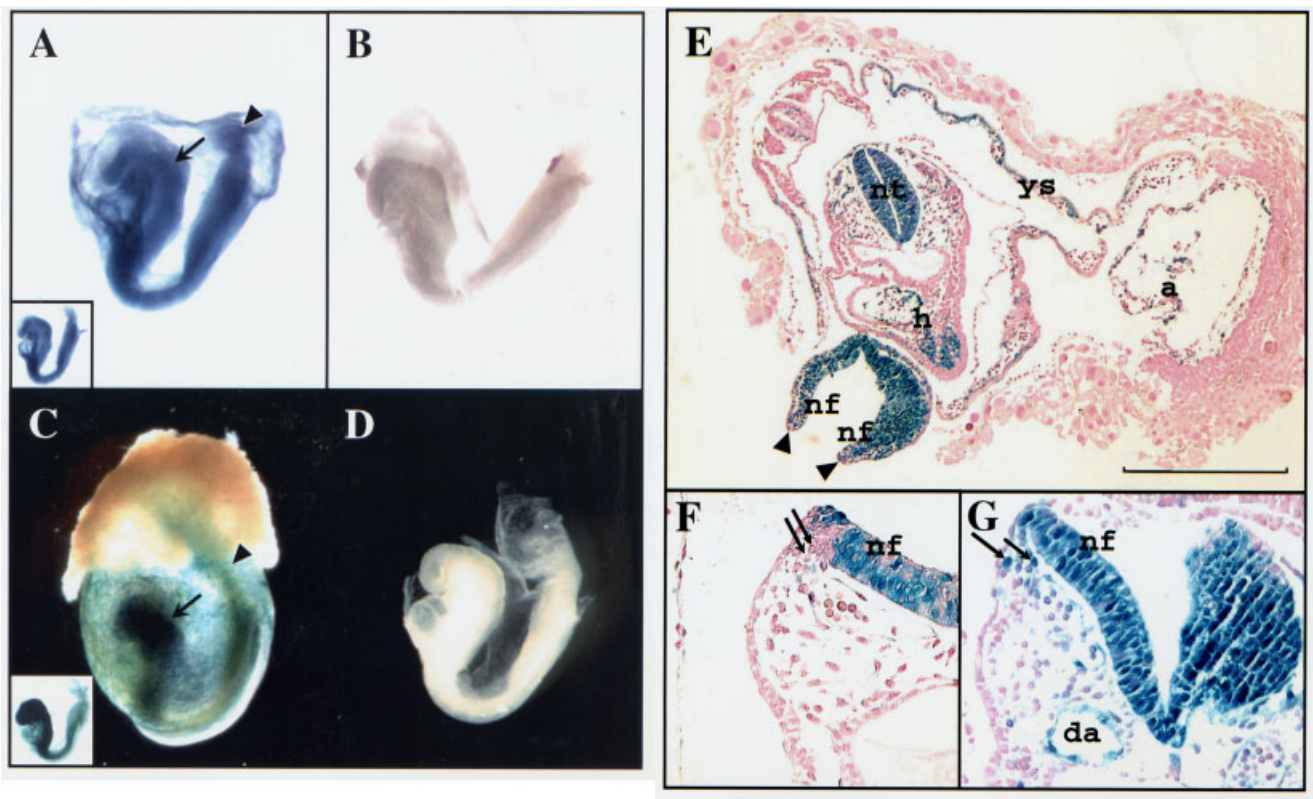

Fig. 4.

in the tela choroidea, which is the thin roof of the fourth ventricle (Fig. 9A). This roof plate consists of a single layer of ependymal cells, which is later covered by the pia mater, the inner layer of the meninges (Rugh, 1994). Significant β-gal expression was detected in the metencephalon and the myelencephalon. In addition, strong β-gal staining was found in the forebrain, including the telencephalon and the diencephalon, the optic chiasma, the tuberculum posterius, and the infundibulum (Fig. 9B). However, only some parts of the mesencephalon were darkly stained while others were lightly stained. In the head region, the epidermal layer, which contains presumptive melanocytes, was also labeled (Fig. 9A).

The retina is the innermost layer of the eye and is derived embryologically from the outgrowth of the developing brain (Martinez-Morales et al., 2004). It is comprised of two major layers, the inner layer (prospective neural layer of the retina) and the outer layer (prospective pigmented epithelium). In the E10.5 transgenic embryo, intense β-gal staining was readily detected in the pigmented epithelium layer of the retina, whereas the neural layer of the retina and the lens show very little expression (Fig. 9C).

As noted above, strong β-gal activity was detected in the mesenchyme of the mandible prominence of the first branchial arch in the E10.5 transgenic embryo (Fig. 9D). The adjacent neural crest cells populating the truncus arteriosus also showed intense labeling. In addition, significant β-gal expression was found in the paraaortic mesenchyme and the heart region. Furthermore, the dorsal aspect of the forming spinal cord and its flanking primordial spinal ganglia were strongly labeled. Together, these results indicate that the *NF2* promoter is strongly expressed in various embryonic ectoderm-derived tissues.

NF2 Promoter-Directed β-gal Expression to the Trigeminal Ganglion and Acoustic Ganglion

At E11.5, the forebrain is separated into a paired telencephalic vesicles and the diencephalon. We observed high levels of β-gal activity in both lobes of the telencephaon and in the diencephalon of the E11.5 transgenic embryo (Fig. 10A). However, the midbrain mesencephalon was only lightly stained with the exception of the dorsal midline closure, which consistently displayed intense staining similar to those seen at earlier stages. Interestingly, we detected a striped pattern of β-gal staining in the hindbrain-derived myelencephalon (Fig. 10B) and the metencephalon (also see below). β-gal expression can also be found in the cranial ganglion VIII, derived from the hindbrain and also known as the acoustic ganglion, and its extending nerve. The β-gal staining was particularly notable in the cells surrounding the acoustic ganglion and extending nerve (Fig. 10B). It should be mentioned that the extending nerve expressed a higher level of S100 immunoreactivity than the ganglion (Fig. 6C). Some of the cells inside the ganglion also expressed β-gal (Fig. 10B). In addition, strong β-gal staining was detected in the cranial ganglion V, which is also called the trigeminal ganglion; both the trigeminal ganglion and its three nerve divisions were robustly labeled (Fig. 10C). Consistent with the β-gal staining, immunostaining revealed that merlin was expressed throughout the trigeminal ganglion (Fig. 6D). Similar to that seen at E10.5, very intense β-gal staining was detected in the pigmented epithelium of the retina (Fig. 10C).

As noted before, the dorsal midline of the spinal cord from the E11.5 embryo was darkly stained for β-gal expression; however, only a few cells inside the spinal cord were labeled (Fig. 10D,E). Interestingly, we noted that the cells in the dorsal midline of neural tube closure expressed a high level of Sox9, a neural crest determinant marker (Fig. 6E). β-gal staining was detected in the cells surrounding the spinal ganglia and in some, but few, cells inside the spinal ganglia. It appeared that the cells along the ventral and dorsolateral pathways of neural crest cell migration were labeled (Fig. 10E). The sclerotome of somites has been shown to play an essential role in neural crest migration of the early ventral pathway (Hogan et al., 1994; Chen et al., 2004; Hay 2005; Honjo and Eisen, 2005). Significantly, we also detected deep β-gal staining in the sclerotome (Fig. 10F).

In addition to intense β-gal staining in the dorsal aorta as seen in earlier stages, the paraaortic mesenchyme were strongly labeled at E11.5 (Fig. 10G). Within the four-chambered heart, the endometrial tissue, including the valves, showed the highest β-gal activity. Intervertebral arteries were also labeled. While some β-gal was expressed in the liver and mesonephros, only weak staining was detected in the gonad (Fig. 10F,G).

Broad β-gal Expression Pattern in Various Neural Tissues During Mid-Embryogenesis

At E12.5, the anterior portion of the telencephalon continued to express high levels of β-gal, while the staining

Fig. 4. The *Nf2* RNA expression and β-gal staining pattern in E8.5 embryos. **A–D:** The pattern of strong *Nf2* RNA expression in the developing neural tube of the wild-type E8.5 embryo was confirmed by the β-gal staining of the E8.5 transgenic embryo. Whole-mount RNA in situ hybridization of wild-type E8.5 embryos was performed using an antisense (A) or sense (B) *Nf2* probe as described in Figure 3. Whole-mount X-gal staining was also performed on transgenic (C) or non-transgenic (D) E8.5 embryos. Note that the developing neural tube (arrow) showed strong *Nf2* RNA or β-gal expression. In addition, *Nf2* expression was also detected in the allantois (arrowhead). The small photograph inset in A and C displays the dissected embryo from in situ hybridization and β-gal staining analysis, respectively. **E–G:** Change of *NF2* promoter activity during neural crest cell migration. **E:** A transverse section of the transgenic E8.5 embryo showed significant β-gal expression in neural fold (nf) of the head region, the developing neural tube (nt) and heart (h), as well as yolk sac (ys) and allantois (a). Note that the tip (arrows) of the neural fold displayed weak β-gal staining compared to the rest of the neural fold, which exhibited strong β-gal activity. Scale bar = 100 μm. **F,G:** Detailed analysis of tissue sections containing the neural fold region revealed that while little β-gal staining was found in the round-shaped neural crest cells (arrows), which were at the moment of delaminating from the dorsal ridge region of the neural fold (F), significant β-gal expression was detected in the neural crest cells already migrating away from the dorsal neural tube (G). da, dorsal aorta.

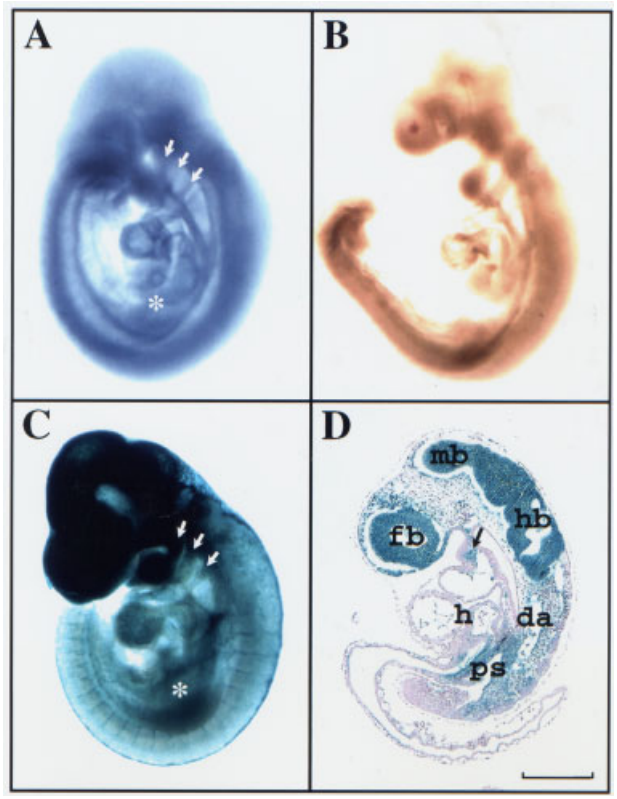

Fig. 5.

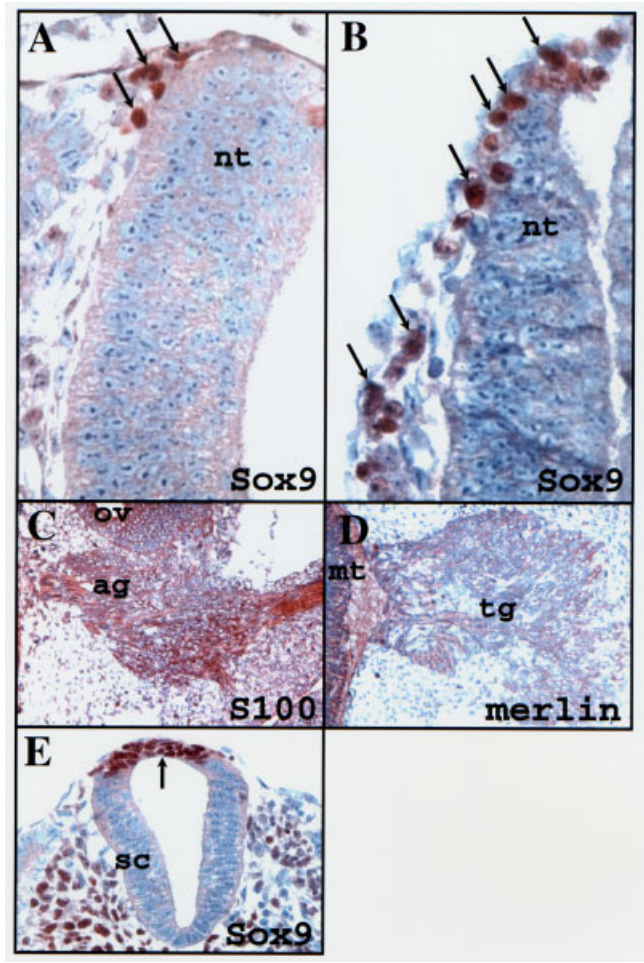

Fig. 6.

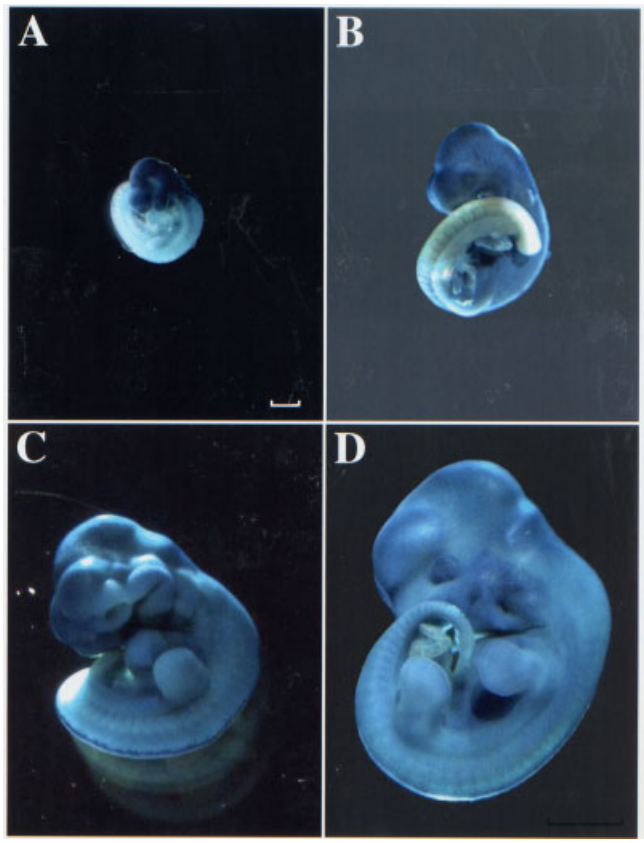

Fig. 7.

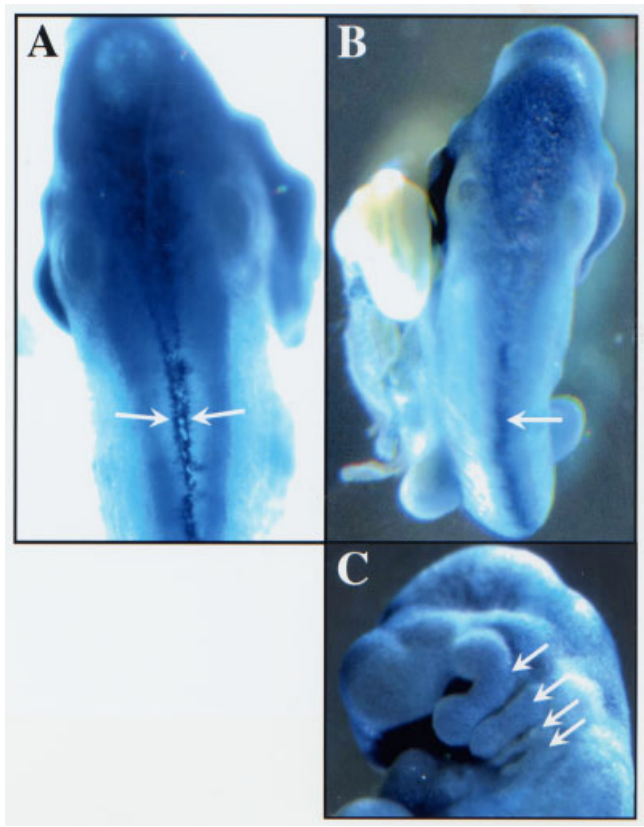

Fig. 8.

in the posterior part was less saturated (Fig. 11A). Similarly, some portions of the diencephalon expressed significant levels of β-gal, whereas other regions were weakly stained (Fig. 11B). Curiously, the pigmented epithelium of the retina continued to be intensely labeled at this stage. The lens epithelium and some cells in the lens also expressed moderate levels of β-gal.

The posterior commissure is the roof of the brain between the anterior limit of the mesencephalon and the posterior portion of the diencephalon. Saturated β-gal staining was observed in the posterior commissure, while only patchy staining was seen in the rest of the mesencephalon (Fig. 11C). However, it appeared that more labeled cells were present in the mesencephalon proximal to the posterior commissure. The isthmus or mesencephalon-metencephalon junction tissue is an organizing center that plays an important role in the midbrain-hindbrain patterning (Wassef and Joyner, 1997). Intriguingly, intense β-gal staining was found in the isthmic tissue of the mesencephalic part (Fig. 11D). In contrast, the metencephalic portion of this junction tissue showed a striped β-gal staining pattern, similar to that of the rest of the metencephalon. Consistent with robust β-gal expression in the tela choroidea observed at earlier stages, the tela choroidea-derived posterior choroid plexus was strongly labeled in the E12.5 embryo. The tuberculum posterius is a thickening in the floor of the brain at the region of the anterior end of the notochord. It represents the posterior margin of the diencephalon and develops into a part of the hypothalamus. We noted that some discrete regions of the tuberculum posterius showed high levels of β-gal activity, while some other parts expressed notably smaller amounts of β-gal (Fig. 11E). At this stage, significant β-gal staining was still seen in the trigeminal ganglion and its nerve divisions; however, unlike the strong labeling throughout the entire ganglion observed at E11.5, the central part of the trigeminal ganglion from the E12.5 embryo appeared to show little β-gal staining (Fig. 11F). Interestingly, the synaptic junction area between the trigeminal ganglion and the hindbrain remained strongly labeled (Figs. 10C and 11F). In addition, similar to that noted at E11.5, cells surrounding spinal ganglia and their extending nerves continued to show significant β-gal expression in the E12.5 embryo (Fig. 11G). Taken together, these results indicate that the *NF2* promoter is widely expressed in neural tissues during embryogenesis.

DISCUSSION

The development of schwannomas on or around the vestibular branch of both eighth cranial nerves has been considered as the hallmark of NF2, but other tumors and ocular abnormalities are observed as well (Neff et al., 2005). Most NF2 patients go on to develop multiple schwannomas that are associated with other cranial nerves, such as the trigeminal nerve and the spinal nerve roots. In addition, cranial and spinal meningiomas and, less frequently, ependymomas occur. Such restricted symptoms and phenotypes associated with NF2 are unusual, given the fact that the *NF2* tumor suppressor protein is widely expressed in many cell types. In this report, we showed that the *NF2* promoter was active at early embryogenesis. *NF2* promoter–directed β-gal expression was detected as early as E5.5 and intense β-gal staining was observed at E6.5 in the embryonic ectoderm containing many mitotic cells. In addition, *NF2* promoter activity was detected in parts of the embryonic endoderm and mesoderm. *NF2* promoter continued to be actively expressed in the neural ectoderm and its derived neural tissues throughout mid-embryogenesis. These results are consistent with earlier findings (Gutmann et al., 1994; McClatchey et al., 1997; Stemmer-Rachamimov et al., 1997) and further indicate that *NF2* is an early expression marker.

Currently, limited information is known about the role of merlin during embryonic development and tissue differentiation. In mice, homozygous *Nf2* inactivation is embryonically lethal (McClatchey et al., 1997). Although these results suggest an essential role for *NF2* during early embryogenesis, the function of merlin in these processes is not understood. Merlin has been shown to regulate cell motility and cell adhesion. In cultured mammalian cells, merlin is concentrated in the membrane ruffle and adherens junction (Gonzalez-Agosti et al., 1996; Shaw et al., 1998; Maeda et al., 1999; Lallemand et al., 2003). In cultured polarized neurons, merlin localizes to synaptic junctions (Gronholm et al., 2005). Merlin can associate with the actin cytoskeleton directly (Xu and Gutmann, 1998) or

Fig. 5. Strong *Nf2* RNA expression and β-gal staining were detected in the developing brain, the branchial arches, and the paraaortic splanchnopleura of E9.5 embryos. In situ hybridization of wild-type E9.5 embryos was performed using an antisense (**A**) or sense (**B**) *Nf2* probe as described before. Whole-mount X-gal staining was also performed on transgenic E9.5 embryos (**C**). Sagittal section of the β-gal stained embryo was obtained (**D**). Arrows point to neural crest cell populated branchial arches and the asterisk marks the location of the paraaortic splanchnopleura. fb, forebrain; mb, midbrain; hb, hindbrain; h, heart; da, dorsal aorta; ps, paraaortic splanchnopleura. Scale bar = 200 μm.

Fig. 6. Immunohistochemical analysis of tissue sections from E9 (**A,B**) and E11.5 embryos (**C–E**). Tissue sections were stained with anti-Sox9 (A,B,D), anti-S100 (C), and anti-merlin (E) antibodies according to the Experimental Procedures section. A hematoxylin was used as a counterstain. The positively stained tissue appeared brown. Arrows point to migrating neural crest cells (A,B) or dorsal midline of the neural tube closure (D). nt, neural tube; sc; spinal cord, ag, acoustic ganglion; ov, otic vesicle; mt, metencephalon; tg, trigeminal ganglion.

Fig. 7. Lateral views of whole-mount X-gal-stained transgenic mouse embryos at various days p.c. (**A**) E 9.5, (**B**) E10.5, (**C**) E12.5, and (**D**) E14.5. Scale bar = 400 μm.

Fig. 8. The most intense β-gal expression was detected along the dorsal closure (arrows) of neural tube in E9.5 (**A**) and E10.5 (**B**) transgenic embryos. Strong β-gal expression was also seen in the Branchial arches I–IV (arrows) of the E10.5 embryo (**C**).

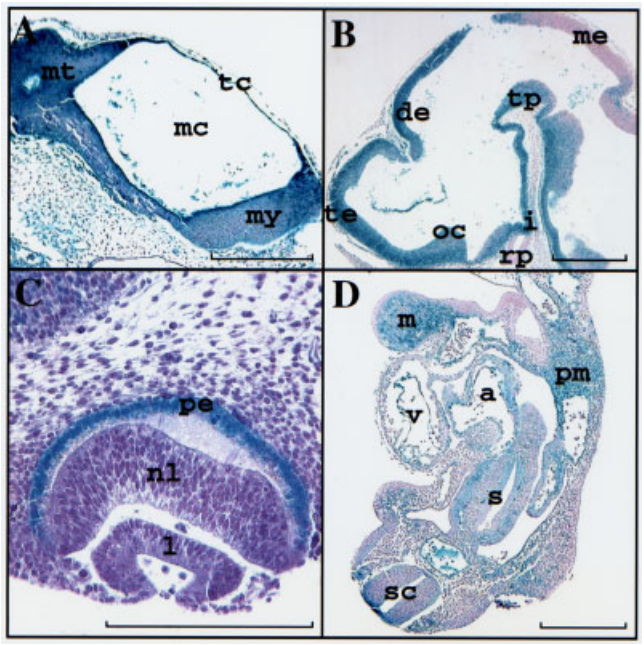

Fig. 9.

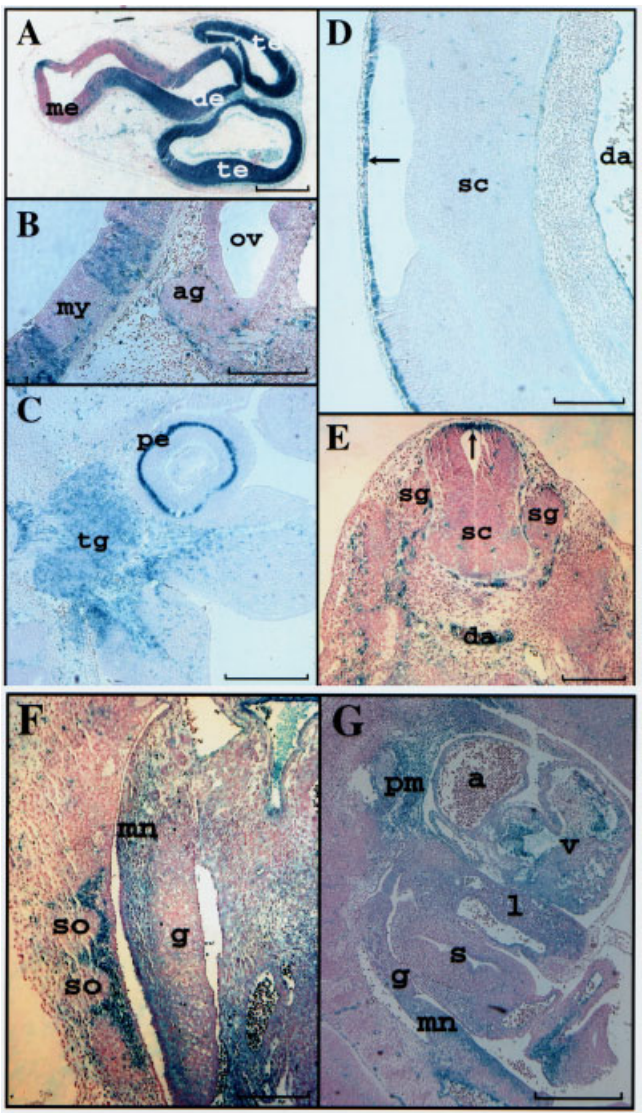

Fig. 10.

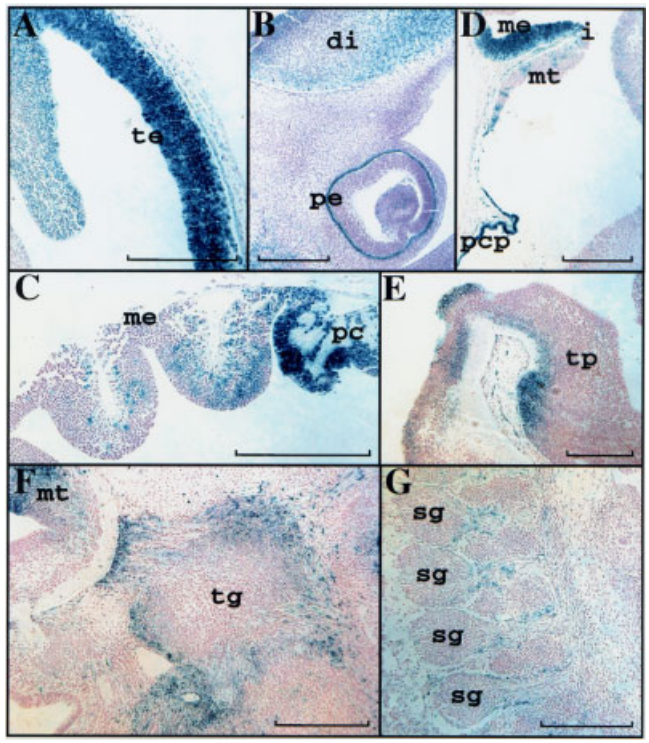

Fig. 11. The β-gal staining pattern in various neural tissue sections from transgenic E12.5 embryos. Whole-mount X-gal stained embryos were prepared and sagittal sections were obtained as described before. **A:** Intense β-gal expression was found in the telencephalon (te). **B:** Deep β-gal staining continued to be detected in the pigmented epithelium of the retina (pe). di, diencephalon. **C:** Strong β-gal staining was observed in the posterior commissure (pc) compared to that in the mesencephalon (me), which showed patchy expression. **D:** The tela choroidea-derived posterior choroid plexus (pcp) in the 4th ventricle area was deeply labeled. me, mesencephalon; i, isthmus; mt, metencephalon. **E:** Only certain areas in the tuberculum posterius (tp) were positive for β-gal staining. **F:** Significant β-gal expression was also observed in the trigeminal ganglion (tg) and its nerve divisions. mt, metencephalon. **G:** Cells surrounding the spinal ganglia (sg) and their extending nerves continued to show β-gal staining. Scale bar = 300 μm.

indirectly by interacting with actin-binding proteins (Scoles et al., 1998; Fernandez-Valle et al., 2002). Re-expression of merlin in *Nf2*-deficient cells attenuates actin cytoskeleton-associated processes, including motility (Gutmann et al., 1999). In addition, over-expression of merlin mutants alters cell adhesion, causing fibroblasts to detach from the substratum (Stokowski and Cox, 2000). Also, *Nf2* deficiency results in an inability of mouse fibroblasts or keratinocytes to undergo contact-dependent growth arrest and to form stable cadherin-containing cell:cell junctions (Lallemand et al., 2003). Merlin may stabilize adherens junctions by inhibiting Rac/Pak signaling and stabilizing the actin cytoskeleton (Shaw et al., 2001; Kissil et al., 2002; Xiao et al., 2002;

McClatchey and Giovannini, 2005). Moreover, *Nf2*-deficient mouse tumor cells are highly motile and metastatic in vivo (McClatchey et al., 1998). Together, these results suggest that merlin may participate in fundamental processes involving the regulation of cell migration, cell adhesion, and cell proliferation during embryonic development.

It has been well documented that during embryogenesis, many cells and tissues undergo complex morphogenetic movements, such as neural crest and progenitor germ cell migration, migration of hematopoietic progenitors into the embryonic hematopoietic rudiments, and neural tube closure (Graham, 2003; Bertrand et al., 2005; Wallingford, 2005); however, the underlying cellular and molecular mechanisms are poorly understood. Studies have shown that cell migration is highly regulated and involves the extension of leading processes, where continuous remodeling of actin and adhesive contacts is required (Li et al., 2005). Interestingly, we observed strong *NF2* promoter activity in sites where migrating cells were located including the neural tube closure, the branchial arches, the dorsal aorta, and the paraaortic splanchnopleura. The most intense activity was detected along the dorsal midline during neural tube closure, the location where the adhesion and fusion of two opposing neural folds and epithelial sheets occur. Similarly, high levels of *NF2* promoter activity were seen at the site of the anterior neuropore closure in the head region. Notably, McLaughlin et al. (2004) recently generated conditional *Nf2* knockout mice in which *Nf2* was deleted throughout the developing central nervous system by using nestin promoter-driving *Cre* recombinase. These mice displayed defects in neural tube closure and tissue fusion. It is known that cell adhesion during dorsal closure relies on the activities of the dynamic actin-based protrusions (Jacinto et al., 2002; Woolner et al., 2005). Since merlin localizes to membrane ruffles and adherens junctions (Gonzalez-Agosti et al., 1996; Shaw et al., 1998; Maeda et al., 1999) and plays critical roles in cell motility and cell adhesion (Gutmann et al., 1999; Stokowski and Cox, 2000; Lallemand et al., 2003), the most intense *NF2* promoter activity along the dorsal midline and at the site of anterior neuropore closure that we detected suggests that merlin may be necessary for cytoskeletal machinery driving cell adhesion and movement during neural tube closure.

In addition, it is tempting to speculate that merlin may participate in neural crest cell migration. The neural crest comprises a group of highly motile cells, which are the precursors of peripheral neurons, Schwann cells, pigment and facial cartilage cells (Le-Douarin and Kalcheim, 1999; Jessen and Mirsky, 2005). Intriguingly, we detected little *NF2* promoter activity in premigratory neural crest cells and the round-shaped neural crest cells, which had just delaminated from the dorsal ridge region of the neural fold. On the contrary, significant *NF2* promoter activity was found in the neural crest cells already migrating away from the dorsal neural tube. Such a transient change of *NF2* promoter activity implies a transcriptional regulation during neural crest cell migration and further corroborates with the role of merlin in cell motility and cell adhesion (McClatchey, 2004; McClatchey and Giovannini, 2005). It is possible that down-regulation of *NF2* promoter expression may allow premigratory neural crest cells to delaminate from the dorsal neural tube. Once migrating away, the neural crest cells turn on the *NF2* gene to ensure cell migration and cell adhesion in order to colonize different parts of the embryo. Recently, several developmentally regulated transcription factors have been implicated in the control of neural crest induction and delamination (Cheung et al., 2005). Thus, it will be important to see whether these transcription factors regulate *NF2* promoter expression during neural crest cell migration.

Analogously, the *NF2* promoter was highly expressed in hematopoietic stem cell–producing tissues such as the yolk sac and the paraaortic mesenchyme. This mesodermally derived intraembryonic region, known as the aorta-gonad-mesonephros region or,

Fig. 9. Strong β-gal staining in the neural ectoderm-derived tissues of E10.5 transgenic embryos. **A:** Intense β-gal staining was detected in the metencephalon (mt), the tela choroidea (tc), and the myelencephalon (my). mc, myelocoel. Scale bar = 400 μm. **B:** Sagittal section of the head region revealed strong β-gal expression in the telencephalon (te), the diencephalon (de), the optic chiasma (oc), the tuberculum posterius (tp), and the infundibulum (i). Striped pattern of β-gal staining was seen in the mesencephalon (me), while little or no expression was detected in the Rathke's pocket (rp). Scale bar = 200 μm. A,D: Parasagittal sections. **C:** Sagittal section of the eye showed that the prospective pigmented epithelium (pe) of retina displayed robust β-gal staining, while the neural layer (nl) of the retina and the lens (l) exhibited very little expression. Scale bar = 100 μm. **D:** Significant β-gal expression was detected in the mandible prominence of the first branchial arch (m), the paraaortic mesenchyme (pm), the atrium (a) and the ventricle (v) of the heart, and the dorsal aspect of the spinal cord (sc). Some β-gal expression was seen in the stomach region (s). Scale bar = 400 μm.

Fig. 10. Significant *NF2* promoter activity was detected in various NF2-affected tissues such as the acoustic ganglion, the trigeminal ganglion, the spinal ganglia, and the pigmented epithelium of the retina in transgenic E11.5 embryos. A,E,F: Transverse sections. B–D,G: Sagittal sections. **A:** Strong β-gal expression was detected in the telencephalon (te) and the diencephalon (de). me, mesencephalon. Scale bar = 500 μm. **B:** The myelencephalon (my) showed a striped pattern of β-gal expression. The peripheral region of the acoustic ganglion (ag; cranial ganglion VIII) and its extending nerve also stained positive for β-gal expression. ov, otic vesicle. Scale bar = 250 μm. **C:** Intense β-gal expression was found in the pigmented epithelium (pe) of the retina. Also, strong β-gal expression was seen in the trigeminal ganglion (tg; cranial ganglion V) and its nerve branches. Scale bar = 250 μm. **D:** Robust β-gal staining continued to be seen along the dorsal midline (arrow) of the spinal cord (sc). Positive β-gal staining was also detected in the wall of the dorsal aorta (da). Scale bar = 200 μm. **E:** Strong β-gal expression was found in the dorsal aspect (arrow) of the spinal cord (sc). Positive β-gal staining was also detected along the dorsolateral and late ventral pathways of neural crest cell migration surrounding the spinal ganglion (sg). da, dorsal aorta. Scale bar = 300 μm. **F:** The sclerotome of somites showed strong β-gal expression. While the mesonephros (mn) exhibited positive β-gal staining, the gonad (g) showed little expression. Scale bar = 200 μm. **G:** Significant β-gal expression was observed in the paraaotic mesenchyme (pm), the heart, particularly the endocardium including the valves, the liver (l), and the mesonephros (mn). a, atrium; v, ventricle; pn, pronephros; s, stomach; g, gonad. Scale bar = 500 μm.

at a slightly earlier developmental stage, the paraaortic splanchnopleura, produces, respectively, potent hematopoietic stem cells and multipotent progenitor cells in addition to the yolk sac (Bertrand et al., 2005). The strong *NF2* promoter activity in these hematopoietic stem cell–producing tissues suggest that merlin may also play a role in the migration of hematopoietic progenitors into these embryonic hematopoietic rudiments including fetal liver, thymus, spleen, and bone marrow during embryonic development.

As mentioned above, in addition to vestibular schwannomas, most NF2 patients develop multiple schwannomas that are associated with trigeminal nerve and spinal nerve roots, and less commonly, meningiomas and ependymomas (McClatchey, 2004; McClatchey and Giovannini, 2005; Neff et al., 2005). We detected significant *NF2* promoter activity in all these affected tissues during embryonic development. In particular, very intense promoter activity was noted in the tela choroidea, which consists of a layer of ependymal cells covered by the meninges.

Significant *NF2* promoter activity was also seen in the acoustic ganglion, trigeminal ganglion, spinal ganglia, and their extending nerves. Furthermore, NF2 patients frequently suffer from juvenile lens opacities and a variety of retinal and optic nerve lesions including defects of the pigment epithelium and pigment epithelial retinal hamartomas (Evans et al., 1992; Parry et al., 1994; Meyers et al., 1995; Hazim et al., 1998; Levine and Slattery, 2003). Consistent with previous observations (Claudio et al., 1995; Huynh et al., 1996), we detected some *NF2* promoter activity in the lens. Strong promoter activity was also seen in the optic chiasma. In the retina, *NF2* promoter is highly expressed in the pigmented epithelium. The fact that the *NF2* promoter is very active in the tissues affected by NF2 during embryonic development further supports the role of merlin in the pathogenesis of this genetic disorder.

It should be noted that the 2.4-kb *NF2* promoter appeared to be sufficient to recapitulate most of the endogenous *Nf2* RNA expression pattern in the embryonic tissues during embryogenesis, as we compared the β-gal staining pattern with the results from the RNA in situ hybridization (Figs. 3–5; McClatchey et al., 1997; McLaughlin et al., 2004). A detailed comparison with embryo sections from in situ hybridization analysis will strengthen this conclusion. However, while the 2.4-kb *NF2* promoter could direct β-gal expression to some extraembryonic tissues such as allantois and yolk sac, no expression was detected in the ectoplacental cone and chorionic ectoderm in transgenic embryos at E6.5–7.5, the time when *Nf2* knockout mice show defects in extraembryonic tissues. We hypothesize that additional elements located in the upstream or downstream region of the *NF2* promoter are required for proper expression in these extraembryonic tissues.

Previously, we (Welling et al., 2000; Chang et al., 2002) showed that while multiple elements are required for full *NF2* promoter activity in transfected cells, a GC-rich sequence, which was located in the promoter proximal region and could be bound by transcription factor Sp1, served as a positive *cis*-acting regulatory element. We are presently conducting experiments to test whether the GC-rich sequence and other *cis*-acting regulatory elements are important for the spatial and temporal expression pattern of the *NF2* promoter. Understanding of the regulation of the *NF2* gene in vivo may provide us new clues regarding merlin's participation in cell migration and cell adhesion during embryonic development.

EXPERIMENTAL PROCEDURES

Transgene Construct and Transgenic Production

The pNF2P(-2092)-Luc plasmid containing the 2.4-kb human *NF2* promoter was described previously (Chang et al., 2002). The MFG-S-nlsLacZ retroviral vector was kindly provided by Dr. Bruce Bunnell (Imbert et al., 1998). To generate the pNF2P(-2092)-nlsLacZ construct, the luciferase expression unit was removed from pNF2P(-2092)-Luc and substituted with the LacZ gene, which contained a nuclear localization signal (nlsLacZ) and was excised from MFG-S-nlsLacZ vector. Subsequently, the splicing signal and the polyadenylation signal sequences isolated from pSV2-βG (Chang et al., 1989) were inserted downstream of the nlsLacZ sequence (Fig. 1A).

The *NF2* promoter-driven nls-*LacZ* expression cassette was excised from the pNF2P2.4-nls-LacZ plasmid by double digestions with *Not*I and *Sal*I enzymes. The *NF2* promoter-nls-LacZ DNA fragment was purified through a Qiaquick Gel Extraction kit (Qiagen, Chatsworth, CA) and microinjected into male pronuclei of fertilized one-cell mouse eggs obtained from superovulated FVB/N female mice (Hogan et al., 1994). Injected embryos were transferred into the oviduct of pseudopregnant female foster mice to allow complete development to term.

To identify transgenic mice, mouse-tail DNA was prepared using the Puregene kit (Gentra) and used in Southern blot analysis. High-molecular-weight mouse-tail DNA was digested with *Bam*HI enzyme, which cut once between the *NF2* promoter and nls-*Lac*Z DNA of the transgene. Digested DNA was electrophoresed onto a 0.7% agarose gel and then transferred to a GeneScreen Plus® hybridization transfer membrane (NEN Life Science). For the probe, the *Lac*Z DNA was labeled with biotinylated dNTP mixture by the random primed method using the NEBlot™ Phototope™ kit (New England Biolabs). Filter membranes containing mouse-tail DNAs were prehybridized in hybridization buffer for one hour, and then hybridized with the biotin-labeled *Lac*Z probe overnight. After hybridization, filters were washed twice in 0.1× SSC and 0.1% SDS at 65°C for 30 min each time. For detecting hybridization signal, the Phototope™-Star Detection Kit for Nucleic Acids (New England Biolabs) was used, and chemiluminescence was captured by the ChemiGenius^2 Image Acquisition System (Syngene) or by exposure to X-ray films. Once identified, transgenic mice were mated with FVB/N mice to generate offspring.

Whole-Mount X-Gal Staining

Transgenic mice were mated with each other. The day when the vaginal plug

was found, the embryo was aged as 0.5 day p.c. (E0.5). On the following day, the embryo was aged as E1.5 and so on. Embryos at various days p.c. were harvested and fixed in the fixative solution containing 1% formaldehyde, 0.2% glutaraldehyde, and 0.02% NP-40 in phosphate-buffered saline (PBS) for 40 min on ice. After fixation, embryos were incubated overnight in the X-gal staining solution, containing 5 mM $K_3Fe(CN)_6$, 5 mM $K_4Fe(CN)_6$, 2 mM $MgCl_2$, and 1 mg/ml of 5-bromo-4-chloro-3-indolyl-β-galactoside, at 37°C with gentle shaking. Stained embryos were rinsed with PBS and photographed under a Leica MZ16FA stereoscope. Embryos were further fixed overnight in 4% paraformaldehyde in PBS at 4°C and then embedded in paraffin. Five-micron tissue sections were obtained using a rotary microtome. Sections were deparaffinized, counter-stained with nuclear fast red, mounted with a coverslip, and then photographed under a Leica DM4000B microscope.

Cloning of Mouse *Nf2* cDNAs

Total RNA was isolated from adult mouse brain using the TRIzol reagent (Invitrogen) and used in RT-PCR to isolate *Nf2* cDNAs (Fig. 1B) as described previously (Chang et al., 2002). The mouse *Nf2* cDNA containing the entire coding region was obtained by RT-PCR using the primers Coding-F and Coding-R (Fig. 1C). The resulting *Nf2* cDNA was cloned into pCRII-TOPO vector (Invitrogen) to generate the pCRII-*Nf2*coding plasmid (Fig. 1B). The *Nf2* cDNA was digested with *Hind*III enzyme to yield the N-terminal 0.9-kb, middle 0.3-kb, and C-terminal 0.6-kb fragments. Each cDNA fragment was subcloned into pCRII-TOPO to generate the pCRII-N, pCRII-M, or pCRII-C subclone, respectively. To obtain the *Nf2* cDNA containing the 5′ untranslated region, RT-PCR was performed using the 5U-F and 5U-R primers (Fig. 1C). The resulting cDNA product was cloned into pCRII-TOPO to generate the pCRII-5U construct (Fig. 1B). Similarly, cDNAs containing the sequences immediately upstream of the translation termination codon and extending into the 3′ untranslated region were obtained using the primer pairs 3U1-F and 3U1-R, or 3U2-F and 3U2-R (Fig. 1C). The resulting cDNAs containing the 3′ untranslated region were also cloned into pCRII-TOPO to generate pCRII-3U1 and pCRII-3U2, respectively (Fig. 1B). All *Nf2* cDNA sequences obtained were confirmed by DNA sequencing.

Whole-Mount RNA In Situ Hybridization

Mouse embryos (E7.5, E8.5, and E9.5) were harvested and fixed in 4% paraformaldehyde in PBS overnight at 4°C. Fixed embryos were rinsed with PBT (PBS plus 0.1% Tween) three times, placed in 100% methanol, and then bleached at room temperature for 5 hr by adding hydrogen peroxide to 6%. After rinsing with 100% methanol three times, embryos were stored in 100% methanol at −20°C.

In situ hybridization was performed as previously described (Wilkinson, 1992) with minor modifications (Correia and Conlon, 2001). Following hydration through a 75, 50, and 25% methanol/PBT series, embryos were treated with 10 mg/ml proteinase K in PBT at room temperature (5 min for E7.5 embryos, 7 min for E8.5 embryos, and 8 min for E9.5 embryos). Treated embryos were washed twice for 5 min with 2 mg/ml glycine in PBT, rinsed three times with PBT, and then refixed with freshly prepared 4% paraformaldehyde/0.2% glutaraldehyde in PBT for 20 min at room temperature.

For riboprobe preparation, transcription plasmids carrying a different portion of the *Nf2* cDNA (pCRII-5U, N, M, C, 3U1, and 3U2) were linearized with an appropriate restriction enzyme, which cuts at the junction between the cDNA and vector sequences. In vitro transcription that produced riboprobes, which incorporate digoxygenin-labeled nucleotides from each linearized plasmid with T7 or SP6 polymerase, was performed using the DIG RNA Labeling Kit (Roche). Both the sense and antisense riboprobes from each transcription plasmid were produced.

For hybridization, embryos were briefly rinsed with hybridization buffer (5× SSC, pH 5, 1% SDS, 50 μg/ml yeast tRNA, 50 μg/ml heparin, and 50% formamide) and then incubated in hybridization buffer for 1 hr at 65°C with gentle shaking. After removing the pre-hybridization buffer, each riboprobe was diluted in hybridization buffer to about 1 μg/ml and then added to the embryos. Hybridization was carried out at 65°C with gentle shaking overnight.

Hybridized embryos were sequentially washed with Wash Solution 1, a 1:1 solution of Wash Solutions 1 and 2, and Wash Solution 2, followed by digestion with 100 μg/ml RNase A and washing with Wash Solution 2 and 3 (Wilkinson, 1992). To detect the hybridization signal, the DIG Nucleic Acid Detection Kit (Roche) was used. Embryos were pre-blocked with 10% sheep serum and then incubated overnight at 4°C with alkaline phosphatase-conjugated anti-digoxigenin antibody, which had been pre-absorbed with embryo powder (Wilkinson, 1992). After extensive washing, embryos were incubated in 1 ml of freshly prepared NTMT (100 mM NaCl, 100 mM Tris-HCl, pH 9.5, 50 mM MgCl2, and 0.1% Tween 20) containing 4.5 μl/ml NBT stock and 3.5 μl/ml BCIP stock (Correia and Conlon, 2001). Incubation was performed in the dark with gentle shaking. When color was developed to the desired extent, embryos were rinsed several times with PBT, stored in a 50/50 mix of glycerol and PBT, and photographed under a Leica MZ16FA stereoscope.

Immunohistochemical Analysis

Embryos at various days p.c. were harvested, fixed in 4% paraformaldehyde, and then embedded in paraffin. Tissue sections were obtained, deparaffinized, and processed for immunostaining with antibodies against Sox 9 (sc-20095; Santa Cruz Biotechnology), S100 (z 0311; Dako), and merlin (sc-331; Santa Cruz Biotechnology) according to previously described procedures (Welling et al., 2002). Negative controls were treated with the same immunostaining procedure except without the primary antibody. Hematoxylin was used as a counterstain.

ACKNOWLEDGMENTS

We sincerely thank Sarah Burns for a critical reading of the manuscript and members of the Chang lab for helpful discussion throughout the work. Part

of the work described in this report was presented at the 2004 and 2005 NNFF Int. Consortium for the Mol. Biol. of NF1 and NF2 in Aspen, CO.

REFERENCES

Bertrand JY, Giroux S, Cumano A, Godin, I. 2005. Hematopoietic stem cell development during mouse embryogenesis. Methods Mol Med 105:273–288.

Bianchi AB, Hara T, Ramesh V, Gao J, Klein-Szanto AJ, Morin F, Menon AG, Trofatter JA, Gusella JF, Seizinger BR, Kley N, 1994. Mutations in transcript isoforms of the neurofibromatosis 2 gene in multiple human tumour types. Nat Genet 6:185–192.

Chang L-S, Yang S, Shenk T. 1989. Adeno-associated virus P5 promoter contains an adenovirus E1A-inducible element and a binding site for the major late transcription factor. J Virol 63:3470–3488.

Chang L-S, Akhmametyeva EM, Wu Y, Zhu L, Welling DB. 2002. Multiple transcription initiation sites, alternative splicing, and differential polyadenylation contribute to the complexity of human neurofibromatosis 2 transcripts. Genomics 79:63–76.

Chen Y, Gutmann DH, Haipek CA, Martinsen BJ, Bronner-Fraser M, Krull CE. 2004. Characterization of chicken Nf2/merlin indicates regulatory roles in cell proliferation and migration. Dev Dyn 229: 541–554.

Cheung M, Briscoe J. 2003. Neural crest development is regulated by the transcription factor Sox9. Development 130: 5681–5693.

Cheung M, Chaboissier MC, Mynett A, Hirst E, Shedl A, Briscoe J. 2005. The transcriptional control of trunk neural crest induction, survival, and delamination. Dev Cell 8:179–192.

Claudio JO, Marineau C, Rouleau GA. 1994. The mouse homologue of the neurofibromatosis type 2 gene is highly conserved. Hum Mol Genet 3:185–190.

Claudio JO, Lutchman M, Rouleau, GA. 1995. Widespread but cell type-specific expression of the mouse neurofibromatosis type 2 gene. Neuroreport 6:1942–1946.

Correia KM, Conlon RA. 2001. Whole-mount in situ hybridization to mouse embryos. Methods 23:335–338.

Evans DG, Huson SM, Donnai D, Neary W, Blair V, Newton V, Strachan T, Harris R. 1992. A genetic study of type 2 neurofibromatosis in the United Kingdom. II. Guidelines for genetic counseling. J Med Genet 29:847–852.

Fernandez-Valle C, Tang Y, Ricard J, Rodenas-Ruano A, Taylor A, Hackler E, Biggerstaff J, Iacovelli J. 2002. Paxillin binds schwannomin and regulates its density-dependent localization and effect on cell morphology. Nat Genet 31:354–362.

Giovannini M, Robanus-Maandag E, van der Valk M, Niwa-Kawakita M, Abramowski V, Goutebroze L, Woodruff JM, Berns A, Thomas G. 2000. Conditional biallelic Nf2 mutation in the mouse promotes manifestations of human neurofibromatosis type 2. Genes Dev 14:1617–1630.

Gonzalez-Agosti C, Xu L, Pinney D, Beauchamp R, Hobbs W, Gusella J, Ramesh V. 1996. The merlin tumor suppressor localizes preferentially in membrane ruffles. Oncogene 13:1239–1247.

Graham A. 2003. The neural crest. Curr Biol 13:R381–384.

Gronholm M, Teesalu T, Tyynela J, Piltti K, Bohling T, Wartiovaara K, Vaheri A, Carpen O. 2005. Characterization of the NF2 protein merlin and the ERM protein ezrin in human, rat, and mouse central nervous system. Mol Cell Neurosci 28: 683–693.

Gutmann DH, Wright DE, Geist RT, Snider WD. 1994. Expression of the neurofibromatosis 2 (*NF2*) gene isoforms during rat embryonic development. Hum Mol Genet 4:471–478.

Gutmann DH, Geist RT, Xu HM, Kim JS, Saporito-Irwin S. 1998. Defects in neurofibromatosis 2 protein function can arise at multiple levels. Hum Mol Genet 7:335–345

Gutmann DH, Sherman L, Seftor L, Haipek C, Hoang Lu K, Hendrix M. 1999. Increased expression of the NF2 tumor suppressor gene product, merlin, impairs cell motility, adhesion and spreading. Hum Mol Genet 8:267–275.

Haase VH, Trofatter JA, MacCollin M, Tarttelin E, Gusella JF, Ramesh V. 1994. The murine NF2 homologue encodes a highly conserved merlin protein with alternative forms. Neuroreport 8: 2025–2030.

Hay ED. 2005. The mesenchymal cell, its role in the embryo, and the remarkable signaling mechanisms that create it. Dev Dyn 233:706–720.

Hazim W, Mautner VF, Christiani B, Hasse W. 1998. Fluorescein angiography of retinal changes in patients with neurofibromatosis 2. Ophthalmologe 95:687–690.

Hogan B, Beddington R, Costantini F, Lacy E. 1994. Manipulating the mouse embryo, a laboratory manual. Plainview, NY: Cold Spring Harbor Laboratory Press.

Honjo Y, Eisen JS. 2005. Slow muscle regulates the pattern of trunk neural crest migration in zebrafish. Development 132: 4461–4470.

Huynh DP, Tran TM, Nechiporuk T, Pulst SM. 1996. Expression of neurofibromatosis 2 transcript and gene product during mouse fetal development. Cell Growth Differ 7:1551–1561.

Imbert AM, Bagnis C, Galindo R, Chabannon C, Mannoni P. 1998. A neutralizing anti-TGF-β1 antibody promotes proliferation of CD34+Thy-1+ peripheral blood progenitors and increases the number of transduced progenitors. Exp Hematol 26: 374–381.

Jacinto A, Wood W, Woolner S, Hiley C, Turner L, Wilson C, Martinez-Arias A, Martin P. 2002. Dynamic analysis of actin cable function during Drosophila dorsal closure. Curr Biol 12:1245–1250.

Jessen KR, Mirsky R. 2005. The origin and development of glial cells in peripheral nerves. Nat Rev Neurosci 6:671–682.

Kalamarides M, Niwa-Kawakita M, Leblois H, Abramowski V, Perricaudet M, Janin A, Thomas G, Gutmann DH, Giovannini M. 2002. Nf2 gene inactivation in arachnoidal cells is rate-limiting for meningioma development in the mouse. Genes Dev 16:1060–1065.

Kissil JL, Johnson KC, Eckman MS, Jacks T. 2002. Merlin phosphorylation by p21-activated kinase 2 and effects of phosphorylation on merlin localization. J Biol Chem 277:10394–10399.

Lallemand D, Curto M, Saotome I, Giovannini M, McClatchey AI. 2003. NF2 deficiency promotes tumorigenesis and metastasis by destabilizing adherens junctions. Genes Dev 17:1090–1100.

LeDouarin N, Kalcheim C. 1999. The neural crest. Cambridge, UK: Cambridge University Press.

Levine RE, Slattery WH III. 2003. Documenting changes in the pre-retinal membrane using the Optical Coherence Tomography 3. Abstract presented to the 2003 NNFF Int. Consortium for the Mol Biol of NF1 and NF2, Aspen, CO.

Li S, Guan J-L, Chien S. 2005. Biochemistry and biomechanics of cell motility. Annu Rev Biomed Eng 7:105–150.

Lutchman M, Rouleau GA. 1995. The neurofibromatosis type 2 gene product, schwannomin, suppresses growth of NIH 3T3 cells. Cancer Res 55:2270–2274.

Maeda M, Matsui T, Imamura M, Tsukita S, Tsukita S. 1999. Expression level, subcellular distribution and rho-GDI binding affinity of merlin in comparison with Ezrin/Radixin/Moesin proteins. Oncogene 18:4788–4797.

Martinez-Morales JR, Rodrigo I, Bovolenta P. 2004. Eye development: a view from the retina pigmented epithelium. BioEssays 26:766–777.

McClatchey AI. 2004. Merlin and ERM proteins: unappreciated roles in cancer development. Nat Rev Cancer 3:877–883.

McClatchey AI, Giovannini M. 2005. Membrane organization and tumorigenesis: the NF2 tumor suppressor, Merlin. Genes Dev 19:2265–2277.

McClatchey AI, Saotome I, Ramesh V, Gusella JF, Jacks T. 1997. The NF2 tumor suppressor gene product is essential for extraembryonic development immediately prior to gastrulation. Genes Dev 11:1253–1265.

McClatchey AI, Saotome I, Mercer K, Crowley D, Gusella JF, Bronson RT, Jacks T. 1998. Mice heterozygous for a mutation at the NF2 tumor suppressor locus develop a range of highly metastatic tumors. Genes Dev 12:1121–1133.

McLaughlin ME, Slocum K, Jacks T. 2004. The NF2 tumor suppressor, merlin, is required for tissue fusion during mouse embryonic development. Abstract presented to the 2004 NNFF Int. Consor-

tium for the Mol Biol of NF1 and NF2, Aspen, CO.

Meyers SM, Gutman FA, Kaye LD, Rothner AD. 1995. Retinal changes associated with neurofibromatosis 2. Trans Am Ophthalmol Soc 93:245–252; discussion 252–257.

Mori-Akiyama Y, Akiyama H, Rowitch DH, de Crombrugghe B. 2003. Sox9 is required for determination of the chondrogenic cell lineage in the cranial neural crest. Proc Natl Acad Sci USA 100:9360–9365.

Neff B, Welling DB, Akhmametyeva E, Chang L-S. 2005. The molecular biology of vestibular schwannomas: dissecting the pathogenic process at the molecular level. Otol Neurotol 27:197–208.

NIH Consens. Statement. 1991. Acoustic neuroma. Consens. Statement 9:1–24.

Parry DM, Eldridge R, Kaiser-Kupfer MI, Bouzas EA, Pikus A, Patronas, N. 1994. Neurofibromatosis 2 (NF2): clinical characteristics of 63 affected individuals and clinical evidence for heterogeneity. Am J Med Genet 52:450–461.

Pelton PD, Sherman LS, Rizvi TA, Marchionni MA, Wood P, Friedman RA, Ratner N. 1998. Ruffling membrane, stress fiber, cell spreading and proliferation abnormalities in human Schwannoma cells. Oncogene 17:2195–2209.

Rong R, Surace EI, Haipek CA, Gutmann DH, Ye K. 2004. Serine 518 phosphorylation modulates merlin intramolecular association and binding to critical effectors important for NF2 growth suppression. Oncogene 23:8447–8454.

Rouleau GA, Merel P, Lutchman M, Sanson M, Zucman J, Marineau C, Hoang-Xuan K, Demezuk S, Desmaze C, Plougastel B, Pulst SM, Lenoir G, Bijlsma E, Fashold R, Dumanshki J, de Jong P, Parry D, Eldridge R, Aurias A, Delattre O, Thomas G. 1993. Alteration in a new gene encoding a putative membrane-organising protein causes neurofibromatosis type 2. Nature 363:515–521

Rugh R. 1994. The mouse: its reproduction and development. Oxford: Oxford University Press.

Scoles DR, Huynh DP, Morcos PA, Coulsell ER, Robinson NG, Tamanoi F, Pulst, SM. 1998. Neurofibromatosis 2 tumor suppressor schwannomin interacts with βII-spectrin. Nat Genet 18:354–359.

Shaw RJ, McClatchey AI, Jacks T. 1998. Localization and functional domains of the neurofibromatosis type II tumor suppressor, Merlin Cell Growth Diff 9:287–296.

Shaw RJ, Paez JG, Curto M, Yaktine A, Pruitt WM, Saotome I, O'Bryan JP, Gupta V, Ratner N, Der CJ, Jacks T, McClatchey, AI. 2001. The Nf2 tumor suppressor, merlin, functions in Rac-dependent signaling. Dev Cell 1:63–72.

Sherman L, Xu HM, Geist RT, Saporito-Irwin S, Howells N, Ponta H, Herrlich P, Gutmann DH. 1997. Interdomain binding mediates tumor growth suppression by the NF2 gene product. Oncogene 15: 2505–2509.

Stemmer-Rachamimov AO, Gonzalez-Agosti C, Xu L, Burwick JA, Beauchamp R, Pinney D, Louis DN, Ramesh V. 1997. Expression of NF2-encoded merlin and related ERM family proteins in the human central nervous system. J Neuropathol Exp Neurol 56:735–742.

Stokowski RP, Cox DR. 2000. Functional analysis of the neurofibromatosis type 2 protein by means of disease-causing point mutations. Am J Hum Genet 66: 873–891.

Surace EI, Haipek CA, Gutmann DH. 2004. Effect of merlin phosphorylation on neurofibromatosis 2 (NF2) gene function. Oncogene 23:580–587.

Tikoo A, Varga M, Ramesh V, Gusella J, Maruta H. 1994. An anti-Ras function of neurofibromatosis type 2 gene product (NF2/Merlin). J Biol Chem 269:23387–23390

Trofatter JA, MacCollin MM, Rutter JL, Murrell JR, Duyao MP, Parry DM, Eldridge R, Kley N, Menon AG, Pulaski K, Haase VH, Ambrose CM, Munroe D, Bove C, Haines JL, Martuza RL, MacDonald ME, Seizinger BJ, Short MP, Buckler AL, Gusella JF. 1993. A novel Moesin-, Exrin-, Radixin-like gene is a candidate for the neurofibromatosis 2 tumor-suppressor. Cell 72:791–800.

Wallingford JB. 2005. Neural tube closure and neural tube defects: studies in animal models reveal known knowns and known unknowns. Am J Med Genet Part C Semin Med Genet 135:59–68.

Wassef M, Joyner AL. 1997. Early mesencephalon/metencephalon patterning and development of the cerebellum. Perspect Dev Neurobiol 5:3–16.

Welling DB, Akhmametyeva EM, Daniels RL, Lasak JM, Zhu L, Miles-Markley BA, Chang L-S. 2000. Analysis of the human neurofibromatosis type 2 gene promoter and its expression. Otolaryngol Head Neck Surg 123:413–418.

Welling DB, Lasak JM, Akhmametyeva E, Ghehari B, Chang L-S. 2002. cDNA microarray analysis of vestibular schwannomas. Otol Neurol 23:736–748.

Wilkinson DG. 1992. In situ hybridization, a practical approach. Oxford: IRL Press. p 75–83.

Woolner S, Jacinto A, Martin P. 2005. The small GTPase Rac plays multiple roles in epithelial sheet fusion: dynamic studies of Drosophila dorsal closure. Dev Biol 282:163–173.

World Health Org. 1992. Prevention and control of neurofibromatosis: Memorandum from a joint WHO/NNFF meeting. Bull. World Health Org 70:173–182.

Xiao GH, Beeser A, Chernoff J, Testa JR. 2002. p21-activated kinase links Rac/Cdc42 signaling to merlin. J Biol Chem 277:883–886.

Xu HM, Gutmann DH. 1998. Merlin differentially associates with the microtubule and actin cytoskeleton. J Neurosci Res 51:403–415.

The Laryngoscope
Lippincott Williams & Wilkins, Inc.

Growth of Benign and Malignant Schwannoma Xenografts in Severe Combined Immunodeficiency Mice

Long-Sheng Chang, PhD; Jacob Abraham, MD; Mark Lorenz, MD; Jonathan Rock, BS; Elena M. Akhmametyeva, MD, PhD; Georgeta Mihai, MS; Petra Schmalbrock, PhD; Abhik R. Chaudhury, MD; Raul Lopez, BS; Jyoji Yamate, PhD; Markus R. John, PhD; Hannes Wickert, PhD; Brian A. Neff, MD; Edward Dodson, MD; D. Bradley Welling, MD, PhD

Objectives: **Models for the development of new treatment options in vestibular schwannoma (VS) treatment are lacking. The purpose of this study is to establish a quantifiable human VS xenograft model in mice.** ***Study Design and Methods:*** **Both rat malignant schwannoma cells (KE-F11 and RT4) and human malignant schwannoma (HMS-97) cells were implanted near the sciatic nerve in the thigh of severe combined immunodeficiency (SCID) mice. Additionally, human benign VS specimens were implanted in another set of SCID mice. Three-dimensional tumor volumes were calculated from magnetic resonance images over the next 6 months.** ***Results:*** **Mice implanted with malignant schwannoma cells developed visible tumors within 2 weeks. Imaging using a 4.7-tesla magnetic resonance imaging and immunohistopathologic examination identified solid tumors in all KE-F11 and HMS-97 xenografts, whereas RT4 xenografts consistently developed cystic schwannomas. VS xenografts demonstrated variability in their growth rates similar to human VS. The majority of VS xenografts did not grow but persisted throughout the study, whereas two of 15 xenografts grew significantly. Histopathologic examination and immunohistochemistry confirmed that VS xenografts retained their original microscopic and immunohistochemical characteristics after prolonged implantation.** ***Conclusions:*** **This study describes the first animal model for cystic schwannomas. Also, we demonstrate the use of high-field magnetic resonance imaging to quantify VS xenograft growth over time. The VS xenografts represent a model complimentary to *Nf2* transgenic and knockout mice for translational VS research.** ***Key Words:*** **Vestibular schwannoma, neurofibromatosis type 2 (NF2), xenograft, severe combined immunodeficiency (SCID) mice, magnetic resonance imaging (MRI), cystic, malignant, gadolinium.**

Laryngoscope, **116:2018–2026, 2006**

INTRODUCTION

Vestibular schwannomas (VS) have no known medical therapies available. However, significant morbidity, including hearing loss and facial weakness, remain major concerns. VS can be divided into four general categories, including unilateral sporadic VS, neurofibromatosis type 2 (NF2)-associated VS, cystic, and malignant schwannomas.[1] Among VS, sporadic unilateral solid tumors are by far the most common, occurring in 10 to 13 persons per million per year. The development of bilateral VS is the hallmark of NF2, an autosomal-dominant disease caused by mutations in the neurofibromatosis type 2 (*NF2*) gene on chromosome 22q12.[2,3] Most of these solid tumors, either sporadic or NF2-associated, grow at a slow rate of approximately 1 to 2 mm per year.[1] Cystic schwannomas are a particularly aggressive group of unilateral schwannomas. They invade the surrounding cranial nerves, splaying them throughout the tumor.[4] Cystic tumors may grow rapidly and are typically more difficult to manage, often resulting in hearing loss and facial nerve paralysis on their removal.[5] In addition to NF2-associated tumors, mutations in the *NF2* gene have been detected in sporadic VS and cystic schwannomas.[6] The most aggressive and rare variant is the malignant VS or triton tumor. These

From the Departments of Pediatrics (L.-S.C., E.M.A.), Otolaryngology (L.-S.C., J.A., B.A.N., E.D., D.B.W.), Pathology (L.-S.C., A.R.C.), and Radiology (G.M., P.S.), The Ohio State University and the College of Medicine (L.-S.C., M.L., J.R., P.S., A.R.C., R.L., E.D., D.B.W.), Columbus, Ohio, U.S.A.; the Center for Childhood Cancer (L.-S.C., E.M.A.), Children's Research Institute, Columbus, Ohio, U.S.A.; Laboratory of Veterinary Pathology (J.Y.), Osaka Prefecture University, Osaka, Japan; Musculoskeletal Diseases Exploratory Clinical Development Unit (M.R.J.), Novartis Pharma AG, Basel, Switzerland; and Hygiene Institut (H.W.), Abteilung Parasitologie, Universitätsklinikum Heidelberg, Heidelberg, Germany.

Editor's Note: This Manuscript was accepted for publication July 18, 2006.

Supported by grants from the U.S. Department of Defense NF Research Program and National Institute of Deafness and Communication Disorders.

Send correspondence to Long-Sheng Chang, Children's Hospital and Department of Pediatrics, The Ohio State University, 700 Children's Drive, Columbus, OH 43205. E-mail: lchang@chi.osu.edu

DOI: 10.1097/01.mlg.0000240185.14224.7d

malignant tumors occur either sporadically or after radiation and are uniformly fatal.[7]

Magnetic resonance imaging (MRI) distinguishes clearly among the various types of VS. Cystic regions within cystic schwannomas are signal intense on T2-weighted images, whereas noncystic components of these tumors enhance on T1-weighted images with gadolinium (Gd) in a manner similar to those seen in sporadic and NF2-associated VS.[1] These represent a unique tumor type clinically and histologically and should not be confused with degenerative regions of larger tumors. The irregular appearance of some heterogeneous tumors on contrast-enhanced T1-weighted images may be accounted for by hemosiderin deposits, which correlates with increasing tumor size,[8] but these tumors do not contain fluid as demonstrated on T2 imaging. Although distinct clinically and by MRI, the underlying molecular differences among the three benign types of VS are not understood. Malignant schwannomas invade surrounding tissues locally and progress rapidly.[7] Most appear solid and enhance on T1-weighted images but lack the capsule of the more common benign VS. Additionally, the optimal treatment regimen for each subtype of VS is not known because of a lack of understanding of fundamental tumor biology and a lack of rigorous clinical outcome studies.

Several studies previously attempted to implant human VS tissues in immunodeficient mice. Lee et al.[9] implanted human schwannomas in nude mice and showed that the tumors grew most consistently when placed in the sciatic nerve region. Charabi et al.[10] and Stidham et al.[11] confirmed that VS tissues could be successfully implanted and maintained in a subcutaneous pocket of nude mice. Although these studies demonstrated macroscopic growth in some of the transplanted VS tissues, an effective means of assessing the survival, growth, and blood supply of tumor xenografts was lacking. In addition, no study to date has compared the growth potential of various types of schwannoma tissues in mice.

We evaluated the growth characteristics of rodent and human malignant schwannoma cells as well as benign human VS xenografts in severe combined immunodeficiency (SCID) mice using a 4.7-T MRI. Our results demonstrated the feasibility of using MRI to quantify VS xenografts in mice. Interestingly, MRI also distinguished two different schwannoma types, which were confirmed by immuno- and histopathologic analysis.

MATERIALS AND METHODS

Experimental Design

The Institutional Animal Care and Use Committee of The Ohio State University approved the animal protocols used in this study. Healthy female SCID mice (Harlan Co., Indianapolis, IN) were housed according to approved procedures. The first series of experiments involved injecting three groups of SCID mice subcutaneously in the thigh with rat malignant schwannoma cells KE-F11[12] and RT4[13] as well as human malignant schwannoma HMS-97 cells.[14] Tumor growth was observed over 4 weeks and measured using a 4.7-T small-animal MRI scanner (Bruker, Billerica, MA). After euthanizing the animals, specimens were harvested for histopathologic analysis. A second set of experiments was performed using human VS specimens. SCID mice were implanted with VS tissues obtained directly from patients undergoing surgical resection. All VS implants were placed in the proximal thigh of the left leg near the sciatic nerve. Tumor growth, if any, was accessed serially by MRI over the subsequent months after xenotransplantation. Histopathologic examination and immunohistochemical analysis were also performed on selected mice to confirm the imaged regions contain viable tumor rather than scar tissues.

Tissue Procurement

A human subject protocol for the acquisition and analysis of human vestibular schwannomas was approved by our Institutional Reviewed Board. Patient consents were obtained before surgery. Each tumor specimen was confirmed by a pathologist as schwannoma. For implantation of human VS tissues into SCID mice, freshly removed specimen was placed in a sterile tube containing Dulbecco modified minimum essential (DME) medium (Invitrogen, Carlsbad, CA) and transported immediately to the animal research facility. Also, a portion of tumor was snap-frozen in liquid nitrogen for future molecular studies.

Growth of Schwannoma Cells

Rat malignant schwannoma KE-F11 and RT4 cells and human malignant schwannoma HMS-97 cells were grown in DME medium supplemented with 10% fetal bovine serum (Invitrogen). For inoculation of rat KE-F11 or RT4 cells into each SCID mouse, 2.5×10^5 cells were washed with phosphate-buffered saline and suspended in 0.2 mL of Matrigel (BD Biosciences, San Jose, CA). For inoculation of human HMS-97 cells into each SCID mouse, 5×10^5 cells were used.

Injection Technique

SCID mice were anesthetized by intraperitoneal injection of Avertin (2,2,2-tribromoethanol + tert-amyl alcohol; Sigma-Aldrich, St. Louis, MO) or by isoflurane inhalation. Under anesthesia, the left flank of mouse was shaved and prepped using aseptic technique. An 18-gauge needle was used to inject 0.2 mL of schwannoma cells 3 mm inferior to the greater trochanter of femur. The thigh was selected for ease of implantation and the ability to grossly observe tumor growth. Additionally, previous studies indicated that proximity to a peripheral nerve might affect growth.[9–11] Injected mice were revived on a warming blanket until recovery and were watched daily for tumor growth.

Surgical Implantation Technique

An incision was made along the long axis of the proximal thigh. The contralateral leg was not dissected and used as a control for imaging. Soft tissues were dissected bluntly to identify the biceps femoris muscle and the sciatic nerve. A piece of VS tumor specimen (1–5 mm in diameter) was implanted en bloc near the nerve and the skin was closed using a single layer of interrupted suture.

Magnetic Resonance Imaging

Mice were anesthetized with Avertin, immobilized on an animal holder, and placed prone in a 4.7-T/cm MRI system with a 120-mm inner diameter gradient coil (maximum 400 mT/m), a 72-mm inner diameter proton volume radiofrequency coil for transmit, and a 4-cm surface receive coil. For T1-weighted axial and coronal images, a spin echo sequence with TR of 550 to 600 ms and TE of 10.5 ms was used. For T2-weighted images, a rapid acquisition with refocusing echoes (RARE) sequence with TR of 2500 to 2600 ms, an effective TE of 47 to 54 ms, and a RARE factor of 4 was used. In-plane resolution was 156 μm on the axial and 195 μm on the coronal images, and the slice thickness was 0.8

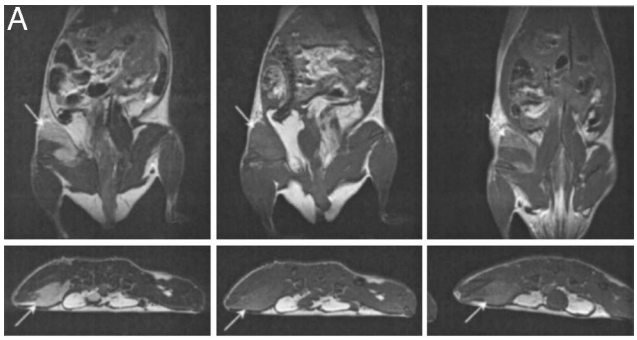

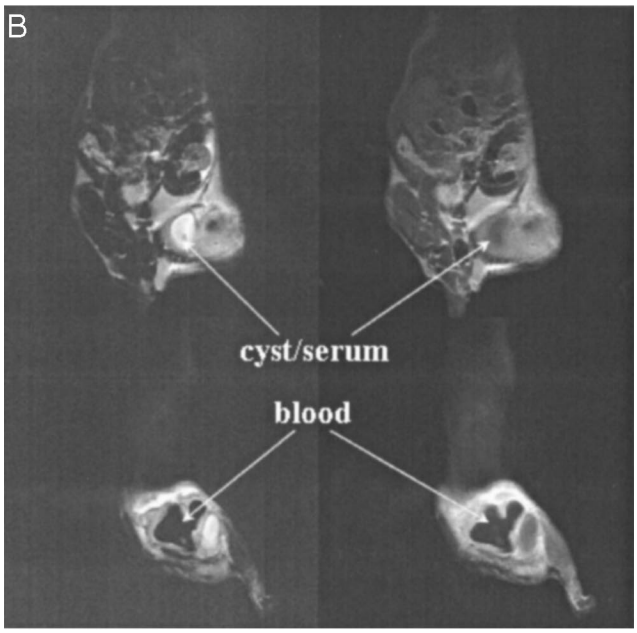

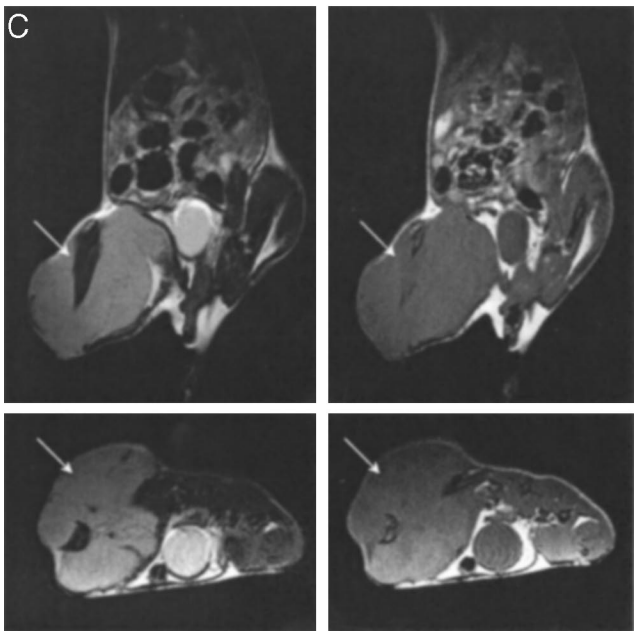

mm with a 0.2-mm gap between slices. Scan time was 5 to 6 minutes per scan.

In addition, contrast-enhanced T1 axial and coronal images were acquired after a bolus injection with Gadodiamide (Omniscan; GE Health Care, Piscataway, NJ; 0.1-mL bolus of 10 mmol/L). The contrast agent was injected through a tail vein catheter using thin polyethylene tubing that reached outside the magnet and allowed quick delivery of the contrast agent without changing the position of the mouse inside the magnet. Mice with rat schwannoma cell implants were imaged within 2 weeks of implantation and those with human schwannoma cell implants were imaged approximately 4 weeks after inoculation. Mice with human VS implants were imaged at indicated times over the course of a year postprocedure.

Multiplanar tumor volumes were determined from T1- and T2-weighted images. For these measurements, tumor areas were manually traced on axial and coronal T1 and T2 images. Postcontrast images were also used when available. Tumor volumes were calculated by adding the traced areas from all slices depicting the tumor and multiplying with the distance between slice (i.e., 0.8-mm slice thickness + 0.2-mm gap = 1 mm). Tumor volumes measured from axial and coronal or T1 and T2 images were in fair agreement. All volume measurements were referenced to the first MRIs taken 1 month after implantation.

Immunohistopathologic Analysis

Tumors grown in mice with schwannoma xenografts were dissected, fixed in 10% buffered formalin, and embedded in paraffin. Five-micron tissue sections were mounted, deparaffinized, and processed for standard hematoxylin–eosin staining or immunostaining with antibodies against S-100 protein (1:200 dilution of anti-S-100 from Dako, Carpinteria, CA), myelin basic protein (MBP) (prediluted anti-MBP from Zymed, San Francisco, CA), and NGF-receptor ($p75^{NGFR}$)/neurotrophin receptor (1:100 dilution of anti-$p75^{NGFR}$ from LabVision/NeoMarker, Fremont, CA) according to previously described procedures.[6] A hematoxylin counterstain was then applied and the stained tissue visualized by light microscopy. Negative controls were treated with the same immunostaining procedure except without the primary antibody.

RESULTS

KE-F11 and HMS-97 schwannoma xenografts developed solid tumor phenotypes, whereas RT4 xenografts produced cystic tumors. SCID mice injected with either the KE-F11 or RT4 rat malignant schwannoma cells produced visible tumors within 1 week after inoculation. On the MRI obtained within 2 weeks of xenotransplantation, the two sets of mice demonstrated significantly different imaging characteristics. All mice implanted with KE-F11

Fig. 1. Magnetic resonance imaging scans of malignant schwannoma xenograft 2 weeks after implantation display the presence of solid tumor mass in the left thigh (arrow). The T2-weighted rapid acquisition with refocusing echoes images (left) and T1-weighted images without (middle) and with contrast agent (right) were obtained according to "Methods." The tumor is seen hyperintense to muscle on T2 and isointense on T1 images and enhances after the injection of contrast agent (arrows). (B) Coronal (top) and axial (bottom) images of a rat RT4 schwannoma xenograft 2 weeks after implantation show the presence of a cystic tumor. Blood appeared hypointense in signal intensity on both T1 and T2 images, whereas the cyst was hyperintense on T2 images (left) and dark on T1 images (right). (C) Magnetic resonance images of a human HMS-97 schwannoma xenograft 4 weeks after implantation demonstrating a large tumor with solid architecture.

cells developed solid tumors, and the presence of tumor created significant asymmetry in the implanted thigh (Fig. 1A). Coronal and axial T2-weighted RARE images showed that the tumor mass appeared homogenous but was hyperintense or brighter to the surrounding musculature. On T1-weighted images, the tumor-containing region was near isointense to muscle and enhanced on post-contrast T1 images (arrows) as is characteristics of human VS tissues in situ. In contrast, all mice injected with RT4 cells demonstrated a distinctive cystic phenotype (Fig. 1B). Within the tumor mass, blood-filled cavities appeared darkest on both T1- and T2-weighted images, whereas the cysts displayed high signal intensity on T2 images but were dark on T1 images. Similar to the KE-F11 xenografts, MRIs revealed that all mice with human malignant schwannoma HMS-97 implants developed large, homogenous, solid tumors by 4 weeks postimplantation as seen on coronal and axial T1- and T2-weighted images (Fig. 1C). There were no cystic changes.

To confirm that the xenografts retained their schwannoma phenotype, histopathologic examination was performed on tumor-bearing mice. No metastatic lesions were found. Macroscopic and microscopic analysis confirmed the solid phenotype for both the KE-F11 and HMS-97 tumors and the cystic phenotype for the RT4 xenografts (Fig. 2). The KE-F11 cell line was derived from a spontaneous malignant schwannoma found in an aged male F344 rat.[12] The KE-F11 xenograft was a grayish, creamy globoid mass, which histologically consisted of actively growing, heterochromatic, oval- or spindle-shaped cells with large pleomorphic nuclei (Fig. 2A). RT4 is a clonal schwannoma cell line derived from a peripheral nervous system tumor induced by ethylnitrosourea injection in a newborn BDIX rat.[13] The xenograft generated by RT4 cells contained multiple cysts; some of the cysts contained dark, viscous blood products, whereas others were filled with serous fluid. Histologically, the RT4 tumor contained compact spindle cells with a high nucleus to cytoplasm ratio and had increased perivascular cellularity (Fig. 2B). The HMS-97 cell line was established from a malignant schwannoma from an adult patient with oncogenic osteomalacia.[14] Similar to KE-F11, the HMS-97 tumor was a large globoid mass comprised of heterochromatic ovoid cells with multiple mitotic figures (Fig. 2C). The HMS-97 xenograft was transplantable. When a small piece of the tumor was transplanted to another SCID mouse, tumor growth was readily seen within 2 weeks (data not shown).

Because Schwann cells originate from the neuroectodermal neural crest, Schwann cell-derived tumors often show immunoreactions to S-100 protein, MBP, and $p75^{NGFR}$.[15–18] Immunostaining with an anti-S-100 antibody showed that tumor cells from the HMS-97 xenograft strongly and diffusely expressed S-100 protein (Fig. 3A). Similarly, HMS-97 tumor cells also stained robustly for MBP expression (Fig. 3B). The staining for $p75^{NGFR}$ expression was weak but detectable (Fig. 3C).

Collectively, these results are consistent with previous reports that malignant schwannomas are transplantable and their Schwann cell characteristics were maintained after xenotransplantation.[12,13] Our study further

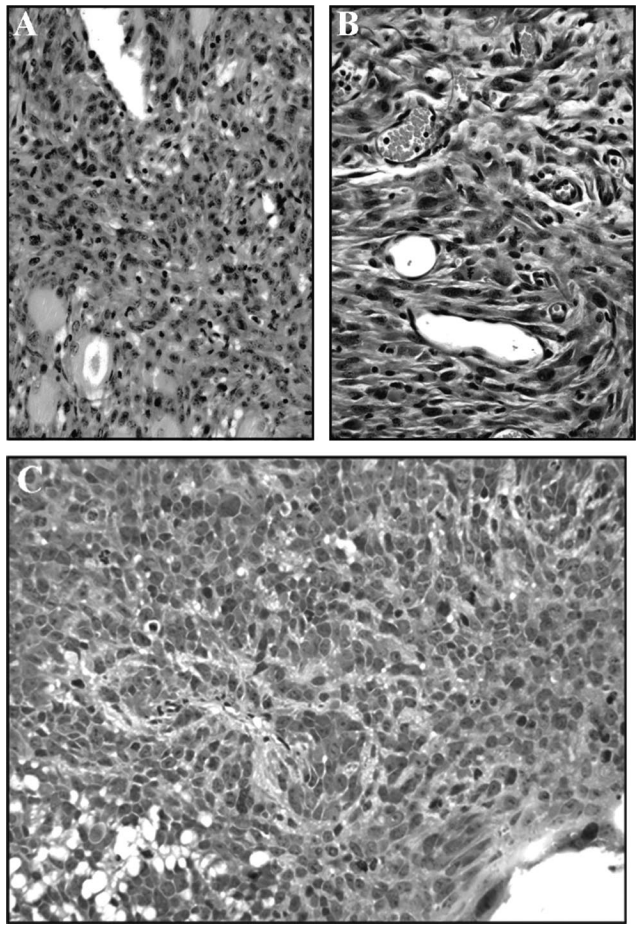

Fig. 2. Histologic analysis of malignant schwannoma xenografts. Malignant-appearing cells with plump, pleomorphic nuclei and densely stained chromatin were present in both the (A) KE-F11 and (B) RT4 tumors. Numerous vascular channels in the RT4 tumor suggest significant tumor angiogenesis. Similarly, malignant-appearing cells with multiple mitotic figures and a high nucleus to cytoplasm ratio were seen in the HMS-97 tumor (C).

demonstrates the feasibility of using MRI to detect the phenotype and growth characteristics of schwannomas in SCID mice. The KE-F11 and HMS-97 xenografts engender malignant solid schwannomas, whereas the RT4 cells produce distinct cystic tumors.

Human VS xenografts persisted for a long period of time and some showed growth in SCID mice. To evaluate potential growth characteristics of human VS, freshly removed tumors were implanted in the thigh of SCID mice. High-field MRI was used to visualize and quantify all VS xenografts in mice as described previously. Analysis of images obtained from each animal at various times after xenotransplantation revealed that the majority of VS xenografts persisted but did not show significant growth (Fig. 4). Most tumor volumes were either unchanged or reduced over the study period. The tumor with the most reduction diminished to about half its original tumor volume over 6 months. It is important to note that even without growth, the xenograft was detectable by MRI scans (Fig. 4A). We were able to maintain one VS xenograft for 13 months until the

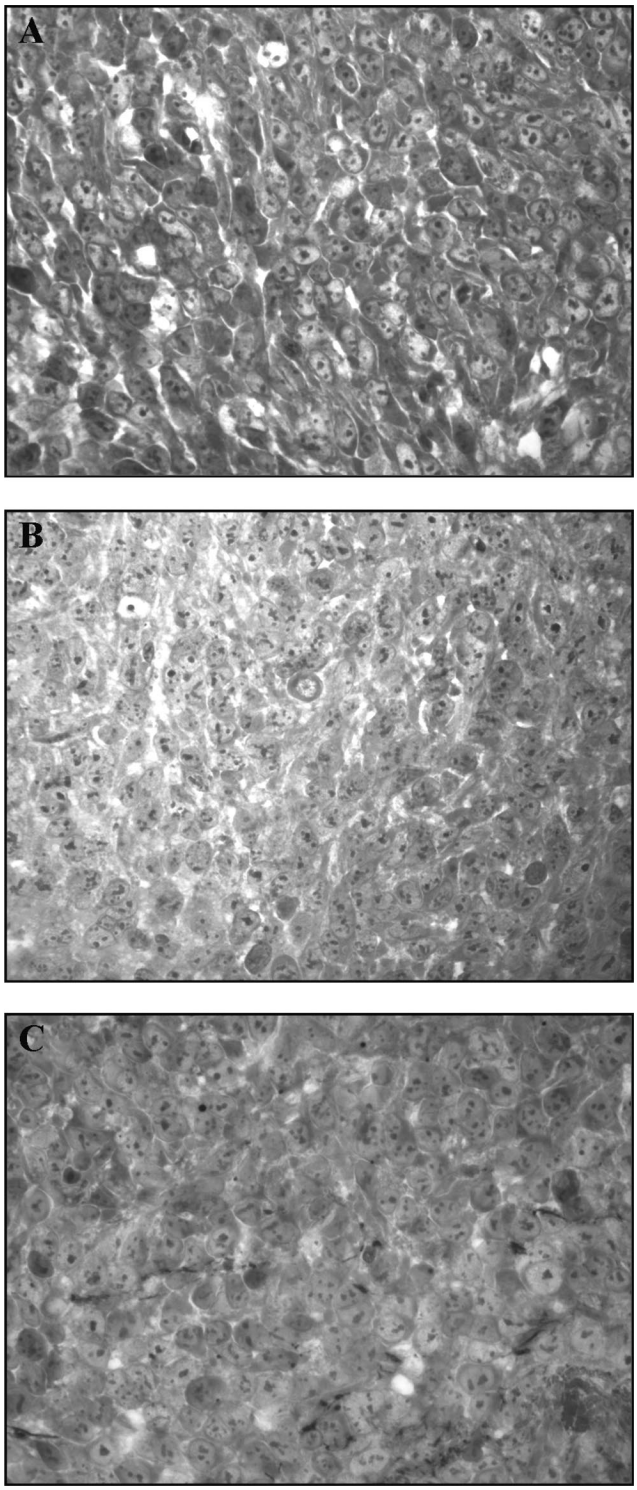

Fig. 3. Immunohistochemical analysis of the HMS-97 xenograft demonstrating continued Schwann cell lineage of tumor cells. Tissue sections containing tumor cells were immunostained with (A) anti-S-100, (B) anti-MBP, and (C) and anti-$p75^{NGFR}$ antibodies. The positively stained tissue appeared brown. All negative controls did not stain (not shown).

animal was killed for histopathologic examination (see subsequently). We also detected an increase in tumor volume in two of 15 VS xenografts over 6 months (Fig. 4B, 4C). One showed a 60% increase in tumor volume, whereas the other grew to 14 times its original volume.

Representative MRIs from the mouse with the VS xenograft whose tumor volume diminished by approximately half over 6 months are shown in Figure 4A. Although the tumor was small and its size decreased over the study period, a persistent mass could be found at the surgical implant site (arrows) in all images obtained. Because this tumor was surrounded by fatty tissue, both T1- and T2-weighted images depicted the tumor. The postcontrast study at month 6 showed only weak marginal enhancement (Fig. 4A, right column).

When similar MRI sequences were performed on the VS xenograft showing significant growth, changes in tumor growth could be easily seen from both the T1- and T2-weighted images (Fig. 4B). Visual comparison of the images obtained at 1 and 2 months postimplantation revealed that the xenograft became larger. By 6 months, the tumor grew so much that it created an obvious asymmetry in the left implanted thigh. T1-weighted, postcontrast images most clearly outlined the tumor and its growth into the adjacent muscle tissue. Together with the T2 scan, these images confirmed the growth of the VS xenograft.

Histopathologic analysis was performed on the mouse with significant tumor growth to confirm that the mass seen on the MRI was in fact schwannoma tissue by phenotype. Gross examination revealed a large globoid mass in the implanted thigh with no sign of metastasis. Histologically, the tumor was encapsulated and consisted of spindle-shaped cells. Alternating compact areas of elongated cells with occasional nuclear palisading (Antoni A pattern) and less cellular, loosely textured Antoni B areas were seen (Fig. 5A). The tumor cells had relatively abundant cytoplasm with discernible cell margins. All of these characteristics were consistent with a primary benign human VS. We also detected strong immunoreactivity to S-100, $p75^{NGFR}$, and MBP antigens in the area containing tumor cells (Fig. 6A–C).

Similarly, we performed a histopathologic examination on the mouse with a VS implant present but without any growth for 13 months. The xenograft tissue could still be detected by MRI (data not shown) and macroscopic analysis confirmed the presence of a small tumor within the implanted region. Microscopically, the tumor was composed of both ovoid and spindle-shaped cells with foci of lipid laden tumor cells characteristic of an aged vestibular schwannoma (Fig. 5B). Similar to those detected in the VS tumor showing significant growth, strong immunoreactivity, to S-100 and $p75^{NGFR}$ proteins was found in the area containing the tumor cells (Fig. 6D, E).

Taken together, these results show that VS xenografts can persist or grow in SCID mice and are readily detectable and quantified by MRI. The tumors retained their original microscopic and immunohistochemical characteristics after prolonged implantation.

DISCUSSION

Meaningful translational research in chemotherapy requires disease-specific, reproducible, quantifiable, and cost-effective animal models. Mice have been an attractive species for such models because they can be bred to have little

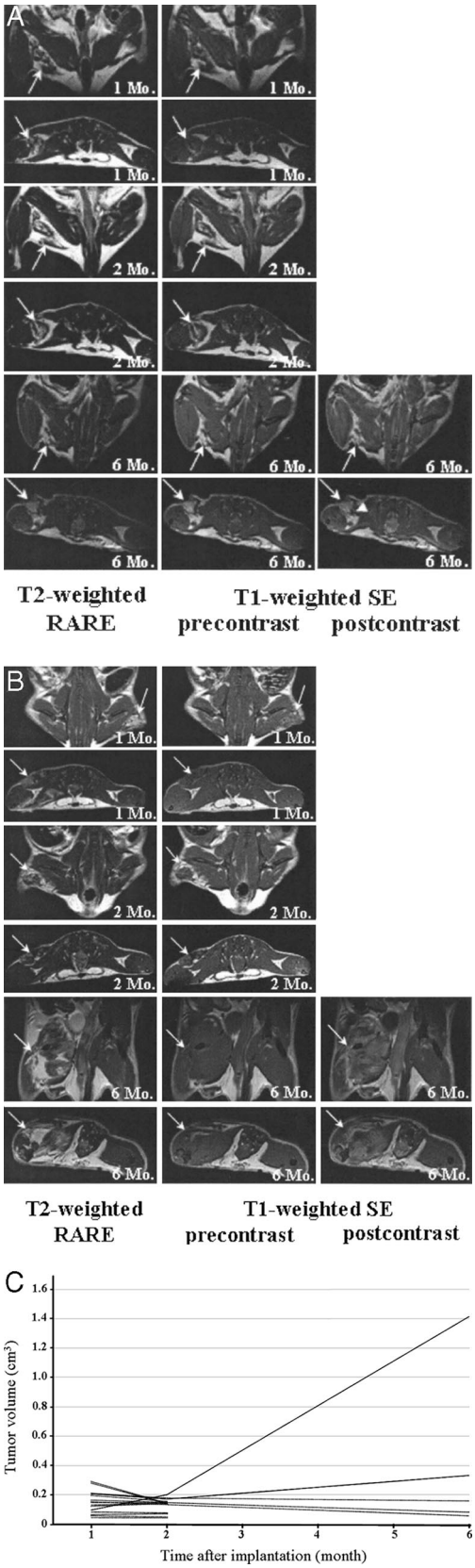

genetic variability and are accessible to genetic manipulation. Over the past decade, most of the in vivo research with schwannomas has focused on *Nf2* transgenic and knockout mice.[16,17] Although soft tissue, peripheral nerve, and central nervous system schwannomas have developed in these animals, no mouse to date has engendered a primary schwannoma on its eighth cranial nerve. Additionally, the conditional *Nf2* mutant mice with schwannomas were found at low frequency only in older mice. Both benign and malignant schwannomas have been found in these mice. This is in contrast to the clearly benign phenotype of VS frequently seen in patients with NF2. Although the reason for these differences is not known, basic schwannoma histology and, perhaps, interspecies differences in normal vestibulocochlear nerve microanatomy may be considered. It should be mentioned that human vestibular bipolar ganglion cells are devoid of myelin sheaths while these cells in rodents are myelinated.[16,17,19] Recently, Stemmer-Rachamimov et al.[20] thoroughly reviewed human and murine schwannomas to create a grading system for these tumors. The World Health Organization describes benign human VS as composed of encapsulated, noninfiltrative tumors composed of mature Schwann cells in Antoni A and Antoni B patterns with Verocay bodies, which are rows of palisading Schwann cell nuclei separated from each other by stroma. The benign schwannomas seen in the *Nf2*-knockout mice were classified as murine genetic engineered mouse I or GEM I tumors because they were most closely related to human VS. Although these benign mouse schwannomas displayed primarily an Antoni A growth pattern with occasional Verocay bodies, they were not encapsulated and were far more infiltrative than human VS. The murine GEM II tumors, which refer to more malignant murine schwannomas, displayed nuclear pleomorphism, increased cellularity, and scattered mitotic figures. These histologic differences between human and mouse schwannomas may make it difficult to directly translate research conclusions drawn from these models to the human disease. For this reason, an alternative model such as the reproducible, quantifiable VS xenograft model that we reported here will be important for translational VS research.

Fig. 4. Quantification of human VS xenografts by magnetic resonance imaging. (A) T2-weighted (left), pre- (middle), and postcontrast T1-weighted images (right) of a vestibular schwannoma (VS) xenograft showed that the tumor persisted in the severe combined immunodeficiency mouse over the 6-month study period. The first coronal and axial magnetic resonance imaging scans were performed 1 month after surgery to ensure that the animals had healed. Follow-up magnetic resonance images were obtained at the 2- and 6-month time points. Note that the tumor is readily visible in a fatty tissue pocket between the thigh musculature on both T1 and T2 images (arrows). T1 postcontrast images obtained at 6 months show some enhancement at the tumor margins (arrowhead). (B) T2-weighted (left), pre- (middle), and postcontrast T1-weighted images (right) of a VS xenograft demonstrating significant growth over a 6-month period. Note that the tumor (arrow) appears larger on the 2-month images. T2-weighted imaging at 6 months showed that the tumor extended into the surrounding muscles. Postcontrast T1-weighted images verified the presence of tumor within the thigh musculature. (C) Volumetric measurement of 15 VS xenografts over a 6-month period. Note that most tumors remained stable or regressed slightly, whereas two xenografts demonstrated significant growth.

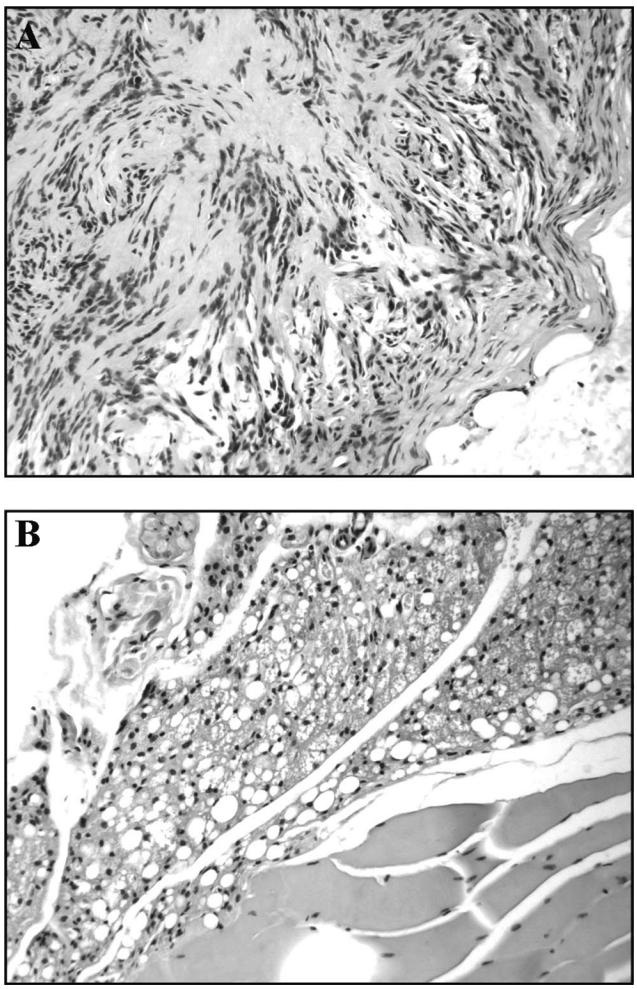

Fig. 5. Histologic analysis of the human vestibular schwannoma (VS) xenografts in severe combined immunodeficiency mice. (A) A tissue section of a VS xenograft harvested 6 months after implantation demonstrated significant tumor growth. The encapsulated tumor mass consisting of spindle cells with no significant atypia and palisading nuclei in Antoni A and Antoni B configurations, all of which are histologic characteristics of benign human VS. (B) A tissue section of a VS xenograft 13 months postimplantation confirmed the presence of tumor cells within the mass seen on magnetic resonance imaging. Note the cells with bland-appearing homogeneous nuclei and some foci of lipid-laden tumor cells in the specimen characteristic of an aged schwannoma.

We have demonstrated the use of MRI in assessing and quantifying schwannoma xenografts in SCID mice. The technique offers investigators the ability to assess an individual xenograft over time without requiring serial surgery or killing the animal. We showed that MRI reliably visualized both human and rat malignant schwannoma xenografts and distinguished between the solid and cystic tumor phenotypes. Immuno- and histopathologic analyses confirmed the MRI findings. The RT4 xenograft is the first description of an animal model for cystic schwannomas in the literature. Human cystic tumors are clinically aggressive, may grow rapidly, and have poorer outcomes. The unique RT4 xenograft may allow the investigation of the basic science behind cystic schwannomas.

MRI of human VS xenografts revealed that although most VS implants diminished slightly and two grew significantly over time, all of the tumors persisted and could be readily imaged. It is important to note that patients with VS in situ demonstrate a similar pattern of disease. Most individuals' tumors persist or grow slowly over time, approximately 5% diminish in size when imaged serially, and approximately 10% grow rapidly.[1] Interestingly, the nongrowing human VS xenografts persisted in SCID mice for 6 to 13 months. We were able to use the high-field MRI to monitor a xenograft for 13 months. Histologically, the persistent xenograft retained characteristics of an aged vestibular schwannoma. In most of the animals imaged over a 6-month period, the variance in tumor volumes was limited. Defining the variance more precisely would require a larger cohort of animals imaged over a 1-year time period. Once established, deviations from the expected variance could be used for evaluating growth-inhibiting effects of potential chemotherapeutic interventions.

The gold standard for evaluating human VS in situ is T1-weighted MRI with gadolinium enhancement.[1] This technique provides sharp contrast between the tumor and surrounding fluid spaces and neural structures. Our MRI analysis of VS xenografts also suggests that T1 postcontrast images best delineate the tumor margins and contrast can be adequately delivered to the mouse using tail vein catheter injections. However, this technique is not without risk to the animal. The volume of gadolinium along with the flush of saline that follows can fluid overload the animal and increase its mortality risk. We have found that T2-weighted RARE images may adequately delineate the xenografts margins and allow for volumetric measurements. Thus, the injection of contrast agent is used in those tumors that are difficult to differentiate from adjacent thigh musculature.

Most human VS tumors are slow growing, whereas only a few proliferate rapidly.[1] Tumor genetics may play a role in the growth potential of these benign tumors. Mutations in the *NF2* gene have been detected in NF2-associated VS, sporadic VS, and cystic schwannomas.[6] Several attempts have been made to correlate clinical expression and specific *NF2* mutations in VS and other NF2-associated tumors. Initially, mutations that cause truncation of the *NF2* protein were reported to cause a more severe phenotype, whereas missense mutations or small in-frame insertions correlated with a mild phenotype. However, there have been reports of severe phenotypes associated with missense mutations in the *NF2* gene, and likewise, large deletions have been reported to give rise to mild phenotypes. In addition, phenotypic variability within NF2 families carrying the same germline mutation has been reported. Given this heterogeneity of clinical response to various mutations, it remains vital to identify key regulatory factors involved in the growth of various types of schwannomas.

Research to better understand VS tumorigenesis has been hampered by the lack of a spontaneous VS cell line available for in vitro study. VS cells are difficult to culture and have a very limited lifespan in vitro. A previous attempt to immortalize VS cells using the human papilloma virus E6–E7 oncogenes yielded the HEI193 cell line with

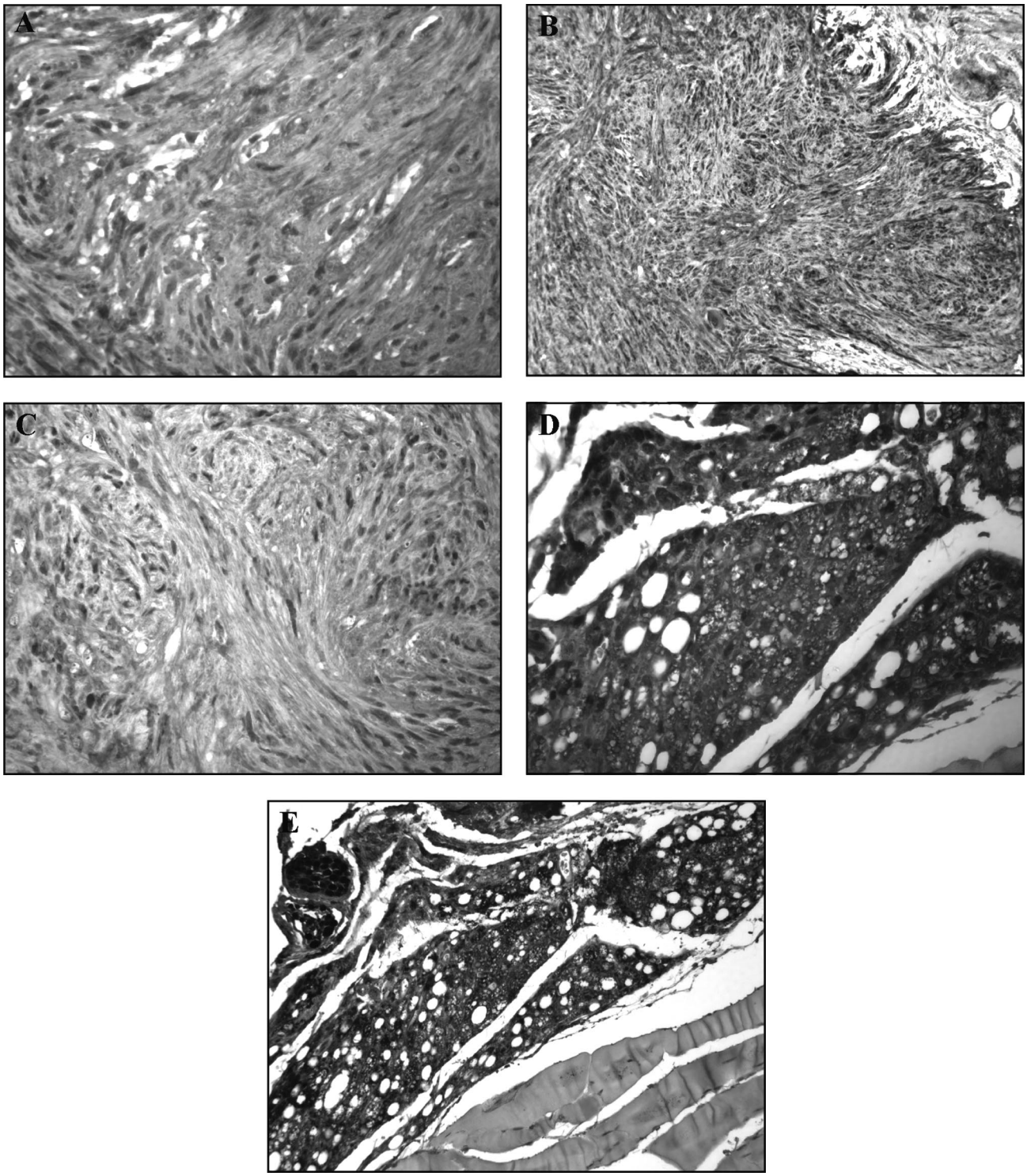

Fig. 6. Immunostained human vestibular schwannoma (VS) xenograft tissue sections. Tissue sections from the VS xenograft showing significant growth over a 6-month period were stained with antibodies to (A) S-100, (B), MBP, and (C) $p75^{NGFR}$. Similarly, sections from a VS xenograft that did not grow but persisted in the mouse for 6 months were stained with (D) anti-S-100 and (E) anti-$p75^{NGFR}$ antibodies. These VS xenografts retained positive immunoreactivity to these Schwann cell markers, whereas the adjacent nontumor cells showed no staining.

altered growth properties such as morphologic changes and independence of Schwann cell growth factors.[21] The fact that some VS xenografts grow in SCID mice and may be transplantable suggests that they may be used as a means to enhance the growth potential of VS cells in culture. By transplanting the growing VS tissue repeatedly through mice, VS cells with enhanced growth capability may be isolated and used to establish a VS cell line.

In summary, this study established a quantifiable human VS xenograft model in SCID mice that uses MRI to measure tumor volumes. VS xenografts demonstrate biologic variability in their growth potential, but although individual grafts may grow, persist, or regress over time, MRI successfully quantifies these tumors noninvasively. VS xenografts represent a model complimentary to *Nf2* transgenic and knockout mice for translational research and improved drug screening.

Acknowledgments

The authors thank Dan Scoles for the RT4 cell line, Peter Wassenaar and Abdulkerim Eroglu for technical assistance, and Sarah S. Burns for critical reading of the manuscript. Mark Lorenz was a recipient of the Young Investigator Award from the Children's Tumor Foundation.

BIBLIOGRAPHY

1. Neff BA, Welling DB, Akhmametyeva E, Chang L-S. The molecular biology of vestibular schwannomas: dissecting the pathogenic process at the molecular level. *Otol Neurotol* 2006;27:197–208.
2. Rouleau GA, Merel P, Lutchman M, et al. Alteration in a new gene encoding a putative membrane-organising protein causes neurofibromatosis type 2. *Nature* 1993;363:515–521.
3. Trofatter JA, MacCollin MM, Rutter JL, et al. A novel Moesin-, Exrin-, Radixin-like gene is a candidate for the neurofibromatosis 2 tumor-suppressor. *Cell* 1993;72:791–800.
4. Charabi S, Klinken L, Tos M, Thomsen J. Histopathology and growth pattern of cystic acoustic neuromas. *Laryngoscope* 1994;104:1348–1352.
5. Fundova P, Charabi S, Tos M, Thomsen J. Cystic vestibular schwannoma: surgical outcome. *J Laryngol Otol* 2000;114: 935–939.
6. Welling DB, Lasak JM, Akhmametyeva EM, Chang L-S. cDNA microarray analysis of vestibular schwannomas. *Otol Neurotol* 2002;23:736–748.
7. Shin M, Ueki K, Kurita H, Kirino T. Malignant transformation of a vestibular schwannoma after gamma knife radiosurgery. *Lancet* 2002;360:309–310.
8. Niemczyk K, Vaneecloo FN, Lecomte MH, et al. Correlation between Ki-67 index and some clinical aspects of acoustic neuromas (vestibular schwannomas). *Otolaryngol Head Neck Surg* 2000;123:779–783.
9. Lee JK, Sobel RA, Chiocca EA, Kim TS, Martuza RL. Growth of human acoustic neuromas, neurofibromas and schwannomas in the subrenal capsule and sciatic nerve of the nude mouse. *J Neurooncol* 1992;14:101–112.
10. Charabi S, Rygaard J, Klinken L, Tos M, Thomsen J. Subcutaneous growth of human acoustic schwannomas in athymic nude mice. *Acta Otolaryngol* 1994;114:399–405.
11. Stidham KR, Roberson JB Jr. Human vestibular schwannoma growth in the nude mouse: evaluation of a modified subcutaneous implantation model. *Am J Otol* 1997;18: 622–626.
12. Yamate J, Yasui H, Benn SJ, et al. Characterization of newly established tumor lines from a spontaneous malignant schwannoma in F344 rats: nerve growth factor production, growth inhibition by transforming growth factor-β1, and macrophage-like phenotype expression. *Acta Neuropathol (Berl)* 2003;106:221–233.
13. Imada M, Sueoka N. Clonal sublines of rat neurotumor RT4 and cell differentiation. I. Isolation and characterization of cell lines and cell type conversion. *Dev Biol* 1978;66: 97–108.
14. John MR, Wickert H, Zaar K, et al. A case of neuroendocrine oncogenic osteomalacia associated with a PHEX and fibroblast growth factor-23 expressing sinusidal malignant schwannoma. *Bone* 2001;29:393–402.
15. Charabi S, Simonsen K, Charabi B, et al. Nerve growth factor receptor expression in heterotransplanted vestibular schwannoma in athymic nude mice. *Acta Otolaryngol* 1996; 116:59–63.
16. Giovannini M, Robanus-Maandag E, Niwa-Kawakita M, et al. Schwann cell hyperplasia and tumors in transgenic mice expressing a naturally occurring mutant NF2 protein. *Genes Dev* 1999;13:978–986.
17. Giovannini M, Robanus-Maandag E, van der Valk M, et al. Conditional biallelic Nf2 mutation in the mouse promotes manifestations of human neurofibromatosis type 2. *Genes Dev* 2000;14:1617–1630.
18. Hung G, Colton J, Fisher L, et al. Immunohistochemistry study of human vestibular nerve schwannoma differentiation. *Glia* 2002;38:363–370.
19. Ona A. The mammalian vestibular ganglion cells and the myelin sheath surrounding them. *Acta Otolaryngol Suppl* 1993;503:143–149.
20. Stemmer-Rachamimov AO, Louis DN, Nielsen GP, et al. Comparative pathology of nerve sheath tumors in mouse models and humans. *Cancer Res* 2004;64:3718–3724.
21. Hung G, Li X, Faudoa R, et al. Establishment and characterization of a schwannoma cell line from a patient with neurofibromatosis 2. *Int J Oncol* 2002;20:475–482.

BMC Cell Biology

BioMed Central

Research article

The role of *Drosophila* Merlin in spermatogenesis

Natalia V Dorogova[1], Elena M Akhmametyeva[2], Sergei A Kopyl[1], Natalia V Gubanova[1], Olga S Yudina[1], Leonid V Omelyanchuk[1] and Long-Sheng Chang*[2]

Address: [1]Institute of Cytology and Genetics, Russian Academy of Sciences, Novosibirsk, Russia and [2]Center for Childhood Cancer, Research Institute at Nationwide Children's Hospital and Department of Pediatrics, The Ohio State University College of Medicine, Columbus, Ohio, USA

Email: Natalia V Dorogova - natdorogova@rambler.ru; Elena M Akhmametyeva - akhmamee@ccri.net; Sergei A Kopyl - kopyl@bionet.nsc.ru; Natalia V Gubanova - nat@bionet.nsc.ru; Olga S Yudina - olya_y@ngs.ru; Leonid V Omelyanchuk - ome@bionet.nsc.ru; Long-Sheng Chang* - lchang@chi.osu.edu

* Corresponding author

Published: 10 January 2008

BMC Cell Biology 2008, **9**:1 doi:10.1186/1471-2121-9-1

Received: 23 July 2007
Accepted: 10 January 2008

This article is available from: http://www.biomedcentral.com/1471-2121/9/1

Abstract

Background: *Drosophila* Merlin, the homolog of the human *Neurofibromatosis 2* (*NF2*) gene, is important for the regulation of cell proliferation and receptor endocytosis. Male flies carrying a Mer^3 allele, a missense mutation (Met^{177}→Ile) in the *Merlin* gene, are viable but sterile; however, the cause of sterility is unknown.

Results: Testis examination reveals that hemizygous Mer^3 mutant males have small seminal vesicles that contain only a few immotile sperm. By cytological and electron microscopy analyses of the Mer^3, Mer^4 (Gln^{170}→stop), and control testes at various stages of spermatogenesis, we show that *Merlin* mutations affect meiotic cytokinesis of spermatocytes, cyst polarization and nuclear shaping during spermatid elongation, and spermatid individualization. We also demonstrate that the lethality and sterility phenotype of the Mer^4 mutant is rescued by the introduction of a wild-type *Merlin* gene. Immunostaining demonstrates that the Merlin protein is redistributed to the area associated with the microtubules of the central spindle in telophase and its staining is less in the region of the contractile ring during meiotic cytokinesis. At the onion stage, Merlin is concentrated in the Nebenkern of spermatids, and this mitochondrial localization is maintained throughout sperm formation. Also, Merlin exhibits punctate staining in the acrosomal region of mature sperm.

Conclusion: *Merlin* mutations affect spermatogenesis at multiple stages. The Merlin protein is dynamically redistributed during meiosis of spermatocytes and is concentrated in the Nebenkern of spermatids. Our results demonstrated for the first time the mitochondrial localization of Merlin and suggest that Merlin may play a role in mitochondria formation and function during spermatogenesis.

Background

Spermatogenesis is a model that facilitates studies of the effect of gene mutations on mitosis, meiosis and the remodeling of many cell structures. During spermatogenesis, primordial germ cells undergo an oriented mitotic division to replace themselves and to produce spermatogonia (reviewed in [1,2]). Each spermatogonium undergoes four rounds of mitotic division, generating 16

spermatogonia that subsequently differentiate into spermatocytes within a cyst. Since the cytokinesis of mitotic divisions is incomplete, the spermatogonia are connected by ring channels. Then, all 16 spermatocytes go through two rounds of meiotic divisions, resulting in a cyst of 64 haploid, round-shaped spermatids. The meiotic cytokinesis is also incomplete so that the spermatids remain interconnected.

During the coalescence stage in early spermatids, the mitochondria aggregate to the side of the nucleus, where the centriole resides [2]. By the onion stage of spermatid differentiation, a dramatic transformation of the mitochondrial mass occurs. The individual mitochondria fuse into two giant mitochondria, which are arranged in a densely-packed sphere consisting of many layers of wrapped mitochondrial membranes [1]. This onion-like structure is termed the Nebenkern.

At the elongation stage, the flagellar axoneme elongates, resulting in a dramatic change in the shape of the spermatid [1]. The two interlocked subunits of the Nebenkern unfold and extend along with the growing axoneme. Despite the structural changes of the two mitochondrial derivatives, both mitochondrial subunits remain aligned and associated with axoneme. As spermatids begin to elongate, their heads, containing nuclei, remain aligned toward the testis wall and their tails are turned aside toward the testicular apex. Simultaneously, the cyst slides down along the testis wall, changing its shape from a disc-like structure to a bundle of elongating spermatids with the nuclear regions of spermatids polarized toward the base of the testis [3]. Following the flagellar elongation, the spermatid nucleus transforms its shape from a spherical structure to a long, thin needle. Subsequently, the process of individualization is initiated by the formation of the individualization complex (IC), containing the actin cones at the head region of the spermatid bundle [4]. Individualization occurs in a cystic bulge, progressing along the entire length of the spermatid bundle. During individualization, membrane remodeling takes place, the channels connecting spermatids are destroyed, and syncytial organization of a cyst is lost [5]. Following coiling of the sperm bundle, mature sperm are released into the testis lumen and then pass into the seminal vesicle.

Although the spermatogenesis process has been well defined, only a limited number of genes whose mutations affect this process has been described, and the role of their protein products are mostly unknown. *Mer*^{3}, a mutation (Met^{177}→Ile) in the gene encoding *Drosophila* Merlin, whose ortholog in human is named the *Neurofibromatosis 2* (*NF2*) gene [6,7], leads to male sterility [8]. Male flies with a *Mer*^{3} allele are viable but sterile; however, the cause of sterility is unknown.

Merlin shares a high degree of homology to the ezrin, radixin, and moesin (ERM) proteins, which belong to the protein 4.1 superfamily, linking the actin cytoskeleton to the plasma membrane [9]. Interaction of the ERM proteins with the actin cytoskeleton is thought to be important for the determination of the cell-shape, cell adhesion, cell motility, cytokinesis, and intracellular signaling [10,11]. In addition to its interaction with the actin cytoskeleton, Merlin can bind to microtubules and regulate the microtubule cytoskeleton [12,13]. Studies in mammalian cells show that Merlin mediates contact inhibition of proliferation [14]. Merlin inactivation leads to tumor formation in several cell types in mammals [15].

Merlin is evolutionally conserved [16]. The Merlin homolog in *Drosophila melanogaster* shows extensive sequence homology to the human protein [17]. This similarity between the fly and human Merlin proteins extends over the entire amino acid sequences with the greatest similarity in the amino terminus of the FERM domain (F for protein 4.1) [9,16-18]. The homology between the fly and human Merlin proteins also exists in the carboxyl terminus, a region in which Merlin diverges from the ERM-family members [10,16].

The *Drosophila Merlin* gene (*D-Mer*) is located at the 18D-E region of the X chromosome. *D-Mer* has been shown to regulate cell proliferation and survival through the Hippo signaling pathway [8,19-23]. In addition, Merlin promotes endocytosis of several membrane signaling receptors [24,25]. Furthermore, *D-Mer* is non-autonomously required to maintain polarity of posterior follicle cells in the oocyte and to limit their proliferation [26].

To better understand the cause of sterility in Merlin mutant flies, we carried out an extensive analysis of cellular events in spermatogenesis. We showed that the Merlin protein was concentrated in the mitochondrial derivatives, and that *Merlin* mutations affected meiosis, cyst polarization, nuclear shaping, and axoneme-Nebenkern association.

Results

The sterility phenotype in Merlin mutants is rescued by the introduction of a wild-type Merlin gene

The *Mer*^{3} allele carries a missense mutation (Met^{177}→Ile), and male flies hemizygous for *Mer*^{3} are viable but sterile [8]. Upon examination of the testis, we noted that seminal vesicles from the *Mer*^{3} males were smaller than those from the control *FM6* flies (compare Figure 1B with Figure 1A). In addition, very few sperm were found in the *Mer*^{3} seminal vesicles, and they were immotile, in contrast to those seen in the control *FM6* siblings obtained from the same cross. Acetic acid/orcein staining showed that the *Mer*^{3} testis had fewer sperm heads in each bundle than the control

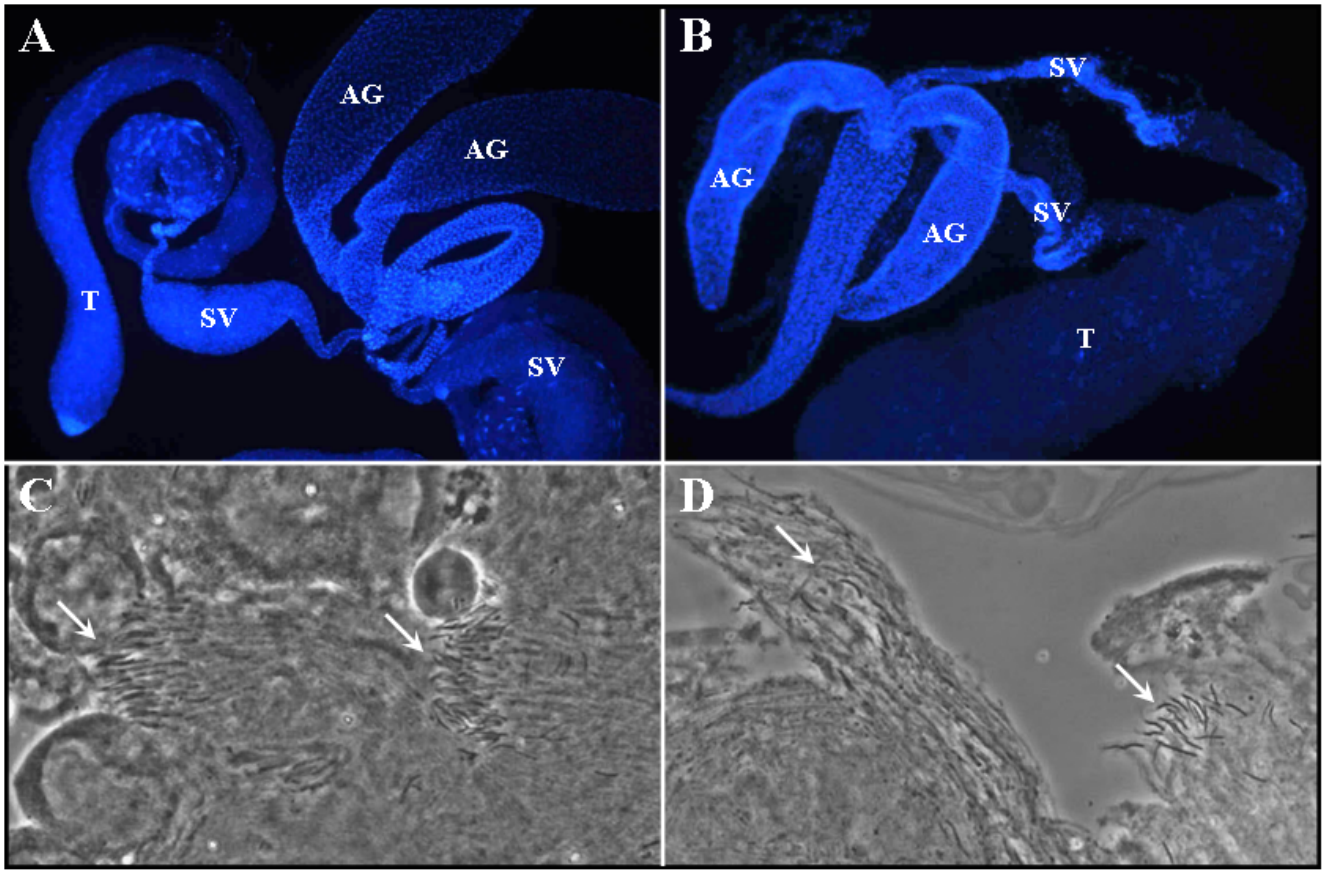

Figure 1
Morphological examination of the testis tissues from young wild-type (panels A and C) and *Mer*^{3} (panels B and D) males. The control *FM6* and *Mer*^{3} mutant males were obtained according to Materials and Methods. The DAPI-stained testis from the control male contained a bulging seminal vesicle (SV) (A). In contrast, a shriveled seminal vesicle was seen in the Mer^3 testis (B). T, testis; AG, accessory gland. Acetic acid/orcein staining revealed that the testis tissue from the control male contained well-organized sperm bundles (arrows) (C), while the Mer^3 testis had fewer sperm in a more disorganized bundle (arrows) (D).

testis (compare Figure 1D with Figure 1C). Also, the sperm in the bundle were arranged in a more disorganized fashion.

Previously, LaJeunesse et al. [8] demonstrated that ectopic expression of a *Mer*$^+$ or *Mer*^{3} transgene using a ubiquitously-expressed Gal4 driver (*T80-Gal4*) in a *Mer*^{4} (Gln^{170}→stop) background rescued *Mer*^{4} lethality. In addition, insertion of a cosmid construct (*P*{*cosMer*$^+$}), carrying the entire *D-Mer* gene, was capable of rescuing various *Mer* mutations. We conducted a similar experiment to test whether a *Mer*$^+$ transgene could rescue the sterility of the *Mer*^{4} allele. Table 1 shows that males carrying both *Mer*^{4} and *P*{*cosMer*$^+$} were viable and fertile. To ensure germline expression of the *Mer*$^+$ or *Mer*^{3}transgene, we cloned the *Mer*$^+$ and *Mer*^{3} sequences into the pUASP vector, and used them to transform embryos. We showed that both pUASP-*Mer*$^+$ and pUASP-*Mer*^{3} could rescue the lethality of *Mer*^{4} mutation when ectopically activated by the *Act5C-Gal4* driver (Table 1). However, only *Mer*$^+$ overexpression restored the fertility of flies with the *Mer*^{4} mutation.

The Merlin protein is dynamically redistributed during meiosis of spermatocytes and is concentrated in the Nebenkern of spermatids

To understand the cause of sterility in the Merlin mutant flies, we studied the subcellular localization of the Merlin protein in the control *FM6* and *Mer*^{3} testes at various stages of spermatogenesis. In the cysts from the control testis, Merlin expression was detected in the cellular cortex of spermatocytes (Figure 2A), as seen in somatic tissues and earlier germ cells [17]. This cortical localization became more pronounced in spermatocytes during prometaphase and metaphase of meiosis (Figures 2B and 2C). Merlin was found to redistribute, and more intense staining was observed in the area associated with the microtubules of the central spindle in telophase (Figure

Table 1: The ability of various transgenes to restore the viability and fertility of the *Mer*^{4} allele.

Genetic cross	Males carrying *Mer*^{4}	Viability	Fertility
♀♀ *y w Mer*^{4}*/FM7i, GFP; +/+; +/+* × ♂♂ *w sn/Y; +/+; P{w*$^+$ *= cosMer*$^+$*}/+*	*y w Mer*^{4}*/Y; +/+; P{w*$^+$ *= cosMer*$^+$*}/+*	+	+
	y w Mer^4*/Y; +/+; +/+*	-	-
♀♀ *y w Mer*^{4}*/M-5, B w*^{a}*; +/+; +/+* × ♂♂ *y w/Y; Act5C-Gal4/If; P{w*$^+$ *= UASP-Mer*$^+$*}/TM6, Tb*	*y w Mer*^{4}*/Y; Act5C-Gal4/+; P{w*$^+$ *= UASP-Mer*$^+$*}/+*	+	+
	y w Mer^4*/Y; Act5C-Gal4/+; +/TM6, Tb*	-	-
	y w Mer^4*/Y; If/+; TM6, Tb/+*	-	-
	y w Mer^4*/Y; If/+; P{w*$^+$ *= UASP-Mer*$^+$*}/+*	-	-
♀♀ *y w Mer*^{4}*/M-5, B w*^{a}*; +/+; +/+* × ♂♂ *y w/Y; Act5C-Gal4/If; P{w*$^+$ *= UASP-Mer*^{3}*}/TM6, Tb*	*y w Mer*^{4}*/Y; Act5C-Gal4/+; P{w*$^+$ *= UASP-Mer*^{3}*}/+*	+	-
	y w Mer^4*/Y; Act5C-Gal4/+; +/TM6, Tb*	-	-
	y w Mer^4*/Y; If/+; TM6, Tb/+*	-	-
	y w Mer^4*/Y; If/+; P{w*$^+$ *= UASP-Mer*^{3}*}/+*	-	-

2D). During cytokinesis, intense Merlin staining remained associated with the microtubules but the intensity was less in the region of the contractile ring (Figure 2E). A similar Merlin distribution pattern was seen during the second meiotic division (data not shown). At the onion stage, Merlin was concentrated in the Nebenkern, a specialized structure formed by the fusion of mitochondria during spermatid differentiation (Figure 2F). This intense Merlin staining in the Nebenkern remained throughout the comet stage of spermatid elongation, during which the Nebenkern split into two parts (Figure 2G). Note that concentrated Merlin immunoreactivity was clearly seen in the two subunits of the Nebenkern in the spermatid (insert in Figure 2G). In the control cyst containing mature sperm, Merlin staining continued to be present in the elongated Nebenkern (Figure 2H). In addition, Merlin was seen as a bright punctate dot in the acrosomal region, a Golgi apparatus-derived structure developed over the anterior part of the sperm's head. We also performed a similar immunostaining on the *Mer*^{3} testis. Although we could detect Merlin staining in the *Mer*^{3} cyst at the comet stage, the *Mer*^{3} spermatid nuclei were scattered throughout the cyst, and the arrangement of spermatids appeared irregular (Figure 2I). The ability of the antibody to detect Merlin staining in the *Mer*^{3} cyst suggests that the missense mutation in *Mer*^{3} did not affect antibody recognition. Using the same antibody, LaJeunesse [8] previously detected a similar cortical localization of Merlin in both the wild-type and *Mer*^{3} imaginal discs. However, the *Mer*^{3} mutation clearly affects Merlin function as the spermatids in the *Mer*^{3} cyst were poorly arranged.

Merlin mutations affect meiotic cytokinesis of spermatocytes, cyst polarization and nuclear shaping during spermatid elongation, and spermatid individualization

Next, we examined if there were any abnormalities during early steps of spermatogenesis in the *Mer*^{3} testis. We dissected testes from both the control and *Mer*^{3} mutant flies. Following staining with acetic acid/orcein, the testes were squashed and examined according to Ashburner [27]. Although we did not find any abnormalities during mitosis of spermatogonia or spermatocyte growth, we observed three types of abnormalities during meiosis of spermatocytes from the *Mer*^{3} testis, as compared with the control testis. The first type of abnormality is shown in Figure 3A, demonstrating a spermatid containing two nuclei of equal size and two Nebenkerns. This type of abnormality was likely caused by cytokinesis failure during the second meiotic division. The second type of abnormality is tripolar spindle in a spermatocyte going through the second meiotic division (Figure 3B). This result suggests incomplete cytokinesis in the previous meiotic division. The third type of abnormality is four-polar spindle in a spermatocyte undergoing the second meiotic division (Figures 3C–E). Note that a secondary *Mer*^{3} spermatocyte contained two pairs of telophase nuclei (Figure 3D). Each pair of nuclei was situated with its own spindle, and two spindles shared a common mid zone (Figure 3C and 3E). This is in contrast with wild-type spermatocytes in telophase showing two daughter nuclei separate from each other along the central spindle (Figure 3F). The four-polar spindle represents another case of abnormal cytokinesis in the first meiotic division. It should be mentioned that we detected the first type of abnormality in about 5% of the mutant cysts, while the second and third types of abnormalities appeared less frequent.

Following meiosis, spermatid elongation ensues [1]. Prior to spermatid elongation, spermatid nuclei group at a defined area of the cyst wall in a process referred to as cyst polarization [3]. We noted that, at this stage, spermatid nuclei were detected as a group in the control cyst (Figure 4A). Intriguingly, spermatid nuclei in the *Mer*^{3} cyst were grouped in two locations (Figure 4B–E), and in some other cysts, nuclei appeared more scattered (Figure 4C–E). We also found a similar abnormality in nuclear grouping

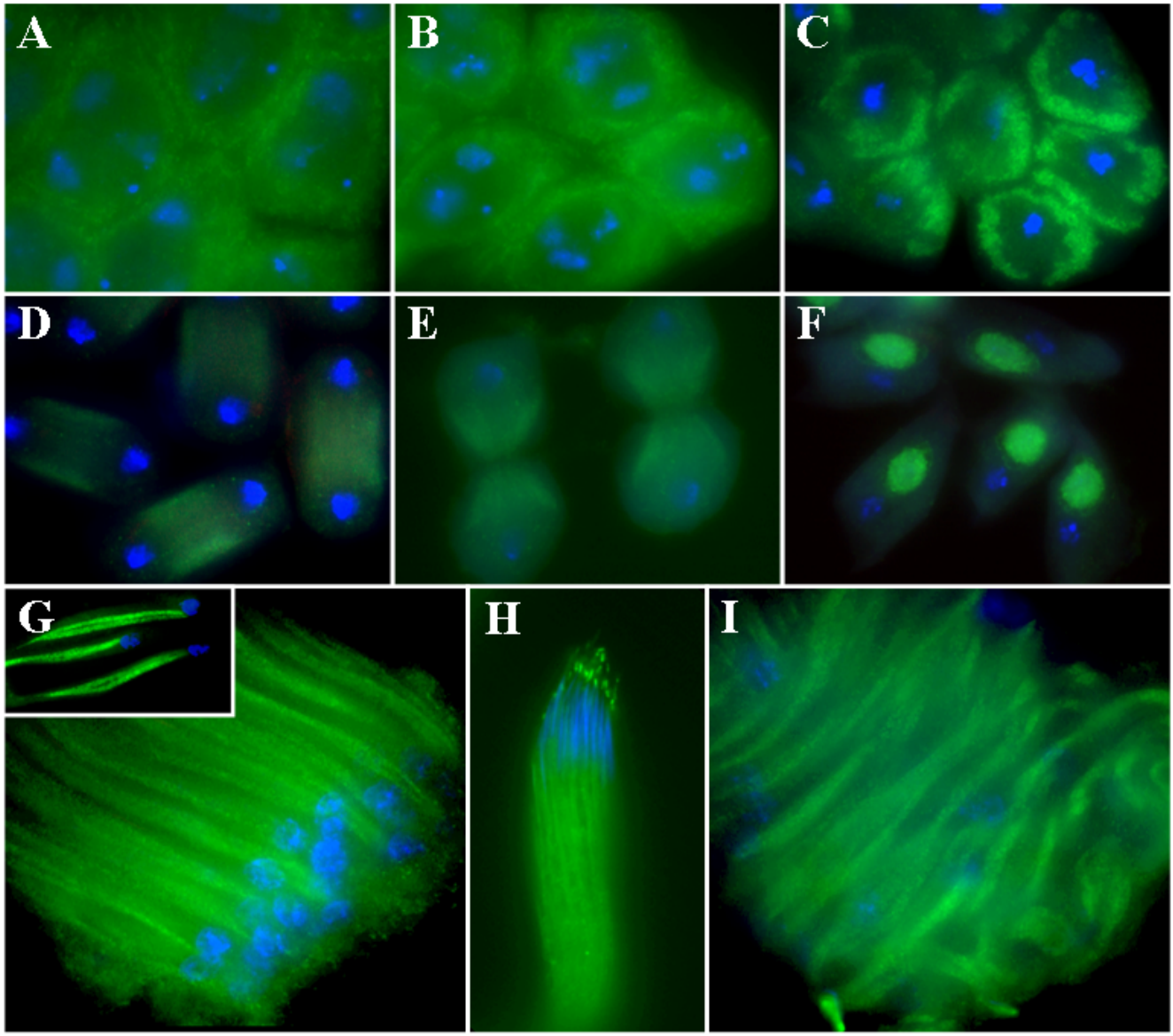

Figure 2
Intracellular distribution of the Merlin protein at various stages of spermatogenesis. In the control cyst, Merlin was detected in the cellular cortex of spermatocytes (A). In prometaphase (B) and metaphase (C) of meiosis, the cortical localization of Merlin became more evident. In telophase (D), Merlin redistributed and accumulated in the area associated with the microtubules of the central spindle. During cytokinesis (E), Merlin staining remained associated with the microtubules but was less intense in the region of the contractile ring. In the onion-stage spermatids (F), Merlin was highly concentrated in the Nebenkern. This localization pattern was maintained through the comet stage of spermatid elongation (G). The insert in panel G shows intense Merlin staining in the two subunits of Nebenkern in spermatids. In the control cyst, containing mature sperm, bright Merlin staining was also seen as a punctate dot in the acrosomal region (H). Merlin staining was still detected in the Mer^3 cyst at the comet stage; however, sperm nuclei were scattered throughout the cyst, and the arrangement of spermatids was irregular (I).

in the Mer^4 cyst. Although Mer^4 is larva-lethal [19], we isolated some rare hemizygous Mer^4 male pupae from the *y* Mer^4/*Binsn* stock, and a few of them were able to grow to pharates adults. When examining testis preparations from these Mer^4 males, we detected spermatid nuclei arranged in two groups (Figures 4F and 4G) or in a scattered manner in all of the mutant cysts (Figure 4H). Also, the cyst polarization defects were more frequently seen in Mer^4 (about 90%) than Mer^3 (about 50%) cysts. These results indicate that *Merlin* mutations affect cyst polarization.

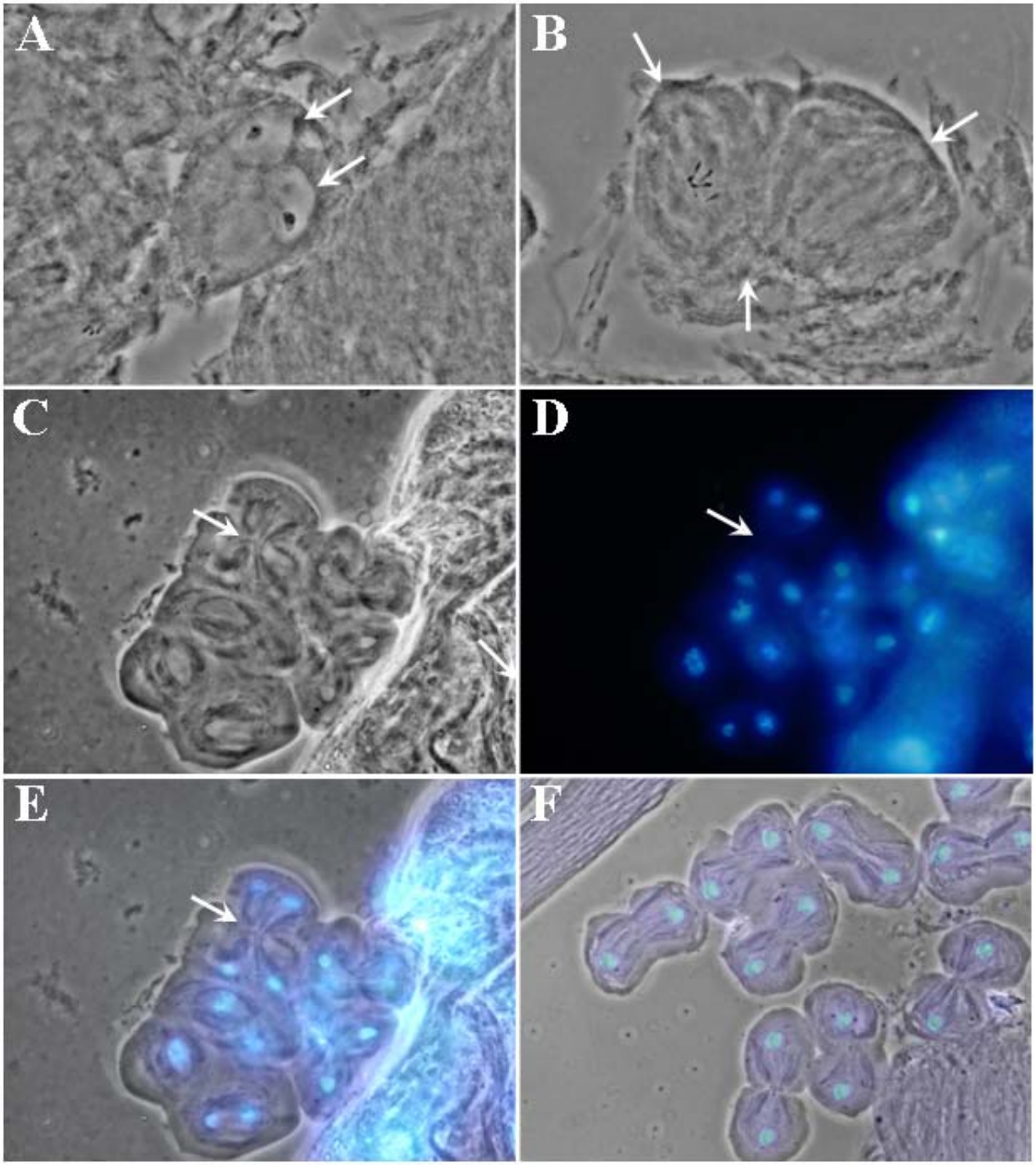

Figure 3
Abnormalities observed during meiosis of Mer^3 spermatocytes: a spermatid containing two nuclei of equal size (arrows) and two Nebenkerns (A), tripolar spindle in a spermatocyte going through the second meiotic division (B), and four-polar spindle in a spermatocyte undergoing the second meiotic division (C-E). Panel C shows the phase contrast image, panel D the DAPI-stained nuclei, and panel E the merged image. Arrow points to the central spindle midzone [29]. For comparison, wild-type meiotic cells in telophase were shown (F).

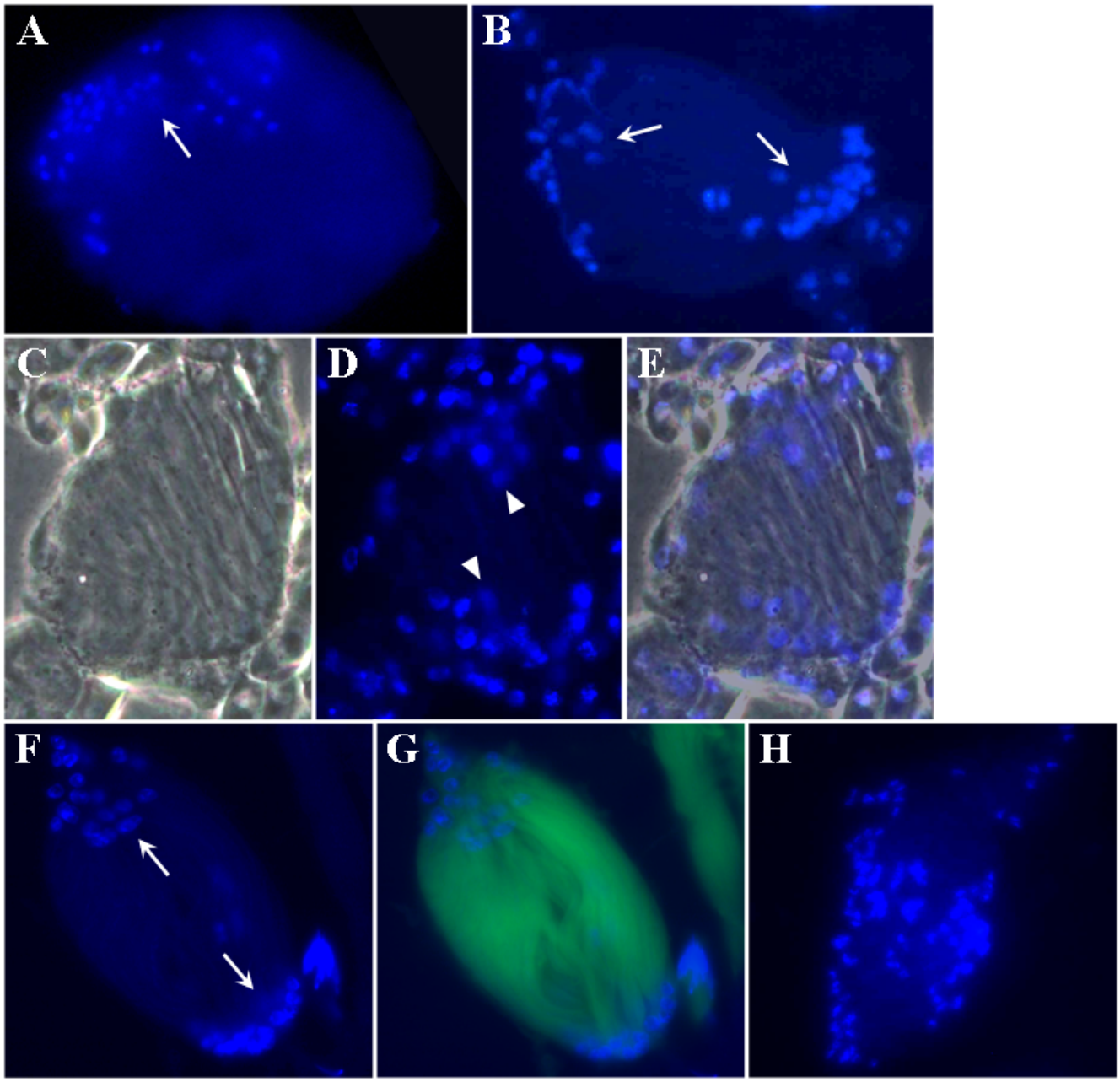

Figure 4
Difference in nuclear grouping during cyst polarization between the control and Merlin mutant spermatids. Dissected testes from the control *FM6* (A), Mer^3 (B-E), and Mer^4 (F-H) males were stained with DAPI and examined as described before. Note that while the spermatid nuclei were grouped in one area (arrow) of the control cyst (A), the spermatid nuclei in the Mer^3 (B-E) and Mer^4 (F-G) cysts were seen as two diffuse groups (arrows). In some cases, the spermatid nuclei were scattered in the mutant cyst (H). Panel C shows a phase-contrast image of a Mer^3 cyst, panel D displays the same cyst stained with DAPI, and panel E represents a merged image. The cyst shown in panels F and G was obtained from a male carrying the Mer^4 mutation and a GFP marker as described in Materials and Methods.

The final stage of spermatogenesis is the process of individualization, followed by sperm coiling [1,2]. The individualization process is initiated at the head of the spermatid cyst, and involves the formation and movement of the actin cones from the head region of the spermatid bundle to the caudal end [4]. Analogous to the previous finding, we detected the actin cones, which moved caudally as a bundle in the control cyst (Figures

5A–D). Note that the sperm heads were grouped in one end of the control cyst, consistent to that seen at the cyst polarization stage (Figures 5B and 5D). Also, the sperm heads became needle-shaped. However, we observed that the sperm nuclei in the *Mer*^{3} cyst appeared scattered (Figure 5E–H) and had variable morphology; some were round, while others were needle shape (Figure 5I). Unlike the control cyst, the *Mer*^{3} cyst had the actin cones located

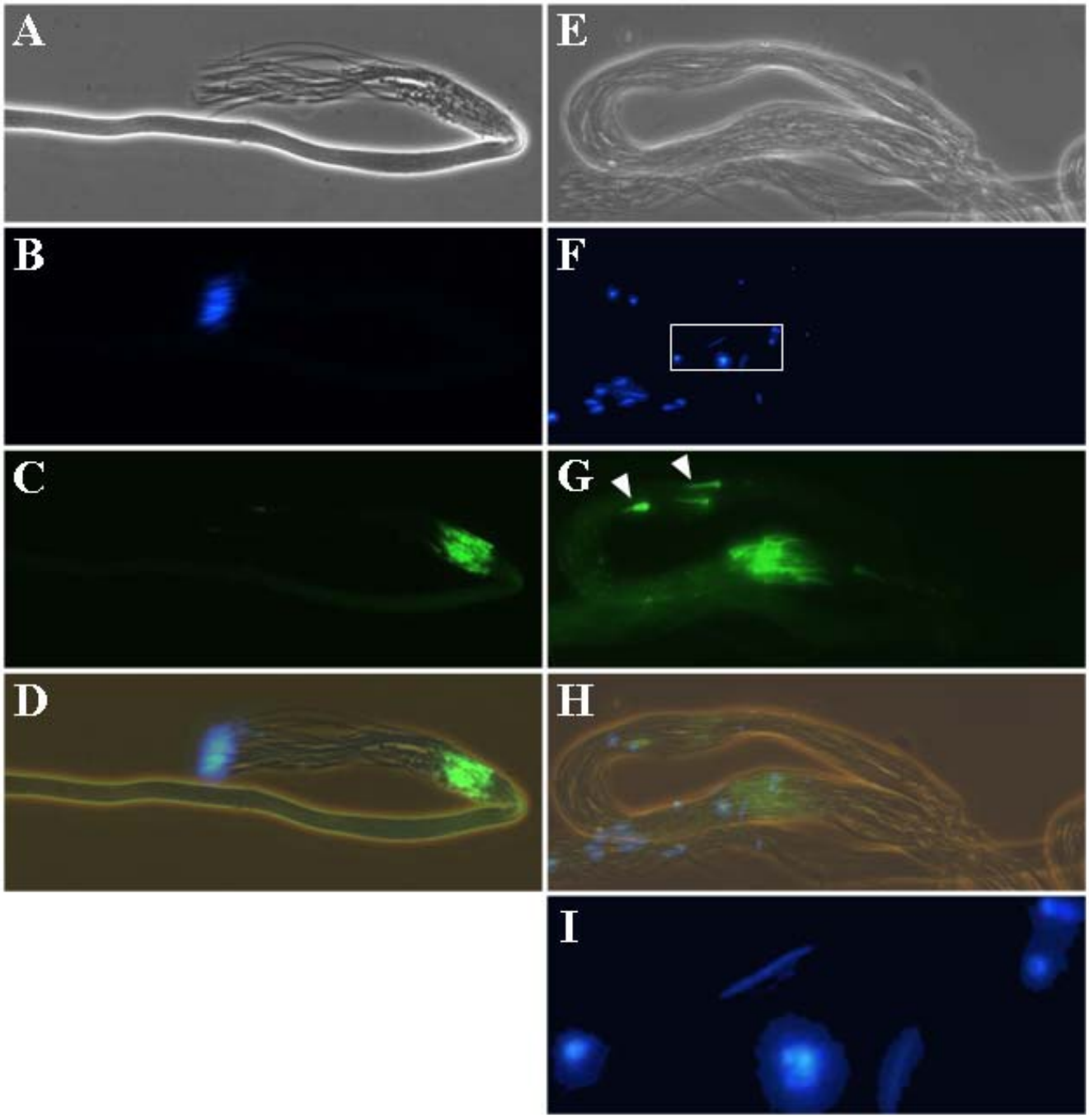

Figure 5
Spermatid individualization in the control (A-D) and *Mer*^{3} (E-I) cysts. Panels A and E illustrate the phase-contrast view of a control or *Mer*^{3} cyst, respectively. Panels B and F show the location of the DAPI-stained sperm nuclei. Panels C and G display the sites (arrowheads) and orientation of the actin cones as visualized by FITC-conjugated phalloidin staining. Panels D and H represent merged images. Panel I is an enlarged view of the rectangular area denoted in panel F.

at multiple sites (Figure 5G). Dispersed actin cones together with scattered nuclei were also found in the Mer^4 cyst (data not shown).

Merlin mutant cysts display abnormalities in Nebenkern-axoneme association

Since we detected intense Merlin staining in the Nebenkern at the onion stage, we employed electron microscopy to further examine Nebenkern transformation from the structure containing two mitochondrial derivatives at the late stage of spermatid elongation into a configuration filled by electron dense material, called the paracrystalline body, at the end of the individualization stage [4]. Thin sections of testes from the control *FM6*, Mer^3, and Mer^4 males were analyzed under a transmission electron microscope. As shown in Figure 6A, we observed that at the late elongation stage, each spermatid in the control cyst contained one major and one minor mitochondrial derivative associated with one axoneme. A paracrystalline body could be seen within the major mitochondrial derivative. However, we found that some of the spermatids in the Mer^3 cyst contained two paracrystalline bodies within the major mitochondrial derivative (Figure 6B). Also, some spermatids had two axonemes. Similarly, two paracrystalline bodies within the major mitochondrial derivative were frequently seen in the elongating spermatids of the Mer^4 cyst (Figure 6C). It should be mentioned that, unlike the spermatids in the control cyst, which displayed cell-cell contact, the spermatids in the Mer^3 cyst were loosely arranged (Figures 6B), and those in the Mer^4 cyst were grossly disorganized (Figure 6C). In addition, some cytoplasmic shedding was present in the Mer^3 cysts (Figure 6B), and excessive amount of cytoplasmic fragments was seen in the Mer^4 cyst (Figure 6C).

At the individualization stage, each of the 64 spermatids in the control cyst contained one axoneme associated with the major and minor mitochondrial derivatives (Figure 6D). Furthermore, the paracrystalline body almost filled the entire major mitochondrial derivative. While some spermatids in the Mer^3 cyst at a similar developmental stage had a paracrystalline body-filled major mitochondrial derivative with axoneme, others containing two paracrystalline body-filled mitochondrial derivatives with abnormal shape or three paracrystalline body-filled mitochondrial derivatives together with one axoneme were also seen (Figure 6E). In addition, spermatids having one or two paracrystalline-filled mitochondrial derivatives but lacking axoneme were observed. Also, the spermatids remained loosely contacted with each other in the Mer^3 cyst. The paired arrangement of axoneme with the mitochondrial derivatives was often lost in the spermatids of the Mer^4 cyst at the individualization stage (Figure 6F). Spermatids with multiple paracrystalline body-filled mitochondrial derivatives but without axoneme, or with two axonemes, were found. Also, cytoplasmic fragmentation together with condensed cytoplasmic remnants and gigantic cytoplasmic bodies were also seen in the Mer^4 cyst.

Consistent with previous observations [1,2,4], we noted that mature spermatids in the control cyst had a substantial reduction in the amount of cytoplasm and a significant reduction in the size of the minor mitochondrial derivative at the end of the individualization stage. The major mitochondrial derivative is filled by a dark-staining paracrystalline material (Figure 6G). Each of the 64 individualized spermatids in the control cyst displayed a highly ordered axoneme-Nebenkern pair. In contrast, a gross disorganization in the arrangement of the individualized spermatids in the Mer^3 cyst was detected (Figure 6H). Although some spermatids exhibited the axoneme-Nebenkern pair, others appeared to be fused together or connected by a thin cytoplasmic extension. In addition, the boundary between the cysts was not evident, and each cystic area contained less than 64 spermatids. The most dramatic alteration was observed in the Mer^4 cyst (Figure 6I). Although axoneme and Nebenkern could be found, very little cytoplasmic material was seen, and the cell-cell boundary could not be easily identified. Insert in Figure 6I illustrates that the structure of axoneme appeared to be intact. Despite this dramatic alteration, the 9+2 microtubule-containing structure of axoneme appeared to be preserved in the *Merlin* mutant cysts, indicating that Merlin is not required for axoneme formation and elongation.

Taken together, our results show that Merlin mutations affect cytokinesis, cyst polarization, nuclear shaping, and spermatid individualization. The observation that Merlin is highly concentrated in the Nebenkern suggests that Merlin may pay a role in mitochondria formation and function during various stages of spermatogenesis.

Discussion

Spermatogenesis is a complicated developmental process, including mitosis, meiosis, cell shape changes, and remodeling of subcellular organelles from the nucleus to mitochondria [1,2]. All of these events appear to involve cytoskeleton reorganization. Merlin has been shown to interact with the actin cytoskeleton and participate in the regulation of cell proliferation, cell adhesion, cell motility, and intracellular signaling [10,11,15]. Merlin can also interact with microtubules and regulate microtubule cytoskeleton [12,13]. In addition, an interaction between Merlin and the myosin heavy chain has been reported [28]. Consistent with findings that Merlin interacts with key components of the cytoskeleton, our results showed that *Merlin* mutations affected meiotic cytokinesis, cyst polarization, nuclear shaping, and spermatid individualization during spermatogenesis. We also showed that the

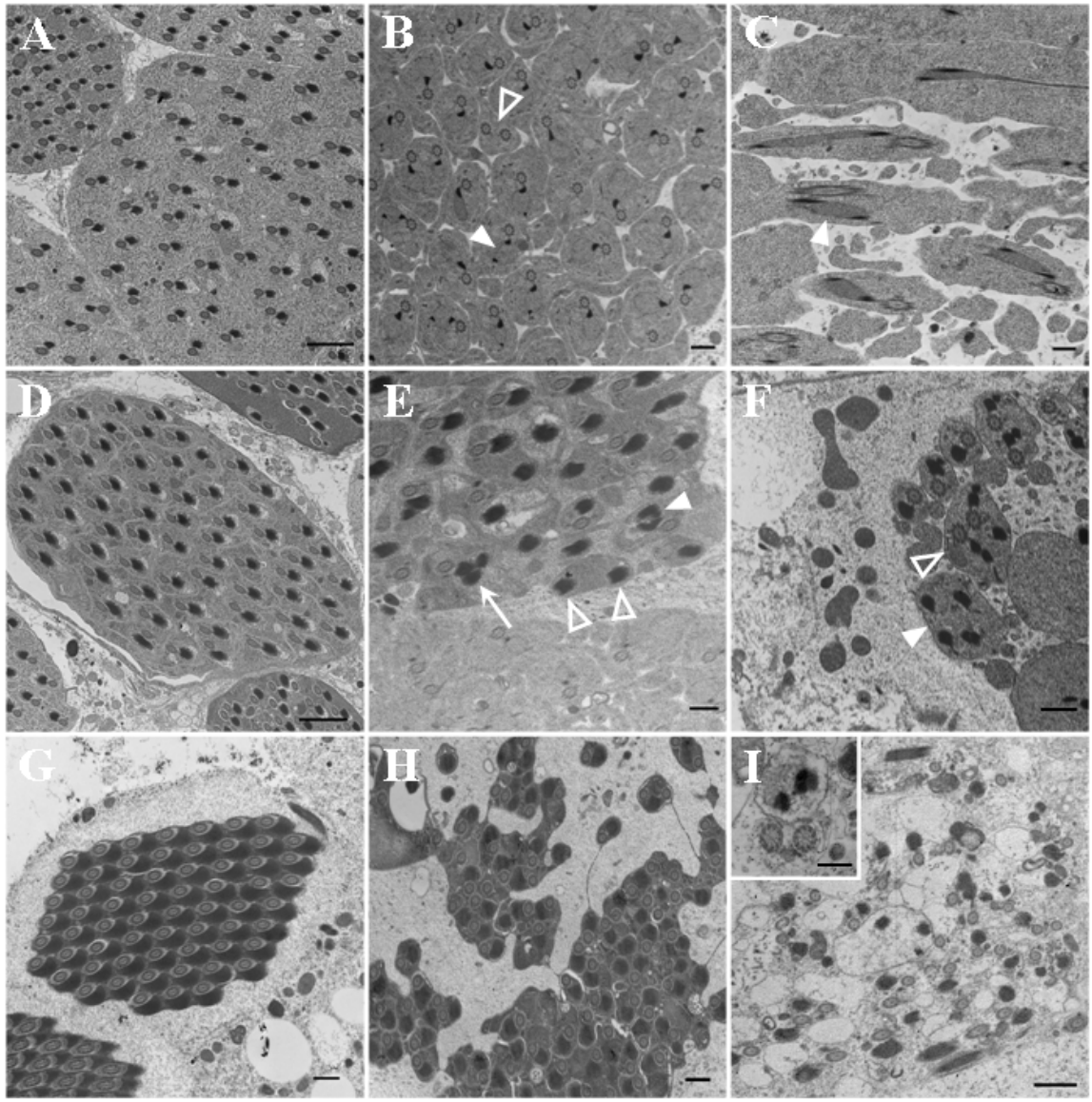

Figure 6
Ultrastructural analysis of the control and Merlin mutant cysts during the elongation and individualization stages. (A-C) Sections of the cysts from the control *FM6* (A), *Mer*^{3} (B), or *Mer*^{4} (C) testis at the elongation stage. (A) A dark paracrystalline body was seen within the major mitochondrial derivative in the control spermatid. Bar = 2 μm. (B) Some of the spermatids in the *Mer*^{3} cyst contained two paracrystalline bodies (filled arrowhead points to one example). Also, some spermatids had two axonemes (open arrowhead). Bar = 0.5 μm. (C) Two paracrystalline bodies within the major mitochondrial derivative were frequently seen in the elongating spermatids of the *Mer*^{4} cyst. Bar = 0.5 μm. (D-F) Cysts from the control *FM6* (D), *Mer*^{3} (E), or *Mer*^{4} (F) testis at the individualization stage. (D) The association of axoneme with the mitochondrial derivatives was seen in the spermatids of the control cyst. Bar = 2 μm. (E) Spermatids in the *Mer*^{3} cyst might contain two abnormally-shaped (filled arrowhead) or three (arrow) paracrystalline bodies together with one axoneme, or have two paracrystalline-filled Nebenkerns but without the axoneme (open arrowhead). Bar = 0.5 μm. (F) Spermatids with multiple Nebenkerns with (open arrowhead) or without (filled arrowhead) axonemes together with cytoplasmic fragmentation were seen in the *Mer*^{4} cyst. Bar = 0.5 μm. (G-I) Cysts from the control *FM6* (G), *Mer*^{3} (H), or *Mer*^{4} (I) testis at the late stage of individualization. (G) Individualized spermatids in the control cyst displayed a highly-ordered axoneme-Nebenkern pair. Bar = 0.5 μm. (H) The spermatids in the *Mer*^{3} cyst were poorly arranged and some of them appeared to be fused together. Bar = 0.5 μm. (I) The *Mer*^{4} cyst showed a complete destruction of spermatid individualization, resulting in empty spermatids with or without axoneme or Nebenkern. Insert illustrates the structure of axoneme appeared to be intact. Bar = 1 μm. Bar in the insert = 0.2 μm.

sterility phenotype of hemizygous male Merlin mutants could be rescued by the introduction of a wild-type *Merlin* gene.

The first abnormality that we found in the *Merlin* mutants during spermatogenesis is cytokinesis failure during meiosis of spermatocytes. Cytokinesis is the process of dividing the cytoplasm and separating two daughter cells. It involves the formation of a contractile ring and the central spindle, two interdependent structures that cooperatively interact throughout the process [29]. The *Drosophila* contractile ring is comprised of actin, non-muscle myosin II, the regulatory light chain of myosin II, and anillin. Intriguingly, we observed that the Merlin expression pattern was closely associated with the microtubules of the spindle during cytokinesis. Given the fact that Merlin interacts with microtubule, actin, and myosin heavy chain, it is possible that Merlin may be involved in the assembly of the spindle and membrane addition. Further colocalization analysis will be needed to better understand the role of Merlin in this meiotic process.

Studies in mammalian cells indicate that Merlin functions both as a growth and tumor suppressor [15]. In *Drosophila*, tumor suppressors often regulate cell proliferation in a tissue-specific manner [30]. Two genes previously reported to have tumor suppressor property in the male gonad are *bam* and *bcgn*. Mutations in these genes result in a large number of cells resembling those in early germline stages [30]. Mosaic analysis in the eye tissue has revealed that *Merlin* mutant clones over-proliferate relative to normal sister clones; however, no tumors were found in the homozygous *Merlin* mutant tissue [8]. This result indicates that *Merlin* mutations belong to the class of overgrowth mutations. Upon careful examination of the Mer^3 and Mer^4 testis tissues, we also did not find any tumors.

Cyst polarization involves nuclear migration to a defined area of the cyst wall [3]. Although specific details about cyst polarization are not understood, it is envisaged that nuclear migration requires the participation of the actin cytoskeleton. Since Merlin interacts and modulates the actin cytoskeleton and other cytoskeletal apparatus, *Merlin* mutations could affect nuclear migration and lead to spermatid nuclei in two disorganized groups or more scattered in the mutant cysts as we have observed. Alternatively, the presence of Merlin in the Nebenkern suggests that Merlin may play a role in cyst polarization through Nebenkern. Nevertheless, *Merlin* represents the first gene whose mutation affects cyst polarization in spermatogenesis. Previously, in a genetic screen for genes functioning in embryonic axis specification, MacDougall et al. [26] found that *gurken* (*grk*) mRNA localization is altered in Mer mutant embryos. Normally, Grk signal instructs about 200 follicle cells to adopt a posterior fate. In turn, the posterior follicle cells send a polarizing signal back to the oocyte. Consequently, it induces the reorganization of oocyte microtubules, determining the localization of different mRNA and oocyte nuclear migration in the oocyte. Despite a broad expression pattern of Merlin in the egg chamber [17], *Merlin* appears to be specifically required non-autonomously only in a small group of follicular cells to maintain the polarity of posterior follicle cells and to limit their proliferation [26]. This finding is consistent with our data showing Merlin also has a role in cyst polarization during the spermatid pre-elongation period.

It should be mentioned that *Merlin* mutations also affect nuclear shaping during spermatid elongation as we observed a few spermatids with a round but not needle-shaped head in the mutant cysts. Recent studies [31-33] have suggested a possible contribution of acrosome to nuclear shaping because defective acrosome development leads to round-headed sperm in mice. The biogenesis of the acrosome, a derivative of the Golgi complex important for sperm-egg penetration, requires the formation of the transient microtubule-containing manchette caudally to the acrosome [34]. In addition, the assembly of an F-actin-containing cytoskeletal plate, called acroplaxome, serves as an anchor for the developing acrosome to the nuclear envelope [35]. Given the well-established relationship between Merlin and the actin filament or microtubule, *Merlin* mutations may affect any of the cytoskeleton-mediated structures required for acrosome formation. It is interesting to note that we have detected intense Merlin staining in the acrosomal region, suggesting a possible role of Merlin in this organelle.

Actin is a major cytoskeletal component of the IC, and individualization is accomplished by the assembly of the cytoskeletal-membrane complex at the nuclear end of the cyst [1,4]. Our results showing scattered nuclei and dispersed actin cones found in the *Merlin* mutant cysts are consistent with the idea that spermatid nuclei provide a physical scaffolding for the assembly of the IC. Intriguingly, several *Drosophila* mutants with scattered nuclei, including Chc^4 (*Clathrin heavy chain*), $scat^1$ (*scattered*), cbx^{05704} (*crossbronx*), EcR^{06410} (*Ecdysone Receptor*), also display the dispersed IC phenotype [4]. The gene *Clathrin heavy chain* has been shown to participate in a number of biological processes, including receptor-mediated endocytosis, neurotransmitter secretion, and sperm individualization. The gene *scattered* is involved in Golgi-to-vacuole transport, retrograde transport from endosome to Golgi, and spermatid individualization. The gene *crossbronx*, encoding a ubiquitin-protein ligase, is important for the ubiquitin cycle and spermatid individualization. The gene *Ecdysone Receptor*, whose protein product responds to hormone stimuli, is essential for embryonic development and organogenesis, including spermatid development.

Curiously, Merlin has been shown to promote endocytosis of several signaling receptors [24,25]. However, how this set of genes is connected to the individualization process remains to be determined.

Spermatid individualization involves membrane remodeling and the outcome of this process is endowing each spermatid with its own plasma membrane and simultaneously removing most of the syncytial cytoplasm from between sperm tails as it proceeds [33,36]. At present, we do not know how *Merlin* mutations lead to excessive cytoplasmic remnants and poorly organized spermatids at the end of individualization. Although Merlin may have a role in membrane remodeling as previously suggested, it is possible that spermatogenesis is such an orchestrated process that perturbation in each stage results in specific abnormalities, which could subsequently affect the following events.

Merlin has been shown to localize underneath the plasma membrane at cell-cell junctions and other actin-rich sites [10,11]. The detection of a high concentration of Merlin protein in the Nebenkern at the onion stage and its maintenance throughout mature sperm formation imply a unique role of Merlin in mitochondria formation and function. The presence of two or multiple paracrystalline bodies in the major mitochondrial derivative of *Merlin* mutant spermatids could result from Merlin dysfunction, leading to such an abnormal Nebenkern structure. A similar abnormality has also been observed in the mutants defective in the gene *fuzzy onion* (*fzo*), encoding a GTPase [37] or *rotund* (*rn*), coding for a Rac GTPase activating protein [38]). However, it is not known whether Merlin function links to these signaling molecules in regulating Nebenkern formation. One fundamental function that mitochondria provide is the production of ATP, which serves as an energy source. The Nebenkern structure is pivotal to sperm motility. Although rare sperm could still be found in the Mer^3 testis, it is likely that without normal Merlin function, sperm motility is impaired.

It should be mentioned that Merlin is not the only growth suppressor whose loss results in male sterility. Like Merlin, the Tumor Suppressor for Lung Cancer 1 (TSLC1) protein, an immunoglobulin superfamily molecule predominantly expressed in the brain, lung and testis, plays important roles in cell adhesion and tumor invasion in mammals [39]. Interestingly, TSLC1-deficient mice also produce round spermatids and are sterile. Thus, it will be important to see whether Merlin deficiency in the testis has any effect on the fertility of mice.

Conclusion

Drosophila Merlin mutant flies are viable but sterile, and the sterility phenotype is rescued by the introduction of a wild-type *Merlin* gene. *Merlin* mutations affect meiotic cytokinesis of spermatocytes, cyst polarization and nuclear shaping during spermatid elongation, and spermatid individualization. The Merlin protein is enriched in the Nebenkern and this mitochondrial localization is maintained throughout sperm formation. These results suggest a role of Merlin in mitochondria formation and function during various stages of spermatogenesis. Further investigation of the action of Merlin in mitochondria is warranted.

Methods

Fly stocks

Flies were maintained at 25°C in standard cornmeal yeast-agar medium. Various *Merlin* mutant strains were generously provided by Rick G. Fehon at University of Chicago, Chicago, IL [40]. Hemizygous Mer^3 males were taken from the strain *w* Mer^3*P{rγ [+t7.2] = neoFRT}19A/FM6, γ B*. The *FM6, γ B* siblings and the *γ w* males from the stock *γ w Pim 19A-FRT/TM6, Tb* (abbreviated here as Pim) were used as controls. The strain *γ w* Mer^4*P{rγ [+t7.2] = neoFRT}19A/FM7i, P{w [+mC] = ActGFP}JMR3* was used as a source of Mer^4 mutant individuals. The *w* sn^3***l(1)18DEb³*** *P{rγ [+t7.2] = neoFRT}19A; P{w [+mC] =* $cosMer^+$*}3/+* strain with an insertion of a genomic fragment containing the entire *Mer* gene was also used. Transgenic strains carrying the pUAST-$MycMer^+$ or pUAST-$MycMer^3$ constructs have been described previously [8]. The strain, containing an insertion of a transposable element carrying the green fluorescent protein (GFP) tag inserted into the *CG8351* gene, was kindly provided by Alain Debec of Université Pierre et Marie Curie, Observatoire Océanologique, Villefranche-sur-mer, France. This strain allowed labeling the cytoplasm of all cells uniformly during spermatogenesis. The strain *γ w; Ki Delta2-3* carrying endogenous transposase activity was a gift from the laboratory of Igor Zhimulev, Institute of Cytology and Genetics, Novosibirsk, Russia.

Acetic acid/orcein and DAPI staining

The females *w* Mer^3*P{rγ [+t7.2] = neoFRT}19A/FM6, γ B* were mated with the males *FM6, γ B/Y* from the same stock. The resulting Mer^3 male *γ w* Mer^3*P{rγ [+t7.2] = neoFRT}19A/Y* and *control FM6, γ B/Y* males were obtained and their testes were dissected. The squashed preparations of testes were performed according to Ashburner [27]. Briefly, testes were dissected in Hanks balanced salt solution (HBSS) and stained in a 1:1 mixture of 1% acetic acid/orcein and 1% acetic acid/carmine for 2 hours at room temperature. Stained testes were examined under phase-contrast optics of an Axiovert-200 microscope (Carl-Zeiss). For DAPI staining, dissected testis tissues were fixed in 3.7% formaldehyde in Dulbecco's phosphate-buffered saline (PBS), pH 7.2, and stained with

DAPI (1.5 μg/ml) prior to visualization under the epifluorescence optics of an Axiovert-200 microscope.

Transgenesis

Genomic DNA were isolated from flies carrying the *UAS-MycMer*$^{+}$ or *UAS-MycMer*^{3} insertion as described above and amplified by PCR to generate *Merlin* cDNAs as previously described [8]. The *Merlin* cDNAs were inserted into the pUASP vector at the *Sac*II and *Xba*I sites. The DNA inserts in the plasmids were confirmed by restriction digestions and direct sequencing. Embryos with the genetic constitution *y w*; *Ki Delta2-3*, carrying the endogenous transposase *Delta2-3*, were injected with the pUASP-*MycMer*$^{+}$ or pUASP-*MycMer*^{3} DNA. After reaching the adult stage, the injected flies were mated with *y w* mating partners. The resulting *w*$^{+}$ progeny were isolated and crossed to establish a strain carrying a transposition. A few independent insertions were obtained for each construct, and the presence of the Merlin coding sequence in the transposants was tested by PCR analysis of genomic DNA described above.

Living cytology

For the examination of sperm motility, seminal vesicles of male flies that had been alone for three days were isolated and checked for movement of sperm heads under Varel contrast optics of an Axiovert-200 microscope. For general spermatogenesis inspection, dissected testes were squashed in HBSS using coverslips as described by Fuller [2]. The unfixed preparations of live cysts were examined for the coiling process according to Cross and Shellenbarger [3].

Antibody staining

Dissected testes were placed onto poly-L-lysine coated slides. To isolate cysts, the dissected testes were pierced using a tungsten needle attached to a Narishigi micromanipulator. Slides with testis tissues attached were fixed in 3.7% formaldehyde in PBS, pH 7.2. After washing in PBS 10 min three times, fixed tissues were permeated with 1% Triton X-100 in PBS for 30 min and then pretreated with the blocking solution containing 1% non-fat dry milk in PBS. Pretreated tissues were incubated with a guinea pig anti-Merlin antibody (1:6000 dilution; [17]) or a mouse anti-α-tubulin antibody (1:500 dilution; Sigma Chemicals) overnight. After washing with PBS three times, a secondary antibody conjugate (Alexa 488-conjugated anti-guinea pig IgG [1:700 dilution], Alexa 568-conjugated anti-mouse IgG [1:200 dilution, or a FITC-conjugated anti-mouse IgG [1:50 dilution]) was added for 2 hours at room temperature. To visualize actin filaments, FITC-conjugated phalloidin (1:50 dilution; Molecular Probe) was used. In some experiments, nuclei were stained with DAPI (1.5 μg/ml). After staining, the slides were mounted in Mowiol with 10% DABCO and examined under the epifluorescence or phase-contrast optics of an Axiovert-200 or an Olympus BX50 microscope.

Electron microscopy

Dissected testes were fixed in 2% glutaraldehyde in PBS, pH 7.4, for 2 hours and then treated with 1% osmium tetraoxide in PBS for 1 hour. Treated tissues were stained with 1% uranyl acetate at 4°C overnight. Following dehydration in ascending ethanol solutions, stained tissues were embedded in Agar-100, mounted in the block, and polymerized at 60°C for two to three days. Ultrathin sections were prepared and contrasted by incubating in 1% uranyl acetate and lead citrate, and examined using a Hitachi H7650 or a JEOL 1000SX transmission electron microscope.

Abbreviations

IC, individualization complex

ERM, the ezrin, radixin, and moesin proteins

NF2, the *Neurofibromatosis 2* gene

FERM, protein 4.1, ezrin, radixin, and moesin

D-Mer, the *Drosophila Merlin* gene

grk, the *gurken* gene

Grk, the Gurken protein

Chc, the *Clathrin heavy chain* gene

scat, the *scattered* gene

cbx, the *crossbronx* gene

EcR, the *Ecdysone Receptor* gene

fzo, the *fuzzy onion* gene

rn, the *rotund* gene

TSLC1, the Tumor Suppressor for Lung Cancer 1 protein

GFP, green fluorescent protein

HBSS, Hanks balanced salt solution

PBS, phosphate-buffered saline

Authors' contributions

NVD performed immunostaining analysis, EMA and NVG carried out electron microscopy, SAK conducted genetic crosses, OSY generated pUASP constructs, LVO helped

with cytological analysis and prepared a draft of the manuscript, and LSC was the principal investigator of the project and participated in the design, coordination, and writing of the manuscript. All authors read and approved the final manuscript.

Acknowledgements

We sincerely thank Rick G. Fehon for providing us various *Merlin* mutant strains and the anti-Merlin antibody. We are also grateful to Alain Debec for the strain with GFP insertion in the *CG8351* gene, and Igor Zhimulev for the *Delta2-3* strain. Special appreciation goes to Cynthia McAllister for EM assistance, and Amanda Simcox and Sarah S. Burns for critical reading of the manuscript. This study was supported by grants from the US Department of Defense Neurofibromatosis Research Program (W81XWH-04-1-0509) and Russian Fund of Fundamental Investigation (05-04-48316).

References

1. Lindsley DL, Tokuyasu KT: **Spermatogenesis.** In *Genetics and Biology of Drosophila* 2nd edition. Edited by: Ashburner M, Wright TR. Academic Press, NY, NY; 1980:225-294.
2. Fuller M: **Spermatogenesis.** In *The Development of Drosophila melanogaster* Edited by: Bate M, Arias AM. Cold Spring Harbor Laboratory Press, NY; 1993:71-147.
3. Cross DP, Shellenbargerr DL: **The dynamics of *Drosophila melanogaster* spermatogenesis in *in vitro* cultures.** *J Embryol Exp Morph* 1979, **53:**345-351.
4. Fabrizio J, Hime G, Lemmon S, Bazinet C: **Genetic dissection of sperm individualization in *Drosophila melanogaster*.** *Development* 1998, **125:**1833-1843.
5. Fuller MT: **Genetic control of cell proliferation and differentiation in *Drosophila* spermatogenesis.** *Semin Cell Dev Biol* 1998, **9:**433-444.
6. Rouleau GA, Merel P, Luchtman M, Sanson M, *et al.*: **Alteration in a new gene encoding a putative membrane-organizing protein causes neurofibromatosis type 2.** *Nature* 1993, **363:**515-521.
7. Trofatter JA, MacCollin MM, Rutter JL, Murrell JR, *et al.*: **A novel Moesin-, Exrin-, Radixin-like gene is a candidate for the neurofibromatosis 2 tumor-suppressor.** *Cell* 1993, **72:**791-800.
8. LaJeunesse DR, McCartney BM, Fehon RG: **Structural analysis of Drosophila merlin reveals functional domains important for growth control and subcellular localization.** *J Cell Biol* 1998, **141:**1589-1599.
9. Algrain M, Arpin M, Louvard D: **Wizardry at the cell cortex.** *Current Biol* 1993, **3:**451-454.
10. Bretscher A, Edwards K, Fehon RG: **ERM proteins and merlin: integrators at the cell cortex.** *Nat Rev Mol Cell Biol* 2002, **3:**586-599.
11. Okada T, You L, Giancotti FG: **Shedding light on Merlin's wizardry.** *Trends Cell Biol* 2007, **17:**222-229.
12. Xu HM, Gutmann DH: **Merlin differentially associates with the microtubule and actin cytoskeleton.** *J Neurosci Res* 1998, **51:**403-415.
13. Muranen T, Gronholm M, Lampin A, Lallemand D, Zhao F, Giovannini M, Carpen O: **The tumor suppressor merlin interacts with microtubules and modulates Schwann cell microtubule cytoskeleton.** *Hum Mol Genet* 2007, **16:**1742-1751.
14. Lallemand D, Curto M, Saotome I, Giovannini M, McClatchey AI: ***NF2* deficiency promotes tumorigenesis and metastasis by destabilizing adherens junctions.** *Genes Dev* 2003, **17:**1090-1100.
15. McClatchey AI, Giovannini M: **Membrane organization and tumorigenesis – the NF2 tumor suppressor, Merlin.** *Genes Dev* 2005, **19:**2265-2267.
16. Golovnina K, Blinov A, Akhmametyeva EM, Omelyanchuk LV, Chang LS: **Evolution and origin of merlin, the product of the *Neurofibromatosis type 2 (NF2)* tumor-suppressor gene.** *BMC Evol Biol* 2005, **5:**69-86.
17. McCartney BM, Fehon RG: **Distinct cellular and subcellular patterns of expression imply distinct functions for the *Drosophila* homologues of moesin and the neurofibromatosis 2 tumor suppressor, merlin.** *J Cell Biol* 1996, **133:**843-852.
18. Chishti AH, Kim AC, Marfatia SM, Lutchman M, *et al.*: **The FERM domain: a unique module involved in the linkage of cytoplasmic proteins to the membrane.** *Trends Biochem Sci* 1998, **23:**281-282.
19. Fehon RG, Oren T, LaJeunesse DR, Melby TE, McCartney BM: **Isolation of mutations in the *Drosophila* homologues of the human Neurofibromatosis 2 and yeast CDC42 genes using a simple and efficient reverse-genetic method.** *Genetics* 1997, **146:**245-252.
20. Hamaratoglu F, Willecke M, Kango-Singh M, Nolo R, Hyun E, Tao C, Jafar-Nejad H, Halder G: **The tumour-suppressor genes NF2/Merlin and Expanded act through Hippo signaling to regulate cell proliferation and apoptosis.** *Nat Cell Biol* 2006, **8:**27-36.
21. Cho E, Feng Y, Rauskolb C, Maitra S, Fehon R, Irvine KD: **Delineation of a Fat tumor suppressor pathway.** *Nat Genet* 2006, **38:**1142-1150.
22. Silva E, Tsatskis Y, Gardano L, Tapon N, McNeill H: **The tumor-suppressor gene fat controls tissue growth upstream of expanded in the hippo signaling pathway.** *Current Biol* 2006, **16:**2081-2089.
23. Pellock BJ, Buff E, White K, Hariharan IK: **The Drosophila tumor suppressors Expanded and Merlin differentially regulate cell cycle exit, apoptosis, and Wingless signaling.** *Dev Biol* 2007, **304:**102-115.
24. Maitra S, Kulikauskas RM, Gavilan H, Fehon RG: **The tumor suppressors Merlin and Expanded function cooperatively to modulate receptor endocytosis and signaling.** *Current Biol* 2006, **16:**702-709.
25. Curto M, Cole BK, Lallemand D, Liu CH, McClatchey AI: **Contact-dependent inhibition of EGFR signaling by Nf2/Merlin.** *J Cell Biol* 2007, **177:**893-903.
26. MacDougall N, Lad Y, Wilkie G, Francis-Lang H, Sullivan W, Davis I: **Merlin, the *Drosophila* homologue of neurofibromatosis-2, is specifically required in posterior follicle cells for axis formation in the oocyte.** *Development* 2001, **128:**665-673.
27. Ashburner M: ***Drosophila*: a laboratory manual.** Cold Spring Harbor Laboratory Press, NY; 1989.
28. Jin H, Sperka T, Herrlich P, Morrison H: **Tumorigenic transformation by CPI-17 through inhibition of a merlin phosphatase.** *Nature* 2006, **442:**576-579.
29. Giansanti MG, Farkas RM, Bonaccorsi S, Lindsley DL, Wakimoto BT, Fuller MT, Gatti M: **Genetic dissection of meiotic cytokinesis in *Drosophila* males.** *Mol Biol Cell* 2004, **15:**2509-2522.
30. Gateff E: **Tumor suppressor and overgrowth suppressor genes of *Drosophila melanogaster*: Developmental aspects.** *Int J Dev Biol* 1994, **38:**565-590.
31. Kang-Decker N, Mantchev GT, Juneja SC, McNiven MA, van Deursen JMA: **Lack of acrosome formation in Hrb-deficient mice.** *Science* 2001, **294:**1531-1533.
32. Yao R, Ito C, Natsume Y, Sugitani Y, Yamanaka H, *et al.*: **Lack of acrosome formation in mice lacking Golgi protein GOPC.** *Proc Natl Acad Sci USA* 2002, **99:**11211-11216.
33. Kierszenbaum AL, Tres LL, Rivkin E, Kang-Decker N, van Deursen JM: **The acroplaxome is the docking site of Golgi-derived myosin Va/Rab27a/b-containing proacrosomal vesicles in wild-type and Hrb mutant mouse spermatids.** *Biol Reprod* 2004, **70:**1400-1410.
34. Kierszenbaum AL, Rivkin E, Tres LL: **The actin-based motor myosin Va is a component of the acroplaxome, an acrosome-nuclear envelope junctional plate, and of manchette-associated vesicles.** *Cytogenet Genome Res* 2003, **103:**337-344.
35. Kierszenbaum AL, Rivkin E, Tres LL: **Acroplaxome, an F-actin-keratin-containing plate, anchors to the acrosome to the nucleus during shaping of the spermatid head.** *Mol Biol Cell* 2003, **14:**4628-4640.
36. Noguchi T, Miller KG: **A role for actin dynamics in individualization during spermatogenesis in *Drosophila melanogaster*.** *Development* 2003, **130:**1805-1816.
37. Hales KG, Fuller MT: **Developmentally regulated mitochondrial fusion mediated by a conserved, novel, predicted GTPase.** *Cell* 1997, **90:**121-129.
38. Bergeret E, Pignot-Paintrand I, Guichard A, Raymond K, Fauvarque MO, Cazemajor M, Griffin-Shea R: **RotundRacGAP functions with Ras during spermatogenesis and retinal differentiation in *Drosophila melanogaster*.** *Mol Cell Biol* 2001, **21:**6280-6291.

39. Yamada D, Yoshida M, Williams YN, Fukami T, *et al.*: **Disruption of spermatogenic cell adhesion and male infertility in mice lacking TSLC1/IGSF4, an immunoglobulin superfamily cell adhesion molecule.** *Mol Cell Biol* 2006, **26:**3610-3624.
40. LaJeunesse DR, McCartney BM, Fehon RG: **A systematic screen for dominant second site modifiers of Merlin/NF2 phenotypes reveals an interaction with blistered/DSRF and scribbler.** *Genetics* 2001, **158:**667-679.

Otology & Neurotology
29:58–68 © 2007, Otology & Neurotology, Inc.

Phosphatidylinositol 3-Kinase/AKT Pathway Activation in Human Vestibular Schwannoma

*Abraham Jacob, *Tina X. Lee, *Brian A. Neff, †Shyra Miller, *Bradley Welling, and ‡Long-Sheng Chang

**Department of Otolaryngology, The Ohio State University, Columbus (Dr. Neff is now with the Mayo Clinic, Rochester, Minnesota); †Department of Pediatrics, Division of Experimental Hematology, Cincinnati Children's Hospital Medical Center, Cincinnati; and ‡Center for Childhood Cancer, Research Institute at Nationwide Children's Hospital, Department of Pediatrics, Children's Hospital, The Ohio State University, Columbus, Ohio, U.S.A.*

Hypothesis: The *neurofibromatosis 2* gene, which encodes the tumor suppressor protein merlin, is frequently mutated in vestibular schwannomas (VS). Merlin can inhibit phosphatidylinositol 3 kinase (PI3 kinase) by binding to PI3 kinase enhancer long isoform. Therefore, we hypothesized that the PI3 kinase/AKT pathway is activated in VS.
Background: Despite advances in diagnosis and treatment, VS continue to cause patient morbidity. A more thorough understanding of the signaling pathways deregulated in VS will aid in the development of novel medical therapeutics. Activation of the PI3 kinase/AKT pathway increases cell survival and cell proliferation and has been observed in a variety of human cancers. However, whether the PI3 kinase/AKT pathway is activated in human VS has not been reported.
Methods: Complementary deoxyribonucleic acid microarrays were performed using cultured Schwann cells, 4 VS specimens, and 2 paired normal vestibular nerves. Immunohistochemical analysis using antibodies to activated phosphorylated-AKT was performed on 14 VS tissue sections. Western blots using various antibodies to components of the PI3 kinase/AKT pathways were conducted.
Results: Microarray analysis demonstrated that total AKT gene expression was upregulated in VS, compared with normal vestibular nerves. Immunohistochemical analysis of 14 VS tissue sections detected positive staining for activated AKT phosphorylated at both serine-473 and threonine-308 in all tumors. Western blots comparing VS specimens with normal vestibular nerves showed that the AKT pathway was activated in VS but not in normal nerve. Total AKT, phosphorylated-AKT, PI3-kinase, phosphorylated-phosphatase and tensin homologue deleted on chromosome 10, phosphorylated-phosphoinositide-dependent protein kinase 1, phosphorylated-forkhead box O, phosphorylated-glycogen synthase kinase 3β, and phosphorylated-mammalian target of rapamycin were upregulated in VS.
Conclusion: The PI3 kinase/AKT pathway is activated in VS. Using our recently reported quantifiable VS xenograft model, novel inhibitors of the PI3 kinase/AKT pathway may be tested for VS growth inhibition in vivo. **Key Words:** Acoustic neuroma—AKT—Apoptosis—Schwann cell—Tumorigenesis—Vestibular schwannoma—PI3 kinase.

Otol Neurotol **29:**58–68, 2008.

Vestibular schwannomas (VS) cause significant patient morbidity by virtue of their critical location. Hearing loss, tinnitus, and balance abnormalities are the most frequently encountered symptoms, but large tumors can result in facial numbness, facial weakness, hydrocephalus, blindness, brainstem compression, and even death (1). Bilateral VS characterize neurofibromatosis Type 2 (NF2), an autosomal dominant disease caused by a gene defect on chromosome 22q12. Merlin, the protein product for the *NF2* gene, is structurally similar to the ezrin/radixin/moesin cytoskeletal proteins (2,3) but has unique tumor-suppressive properties. Overexpression of merlin suppresses growth of rat schwannoma cells (4,5), whereas merlin inactivation leads to loss of contact inhibition and increased cell proliferation (6). Merlin cycles between a growth-suppressive closed conformation and an open growth-permissive state based on serine-518 phosphorylation (7). VS are classified as sporadic, NF2-associated VS, and cystic schwannomas, and most tumors grow 1 to 2 mm per year (8,9).

Address correspondence and reprint requests to Abraham Jacob, M.D., Department of Otolaryngology, The Ohio State University, Cramblett Hall Suite 4A, 456 West 10th Ave, Columbus, OH 43210; E-mail: Abraham.jacob@osumc.edu

The phosphatidylinositol 3 kinase (PI3K)/AKT signaling pathway is a growth-promoting system in many human malignancies. AKT has been implicated in cell survival, growth, insulin response, motility, differentiation, apoptosis, and tumorigenesis (10). A comprehensive discussion on the pathway is well beyond the scope of this manuscript, but Figure 1 delineates the salient features of AKT signaling relevant to our investigations. PI3K is a membrane-associated lipid kinase that catalyzes the conversion of phosphatidylinositol diphosphate (PIP2) to phosphatidylinositol triphosphate (PIP3) (11). This event recruits AKT from the cytoplasm to the plasma membrane through a direct interaction between PIP3 and AKT's pleckstrin homology domain (10,12). AKT is activated by phosphoinositide-dependent protein kinase (PDK) 1 via phosphorylation of AKT's threonine-308 site (13). Maximal AKT activation requires a second phosphorylation event at serine-473. It is unclear whether this second event is mediated by autophosphorylation or by a yet unidentified kinase dubbed PDK2 (14).

The major negative regulator of AKT activation is phosphatase and tensin homologue deleted on chromosome 10 (PTEN). PTEN is composed of a phosphatase domain and a C2 lipid-binding domain that allows it to localize to the plasma membrane (15). Its PIP-phosphatase domain has high affinity for PIP3 and catalyzes the conversion of PIP3 to PIP2. PTEN and PI3K have opposing functions in regulating cell proliferation/survival. Importantly, PTEN activity is regulated by phosphorylation. In fact, phosphorylation of PTEN is thought to decrease it phosphatase activity. Casein kinase 2 (CK2) is the dominant kinase responsible for PTEN phosphorylation (15), but recent reports suggest that glycogen synthase kinase (GSK) 3β, a downstream effector of the AKT pathway, can phosphorylate PTEN at several serine residues. Together, CK2 and GSK3β can reduce PTEN phosphatase activity by 30% (16).

AKT exists as 3 isoforms in mammals—AKT1, AKT2, and AKT3. It is involved in signal transduction, cell proliferation, control of cell size, genomic

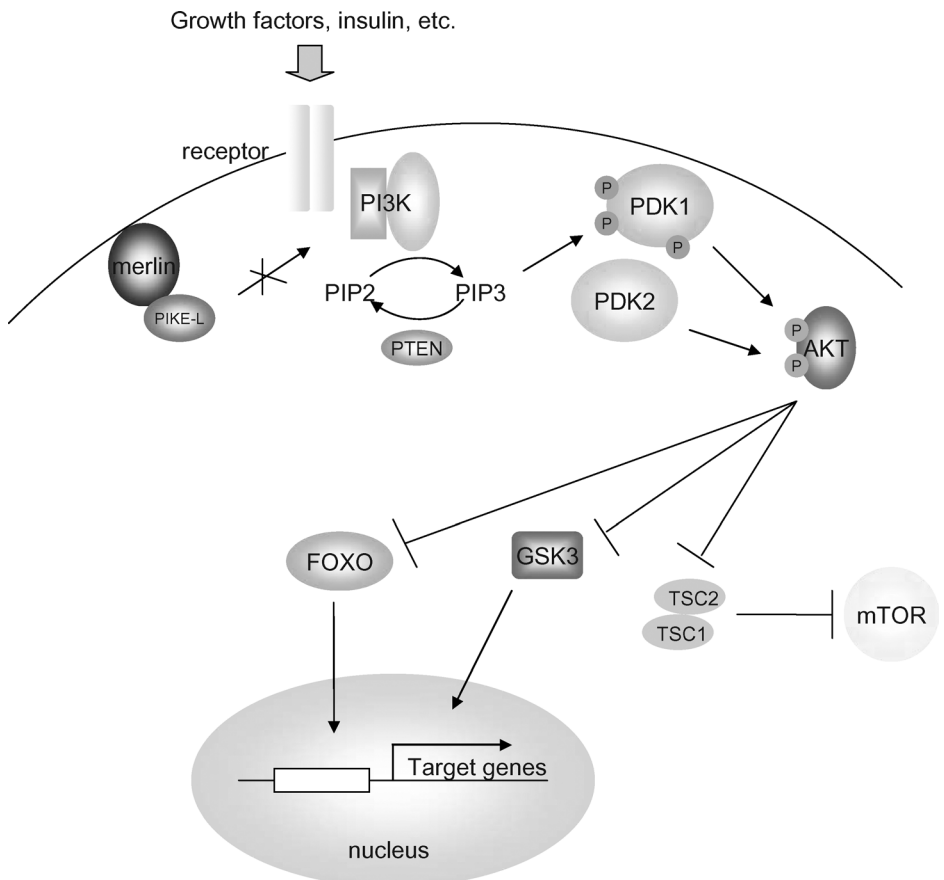

FIG. 1. Salient features of PI3K/AKT signaling. Insulin and other growth factors activate cell surface tyrosine kinase receptors that stimulate PI3K activity. PI3K converts PIP2 to PIP3. PTEN is a negative regulator of the AKT pathway that catalyzes the conversion of PIP3 back to PIP2. PDK1 and PDK2 maximally activate AKT. Phosphorylation of downstream effectors of the AKT pathway such as FOXO, GSK3, and TSC1/TSC2 inhibit these proteins. Existing as a complex, TSC1 and TSC2 normally inhibits mTOR activity. However, when TSC2 is phosphorylated by AKT, it dissociates from TSC1, and mTOR becomes active. Active GSK and FOXO function within the nucleus as transcriptional regulators that activate genes promoting apoptosis. Merlin, the *NF2* gene product, can bind PIKE-L and inactivate PI3K. OSU-03012 is PDK1 inhibitor that inhibits phosphorylation of AKT at the 308 site.

stability, cell survival, apoptosis, and neovascularization (17). Perturbations in AKT signaling have been shown to induce malignant transformation in ovarian cancer, non-Hodgkin lymphoma, pancreatic cancer, hepatocellular carcinoma, gastric cancer, prostate cancer, thyroid cancer, and others (11). Deregulation of upstream components of the AKT pathway such as PI3K and PTEN as well as downstream effectors such as forkhead box O (FOXO), GSK3β, and tuberous sclerosis complex (TSC) 1/TSC2–mammalian target of rapamycin (mTOR) are implicated in tumorigenesis (10).

FOXO transcription factors are characterized by a unique deoxyribonucleic acid (DNA)–binding domain called the "forkhead box" and are major substrates for activated AKT (18). This group of proteins consists of FOXO1, FOXO3, FOXO4, and FOXO6. In the absence of activated AKT, FOXO factors localize to the nucleus where they upregulate growth arrest and apoptotic genes by binding to their DNA-binding element (19). They also contribute to DNA repair and genomic stability. Phosphorylation of FOXO proteins by activated AKT sequesters FOXO to the cytoplasm where it is targeted for degradation by the ubiquitin-proteosome pathway (19). In this way, activated AKT inhibits FOXO, and cells enter a more genomically unstable growth-permissive state.

Like FOXO, GSK3β is a downstream target for activated AKT. GSK3β is widely expressed and was named for its ability to phosphorylate and inactivate glycogen synthase. It regulates a diverse group of metabolic and signaling proteins, structural proteins, and transcription factors. GSK3β is controlled primarily by phosphorylation, but it may also be regulated by protein complex formation and intracellular localization (20). Functional GSK3β activates genes in the nucleus that promote growth arrest. Serine-9 phosphorylation by AKT inactivates GSK3β (20).

Another downstream mediator of AKT is mTOR. Phosphorylated AKT indirectly activates mTOR by way of the TSC. An intact functional TSC consists of TSC1 and TSC2, which inhibit mTOR activity. Activated AKT phosphorylates and stabilizes TSC2, permitting it to dissociate from TSC1. The TSC complex no longer inhibits mTOR, and mTOR is able to phosphorylate downstream effectors such as 4EBP1 and S6K1. Phosphorylated 4EBP1 dissociates from eIF4E. Free eIF4E interacts with other proteins to form the eIF4F complex, which initiates cap-dependent protein translation (21). Phosphorylated S6K1 recruits the 40S ribosomal subunit into an actively translating proteosome capable of protein translation (21). As a result, AKT is able to upregulate the protein synthesis through mTOR.

Active AKT targets a variety of other proteins implicated in apoptosis, including Bcl-2–associated death promoter (BAD) and caspase 9. Caspase 9, a cysteine protease important for programmed cell death and the inflammatory response, is regulated by AKT through phosphorylation of procaspase 9 at serine-196 (22). This inhibits proteolytic processing and prevents downstream targeting of effectors such as the nuclear laminins, inhibitor of caspase-activated DNase or DNA fragmentation factor 45, and poly (adenosine diphosphate) ribose polymerase and P21-activated kinase 2. BAD regulates cell apoptosis by forming heterodimers with Bcl-xL and Bcl-2 and reversing their death repressor activity. Datta et al. (23) demonstrated that activated AKT phosphorylates BAD, thereby inhibiting cell death.

Recent studies indicate that the functional *NF2* gene product, merlin, may play a role in controlling AKT pathway activation. Merlin is capable of inhibiting PI3K activity through its interaction with PI3K enhancer long isoform (PIKE-L) (Fig. 1) (24). PIKE-L is a GTPase that exists in both the cytoplasm and nucleus. It couples PI3K to the metabotropic glutamate receptor (25). Metabotropic glutamate receptor stimulates phospholipase activation and the hydrolysis of phosphoinositide phospholipids in the plasma membrane (26). This reaction provides the necessary substrate (PIP2) for PI3K activity. Normally functioning merlin binds PIKE-L, prevents PIKE-L from binding to PI3K, and limits PI3K access to phosphoinositide lipids like PIP2. Therefore, mutations in the *NF2* gene that inactivate merlin function may account for the observed increase in PI3K/AKT activity in VS.

A more thorough understanding of the signaling pathways deregulated in VS will aid in developing novel medical therapeutics. Here, we report first evidence for the activation of the PI3K/AKT pathway in human VS. A better understanding of AKT deregulation in VS may be directly relevant to clinical care for patients with this disease. Novel inhibitors to this pathway are currently in various stages of preclinical development at our institution, other academic medical centers, and within the pharmaceutical industry. Our group plans to test several such inhibitors using both in vitro and in vivo techniques. Perhaps patients will 1 day have a chemotherapeutic option for treating VS.

MATERIALS AND METHODS

Tissue Acquisition

The Ohio State University Institutional Review Board approved a Human Subjects Protocol for the acquisition of VS specimens and normal nonfunctioning adjacent nerves as needed from patients undergoing surgery. This material was obtained fresh and was confirmed as VS by a clinical pathologist. Paraffin-embedded tissue sections were examined for histology and immunohistochemistry. Part of each tumor specimen was frozen in the operating room with liquid nitrogen, identifying information was removed by tissue-procurement staff at the medical center, and the specimens were transported to our laboratory for RNA and/or protein analysis.

Microarray Analysis

Using frozen tissue, total RNA was prepared from 2 vestibular nerves and 4 VS specimens using the TRIzol method (Life Technologies, Grand Island, NY, USA). Ribonucleic acid concentrations were determined by optical density, and the quality of RNA was checked by electrophoresis. Tissue RNA was then

reverse transcribed into double-stranded complementary DNA (cDNA) per the One-Cycle cDNA Synthesis Affymetrix Protocol. The cDNA was cleaned using the Affymetrix Cleanup Module, and biotin-labeled complementary RNA (cRNA) was synthesized using the Affymetrix GeneChip IVT labeling kit. This was cleaned and quantified using spectrophotometric analysis. cRNA quality was determined using electrophoresis and fragmented. The fragmented cRNA was then added to the Affymetrix hybridization mixture, incubated, and exposed to cDNA probe microarray for 16 hours at 45°C. The array was postwashed with nonstringent wash buffer, stained with Streptavidin Phycoerythrin stain solution, and analyzed. Fold differences for gene expression between normal vestibular nerves and VS specimens were referenced to results from cultured Schwann cells (SCs). Although these data were quantified, the small number of specimens precluded statistical analysis.

Immunohistochemistry

Fourteen paraffin-embedded VS tissue slides were deparaffinized, hydrated, and incubated at 120°C in Biogenex Antigen

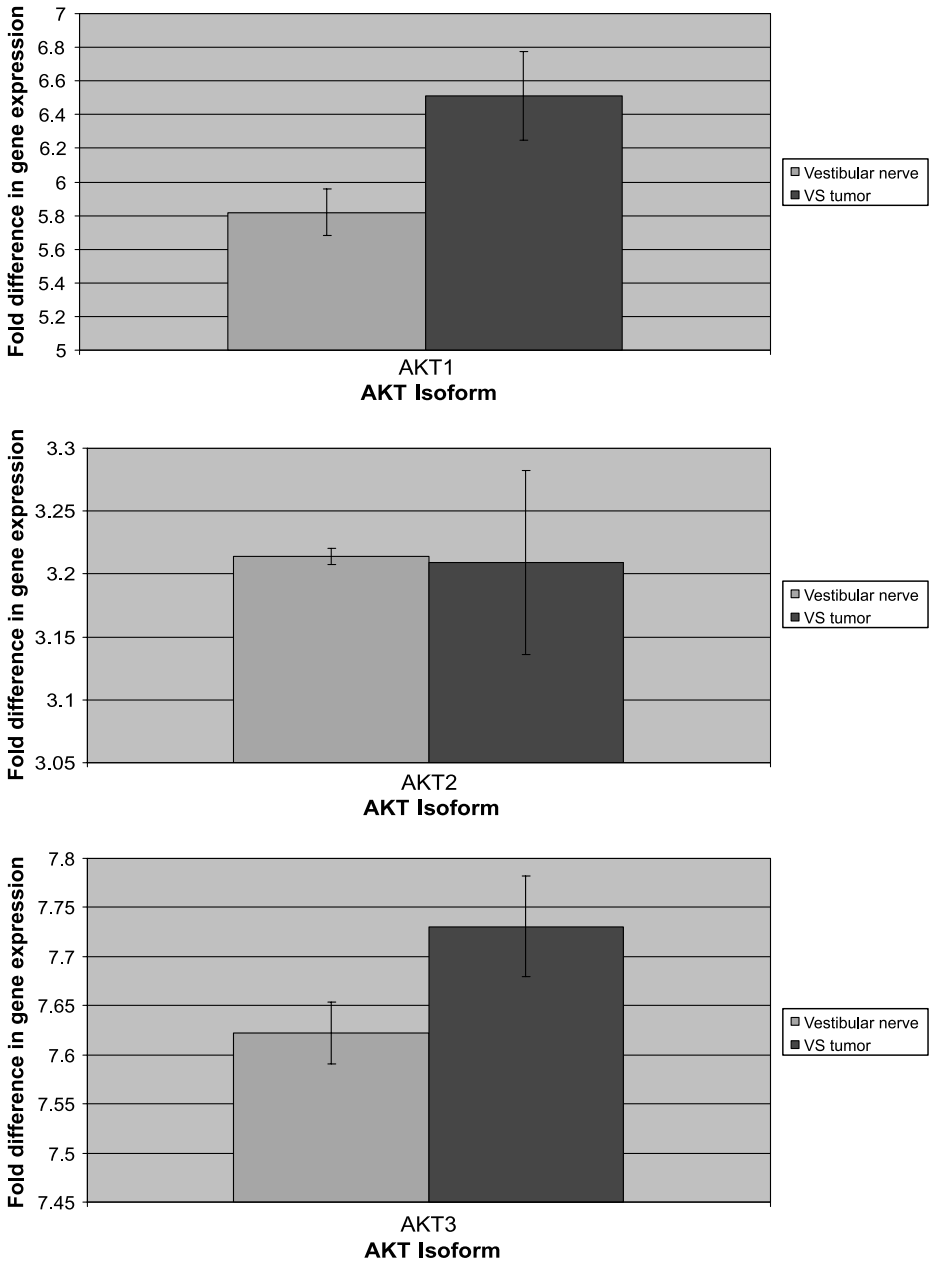

FIG. 2. cDNA microarray data comparing cultured SC gene expression with 4 VS specimens and 2 normal vestibular nerves. Fold differences in AKT1, AKT2, and AKT3 gene expression for tumor and nerve are expressed relative to gene expression in cultured SCs. There is a near one-fold increase in AKT1 gene expression for tumor versus normal nerve. Standard deviation *bars* are provided, but no formal statistical analysis has been performed because of the limited number of specimens. No difference was seen for AKT 2, whereas AKT3 demonstrated a small absolute increase in expression for tumors versus nerve controls.

retrieval citra solution (San Ramon, CA, USA) for 30 minutes. The slides were then placed in 3% hydrogen peroxide for 15 minutes, exposed to Biogenex Power Block for 10 minutes, and incubated with the appropriate primary antibody (either serine 473 or threonine 308 polyclonal phosphorylated AKT [p-AKT] antibody; Cell Signaling, Danvers, MA, USA) at 4°C overnight. Secondary antibody was then applied for 20 minutes followed by an exposure to Biocare Medical Streptavidin-HRP labeling solution (Concord, CA, USA). 3-Amino-9-ethylcarbazole developer was applied for 10 minutes. The slides were counterstained with hematoxylin and mounted using Permount (Fisher Scientific, Hampton, NH, USA). Paraffin-embedded breast cancer sections were used as positive controls, whereas within the breast cancer specimens, fibrofatty stromal elements served as negative controls.

Western Blot Analysis

It is often difficult to find normal-appearing vestibular nerve tissue adjacent to a VS in patients undergoing surgery. However, in patients with smaller tumors or tumors located primarily in the cerebellopontine angle (rather than the internal auditory canal), normal-appearing segments of uninvolved vestibular nerve can be harvested for research purposes. Vestibular nerves served as controls for Western blot analyses looking at differences in protein expression for components of the AKT pathway. In total, we used 12 VS tumors and 7 vestibular nerve controls by Western blot. However, obtaining paired vestibular nerve from the same patient undergoing VS tumor resection is the best control. This obviates potentially confounding factors such as genetic variability between patients, age, sex, time since diagnosis, and tumor growth rate from the data analysis. The data are cleaner and most accurately reflect the molecular changes that occur during VS formation.

In Experiment 1, a single tumor specimen was analyzed to determine the optimal primary antibody exposure times. In Experiment 2, 4 tumor specimens from different patients and 1 nonpaired vestibular nerve serving as a control were evaluated using the protocol established in Experiment 1. Experiment 3 used VS tumor specimens and paired normal vestibular nerve from 2 patients. Band intensities from Experiment 3 were quantified, normalized to band intensities for actin controls, and used to determine relative expression levels for total AKT, serine-473 p-AKT, threonine-308 p-AKT, and β-actin controls using image analysis software (Eastman Kodak Company; Rochester, NY, USA). The x-ray films were scanned, analyzed for image intensity, and normalized to the intensity signals for β-actin controls. In Experiment 3, fold differences in the expression levels for total AKT and p-AKT (serine-473 and threonine-308) between tumor specimens and corresponding paired control nerves were quantified. Since the initial submission of this article, several other paired and unpaired

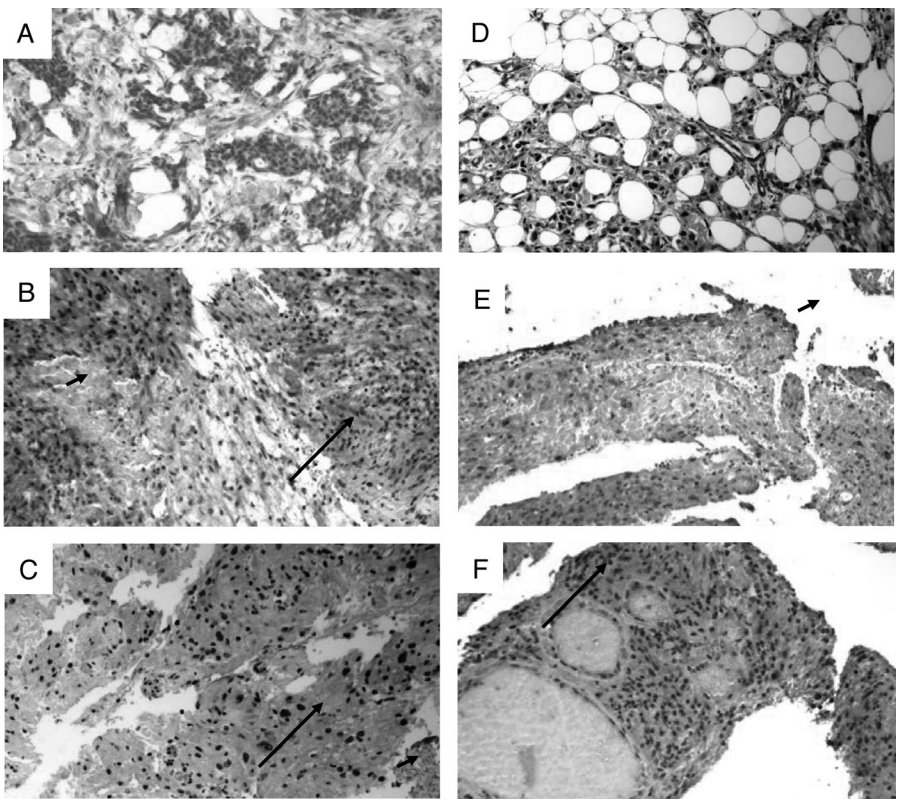

FIG. 3. Immunohistochemistry using antibodies to active p-AKT at the serine-473 and threonine-308 sites. Panels *A* to *C* demonstrate positive staining for serine-473 p-AKT in breast cancer controls (*A*), and 2 VS specimens (*B* and *C*). Panels *D* to *F* demonstrate positive staining for threonine-308 p-AKT staining in breast cancer controls (*D*) and 2 VS specimens (*E* and *F*). All sections were obtained from patients undergoing VS resection at The Ohio State University and were embedded in paraffin. Note the robust staining in hypercellular regions (Antoni A; *long arrows*) and lack of staining in areas of tissue necrosis (*short arrows*). Whereas the breast cancer cells in our control slides (*A* and *D*) were positive for p-AKT, the fibrous stroma present in those slides did not pick up AKT stain for either serine-473 or threonine-308 (original magnification, ×20).

specimens have been analyzed using Western blot. For these samples, upstream and downstream components of the AKT pathway were not evaluated. These data are presented to further demonstrate that AKT activation in VS is a consistent finding at the protein level.

To evaluate whether the growth factors neuregulin (NRG) and forskolin might enhance human SC proliferation through the AKT pathway, Western blots for total AKT and p-AKT were also performed on cultured human SCs grown in the presence and absence of these growth factors. Neuregulin is a growth factor known to enhance SC proliferation in culture (see Discussion). Three sets of human SCs were grown in culture. One set was grown in Dulbecco modified Eagle medium (DMEM) containing fetal bovine serum, NRG, and forskolin. One set had NRG/forskolin withheld for 1 day, whereas the third set had these growth factors withheld for a total of 3 days. Cell lysates from each SC population were isolated and analyzed by Western blots with antibodies against p-AKT (serine-473), p-AKT (threonine-308) and total AKT. α-Tubulin was measured as a loading control for these samples.

Frozen VS tissue was pulverized and suspended in Radio-Immuno Precipitation Assay (RIPA) buffer containing protease inhibitors and phosphatase inhibitor cocktail A (Santa Cruz Biotechnology, Inc., Santa Cruz, CA, USA). After incubation on ice for 45 minutes, the tissue sample was centrifuged, and the supernatant was retained. The protein concentration was determined using a Bio-Rad Protein Assay. The cell lysates containing 20 μg of total protein were separated on a sodium

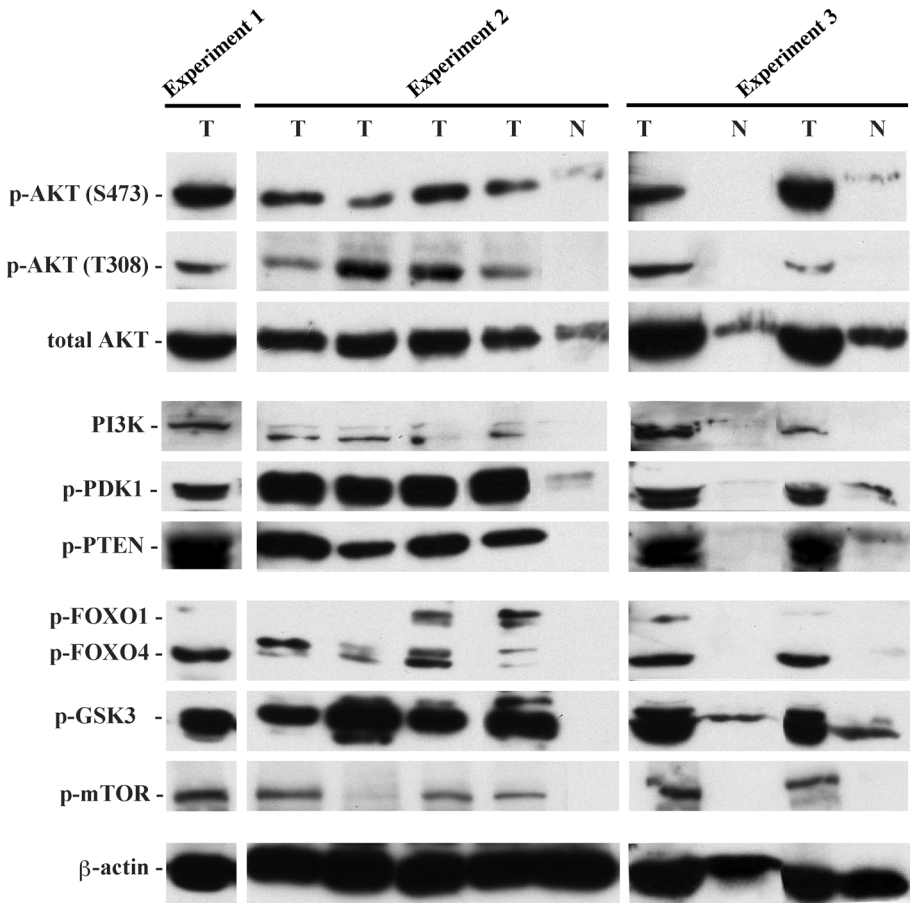

FIG. 4. Western blots from 3 experiments using 7 VS tumor specimens (*T*) and 3 normal vestibular nerve controls (*N*). Experiment 3 includes sets of paired VS tumor and normal vestibular nerve from 2 patients. Polyclonal antibodies to total AKT and p-AKT at the serine-473 (*S473*) and threonine-308 (*T308*) sites were used to evaluate AKT activation. Polyclonal antibodies to activated PI3K, activated PDK1, and inactivated PTEN were used for evaluating upstream components of the AKT pathway, whereas polyclonal antibodies to phosphorylated FOXO1, p-FOXO4, p-GSK3β, and p-mTOR were used to evaluate downstream effectors. The control lane (β-actin) shown applies to all the blots because they were probed with different antibodies after stripping. Total AKT was present in both tumor and nerve samples but was increased in tumors as compared with vestibular nerve controls. Bands were present for p-AKT at the threonine-308 site in all 7 tumor specimens but were absent in the nerve controls. Bands were present for p-AKT at the serine-473 site in all the tumor specimens. Weak bands for serine-473 were present in 2 of the 3 normal nerve samples. Activated PI3K and PDK1 were present in all VS tumors. A weak band for PI3K was present in 1 of the 3 normal nerve controls. Weak bands were seen for PDK1 in 2 of the 3 control nerves. Strong bands were seen for inactive p-PTEN in all tumor samples. One of the 3 normal control nerves demonstrated a weak p-PTEN band. p-FOXO was increased in tumors as compared with control nerves. p-FOXO1 was present in 5 of 7 tumors, whereas p-FOXO4 was present in all 7 of 7 tumor specimens. Only the vestibular nerve control from Pair 2 of the paired VS/normal nerve sample demonstrated a weak band for p-FOXO4. p-GSK3β was increased in all 7 tumor specimens as compared with control nerves. Two of 3 control nerves showed weak bands for p-GSK3β. p-mTOR was clearly active in all 6 of 7 tumors and absent from all control vestibular nerves. The remaining VS specimen had a very faint band for p-mTOR.

dodecyl sulfate–polyacrylamide gel electrophoresis and electroblotted onto an Immobilon-P membrane (0.45 μm, Millipore Corp., Bedford, MA, USA) using a Bio-Rad Mini Trans-Blot electrophoretic transfer cell. Nonspecific binding was blocked using blocking buffer (5% [wt/vol] nonfat dry milk, 1X Tris-buffered saline, 0.1% Tween 20) for 1 hour at room temperature. The membrane was incubated with primary antibody (1:1,000) overnight at 4°C. Then, after incubation with HRP-conjugated antirabbit immunoglobulin G (1:2,000) for 1 hour at room temperature, a mixture of LumiGOLDTM ECL reagents A and B (SignaGen Laboratories, Gaithersburg, MD, USA) was added to the membrane. The chemiluminescent activity was then captured by exposure to Fiji medical x-ray film. The following primary antibodies used were purchased from Cell Signaling: AKT antibody, p-AKT (serine-473) antibody, p-AKT (threonine-308) antibody, PI3K p110γ antibody, p-PDK1 (serine-241) antibody, p-PTEN (serine-380/threonine-382/383) antibody, p-GSK-3β (serine-9) antibody, p-mTOR (serine-2448) antibody, p-FOXO1 (serine-256) antibody. β-actin was used as a control.

RESULTS

Microarray data comparing 4 VS specimens with 2 normal vestibular nerves demonstrated upregulation of AKT gene expression in tumors (Fig. 2). Relative AKT gene expression for the mammalian isoforms AKT1, AKT2, and AKT3 was determined for 4 VS specimens and 2 normal vestibular nerves. These data were normalized to the gene expression profile in cultured SCs. AKT1 gene expression was increased nearly onefold. There was no difference in AKT2 gene expression and a slight increase in AKT3 for VS specimens compared with controls. No statistical analysis was performed because of the small number of samples; however, standard deviation bars are provided.

Immunohistochemistry demonstrated AKT activation in patients with VS (Fig. 3). VS are characterized by areas of Antoni A (hypercellular) and Antoni B (hypocellular) architecture. The cells are typically spindle shaped and lack significant nuclear pleomorphism. All 14 VS specimens were stained with polyclonal antibodies to p-AKT (serine-473) and p-AKT (threonine-308). The Antoni A regions had the most robust staining. Breast cancer tissue was used as a positive control and demonstrated p-AKT staining with both antibodies. The surrounding fibrous stroma within the breast cancer slides was used as a negative control and did not stain for p-AKT.

Western blots demonstrated that both total AKT and p-AKT levels were increased in human VS. Western blots for Experiments 1 through 3 evaluated total AKT and p-AKT levels as well as levels of several upstream and downstream components of the AKT pathway (Fig. 4). Total AKT protein was present in both VS tissue and normal vestibular nerve. However, the signal intensity for total AKT was consistently greater in all 7 tumor specimens compared with vestibular nerve controls. Band intensities for total AKT was quantified in Experiment 3 and normalized to actin controls for the 2 paired samples of VS/normal nerve. Recall that paired samples are vestibular nerve and VS tumor obtained from the same patient. There was a 3.9-fold increase in total AKT band intensity for tumor compared with normal vestibular nerve in Pair 1 and a 1.6-fold difference in Pair 2 (Fig. 5). This modest increase was consistent with AKT gene expression detected in our microarray data. Activated AKT phosphorylated at the serine-473 site was present in all tumor specimens (Fig. 4A). Band intensity was quantified in the 2 samples of paired vestibular nerve and VS tumor obtained from 2 patients. The p-AKT levels were increased 17.9-fold higher in the VS tumor specimen from Pair 1 and 6.6-fold higher in Pair 2 (Fig. 5). Probing with

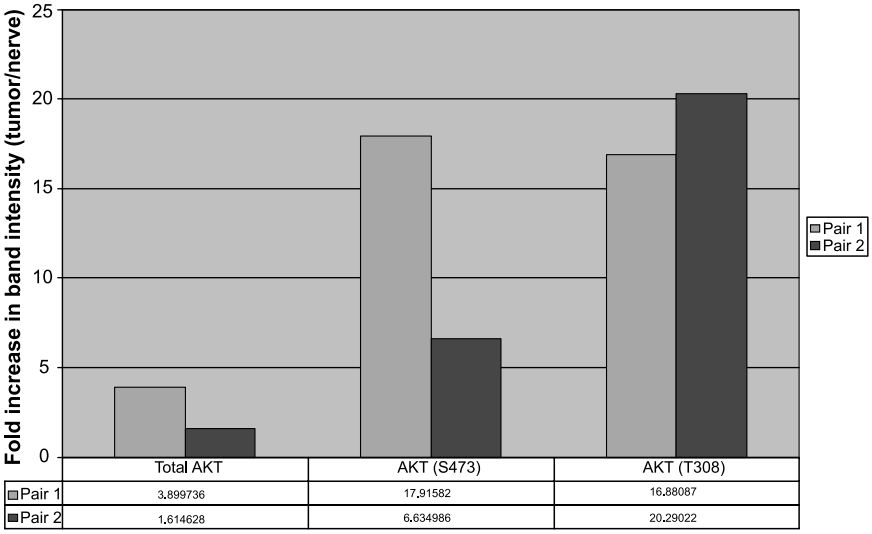

FIG. 5. Band intensity from Western blots using polyclonal antibodies to total AKT and p-AKT at the serine-473 (*S473*) and threonine-308 (*T308*) sites was quantified for total AKT and p-AKT at serine-473 and threonine-308 in the 2 paired VS/normal vestibular nerve samples. This was then normalized to band intensities for actin loading controls. VS tumors had modestly increased amounts of total AKT protein (1.6- to 3.9-fold differences in tumor versus nerve) but had between 6.6- and 20.3-fold increases in phosphorylated (active) AKT.

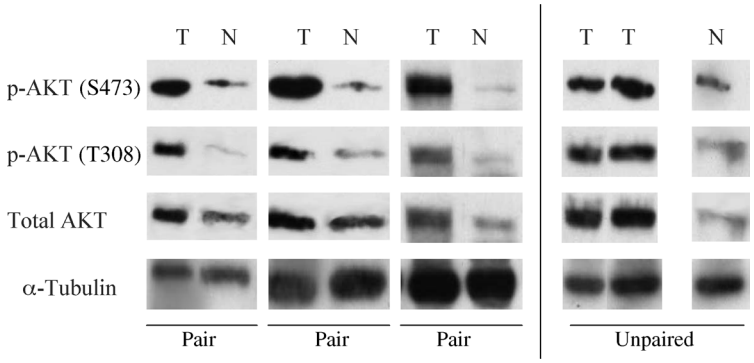

FIG. 6. Western blots were performed for total AKT and activated p-AKT using 3 VS tumor/normal vestibular nerve pairs and an unpaired sample of 2 VS tumors and 1 vestibular nerve. All samples consistently demonstrated upregulation of both total and p-AKT levels in tumors. The difference in band intensity for p-AKT between tumors and normal nerves was more dramatic than differences in band intensity for total AKT. α-Tubulin was used as a loading control.

polyclonal antibody against activated AKT phosphorylated at the threonine-308 site demonstrated robust bands in all VS tumor specimens, whereas no bands were seen for any of the normal nerve specimens (Fig. 4). The p-AKT (threonine-308) band intensity was 16.9-fold higher in the tumor specimen from Pair 1 than in the corresponding normal vestibular nerve. It was 20.3-fold higher in Pair 2 (Fig. 5). In summary, whereas total AKT protein was modestly upregulated in VS tumors, a dramatic increase in posttranslational AKT activation was observed. Three additional tumor/nerve paired specimens as well as 2 tumors and 1 unpaired vestibular nerve specimen were evaluated for total AKT and p-AKT (Fig. 6). Upstream and downstream components of the AKT pathway were not looked at for these specimens. The results confirmed consistent upregulation of both total AKT and p-AKT at both serine and threonine phosphorylation sites.

Western blots demonstrated that activated PI3K and p-PDK were both increased in human VS as compared with normal vestibular nerve controls (Fig. 4). PI3K and PDK1 are upstream components of the pathway that contribute directly to AKT activation. PI3K levels were upregulated in all 7 VS tumor samples. Only 1 of 3 normal nerve specimens demonstrated a weak band for PI3K. This weak band was seen in the control vestibular nerve specimen from paired Sample 1. Phosphorylated (active) PDK1 was upregulated in all 7 VS tumor specimens. Significantly weaker bands were present for PDK1 in 1 unpaired normal nerve control and 1 of the 2 paired normal vestibular nerves.

Western blots demonstrated that the inactive phosphorylated form of PTEN (p-PTEN) was increased in VS as compared with normal vestibular nerves (Fig. 4). PTEN is a key negative regulator of the AKT pathway. In its phosphorylated form, PTEN is no longer able to function as an effective phosphatase. Our Western blots demonstrated that p-PTEN was strongly expressed in all 7 tumor specimens. A significantly weaker band was seen in only 1 of 3 normal nerve controls.

Western blots demonstrated that phosphorylated FOXO, GSK3β, and mTOR (p-FOXO, p-GSK3β, and p-mTOR, respectively) levels were increased in human VS as compared with normal vestibular nerves (Fig. 4). Activated AKT is able to phosphorylate FOXO and GSK3β, thereby inhibiting their activities. As mentioned in the Introduction, mTOR phosphorylation occurs as the end result of p-AKT inhibiting the TSC. Phosphorylated FOXO1 was present in 5 of 7 tumors. Band intensity was variable, however, with weak bands present in 2 of the 5 positive specimens. Phosphorylated FOXO4 was

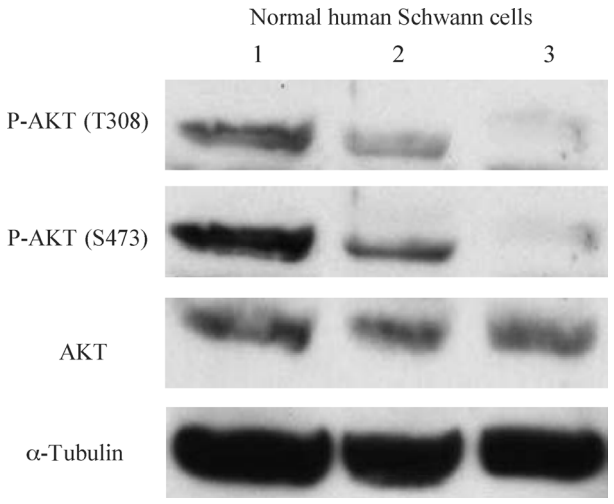

FIG. 7. Neuregulin and forskolin stimulate AKT phosphorylation in normal human SCs. *Lane1*, human SCs grown in advanced DMEM-5% FBS containing 10 nmol/L NRG and 0.5 mmol/L forskolin. *Lane 2*, human SCs grown in advanced DMEM-5% FBS that were deprived on NRG/forskolin for 1 day. *Lane 3*, human SCs grown in advanced DMEM-5% FBS for 2 days and in advanced DMEM containing 1% FBS for 1 day. These cells were deprived of NRG/forskolin for a total of 3 days, and they returned to quiescence in culture. Cell lysates from each SC population were isolated and analyzed by Western blots with antibodies against p-AKT (serine-473), p-AKT (threonine-308) and total AKT. α-Tubulin was measured as a loading control for these samples.

present in all 7 of 7 tumor specimens. The vestibular nerve control from Pair 2 of the paired VS/normal nerve sample demonstrated a weak band for p-FOXO4. Phosphorylated GSK3β was increased in all 7 tumor specimens as compared with control nerves. Bands were present for GSK3β in the normal nerves from the paired samples, but these bands were significantly weaker than the bands from the corresponding tumor specimens. A band for p-GSK3β was undetectable in the nonpaired control nerve. A band for the phosphorylated active form of mTOR was clearly present in 6 of 7 tumors and absent from all control vestibular nerves. The remaining VS tumor specimen had a faint band for mTOR.

Western blots demonstrate that exposure to the growth factors NRG and forskolin enhance activation of AKT in cultured human SCs. Several previous reports have suggested that exposure to growth factors enhances SC proliferation/survival in culture (see Discussion). We sought to identify whether exposure to NRG and forskolin affect the AKT pathway. SCs were initially exposed to these growth factors to establish viable primary cultures. These cells were then deprived of NRG/forskolin for either 1 or 3 days. Our findings demonstrate that although the lack of NRG/forskolin does not appreciably change total AKT expression in cultured human SCs, the levels of activated p-AKT are clearly decreased over a 3-day period without these growth factors (Fig. 7). Cells in culture become quiescent after 3 to 4 days in the absence of NRG/forskolin.

DISCUSSION

In this study, microarray analysis, immunohistochemistry, and Western blots demonstrated that the PI3K/AKT pathway is activated in human VS. Microarray studies identified a modest increase in AKT gene expression (isoforms AKT1 and AKT3) within human VS specimens, and this finding was confirmed by Western blots for total AKT protein. However, Western blots probed for active p-AKT protein revealed that p-AKT was dramatically increased in the VS specimens. Band intensities were quantified for 2 paired tumor/vestibular nerve specimens. Total AKT protein was up only 1.6- to 3.9-fold in tumor versus nerve, whereas p-AKT expression was increased up to 20.3-fold. Therefore, posttranslational AKT phosphorylation may be the dominant mechanism for AKT activation in human VS. Immunohistochemical analysis in 14 tumors using antibodies to both AKT phosphorylation sites (serine-473 and threonine-308) found that AKT was phosphorylated (activated) at both locations. Furthermore, upstream and downstream components of the pathway were evaluated in tumors and vestibular nerve controls using Western blots to demonstrate that the pathway was in fact active. In summary, this study found evidence for AKT activation in a total of 30 VS tumors.

Activation of antiapoptotic growth-promoting pathways such as the PI3K/AKT system may be a key mechanism whereby neoplasms gain a survival advantage. It is well known that SCs do not grow well in culture unless stimulated by growth factors such as NRG and insulin-like growth factor 1. Several previous reports have suggested that the PI3K/AKT pathway may mediate the observed increased proliferation and survival seen in cultures containing growth factors. Li et al. (27) demonstrated that NRG activates ErbB2/ErbB3, which stimulates PI3K and activates AKT in SC culture. Cheng et al. (28) found that insulin-like growth factor 1 promotes SC survival and motility in culture by activating AKT. Monje et al. (29) demonstrated that cyclic adenosine monophosphate synergistically enhances the NRG-induced intracellular signaling in cultured SCs by prolonging the activated state of extracellular signal-regulated kinase and intensifying AKT activation. Our Western blot experiments looking at AKT expression in cultured human SCs exposed to growth factors have confirmed that exposure to NRG and forskolin stimulates increased levels of activated p-AKT. This, along with our finding that human VS contain predominantly activated AKT, suggests that AKT activation may be a necessary step for VS proliferation and survival in vivo.

Several downstream targets of AKT were evaluated to ensure that the pathway was active in the VS tumors. Our Western blots demonstrated increased levels of phosphorylated FOXO, GSK3β, and mTOR in tumors versus control vestibular nerves. Phosphorylation of FOXO and GSK3β downregulates proapoptotic genes, whereas mTOR activity in VS may stimulate its protein translation machinery. The mTOR pathway can feed back to upregulate AKT phosphorylation in some cell types. It has been demonstrated that the mTOR complex mTORC2, consisting of mTOR, rictor, Sin1, and mLST8, can regulate Akt activity and actin polymerization (30–33). Inhibitors to mTOR are under investigation as treatment for various tumors, but to date, it is unclear whether targeting mTOR will be effective for treating VS.

One other important finding from our study was that PTEN, which normally antagonizes PI3K activity, was consistently in its inactive (phosphorylated) state in our tumor specimens. Studies are underway to define whether this is the result of AKT downstream effects on GSK3β or the result of increased CK2 activity.

Therapeutic options for patients with VS currently include radiation and surgical resection. Our data suggest that AKT may be potential target for chemotherapeutic interventions. The AKT pathway has a variety of known chemical inhibitors. Imatinib or Gleevec (Novartis Pharmaceuticals Corp., East Hanover, NJ, USA), a tyrosine kinase inhibitor upstream from PI3K, has been used clinically to treat gastrointestinal stromal tumors and chronic myeloid leukemia. Wortmannin, a fungal metabolite derived from *Penicillium fumiculosum*, can inactivate PI3K by covalent modification of Lys-802 (34) and has demonstrated efficacy at the in vitro level.

LY209002, another potent PI3K inhibitor, promotes G1 cell cycle arrest and apoptosis in cancers such as Hodgkin lymphoma (35). The AKT/protein kinase B signaling inhibitor 2 specifically inhibits AKT kinase activity without targeting upstream components such as PI3K or PDK1 (36). OSU-03012, a novel PDK1 inhibitor derived from celecoxib, is currently under investigation using various in vitro and in vivo models of malignancy (37). Rapamycin, CCI-779 (temsirolimus), RAD001 (everolimus), and AP23573 are examples of mTOR inhibitors undergoing clinical trials for endometrial cancer, renal cell carcinoma, breast cancer, lymphoma, glioblastoma, gastrointestinal stromal tumors, and sarcomas (38,39).

Whereas inhibition of AKT does promote apoptosis, AKT signaling is also important for normal cellular functions. Therefore, concerns have been raised regarding the detrimental effects of AKT inhibition on normal cells. Fortunately, studies suggest that neoplastic cells may be more dependent on AKT activation for survival than normal cells. Tumor cells appear to be more sensitive to chemotherapeutic AKT blockade (13,36,40). However, long-term effects of AKT inhibition on normal human physiology are unclear and require further study.

We would like to end our discussion by introducing OSU-03012, an exciting preclinical chemotherapeutic agent developed at our institution for selectively targeting the AKT pathway. This drug was derived from the COX-2 inhibitor celecoxib (Celebrex) but does not have any COX-2 activity (41). It is a highly selective PDK1 inhibitor. In vitro, this drug has demonstrated efficacy in killing pancreatic cancer cells (42), lymphoma (43), glioblastoma (44), and breast cancer (45). Early in vivo studies using murine xenograft models for prostate cancer have demonstrated suppression of tumor growth, whereas dosing regimens up to 1 month have found no overt signs of toxicity in mice (personal communication, C. S. Chen). Our group has recently presented early in vitro data suggesting that OSU-0312 suppresses VS proliferation, decreases AKT phosphorylation in primary human VS cultures, and induces apoptosis with IC50 doses in the low micromolar concentrations (Abstract P36, pp143-144 presented at the 2007 Children's Tumor Foundation Neurofibromatosis Conference). We are currently evaluating this drug's efficacy using a variety of in vitro human and mouse cell culture systems. Our group has also recently described a quantifiable xenograft model for VS (46). In upcoming months, we plan to use this animal model for testing OSU-03012 and other novel AKT pathway inhibitors in vivo.

REFERENCES

1. Welling DB. Clinical manifestations of mutations in the neurofibromatosis type 2 gene in vestibular schwannomas (acoustic neuromas). *Laryngoscope* 1998;108:178–89.
2. Rouleau GA, Merel P, Lutchman M, et al. Alteration in a new gene encoding a putative membrane organizing protein causes neurofibromatosis type 2. *Nature* 1993;363:515–21.
3. Trofatter JA, MacCollin MM, Rutter JL, et al. A novel moesin-, ezrin-, radixin-like gene is a candidate for the neurofibromatosis 2 tumor suppressor [published erratum appears in *Cell* 1993; 75:826]. *Cell* 1993;72:791–800.
4. Gutmann DH. Minsights into neurofibromatosis 2. *Neurobiol Dis* 1997;3:247–61.
5. Sherman L, Xu HM, Geist RT, et al. Interdomain binding mediates tumor growth suppression by the NF2 gene product. *Oncogene* 1996;15:2505–09.
6. Huynh DP, Pulst SM. Neurofibromatosis 2 antisense oligodeoxynucleotides induce reversible inhibition of schwannomin synthesis and cell adhesion in STS26T and T98G cells. *Oncogene* 1996; 13:73–84.
7. Gonzalez-Agosti C, Wiederhold T, Herndon ME, et al. Interdomain interaction of merlin isoforms and its influence on intermolecular binding to NHE-RF. *J Biol Chem* 1999;274:34438–42.
8. Welling DB, Lasak JM, Akhmametyeva E, et al. cDNA microarray analysis of vestibular schwannomas. *Otol Neurotol* 2002;23: 736–48.
9. Yoshimoto Y. Systematic review of the natural history of vestibular schwannoma. *J Neurosurg* 2005;103:59–63.
10. Toker A, Newton AC. Cellular signaling: pivoting around PDK-1. *Cell* 2000;103:185–8.
11. Altomare DA, Testa JR. Perturbations of the AKT signaling pathway in human cancer. *Oncogene* 2005;24:7455–64.
12. Toker A, Yoeli-Lerner M. Akt signaling and cancer: surviving but not moving on. *Cancer Res* 2006;66:3963–6.
13. Mora A, Komander D, van Aalten DM, et al. PDK1, the master regulator of AGC kinase signal transduction. *Semin Cell Dev Biol* 2004;15:161–70.
14. Dong LQ, Liu F. PDK2: the missing piece in the receptor tyrosine kinase signaling pathway puzzle. *Am J Physiol Endocrinol Metab* 2005;289:E187–96.
15. Gericke A, Munson M, Ross AH. Regulation of the PTEN phosphatase. *Gene* 2006;374:1–9.
16. Al-Khouri AM, Ma Y, Togo SH, et al. Cooperative phosphorylation of the tumor suppressor phosphatase (PTEN) by casein kinases and glycogen synthase kinase 3? *J Biol Chem* 2005;280: 35195–202.
17. Bellacosa A, Kumar CC, Di Cristofano A, et al. Activation of AKT kinases in cancer: implications for therapeutic targeting. *Adv Cancer Res* 2005;94:29–86.
18. Kaestner KH, Knochel W, Martinez DE. Unified nomenclature for the winged helix/forkhead transcription factors. *Genes Dev* 2000; 14:142–6.
19. Greer EL, Brunet A. FOXO transcription factors at the interface between longevity and tumor suppression. *Oncogene* 2005;24: 7410–25.
20. Grimes CA, Jope RS. The multifaceted roles of glycogen synthase kinase 3β in cellular signaling. *Prog Neurobiol* 2001;65:391–426.
21. Mendez R, Myers MG, Jr, White MF, et al. Stimulation of protein synthesis, eukaryotic translation initiation factor 4E phosphorylation, and PHAS-I phosphorylation by insulin requires insulin receptor substrate 1 and phosphatidylinositol 3-kinase. *Mol Cell Biol* 1996;16:2857–64.
22. Cardone MH, Roy N, Stennicke HR, et al. Regulation of cell death protease caspase-9 by phosphorylation. *Science* 1998;282: 1318–21.
23. Datta SR, Dudek H, Tao X, et al. AKT phosphorylation of BAD couples survival signals to the cell-intrinsic death machinery. *Cell* 1997;91:231–41.
24. Rong R, Xiaoling T, Gutmann DH, et al. Neurofibromatosis 2 (NF2) tumor suppressor merlin inhibits phosphatidylinositol 3-kinase through binding to PIKE-L. *PNAS* 2004;101:18200–5.
25. Rong R, Ahn JY, Huang H, et al. PI3 kinase enhancer-Homer complex couples mGluRI to PI3 kinase, preventing neuronal apoptosis. *Nat Neurosci* 2003;6:1153–61.
26. Ahn JY, Ye K. PIKE GTPase signaling and function. *Int J Biol Sci* 2005;1:44–50. Epub 2005 Apr 1.
27. Li L, Tennekoon GI, Birnbaum M, et al. Neuregulin signaling through a PI3K/Akt/Bad pathway in Schwann cell survival. *Mol Cell Neurosci* 2001;17:761–7.

28. Cheng HL, Steinway M, Delaney CL, et al. IGF-1 promotes Schwann cell motility and survival via activation of AKT. *Mol Cell Endocrinol* 2000;170:211–5.
29. Monje PV, Bunge MB, Wood PM. Cyclic AMP synergistically enhances neuregulin-dependnet ERK and Akt activation and cell cycle progression in Schwann cells. *Glia* 2006;53:649–59.
30. Sarbassov DD, Guertin DA, Ali SM, et al. Phosphorylation and regulation of Akt/PKB by the rictor-mTOR complex. *Science* 2005;307:1098–101.
31. Jacinto E, Facchinetti V, Liu D, et al. SIN1/MIP1 maintains rictor-mTOR complex integrity and regulates Akt phosphorylation and substrate specificity. *Cell* 2006;127:125–37.
32. Jacinto E, Loewith R, Schmidt A, et al. Mammalian TOR complex 2 controls the actin cytoskeleton and is rapamycin insensitive. *Nat Cell Biol* 2004;6:1122–8.
33. Sarbassov DD, Ali SM, Kim DH. Rictor, a novel binding partner of mTOR, defines a rapamycin-insensitive and raptor-independent pathway that regulates the cytoskeleton. *Curr Biol* 2004;14: 1296–1302.
34. Wymann MP, Bulgarelli-Leva G, Zvelebil MJ, et al. Wortmannin inactivates phosphoinositide 3-kinase by covalent modification of Lys-802, a residue involved in the phosphate transfer reaction. *Mol Cell Biol* 1996;16:1722–33.
35. Georgakis GV, Yang L, Rassidakis GZ, et al. Inhibition of the phosphatidylinositol-3 kinase/AKT promotes G1 cell cycle arrest and apoptosis in Hodgkin lymphoma. *Br J Haematol* 2005;132: 503–11.
36. Yang L, Dan HC, Sun M, et al. Akt/protein kinase B signaling inhibitor-2, a selective small molecule inhibitor of Akt signaling with antitumor activity in cancer cells overexpressing Akt. *Cancer Res* 2004;64:4394–9.
37. Johnson AJ, Smith LL, Jiuxiang Zhu, et al. A novel celecoxib derivative, OSU03012, induces cytotoxicity in primary CLL cells and transformed B-cell lymphoma via a caspase and Bcl-2 independent mechanism. *Blood* 2005;105:2504–9.
38. Yu K, Toral-Barza L, Discafani C, et al. mTOR, a novel target in breast cancer: the effect of CCI-779, an mTOR inhibitor, in preclinical models of breast cancer. *Endocr Relat Cancer* 2001;8: 249–58.
39. Faivre S, Kroemer G, Raymond E. Current development of mTOR inhibitors as anticancer agents. *Nature Rev Drug Discov* 2006;5: 671–88.
40. Boulay A, Zumstein-Mecker S, Stephan C, et al. Antitumor efficacy of intermittent treatment schedules with the rapamycin derivative RAD001 correlates with prolonged inactivation of ribosomal protein S6 kinase 1 in peripheral blood mononuclear cells. *Cancer Res* 2004;64:252–61.
41. Zhu J, Huang J, Tseng P, et al. From the cyclooxygenase-2 inhibitor celecoxib to a novel class of 3-phosphoinositide-dependent protein kinase-1 inhibitors. *Cancer Res* 2004;64: 4309–18.
42. Li J, Zhu J, Melvin WS, et al. A structurally optimized celecoxib derivative inhibits human pancreatic cancer cell growth. *J Gastrointest Surg* 2006;10:207–14.
43. Johnson AJ, Smith LL, Zhu J. A novel celecoxib derivative, OSU-03012, induces cytotoxicity in primary CLL cells and transformed B-cell lymphoma cell line via a caspase- and Bcl-2-independent mechanism. *Blood* 2005;105:2504–9.
44. McCubrey JA, LaHair MM, Franklin RA. OSU-03012 in the treatment of glioblastoma. *Mol Pharmacol* 2006;70:437–9.
45. Kucab JE, Lee C, Chen CS, et al. Celecoxib analogues disrupt Akt signaling, which is commonly activated in primary breast tumours. *Breast Cancer Res* 2005;7:R796–807.
46. Chang LS, Jacob A, Lorenz M. Growth of benign and malignant schwannoma xenografts in severe combined immunodeficiency mice. *Laryngoscope* 2006;116:2018–26.

Drosophila Merlin Genetically Interacts with the Clathrin Adaptor Protein LAP

Sergei A. Kopyl[1], Elena M. Akhmametyeva[2], Natalia V. Dorogova[1], Leonid V. Omelyanchuk[1], and Long-Sheng Chang[2,*]

[1]*Institute of Cytology and Genetics, Russian Academy of Sciences, 10 Lavrent'ev Ave., 630090, Novosibirsk, Russia,* [2]*Center for Childhood Cancer, Children's Research Institute, and Department of Pediatrics, The Ohio State University College of Medicine, 700 Children's Drive, Columbus, OH 43205, USA*

Running title: Merlin-Lap genetic interaction

Keywords: *Drosophila* Merlin, the *Neurofibromatosis type 2* (*NF2*) gene, receptor-mediated endocytosis, Like AP-180 (Lap), epidermal growth factor receptor (EGFR) signaling,

[*]Corresponding author:

Dr. Long-Sheng Chang, Center for Childhood Cancer, Children's Research Institute, and Department of Pediatrics, The Ohio State University, 700 Children's Drive, Columbus, Ohio 43205; Phone: 614-355-2658; Fax: 614-722-5895; E-mail: lchang@chi.osu.edu

ABSTRACT

Background: Merlin, the *Drosophila* homologue of the protein encoded by the human *Neurofibromatosis 2* (*NF2*) gene, is important for the regulation of cell proliferation and differentiation in the eye and wing. Recent studies show that Merlin and Expanded cooperatively regulate the recycling of membrane receptors, such as the epidermal growth factor receptor (EGFR).

Results: By performing a search for potential genetic interactions between *Merlin* and the genes important for vesicular trafficking, we found that ectopic expression of the clathrin adaptor protein Lap, an adapter protein involved in clathrin-mediated receptor endocytosis, in the wing pouch resulted in the formation of extra vein materials. On the other hand, co-expression of wild-type *Merlin* and *lap* in the wing pouch restored normal venation, while over-expression of a dominant-negative *Merlin* mutant $Mer^{\Delta BB}$ together with *lap* enhanced ectopic vein formation. Using various *Merlin* truncation mutants, we identified the C-terminal portion of Merlin to be important for the *Merlin-lap* genetic interaction. Furthermore, we showed that the Merlin and Lap proteins colocalized at the cellular cortex in the wing imaginal disc cells.

Conclusion: *Merlin* genetically interacts with *lap*. Both the Merlin and Lap proteins colocalize at the cellular cortex within the wing imaginal disc cells. Together with previous findings, our results suggest that Merlin may regulate receptor-mediated endocytosis through interaction with Lap.

INTRODUCTION

Vein patterning in the *Drosophila* wing involves a complex network of signaling events, including the epidermal growth factor receptor (EGFR), Decapentaplegic (Dpp), Hedgehog (Hh), Notch, and Wingless (Wg) signaling pathways (reviewed in Held, 2002; Blair, 2007). Anterior/posterior (A/P) and dorsal/ventral (D/V) compartment borders serve as reference points for vein positioning. The positions of veins 3 and 4 are controlled by the Hh signal, while those of veins 2 and 5 are determined by the Dpp signal, using the A/P compartment border as the reference point. Vein 1 positioning is regulated by a combination of Dpp and Wg signals, and is governed by both compartment borders. In addition, expression of an activated form of *Egfr* or the gain-of-function allele $Egfr^{Elp}$ results in ectopic vein formation. Furthermore, the refinement of proveins is regulated by both positive and negative feedback signals. The Blistered protein is expressed in the intervein regions and negatively regulates vein fate. Blistered itself is negatively regulated by EGFR. Thus, competition between Blistered and EGFR in the wing cells is used to refine the vein pattern.

Drosophila Merlin, a homolog of the gene product encoded by the human *Neurofibromatosis 2* (*NF2*) gene, is important for the regulation of cell proliferation and receptor endocytosis (LaJeunesse et al. 1998; Maitra et al., 2006). The Merlin protein shares a great deal of homology with ezrin, radixin, and moesin (ERM), which belong to the protein 4.1 superfamily of cytoskeletal proteins (Rouleau et al., 1993; Trofatter et al., 1993; Algrain, 1993; Golovnina et al., 2005). *Drosophila* cells lacking Merlin function in the eye and wing over-proliferate relative to their neighbors (LaJeunesse et al., 1998). Mutational analysis reveals that the plasma membrane–associated N-terminal 350 amino acids are required for the regulation of cell proliferation. Removal of the Blue-Box (BB), a sequence containing seven conserved residues in the N-terminal domain of the Merlin protein ($Mer^{\Delta BB}$), results in a dominant-negative form of Merlin that stably associates with the plasma membrane. Ectopic

expression of $Mer^{\Delta BB}$ in the wing causes over-proliferation and disturbs venation. Via a genetic screen for modifiers of the extra vein phenotype, LaJeunesse et al. (2001) found that Merlin antagonized the function of the EGFR signaling pathway and interacted with other proteins involved in vein-intervein fate determination. In addition, Merlin and Expanded, another member of the protein 4.1 family, function together to regulate the steady-state levels of several signaling and adhesion receptors (Maitra et al., 2006). Loss of Merlin and Expanded causes hyperactivation of associated signaling pathways, including the EGFR signaling pathway.

The process of receptor endocytosis begins with the redistribution of membrane proteins into a clathrin-coated pits (Seto et al., 2002). Transmembrane receptors bind to the heterotetrameric adaptor protein complex AP-2 at the plasma membrane (Kirchhausen et al. 1997). The monomeric adaptor protein AP180, whose homolog in *Drosophila* is called Like AP180 (LAP), can also mediate clathrin-binding to the plasma membrane (Zhang et al. 1998, 1999). The receptor–AP-2 complex then binds clathrin, allowing clathrin to polymerize into a basket-shaped lattice that pulls the membrane inside. Once the inward budding of the membrane is complete, an interaction between AP-2 and the GTPase Dynamin (or Shibire in *Drosophila*) facilitates separation of the forming vesicle from the membrane (Wang et al. 1995; Ringstad et al. 1997). Following vesicle formation, the clathrin coat is rapidly disassembled by auxilin and synaptojanin (Newmyer and Schmid 2001). These primary endocytic vesicles fuse with the early endosome. The degradation enzymes are transported from the Golgi to the lysosome via the AP3 protein. The cell surface proteins from the early endosome are then transferred to the late endosome, where they are sorted into special internal vesicles (Griffiths and Gruenberg 1991; Murphy 1991). After the late endosome fuses with the lysosome (Seaman and Luzio 2001), the proteins are degraded.

Presently, the mechanism by which Merlin regulates receptor endocytosis is not

understood. Merlin is located cortically to the plasma membrane. In cultured S2 cells, Merlin is also found in the internalized granules (LaJeunesse et al., 1998). When a green fluorescent protein (GFP)-Mer$^{\Delta BB}$ fusion protein is expressed in S2 cells, the fusion protein is properly targeted to the plasma membrane but is not internalized. This result indicates that BB is essential for Merlin function in endocytosis. It is possible that Merlin may interact with proteins involved in the endocytosis process and regulate signaling receptors like EGFR.

To better understand the role of Merlin in receptor endocytosis, we performed a search for the vesicular trafficking genes that could genetically interact with Merlin. We showed that *Merlin* could suppress the formation of extra vein materials induced by ectopic *lap* expression in the wing pouch. We also found that the C-terminal region of Merlin was required for the *Merlin*:*lap* interaction. In addition, we demonstrated that Merlin colocalized with the Lap protein at the cellular cortex of the wing imaginal disc cells.

MATERIALS AND METHODS

Fly stocks. Strains carrying various *Mer* alleles or constructs were kindly provided by Rick G. Fehon of University of Chicago, Chicago, IL and include (1) *w Mer^{3} 19AFRT/FM6, y B*, (2) *w;P{UAS-Mer$^{\Delta BB}$.myc}*, (3) *w;P{UAS-Mer^{+}.myc}*, (4) *w;P{UAS-Mer$^{1-169}$.myc}*, (5) *w;P{UAS-Mer$^{1-330}$.myc}*, (6) *w;P{UAS-Mer$^{1-375}$.myc}*, (7) *w;P{UAS-Mer$^{1-600}$.myc}*, (8) *w;P{UAS-Mer$^{351-601}$.myc}*, and (9) *w;P{UAS-Mer$^{351-635}$.myc}* (LaJeunesse et al., 1998). Strains carrying the *UAS-sugarless (sgl)* or *UAS-fringe connection (frc)* construct were kindly provided by Norbert Perrimon of Harvard Medical School, Boston, MA (Selva et al., 2001). Strains containing the *UAS-Rab-protein 5 (Rab5)* or *UAS-Rab-protein 7.Q67L (Rab7^{Q67L})* construct were obtained from Marcos A. Gonzalez-Gaitan of Max Planck Institute of Molecular Cell Biology, Dresden, Germany (Entchev et al. 2000). The strain carrying the *UAS-porcupine (porc)* construct was a gift from Tatsuhiko Kadowaki, Nagoya University,

Chikusa, Nagoya, Japan (Tanaka et al. 2002). The strain carrying the *UAS- shibire^{K44A}* (*shi^{K44A}*) construct was provided by Amy Bejsovec, Northwestern University, Evanston, IL, USA. The strain carrying the *UAS-like AP-180 (lap)* construct was obtained from Bing Zhang of The University of Texas at Austin, TX (Zhang et al., 1998). Strains containing an EP-element insertion in the *Damp* [*w^{1118};P{w^{+mC}=EP}Amph^{EP2175}*], *garnet* [*w^{1118} P{w^{+mC}=EP}g^{EP514}*], *α-Adaptin* [*{EP}α-Adaptin^{EP896}*], *Cirl* [*y^{1} w^{67c23};P{w^{+mC} y$^{+mDint2}$=EPgy2}Cirl^{EY12930}*], *GDP dissociation inhibitor* [*y^{1} w^{67c23};P{w^{+mC} y$^{+mDint2}$=EPgy2}Gdi^{EY00735}/CyO*], *AP-47* [*w^{1118};P{w^{+mC}=EP}AP-47^{EP1112}/TB6B, Tb^{1}*], *Ras opposite* [*bw^{1}; Rop^{G27} st^{1}/TM6B, Tb*], *like AP-180* [*y^{1} w^{67c23}; P{w^{+mC} y$^{+mDint2}$=EPgy2}lap^{EY1171}*], and *Scamp* [*w^{1118} P{w^{+mC}=EP}EP1593*] were purchased from Bloomington *Drosophila* Stock Center. The strain *w^{1118} P{w$^{+mW.hs}$=GawB}Bx^{MS1096}*, carrying the *1096-Gal4* driver, was also obtained from Bloomington *Drosophila* Stock Center. This driver has been shown to be active during the larval and pupal stages (Capdevila and Guerrero, 1994, Coelho and Leevers, 2000). Strains, containing an EP element insertion in the *Csp* gene [*P{EP}Csp^{EP3141}*], were obtained from Szeged Stock Center. All *Drosophila* strains were maintained on standard corn meal, yeast, molasses, and agar medium.

Over-expression phenotype assay. The balancer *T(2;3)TSTL, Tb* (Inoue and Glover, 1998) was introduced into the *1096-Gal4* strain and female flies with the genotype of *1096-Gal4;+/T(2;3)TSTL, Tb/+* were crossed with males carrying a UAS construct or an EP-element insertion as described above. The resulting progeny were grown to adults, and they were analyzed for the presence of any abnormalities in the wing due to transgene expression. To generate a strain over-expressing both *Mer^{ΔBB}* and *lap^{EY1171}*, the *1096-Gal4;+/ T(2;3)TSTL, Tb/+* females were crossed with the *y w; +/+; lap^{EY1171}/TM6, Ubx* males. The male progeny with the genotype *1096-Gal4/Y;+/T(2;3)TSTL, Tb/ lap^{EY1171}* were collected and crossed with the *FM7, B;P{UAS-Mer^{ΔBB}.myc}/T(2;3)TSTL, Tb/+* females to generate the

1096-Gal4/ FM7, B;+/ P{UAS-Mer$^{\Delta BB}$.myc};+/ lap^{EY1171} females for the analysis of an enhanced *lap* phenotype in the wing.

Antibody staining. An affinity-purified anti-Merlin antibody, kindly provided by Rick G. Fehon, and an anti-Lap antibody, a gift from Bing Zhang, were used as described previously (McCartney and Fehon, 1996; Zhang et al., 1998). Imaginal wing discs were dissected from the third-instar larvae and fixed in 3.7 % formaldehyde in phosphate-buffered saline (PBS), pH 7.2. After washing in PBS for 10 min three times, fixed tissues were permeated with 1% Triton-X100 in PBS for 30 min, treated with the blocking solution containing 1 % non-fat dry milk in PBS for one hour, and incubated with an anti-Merlin (1:6000 dilution) or anti-Lap (1:200) antibody overnight. Antibody-treated imaginal discs were washed with PBT (0.05% of Tween-20 in PBS) for 10 min three times and then incubated with a secondary antibody [Alexa 488-conjugated anti-guinea pig IgG (1:700 dilution; Molecular Probe) or Rhodamine-conjugated goat anti-Rat IgG (1:200; Abcam)] at 37^{o}C for 1 hour. Stained discs were washed extensively with PBS, mounted in Mowiol with 10% DABCO (Sigma), and examined under the epifluorescence optics of an Axiovert-200 or an Axioskop-2 microscope (Carl Zeiss).

RESULTS

To examine how Merlin might participate in the endocytic process, we performed a search for potential genetic interactions between *Merlin* and the genes important for vesicular trafficking. We first checked FlyBase for the available strains, carrying a UAS construct containing a gene important for vesicular trafficking. Strains with an EP-element insertion near or in the vesicular trafficking genes were also identified. Seven UAS-containing strains for the *sgl*, *frc*, *Rab5*, *porc*, *lap*, *shi^{K44A}* or *Rab7^{DN}* gene or allele, as well as 10 other strains carrying an EP-element insertion for the *Csp^{EP3141}*, *Amph^{EP2175}*, *g^{EP514}*, *α- Adaptin^{EP896}*, *Rop^{G27}*, *Scamp^{EP1593}*, *Cirl^{EY12930}*, *Gdi^{EY00735}*, *AP-47^{EP1112}*, or *lap^{EY1171}* allele were obtained. By

crossing these strains with flies carrying the wing pouch-specific Gal4 driver 1096, we examined the effect of ectopic expression of these vesicular trafficking genes on wing morphology. Among the strains tested, only ectopic expression of *porc*, shi^{K44A}, or lap^{EY1171} gave rise to an apparent abnormal wing morphology in heterozygous *1096-Gal4* females (Figure 1). Ectopic expression of *porc* in the wing pouch resulted in flies having small wings but without venation and the medial triple row (MTR) of bristles. Ectopic expression of the dominant-negative allele of *shi* yielded flies with wings of a reduced size. In addition, the MTR were found only in some areas of the D/V boundary of the wing, and venation was absent in the wings. Intriguingly, over-expression of lap^{EY1171} resulted in flies with normal wing structure but with ectopic vein materials at the distal end of vein V and the posterior crossvein (Figures 1 and 2). Similar results were obtained when *lap* was over-expressed using the strain carrying a *UAS-lap* transgene, instead of the EP element insertion (data not shown). It should be mentioned that female flies with homozygous *1096-Gal4* displayed disruption of the posterior crossvein (Milan et al., 1998), similar to those observed in the wings of the $Mer^{\Delta BB}$–over-expressing strain (LeJeunesse et al., 1998). However, heterozygous *1096-Gal4* females did not show any posterior crossvein disruption. The use of *1096-Gal4* heterozygotes represents a sensitive genetic method to examine the effect of ectopic transgene expression.

Recent data link Merlin function to EGFR signaling, which has been shown to be important for vein formation (LeJeunesse et al., 2001; Maitra et al., 2006). Since over-expression of *lap* resulted in the formation of ectopic vein materials, we investigated the possibility of a genetic interaction between *Merlin* and *lap*. Consistent with previous findings (LeJeunesse et al., 1998, 2001), we observed that over-expression of Mer^{+} did not alter wing structure, while ectopic expression of the BB mutant of *Merlin*, $Mer^{\Delta BB}$, led to formation of a slightly larger wing and disruption of the posterior crossvein (Figure 2). Remarkably, over-

expression of both *lap* and $Mer^{\Delta BB}$ resulted in excessive ectopic vein materials, which were even more extensive than those of *lap* alone and could be seen in many parts of the wing blade. In contrast, simultaneous over-expression of both Mer^{+} and *lap* in the wing pouch yielded wings with normal or almost normal vein patterning (Figure 2). These results suggest a genetic interaction between *Merlin* and *lap*.

To examine the protein domain of Merlin required for a genetic interaction with *lap*, we simultaneously over-expressed *lap* together with various truncated *Merlin* constructs in the wing pouch using the 1096 driver as described above. When Mer^{1-169} was over-expressed together with *lap*, ectopic vein materials were still observed in the wing (Figure 3). Similarly, when constructs containing other N-terminal regions of *Merlin*, Mer^{1-330} and Mer^{1-375}, were over-expressed together with *lap*, ectopic vein materials were also found in the wing. In addition, when the construct containing the first 600 amino acids of Merlin, Mer^{1-600}, was co-expressed with *lap*, some ectopic vein materials were still present in the wing. In contrast, when the construct containing the C-terminal region of *Merlin*, $Mer^{351-635}$, was over-expressed with *lap*, wings with a normal vein pattern, similar to those found in the case of simultaneous over-expression of Mer^{+} and *lap*, were observed (Figure 3). It should be mentioned that over-expression of $Mer^{351-635}$ alone in the wing pouch did not alter wing morphology or venation (data not shown). These results indicate that the C-terminal region of *Merlin* is important for the genetic interaction with *lap*.

Next, we investigated the possibility of colocalization of the Merlin and Lap proteins in the cells of the wing imaginal disc. Figure 4 shows that the Merlin protein had a cortical localization within the cells, analogous to that reported previously (LaJeunesse et al., 1998). Interestingly, the Lap protein displayed a similar cortical localization pattern, and both Merlin and Lap colocalized at the cellular cortex in the wing imaginal disc cells. However, Lap staining appeared more granular. Together, these results suggest that Merlin may directly

interact with protein(s) involved in vesicular trafficking.

DISCUSSION

Clathrin-mediated endocytosis regulates the levels of growth factor receptors, neurotransmitter receptors, and neurotransmitter transporters on the cell surface. In addition, it is involved in synaptic vesicle recycling to regulate previously exocytosed synaptic vesicle membrane proteins and lipids (Kirchhausen, 2000; Slepnev and De Camilli. 2000; Lafer, 2002). During this process, adapter proteins, such as AP-1, AP-2, AP180, and auxilin, promote the assembly of the clathrin cage. AP180 was originally identified as a clathrin-binding protein in rodent brains and is a monomeric protein expressed in neurons (Zhou et al., 1992; Schroder et al., 1995), although its homologs exist and have been found outside the nervous system (Lafer, 2002). The *Drosophila* AP180 homolog, Lap for Like AP180, localizes to endocytic synaptic vesicles and regulate their size (Zhang et al. 1998); however, it is not known whether the *Drosophila* Lap protein is expressed in non-neuronal tissues, and if so, what its function is in this context. By immunostaining analysis, we detected the Lap protein in the wing imaginal disc cells. Interestingly, the Lap protein colocalized with Merlin at the cellular cortex. If Lap is involved in receptor endocytosis, like its mammalian counterpart AP180, these results would imply that Merlin may be linked to the endocytic compartment through Lap. This hypothesis is supported by our over-expression analysis, which demonstrated a genetic interaction between *Merlin* and *lap*.

Over-expression of *lap* in the wing pouch resulted in the formation of ectopic vein materials at the distal end of vein V and the posterior crossvein, suggesting that Lap may be involved in endocytosis of certain growth factor receptors that regulate vein formation. Previously, LeJeunesse et al. (2001) showed that over-expression of a dominant-negative $Mer^{\Delta BB}$ in the wing using an *engrailed-Gal4* driver led to defects in venation. This

phenotype could be modified by mutations in the genes regulated by EGFR signaling. Maitra et al. (2006) further demonstrate that Merlin and Expanded, another protein 4.1-family member, functions to regulate the steady-state levels of signaling receptors, including EGFR, and that loss of these proteins causes hyperactivation of associated signaling pathways. Studies in mammalian cells also shows that Merlin negatively regulates EGFR signaling by restraining the EGFR into a membrane compartment from which it could neither signal nor be internalized (Curto et al., 2007). It is possible that Merlin may counteract Lap function in the regulation of EGFR signaling in the *Drosophila* wing. Over-expression of a wild-type Merlin restored the normal vein pattern, despite of the presence of an excessive amount of the Lap protein. Conversely, inactivation of Merlin function by $Mer^{\Delta BB}$ in conjunction with Lap over-expression further amplified ectopic vein formation.

The "Blue Box" was originally identified as the seven functionally important amino acid residues (^{170}YQMTPEM^{177}) in the N-terminal domain of *Drosophila* merlin. Deletion of these residues results in a dominant-negative phenotype (LeJeunesse et al., 1998). The functional significance of these seven amino acids is further supported by their conservation in the Merlin sequences of vertebrates, fruit flies, and honeybees. However, these residues are not conserved in the ERM proteins (Golovnina et al., 2005). The phenotype from over-expression of $Mer^{\Delta BB}$ in the wing pouch using the 1096 driver is consistent with the dominant-negative effect on Merlin function. In contrast to $Mer^{\Delta BB}$, the C-terminal fragment of Merlin, $Mer^{351-635}$, appears to act in a dominant-active manner, similar to Mer^{+}, in suppressing the phenotype of Lap over-expression. These results suggest that the domain required for the genetic interaction with *lap* resides in the C-terminal half of the Merlin protein. Consistent with this notion, deletion of the C-terminal region of Merlin, e.g., Mer^{1-169}, Mer^{1-300}, Mer^{1-375}, and Mer^{1-600}, abolishes its ability to genetically interact with *lap*. The fact that $Mer^{351-635}$, but not Mer^{1-600}, could suppress the phenotype of Lap over-expression

further emphasizes the importance of the last 35 amino acids of the *Drosophila* Merlin protein for such a genetic interaction. Intriguingly, conservation of these C-terminal residues has been found between the fly and human Merlin proteins (Golovnina et al., 2006). Also, the isoform II species of the human Merlin protein differs from the alternatively spliced isoform I by the last 16 amino acids and can not suppress cell growth (Gutmann et al., 1999). We are presently conducting experiments to explore the possibility of a protein-protein interaction between the C-terminal region of Merlin and Lap.

As mentioned above, AP-1, AP-2, and Lap can promote clathrin assembly; however, unlike Lap, ectopic expression of α-adaptin, a subunit of the AP-2 complex, or AP-47, a subunit of the AP-1 complex in the wing pouch, did not affect wing structure and venation. Although AP-1 is involved primarily in protein sorting and transport from the *trans* Golgi network to the endosome, the AP-2 complex has been shown to play an important role in receptor-mediated endocytosis. It is possible that the endocytosis of signaling receptors important for vein formation in the wing is not affected by the excessive amount of α-adaptin, while Lap may have additional functions in receptor recycling. However, this hypothesis remains to be tested.

The *porc* gene encodes the Porcupine protein, which has acyltransferase activity. The Porcupine protein can bind to the Wg protein and stimulates its posttranslational N-glycosylation in the endoplasmic reticulum, thus playing an important role in regulating the Wg signaling pathway (Zhai et al., 2004, Nusse, R. 2003). Stout bristles grow from the cells of the D/V compartment border, which normally expresses the Wg morphogen (Held, 2003). In addition, both the mechanosensory and chemosensory bristles are developed as the result of Wg induction (Johnston and Edgar, 1998). Therefore, the absence of both stout and sensory bristles due to ectopic expression of *porc* in the wing pouch can be attributed to altered production of active Wg protein. Consistently, we observed the absence of the Wg

stripe at the D/V border of the wing imaginal disc when *porc* was over-expressed in the wing pouch (data not shown).

The *shi* gene codes for the protein Shibire or Dynamin, which possesses GTPase activity. The adapter protein AP-2 binds to Shibire, allowing fission of vesicles from the plasma membrane. Shibire also interacts with actin filaments and microtubules and is important for the cytoskeleton-mediated processes. Because of the role of Shibire in receptor-mediated endocytosis, it is not surprising that over-expression of the dominant-negative shi^{K44A} in the wing pouch resulted in the abnormal wing structure. However, the presence of MTR in some areas of the D/V boundary of the wing when shi^{K44A} was ectopically expressed in the wing pouch suggests that the Wg signaling still functions at the D/V border but does not work to its full extent. On the contrary, the lack of venation due to shi^{K44A} over-expression implies that the signaling pathways necessary for vein formation, such as the EGFR or Notch signaling pathways, may be affected. Further examination of the proteins involved in vesicular trafficking and its potential interaction with Merlin should allow us to better understand the molecular mechanism underlying Merlin function in receptor-mediated endocytosis.

CONCLUSION

Merlin genetically interacts with *lap*, a gene encoding an adapter protein involved in clathrin-mediated receptor endocytosis. The C-terminal domain of Merlin is important for the *Merlin-lap* genetic interaction. Furthermore, both the Merlin and Lap proteins colocalize at the cellular cortex within the wing imaginal disc cells. These results suggest that Merlin may regulate receptor-mediated endocytosis through interaction with Lap.

LIST OF ABBREVIATION USED

EGFR, epidermal growth factor receptor

Dpp, the Decapentaplegic protein

Hh, the Hedgehog protein

Wg, the Wingless protein

A/P, anterior/posterior

D/V, dorsal/ventral

NF2, the *Neurofibromatosis 2* gene

ERM, ezrin, radixin, and moesin

BB, Blue Box

Merlin, the *Merlin* gene

Lap, the Like AP180 protein

lap, the *like AP180* gene

GFP, green fluorescent protein

shi, the *shibire* gene

porc, the *porcupine* gene

MTR, medial triple row

PBS, phosphate-buffered saline

AUTHORS' CONTRIBUTION

SAK performed genetic crosses, EMA participated in data analysis, and NVD carried out immunostaining, LVO helped with the phenotypic examination, and LSC was the principal investigator of the project and wrote the manuscript. All authors read and approved the final manuscript.

ACKNOWLEDGEMENTS

We sincerely thank Amy Bejsovec, Rick G. Fehon, Marcos A. Gonzalez-Gaitan,

Tatsuhiko Kadowaki, Norbert Perrimon, and Bing Zhang for various fly strains and antibodies. Special appreciation goes to D. Bradley Welling and Sarah S. Burns for critical reading of the manuscript. This study was supported by grants from the US Department of Defense Neurofibromatosis Research Program and the Russian Fund of Fundamental Investigation.

REFERENCES

Algrain, M., Arpin, M., Louvard, D. 1993. Wizardry at the cell cortex, Current Biol. 3:451-454.

Blair, S.S. 2007. Wing vein patterning in Drosophila and the analysis of intercellular signaling. Ann. Rev. Cell Dev. Biol. 23:293-319.

Capdevila, J., Guerrero, I. 1994, Targeted expression of the signaling molecule decapentaplegic induces pattern duplications and growth alterations in Drosophila wings. EMBO J. 13: 4459-4468.

Coelho, C.M., Leevers, S.J. 2000. Do growth and cell division rates determine cell size in multicellular organisms? J. Cell Sci. 113:2927-2934.

Curto, M., Cole, B.K., Lallemand, D., Liu, C.H., McClatchey, A.I. 2007. Contact-dependent inhibition of EGFR signaling by Nf2/Merlin. J. Cell Biol. 177:893-903.

Entchev, E.V., Schwabedissen, A., Gonzalez-Gaitan, M. 2000 Gradient formation of the TGF-beta homolog Dpp. Cell 103:981-991.

Golovnina, K., A. Blinov, E.M. Akhmametyeva, L.V. Omelyanchuk, and L.-S. Chang. 2005. Evolution and Origin of Merlin, the Product of the *Neurofibromatosis Type 2* (*NF2*) Tumor-Suppressor Gene. BMC Evol. Biol. 5:69-86.

Griffiths, G. and Gruenberg, J. 1991. The arguments for preexisting early and late endosomes. Trends Cell Biol. 1:5.

Gutmann, D.H., Sherman, L., Seftor, L., Haipek, C., Hoang Lu, K., and Hendrix, M. 1999. Increased expression of the NF2 tumor suppressor gene product, merlin, impairs cell motility, adhesionand spreading. Hum. Mol. Genet. 8:267-275.

Held, L.I. 2002. Imaginal discs. The genetic and cellular logic of pattern formation. Cambridge University Press, Cambridge, UK.

Inoue, Y.H., Glover, D.M. 1998. Involvement of the rolled/MAP kinase gene in Drosophila mitosis: interaction between genes of the MAP kinase cascade and abnormal spindle. Mol. Gen. Genet. 258:334-341.

Johnston, L.A., Edgar, B.A. 1998. Wingless and Notch regulate cell-cycle arrest in the developing Drosophila wing. Nature 394:82-84.

Kirchhausen, T. 2000. Clathrin. Annu. Rev. Biochem. 69:699-727.

Kirchhausen, T., Bonifacino, J.S., and Riezman, H. 1997. Linking cargo to vesicle formation: Receptor tail interactions with coat proteins. Curr. Opin. Cell. Biol. 9:488-495.

Lafer, E.M. 2002. Clathrin-protein interactions. Traffic 3 :513-520.

LaJeunesse, D.R., McCartney, B.M., Fehon, R.G. 1998. Structural analysis of Drosophila merlin reveals functional domains important for growth control and subcellular localization. J. Cell Biol. 141:1589-1599.

LaJeunesse, D.R., McCartney B.M., Fehon, R.G. 2001. A Systematic Screen for Dominant Second-Site Modifiers of Merlin/NF2 Phenotypes Reveals an Interaction With blistered/DSRF and scribbler. Genetics 158:667-679.

Maitra, S., Kulikauskas, R.M., Gavilan, H., Fehon, R.G. 2006. The Tumor Suppressors Merlin and Expanded Function Cooperatively to Modulate Receptor Endocytosis and Signaling. Current Biology 16:702-709.

McCartney, B.M., Fehon, R.G. 1996. Distinct cellular and subcellular patterns of expression imply distinct functions for the Drosophila homologues of moesin and the

neurofibromatosis 2 tumor suppressor, merlin. J. Cell Biol. 133:843-852.

Murphy, R.F. 1991. Maturation models for endosome and lysosome biogenesis. Trends Cell Biol. 1:77-82.

Newmyer, S.L. and Schmid, S.L. 2001. Dominant-interfering Hsc70 mutants disrupt multiple stages of the clathrin-coated vesicle cycle in vivo. J. Cell Biol. 152:607-620.

Nusse, R. 2003. Wnts and Hedgehogs: lipid-modified proteins and similarities in signaling mechanisms at the cell surface. Development 130:5297-5305.

Ringstad, N., Nemoto, Y., and De Camilli, P. 1997. The SH3p4/Sh3p8/SH3p13 protein family: Binding partners for Synaptojanin and Dynamin via a Grb2-like Src homology 3 domain. Proc. Natl. Acad. Sci. USA 94:8569-8574.

Rouleau, G.A., Merel, P., Luchtman, M., Sanson, M., et al. 1993. Alteration in a new gene encoding a putative membrane-organizing protein causes neurofibromatosis type 2. Nature 363:515-521.

Schroder, S., Morris, S.A., Knorr, R., Plessmann, U., Weber, K., Vinh, N.G., Ungewickell, E. 1995. Primary structure of the neuronal clathrin-associated protein auxilin and its expression in bacteria. Eur. J. Biochem. 228:297-304.

Seaman, M.N.J., Luzio, J.P. 2001. Lysosomes and other late compartments of the endocytic pathway. Oxford University Press, New York, NY.

Selva, E.M., Hong, K., Baeg, G.H., Beverley, S.M., Turco, S.J., Perrimon, N., Hacker, U. 2001. Dual role of the fringe connection gene in both heparan sulphate and fringe-dependent signalling events. Nature Cell Biol. 3:809-815.

Seto, E.S., Bellen, H.J., and Lloyd, T.E. 2002 When cell biology meets development: endocytic regulation of signaling pathways. Genes Dev. 16:1314-1336.

Slepnev, V.I., De Camilli, P. 2000. Accessory factors in clathrin-dependent synaptic vesicle endocytosis. Nature Rev. Neurosci. 1:161-172.

Tanaka, K., Kitagawa, Y., Kadowaki, T. 2002. Drosophila segment polarity gene product porcupine stimulates the posttranslational N-glycosylation of wingless in the endoplasmic reticulum. J. Biol. Chem. 277:12816-12823.

Trofatter, J.A., MacCollin, M.M., Rutter, J.L., Murrell, J.R., et al. 1993. A novel Moesin-, Exrin-, Radixin-like gene is a candidate for the neurofibromatosis 2 tumor-suppressor. Cell 72:791-800.

Wang, L.H., Sudhof, T.C., Anderson, R.G. 1995. The appendage domain of alpha-adaptin is a high affinity binding site for Dynamin. J. Biol. Chem. 270:10079-10083.

Zhang, B., Koh, Y.H., Beckstead, R.B., Budnik, V., Ganetzky, B., and Bellen, H.J. 1998. Synaptic vesicle size and number are regulated by a clathrin adaptor protein required for endocytosis. Neuron 21:1465-1475.

Zhang, B., Ganetzky, B., Bellen, H.J., Murthy, V.N. 1999 Tailoring uniform coats for synaptic vesicles during endocytosis. Neuron 23:419-422.

Zhai, L., Chaturvedi, D., Cumberledge, S. 2004. Drosophila wnt-1 undergoes a hydrophobic modification and is targeted to lipid rafts, a process that requires porcupine. J. Biol. Chem. 279:33220-33227.

Zhou, S., Sousa, R., Tannery, N.H., Lafer, E.M. 1992. Characterization of a novel synapse-specific protein. II. cDNA cloning and sequence analysis of the F1-20 protein. J. Neurosci, 12:2144-2155.

Figure Legends:

Figure 1. Abnormal wing morphology resulted from ectopic expression of *porc*, *shi*^{K44A}, or *lap*. Female flies with the genotype of *1096-Gal4;+/T(2;3)TSTL, Tb/+* were crossed with males carrying a UAS construct or an EP-element insertion as described in Materials and Methods. The resulting progeny were grown to adults, and females were analyzed for the presence of any abnormalities in the wing due to over-expression of the transgene.

Figure 2. Genetic interaction between Mer and lap. Ectopic expression of various transgenes in the wing pouch was performed and adult flies were analyzed as described in Figure 1. Over-expression of *Mer*$^{+}$ together with *lap* restored the normal wing morphology. Black arrowheads denote the sites of ectopic vein materials. Female wings are shown.

Figure 3. The C-terminal region of Merlin is required for the genetic interaction with Lap. Arrowheads point to ectopic vein materials.

Figure 4. Co-localization of the Merlin and Lap proteins in the wing imaginal disc cells. The wing imaginal discs were stained with an anti-Merlin (A) or anti-Lap (B) antibody. A merged image is shown in panel C.

Figure 1

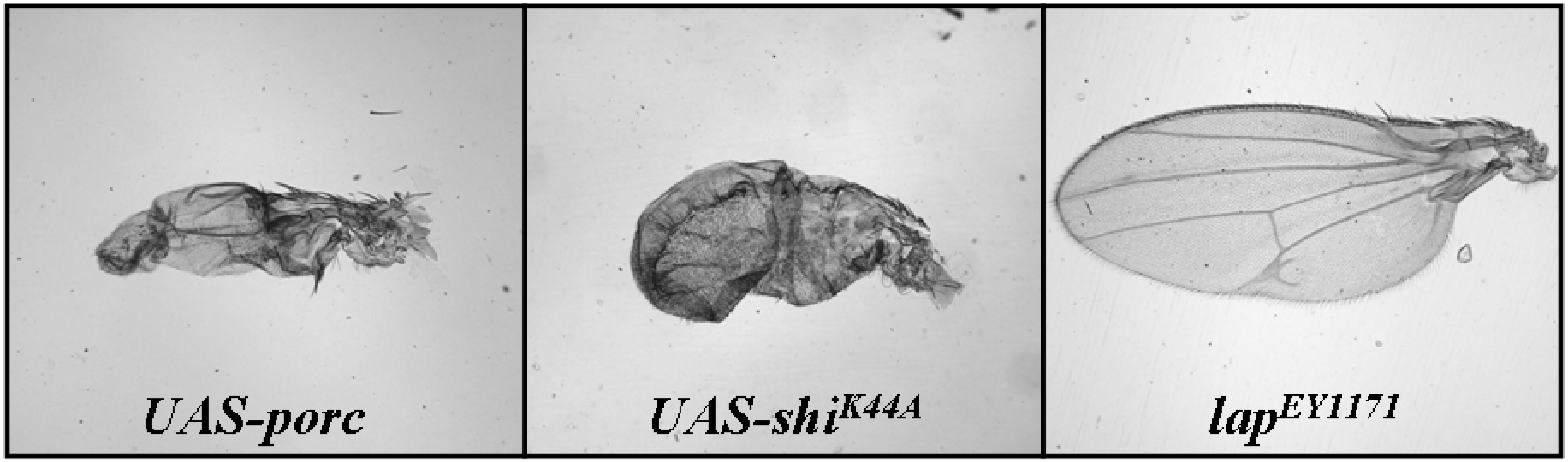

Figure 2

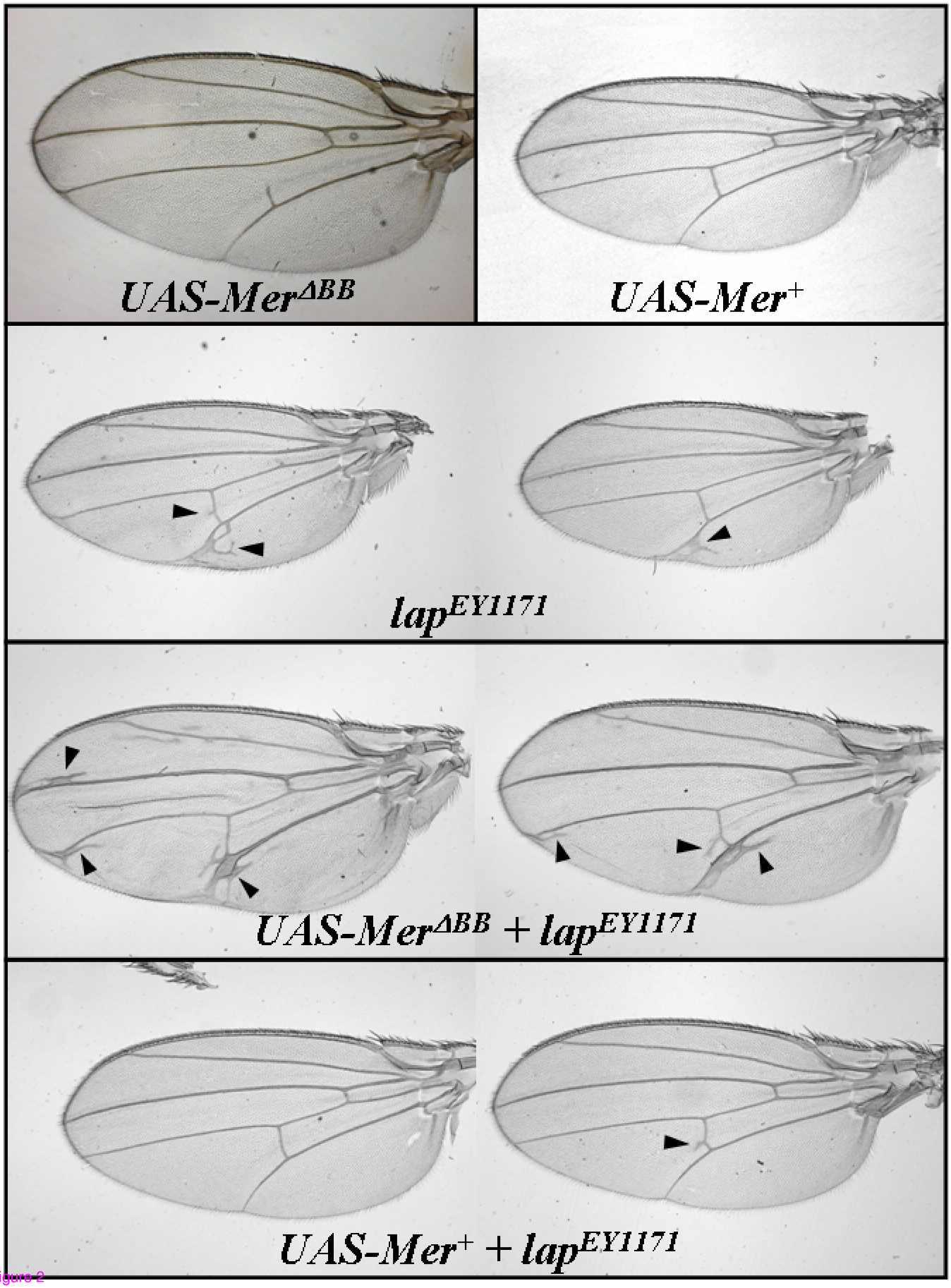
UAS-Mer^ΔBB
UAS-Mer+
lapEY1171
UAS-Mer^ΔBB + lapEY1171
UAS-Mer+ + lapEY1171

Figure 3

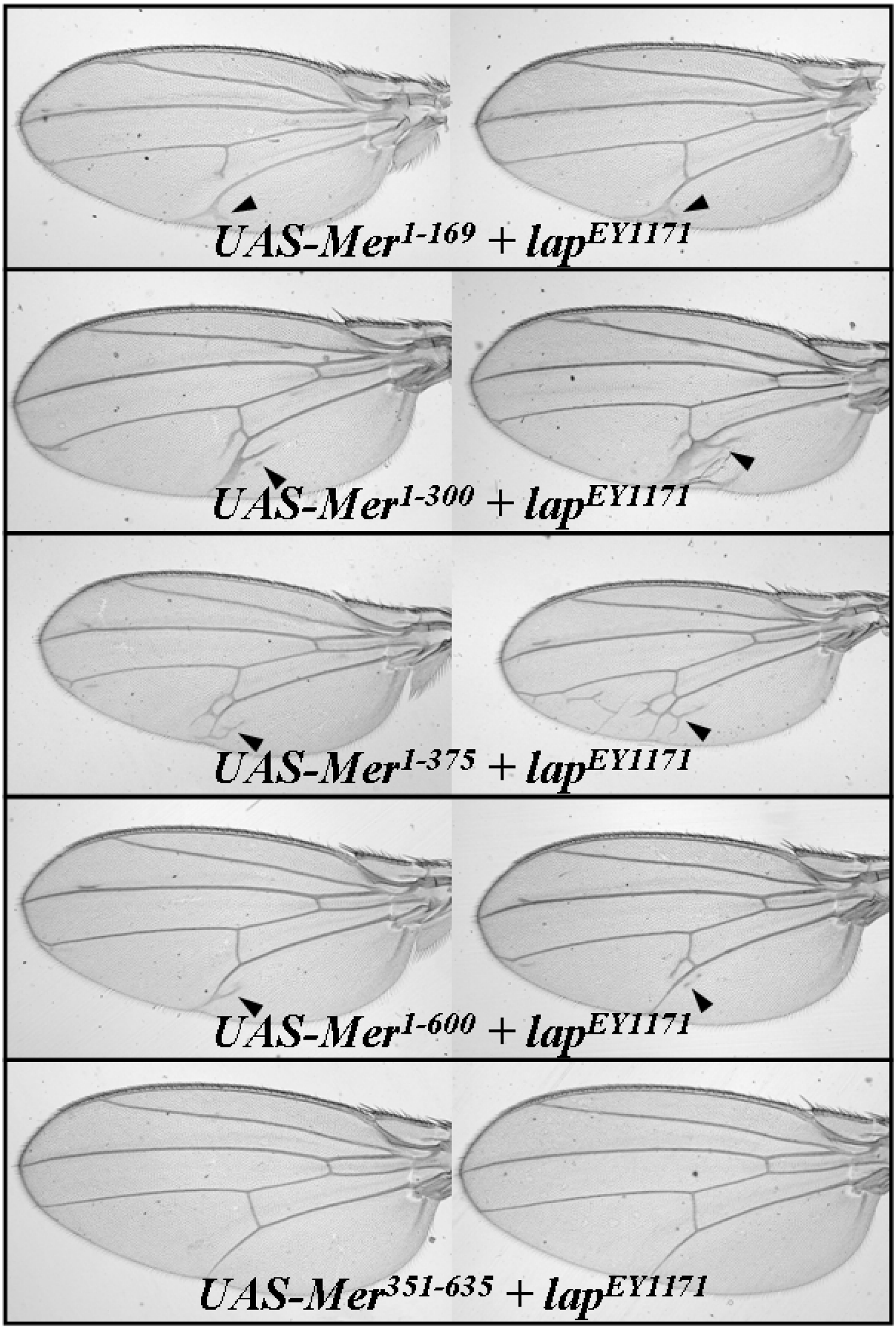
UAS-Mer1-169 + lapEY1171
UAS-Mer1-300 + lapEY1171
UAS-Mer1-375 + lapEY1171
UAS-Mer1-600 + lapEY1171
UAS-Mer351-635 + lapEY1171

Figure 4